Geosphere and biosphere dynamics during late Ordovician climate change

Thomas J. Challands

Geosphere and Biosphere dynamics during Late Ordovician climate change

Thomas J. Challands
Department of Earth Sciences
Durham University

A thesis submitted for the degree of
Doctor of Philosophy

May 2008

Declaration

I declare that the work contained in this thesis was the result of my independent research except where otherwise stated.

Signed 

Thomas James Challands

May 2008

Acknowledgements

This study was funded by a Durham University Postgraduate Scholarship, the Durham University Department of Earth Sciences and a grant from the British Geological Survey British Universities Funding Initiative (BUFI). Additional funding to attend IGCP 503 2006 annual meeting in Glasgow was provided by the IGCP 503 chairing committee. Funding to visit the Research Unit Palaeontology at the University of Ghent to study chitinozoan type material was secured through a 2006 Palaeontological Association Sylvester Bradley Award and a Grant-in-Aid Award from The Micropalaeontological Society. I am grateful to all of these institutions for providing me with the means to complete this study.

Completion of this thesis would not have been possible without the dedication, criticism and support of my supervisors, both internal and external. From Durham University, my principal supervisor, Dr Howard Armstrong, has provided me with meticulous and detailed feedback for all my work, from which it has improved considerably. He has been behind the project from its inception and encouraged me, in his unique manner, to see it through to the end. Dr Stuart Jones has supported, encouraged me and given me advice, within and outwith my PhD research, in taking my research outwith the academic world. Additionally, he has encouraged me at every stage in finding employment prior to completing this thesis. From the British Geological Survey, I thank Drs Jerry Davies, Dave Wilson and Dick Waters (retired) for their assistance in the field, helping me become acquainted with the intricacies of Welsh Ordovician lithostratigraphy and providing invaluable feedback to my work at all stages. I also thank them for initiating and filling in the relevant paper work along the way that has been required for my receipt of the BUFI grant. I am in debt to Dr Alan Owen of the University of Glasgow for his dedication in the final month of my writing up, for his support and encouragement and for giving up his time to read through and make crucial comments on the final versions of each chapter.

Dr Mark Williams from the University of Leicester was involved in the initiation of this project though subsequently could no longer be involved formally due to

work commitments. However, in his free time, he has provided advice, encouragement and support in commenting on manuscripts and helping in the field. Also from the University of Leicester, Dr Jan Zalasiewicz and Andrea Snelling have contributed stimulating discussion and suggestions on palaeoecology of graptolites and chitinozoans in the Upper Ordovician and Lower Silurian. It was a pleasure to help them on fieldwork at Dob's Linn collecting from the *complanatus* graptolite Biozone.

I am indebted to Dr Thijs Vandenbroucke and Prof. Jacques Verniers of the Research Unit Palaeontology at the University of Ghent who have been supportive of my chitinozoan work herein and who made me feel most welcome and assisted me endlessly during my short stay in Ghent. I must especially thank Thijs and his partner Katherine for their hospitality during my visit to Ghent. Thankyou also to Dr Jan Vanmeirhaeghe (formally of the University of Ghent) for his discussion and help in identification of Ashgillian chitinozoans.

Within Durham University Department of Earth Sciences are some very special people I would like to thank. Dom Maloney and Mike Williams for their detailed and informative contribution to the ichnofossil study in this work. Lester Smith for his assistance in the field and on the crag. It has been a pleasure working with Alex Finlay and Dr Dave Selby on the geochemistry of the Silurian GSSP at Dob's Linn. I have learnt a great deal from their enthusiasm, for their subject and outwith their subject, about geochemistry and rifle shooting amongst many other things. Dr Geoff Nowell and Dr Chris Ottley have provided assistance with sampling strategies, processing and running of samples for trace elements and all the $\delta^{13}C$ analyses included would not have possible without the assistance of Dr Colin Macpherson and Joanne Peterkin. Dr Jeroen van Hunen and Peter Holt provided help with getting to grips with Matlab and directions with which to approach carbon isotope modeling. Dr Darren Gröcke for his discussion, comments and imparting upon me his knowledge of carbon isotope systems. Thanks to Dave Stevenson and Gary Wilson for their help with all matters IT and for help in printing various posters at the last minute before conferences. Alan Carr for his help on the (now retired) department SEM and for getting things to magically work e.g. the water bath. Karen Atkinson, Janice Oakes and Carole Blair for their assistance in keeping track of my lab and fieldwork account, booking rooms for DUMC meetings and being there to have a good whinge at (not directed to them of course). I would like to extend my thanks to all others in the department

with whom I have had various discussions, research related or not, and for their kindness and support.

It is needless to say that this project would never, ever have approached anything near completion without the support of the most important people to me, my friends and family. In Durham, Vicky Martin for the endless cups of tea and gossip not to mention her introducing me to LaTeX(I can never go back now). Toni Hamill has always been around should I have needed a break to go and play in Newcastle. Jo Morris for her enthusiasm and allowing me to steal her 'cuppa-soups'. Tom Sinclair who, despite now being based in the Netherlands, has still managed to shout encouragement from afar. After all, he was in the same position a year ago. Charlie Wilson and Jen Waters for sharing the same bay and lab as me and for their uplifting and informative perspective on both geology and life. My lunchtime running partners, Chris Dale and Steve Smith. All of my peers, fellow PhD students in the department who have all been in the same boat.

At home, here in Edinburgh, first and foremost, Mr Sam 'Trumpy' Lowndes, JimTony Reid and Chris Brooks. Without their reassurance and sympathy for me whilst enduring 'The Bad Pudding' I would not have been able to sustain my motivation for three and a half years. Dougal Ranford, Susie Alison, Erica Revie, Clare Walmsley, Jenny Lonnen, Eva and especially Jeff Liston in the last week of it all.

My biggest thanks of all go to my family who have had to endure my perpetual state of PhD frustration for the duration. My Mum, Dad and Gran, all those on the Fell side of the clan, both in the UK and Canada (Dave, Kim and Jon), and Derby branch of the Challands' (Norman, Chris, Kate and Anna). Simon, without whom I would not have even begun to have complete Appendix V, and especially Emily for letting me know that it takes a right whippet to finish a PhD. Sheila and Geoffrey de Bellaigue for their support and help in naming chitinozoan taxa and Christina, Ben and Felix for encouraging me to the end. Finally, and certainly by no means least, my biggest thanks of all to my girlfriend, Diana, for her endless love, support and tolerance over the last four years.

Edinburgh, April 27^{th}, 2008

Abstract

The late Ordovician was a period of major climatic and biological change, much of which is poorly understood. Global cooling began in the Caradoc (early Katian) with the build-up of ice in southern polar regions of the palaeocontinent of Gondwana. Cooling continued into the Ashgill (late Katian) but may have been interrupted by a brief period of global warming, the Boda Event, in the Cautleyan-Rawtheyan immediately prior to the Hirnantian glacial maximum. The proceeding Hirnantian Stage of the Upper Ordovician was a period of abrupt global change in the biosphere, climate and ocean geochemistry. These events are marked by: (1) an abrupt positive Hirnantian isotopic carbon excursion (HICE); (2) one of the three global Phanerozoic mass extinctions and (3) an extensive drop in sealevel associated with the maximum extent of the Gondwanan ice sheet.

Biostratigraphic correlation for the Late Ordovician between basin and shelf sections in the Welsh Basin is limited. The current study describeS three new chitinozoan taxa, *Spinachitina penbryniensis, Belonechitina reticulatus* and *Belonechitina ceredigionensis* and developed a chitinozan biostratigraphic scheme for the Welsh Basin. Four of the six Avalonian Ashgill chitinozoan biozones are recognized: the *bergstroemi*, *fossensis*, *umbilicata* and *taugourdeaui* Biozones. The Baltoscandian and Laurentian index taxon *Hercochitina gamachiana* is recorded for the first time in Avalonia and a new lower Hirnantian regional biozone, the new *Belonechitina reticulatus* n. sp. Biozone is erected. The Cautleyan-Rawtheyan (late Katian) *rugata* Biozone was not recorded.

Four depth-facies biotopes for chitinozoa from the upper Katian–Hirnantian (Upper Ordovician) of Avalonia have been identified herein. These are: 1) an open ocean shallow-water epipelagic biotope which includes *Cyathochitina campanulaeformis*; 2) an open ocean middle-depth mesopelagic biotope comprising *Hercochitina* and *Spinachitina*; 3) an open ocean deep-water meso-bathypelagic biotope characterized by *Bursachitina umbilicata* and 4) a shelf biotope containing predominantly *Desmochitina.* The taxonomic composition of the open ocean middle-depth mesopelagic biotope changes from one dominated by *Hercochitina* and

Spinachitina in the Upper Katian to one comprising *Ancyrochitina* in the Hirnantian post-glacial transgression. The distribution of the deep-water mesobathypelagic biotope and the shelf biotope is affected by basin hydrography and sea level respectively. Changing hydrography induced by climate belt reconfiguration along the southern margin of Iapetus in the Rawthean (late Katian), displaced deep-water taxa into the semi-restricted Welsh Basin. With sea level fall in the early Hirnantian, taxa from the shelf biotope expanded into the shallower basin. Origination of biostratigraphically useful taxa in such segregated environments, e.g. *Bursachitina umbilicata*, restricts their distribution to periods of climatic and environmental change. Gradual change in climate and, hence, distribution of important biozone taxa, leads to diachroneity of chitinozoan biozones.

During the Katian and Hirnantian, the Welsh Basin, UK, lay on the northern margin of the palaeocontinent of Avalonia at mid-latitudes (estimated between 32-45^o S), within the boundaries of the present-day position of the STHP. It therefore provides a suitable environment to test for sensitivity of palaeo-climate belt movement in a mid-palaeolatitude setting (Armstrong *et al.*, in revision).

When the Inter-Tropical Convergence Zone (ITCZ) and Sub-Tropical high pressure belt (STHP) were in a southerly position, mid-palaeolatitudes, which includes the Welsh Basin, were positioned beneath south-easterly trade winds. This climate belt configuration is recorded in the Welsh Basin by the deposition of organic-rich laminated hemipelagites deposited during wind-driven coastal upwelling. Coastal upwelling, increased productivity and organic carbon burial are recorded by increased Ba/Th, increased TOC wt% and negative δ^{13}C. Negative δ^{13}C excursions are interpreted to represent remobilization of ^{12}C-enriched waters during upwelling from the deep-ocean.

The onset of the expression of climate belt movement during Boda Event times is later in the Welsh Basin than at low-palaeolatitudes. At low-palaeolatitudes the δ^{18}O response to shifting ITCZ occurred in the Cautleyan whilst in the Welsh Basin the isotopic and lithological response to moving STHP began in the Rawtheyan. This delay in expression of events is accounted for by ice-sheet-moderated rectification of insolation in the run-up to the glacial maximum. The onset of the Hirnantian glacial maximum is orbitally-moderated and is interpreted to represent an orbital configuration when eccentricity was high, obliquity low and aphelion occurred during Austral summer. It represents a threshold at which the

Gondwanan ice-sheet was able to survive precession and obliquity-induced ablation. Once this threshold had been reached, global climate belt position stabilized in a position where the ITCZ lay north of the equator and the STHP lay north of Avalonia.

Four positive $\delta^{13}C_{org}$ excursions in Hirnantian-age rocks from the Welsh Basin have been recognized in this study and are considered to represent the HICE. They correlate well between basin and shelf environments and also with a proposed sequence stratigraphic model for the Hirnantian in the Welsh Basin. Two excursions of up to 3 ‰ occur in the lower Hirnantian *reticulatus* chitinozoan Biozone and two excursions of 1 ‰ are present in the late Hirnantian *taugourdeaui* Biozone. Higher carbon storage in the basin, coincident with positive $\delta^{13}C_{org}$ excursions during glacial periods, indicate a shift in the locus of carbon burial from the shelf to the basin during low sealevel. The topology of the regional Hirnantian isotope curve for the Welsh Basin compares with only a few curves from other parts of the world indicating strong regional carbon cycling. Comparison of the relative timing of the onset of HICE and peak HICE values from other palaeocontinents demonstrate little, if any, consistency with palaeolatitude or basin setting. It is demonstrated that this chemostratigraphic diachroneity of HICE can be attributed to the process of signal rectification of $\delta^{13}C$ records most likely due to numerous local carbon cycling processes.

Contents

List of Figures

List of Tables

List of Plates

Chapter 1

Introduction

This study addresses responses at mid-palaeolatitudes of sedimentary and biotic processes in shelf and basin marine environments to changing global climate in the Late Ordovician (late Katian – Hirnantian, 455.8-443.7 Ma). The Welsh Basin, UK is used herein as a case study to test predictions of biotic, geochemical and sedimentary response to proposed pre-glacial warming (Fortey & Cocks, 2005) and the onset of the Hirnantian glacial maximum.

The project was conceived during the 2002 Ludlow Research Group field trip to Cardigan Bay, west Wales, where, working alongside British Geological Survey geologists mapping the area at the time, it was realized that the stratigraphy in the region was complete enough for the late Katian and Hirnantian (Ashgill) to use the Welsh Basin as a region to test contended hypotheses of current Late Ordovician climate change. Furthermore, following completion of mapping the Cardigan and Dinas Island sheet (Sheet 193) and the Llangranog sheet (Sheet 194), the British Geological Survey commenced re-mapping in the historical type Llandovery region in south central Wales in 2005. From the developing lithostratigraphical model for this area it became apparent that the study could be extended inland to include and compare basin processes (Cardigan area) with shelfal processes in the recently revised Llandovery area. The Cardigan-Llangranog region in this study refers to the area covered by British Geological Survey England and Wales Sheet 193, Cardigan and Dinas Island (2004) and British Geological Survey England and Wales Sheet 194, Llangranog. The Llandovery area, as described in this work, refers to the area covered by the British Geological Survey sheets 196, Builth, sheet 212, Llandovery (*unpublished*), and parts of sheet 179, Rhayader (Figure 1.1).

A multi-proxy approach using biological, sedimentological and geochemical data has been used to address two key issues of Upper Ordovician climate: a possible pre-glacial warming event, the Boda Event, and the onset and pacing of the proceeding Hirnantian glacial maximum (HGM).

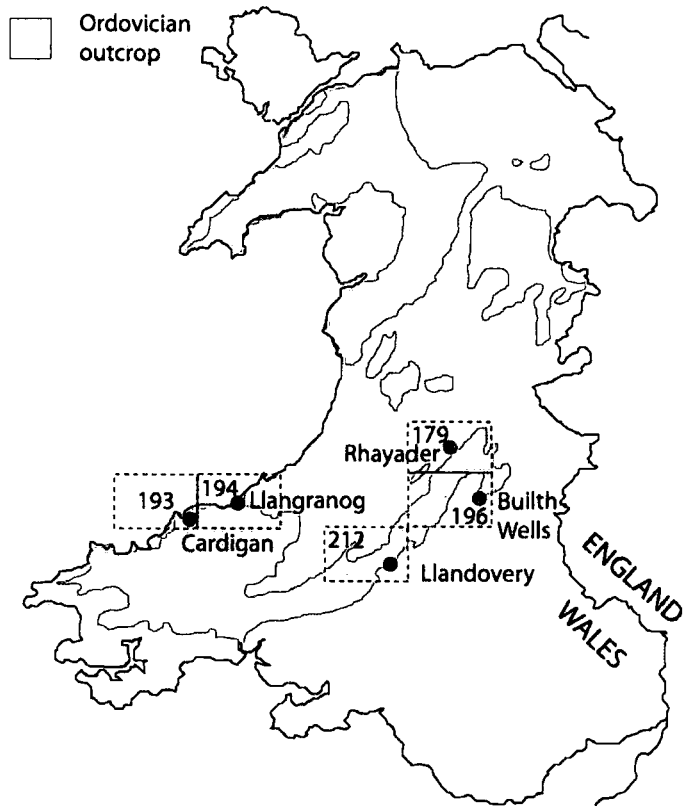

Figure 1.1: Ordovician outcrop and British Geological Survey map sheets covering study areas in Wales (modified from Fortey *et al.*, 2000).

1.1 Basin History: Cambrian to early Silurian

"It is a great slate country"

W. Keeping (1882) Geology of Cardigan Town, p.521.

The quotation above above sums up the approach taken to understanding in detail the geology of the late Katian (Ashgill) sequences in Mid-Central Wales over the past century and a half. The formation and development of the Welsh Basin is complex and warrants a separate study in itself. Here the key evolutionary phases are highlighted based on the comprehensive review by Woodcock & Strachan (2000) and serve to illustrate the changing depositional environments, volcanic and tectonic episodes throughout the Welsh Basin that occurred during the Ordovician. Detailed descriptions of the regional lithostratigraphy can be found in each chapter and in Davies *et al.* (1997), Davies *et al.* (2003), Schofield *et al.* (2004) and Davies *et al.* (2006).

The late Katian of the Welsh Basin between the Llandovery area and the Cardigan area records deposition from shelf setting, beyond the mud line, through the shelf-break, approx-

imated by the Garth Fault system, and into a basin setting which includes all deposits west of the shelf-break (Figure 1.2). Ordovician rocks crop out along the complex Tywi lineament from St.David's towards the Rhayader district in central Wales (Figure 1.2). South of this belt, Lower-, Middle- and Upper Ordovician rocks are developed exhibiting diverse facies. Katian rocks west of the Tywi lineament comprise deep water turbidites, argillites and graptolitic shales (around the Cardigan area).

Three megasequences bound by unconformities are recognised in the Welsh Basin corre-

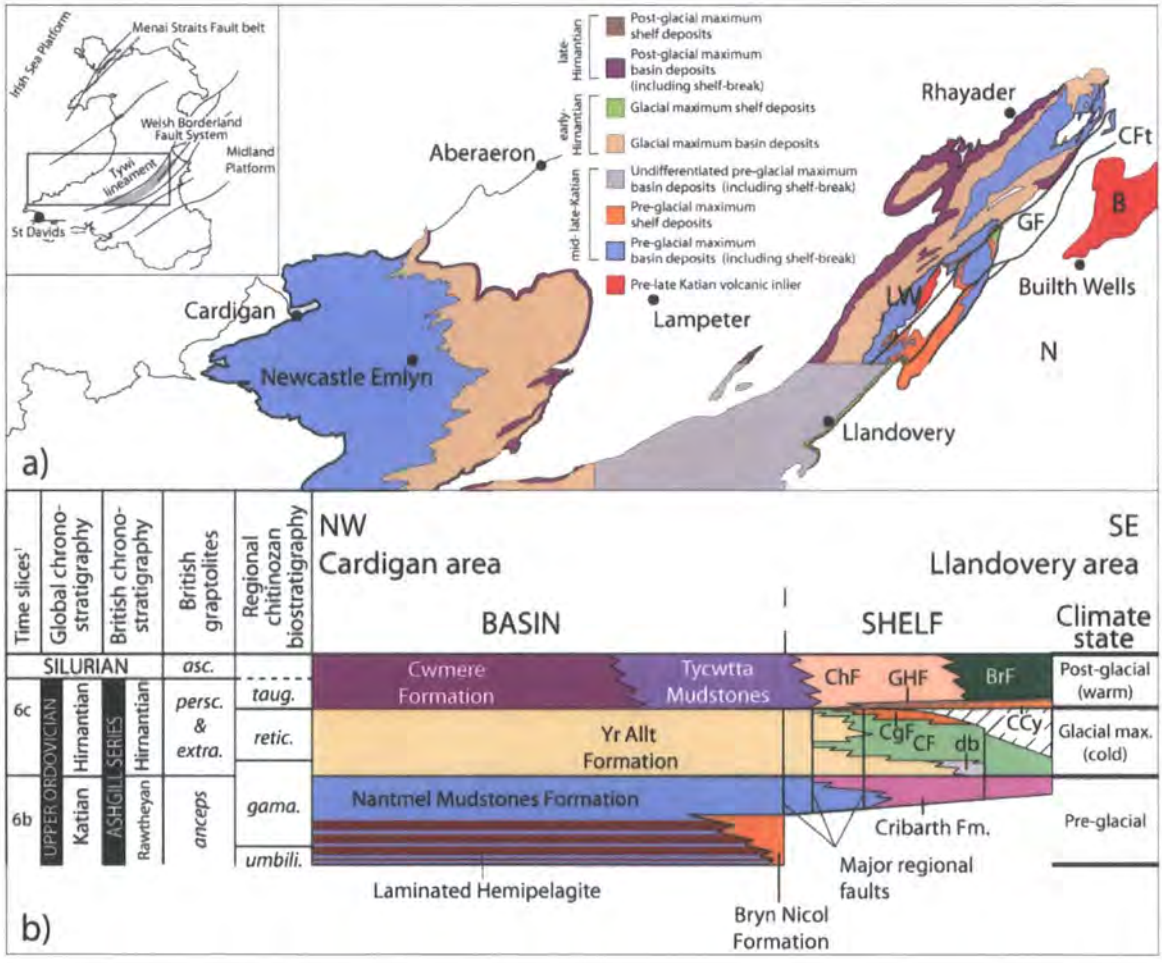

Figure 1.2: Mid- to late Katian and Hirnantian outcrop of the study area and general structural setting (inset). The shelf-basin transition is approximated by the Garth Fault system. b) General lithological relation diagram for formations comprising basin and shelf sediments for the pre-glacial maximum, glacial maximum and post-glacial of the late Katian and Hirnantian of the south central Welsh Basin. B=Builth inlier (including Builth Volcanic Group, BrF=Bronydd Formation, db=disturbed beds, CCy=Cwm Clyd Sandstone Formation, CF=Ciliau Formation, CFt=Crychan Fault, CgF=Cwmcringlyn Formation, ChF=Chwefri Formation, db=disturbed beds of the Ciliau Formation, GF=Garth Fault, GHF=Garth House Formation, LW-Llanwrtyd Wells Volcanic inlier.

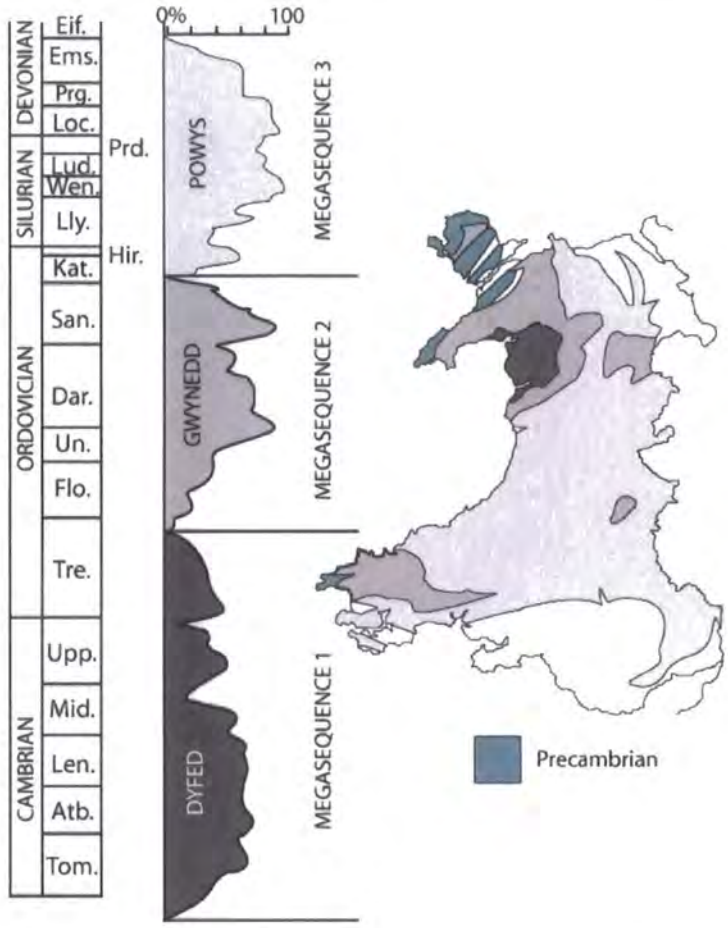

Figure 1.3: Sequence stratigraphy of the Welsh Basin represented as a rock preservation curve, after Woodcock (1990). The late Katian and Hirnantian succession of this study comprises the lowermost part of Megasequence 3, the Powys Supergroup, bound at the base by the Caradoc-Ashgill unconformity. The mid-Hirnantian unconformity expressed in the Llandovery region was not recognised by Woodcock at the time of the development of this scheme. Tom.=Tomocian, Atb.= Atdabanian, Len.= Lenian , Mid.= Middle Cambrian , Upp.= Upper Cambrian, Tre.=Tremadocian, Flo.=Floian, Un.=unnamed, Dar.=Darriwilian, San.=Sandbian, Kat.=Katian, Lly.=Llandovery, Wen.=Wenlock, Lud.= Ludlow, Loc. = Lochkovian, Prg.= Pragian, Ems.= Emsian, Eif.= Eifelian.

sponding to the Dyfed, Gwynedd and Powys Supergroups, broadly corresponding to Cambrian, Ordovician and Silurian-Devonian strata respectively (Woodcock, 1990), and each megasequence has important tectonic controls relating to the separation of Avalonia from Gondwana and its subsequent docking with Baltica and Laurentia (see Figure 1.3).

The sedimentary and tectonic history of the Welsh Basin, while still part of Gondwana, is recorded in Megasequence 1 and ranges from Cambrian to Tremadocian. It comprises marine strata on the episodically-rifted southern margin of Iapetus with an early shallow marine phase of deposition bought about by pulsed transgression (Verniers *et al.*, 2002). The extru-

sion of great thicknesses of volcanics during the late-Tremadocian to early-Floian records the onset of subduction of the Iapetus Ocean beneath Avalonia. Megasequence 2, the Gwynedd Supergroup, ranges from Floian to late Katian age and contains predominantly muddy marine facies deposited in a developing back-arc basin setting with associated subduction-related volcanics (see below). The upper limit of the Gwynedd Supergroup is at the level of the 'sub-Ashgill' (mid-Katian) unconformity (N. Wales) which is not pervasive in south Wales (Davies et al. 1997). The Powys Supergroup of Megasequence 3 records deposition in the Welsh Basin during marine transgression following the Hirnantian glacial maximum sealevel lowstand and subsequent shallowing from the Ludlow with emergence in the Přídolí to Lochkovian and terrestrial deposition of the Old Red Sandstone alluvial facies.

From the Tremadocian until the incipient amalgamation with Baltica and Laurentia, the Welsh Basin lay on the north-western margin of the microcontinent of Avalonia which was moving northward having rifted from Gondwana forming the Rheic Ocean in its wake (Figure 1.5). At this time the Welsh Basin was bounded to the east by the Midland Platform and to the west by the Irish Sea Platform. The Welsh Basin between the Welsh Borderland fault system and the Menai Straits Fault belt experienced significantly higher subsidence rates relative to the Midland Platform and the Irish Sea Platform from the Cambrian (Woodcock & Strachan, 2000). The northward movement of Avalonia, from around 60°S to about 30°S during the Ordovician, opened the Rheic Ocean between Gondwana and Avalonia and the simultaneous subduction of the Iapetus Ocean beneath Avalonia resulting in episodic subduction-related calc-alkaline volcanism from the late Tremadocian to the late early-Katian. Bimodal basic/acid marginal volcanism occurred during lulls in arc-related volcanic activity, controlled by north-south fault movement during east-west basin extension (Woodcock & Strachan, 2000). During volcanic quiescence in the early Floian, marine mudstones with rare tuffs and bentonitic clays were deposited throughout the Welsh Basin. Eruption of bimodal basic/acid lavas in the early Darriwilian (late Arenig) from new volcanic centres heralded the start of volcanism in an extended marginal basin behind a volcanic arc and the subsequent development of new volcanic centres along the south-east of the Welsh Basin margin throughout Llanvirn times (Woodcock & Strachan, 2000) (e.g. the Builth Volcanic Group in the Llandovery area). Sedimentation was dominated by marine fine-grained clastic rocks with localised sandstones and conglomerates derived from volcanic bodies but during relative sealevel fall in the Darriwilian (late Arenig and Llanvirn), erosion and the development of unconformity is recorded throughout the Welsh Basin. Avalonia was a separate entity at this time and no record of external sediment sources are apparent and sediment supply from the emergent Midland Platform must have been restricted by its low relief (Woodcock & Strachan, 2000). Above the upper Darriwilian (late Llanvirn) unconformity,

the late-Darriwilian to early-Katian (latest Llanvirn to early Caradoc) *gracilis* transgression is associated with a eustatic sealevel rise and the deposition in the Welsh Basin of turbiditic mudstones, sandstones and hemipelagites and, in the Llandovery area, the extrusion of the Llanwrtyd Volcanic Group.

In Sandbian (early Caradoc) times, basin extension and back-arc volcanism continued in the north of the Welsh Basin and deep marine organic-rich mudstone deposition associated with basin anoxia dominated regions away from the volcanic centres. At the beginning of the Katian (mid-Caradoc) arc-related volcanism ceased and strike-slip fault activity was initiated associated with chemically-distinctive volcanic rocks and minor intrusions included in the Builth and Llanwyrtyd volcanic inliers. Thermal subsidence coupled with eustatic sealevel rise during the *gracilis* transgression precipitated the deposition of fine-grained siliciclastic marine deposits across the region. In the Cardigan area these include the Dinas Island Formation and in the Llandovery region, the St. Cynllo's Church Formation.

The mid-Katian (late Caradoc and early Ashgill) world experienced a pulsed eustatic sealevel fall (Nielsen, 2004). Nevertheless, the Welsh Basin was still subsiding more rapidly than the adjacent emergent or shallow marine Midland and Irish Sea Platforms and marine deposition persisted. An abrupt trans-Iapetus change from anoxic to bioturbated oxic facies occurs at around the mid-Katian (Caradoc-Ashgill boundary; see Vandenbroucke *et al.*, 2008) and is inferred to have been brought about by the initiation of thermohaline circulation during the development of a global ice-house climate, the Late Ordovician glaciation (Armstrong & Coe, 1997). However, at this time local uplift of discrete fault blocks in the north of the Welsh Basin caused erosion and the development of unconformity around the mid-Katian, Caradoc-Ashgill boundary (Fortey & Cocks, 1986). Strike-slip movement along the Welsh Borderland Fault system, penetrating Darriwilian volcanic rocks of the Builth Inlier which are overstepped by Llandovery deposits, testify to tectonic activity during the late Katian (Ashgill). Active deposition of conglomerates and sands and progressive increase in truncation of older strata to the east in the Llandovery area demonstrate localised fault movement along the Welsh Borderland Fault system at this time. This tectonic episode has been termed the Shelveian deformation event (Lynas, 1988; Toghill, 1992). Contemporaneous with fault activity in the Hirnantian was a dramatic lowering of eustatic sealevel during the onset of the Hirnantian glacial maximum. During this brief event (< 1Myr, Sutcliffe *et al.*, 2000) the Midland Platform was emergent and the basin received vast amounts of sedimentary debris from the eroding hinterland and destabilised basin platforms producing thick, slumped sandy deposits in the deeper parts of the basin, with sediment bypassing the shallower shelves, whilst muddy-sand, tidally-influenced deposits accumulated in basin margin settings. (Figure 1.4).

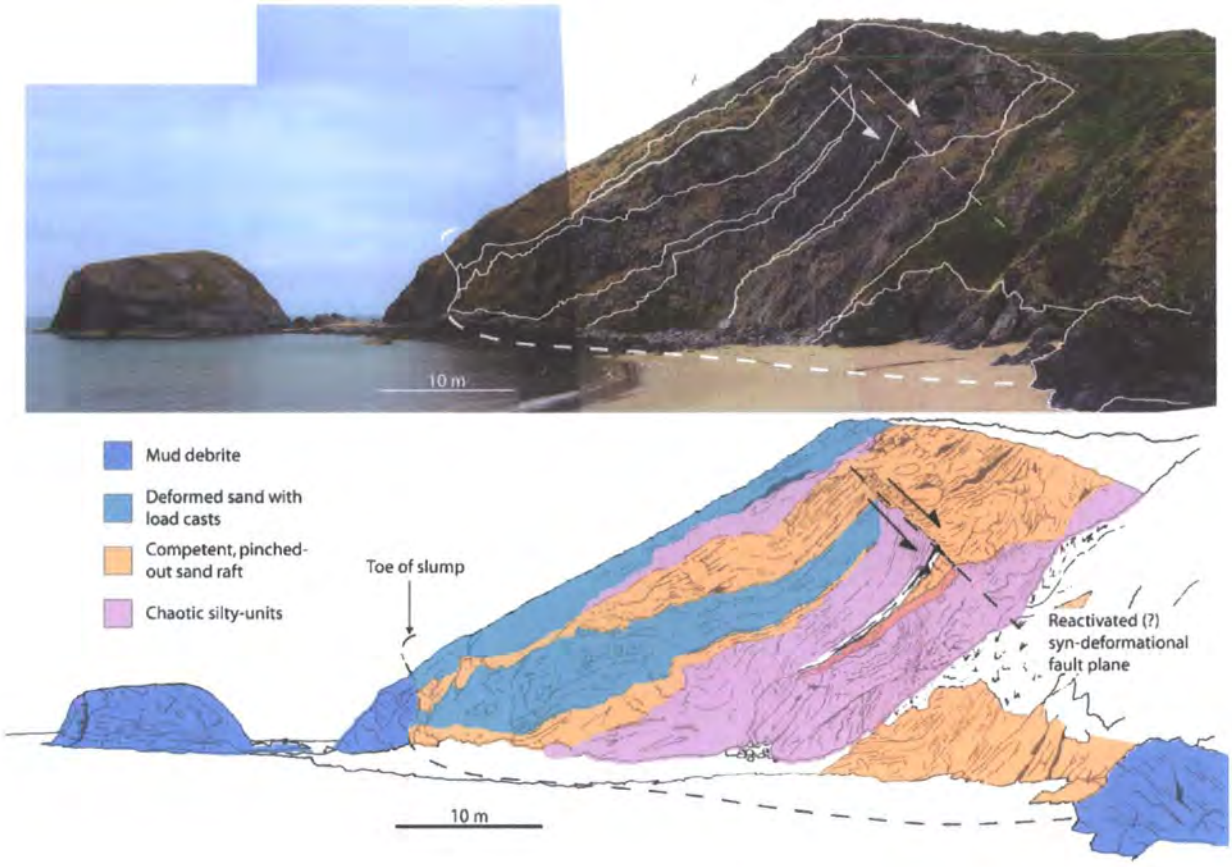

Figure 1.4: Photograph and interpretation looking NE at a large-scale slumped sandstone raft on debrite cushion in the Hirnantian basinal Yr Allt Formation deposited during the Hirnantian glacial maximum. Location: Traeth Bach, Carreg-y-Ty near Llangranog (SN 301 535)

Postglacial conditions resumed in the latest Hirnantian and deep marine sedimentation resumed over much of the Welsh Basin. Initially sedimentation took place under oxic conditions, represented by the Mottled Mudstone Member, ubiquitous in the Welsh Basin, but soon anoxic conditions resumed and organic-rich laminated hemipelagite deposition occurred in slope apron settings (Schofield *et al.*, 2004).

1.1.1 Palaeogeographical setting of the Welsh Basin: Avalonia in the Late Ordovician

From isolation from Gondwana in the Arenig, to the initiation of docking with Baltica in the Late Ordovician, the Welsh Basin lay on the northern margin of the micropalaeocontinent of Avalonia. To the south, Avalonia was separated from Gondwana by the Rheic Ocean and to the north lay the Iapetus Ocean and Laurentia. Avalonia was separated from Baltica by

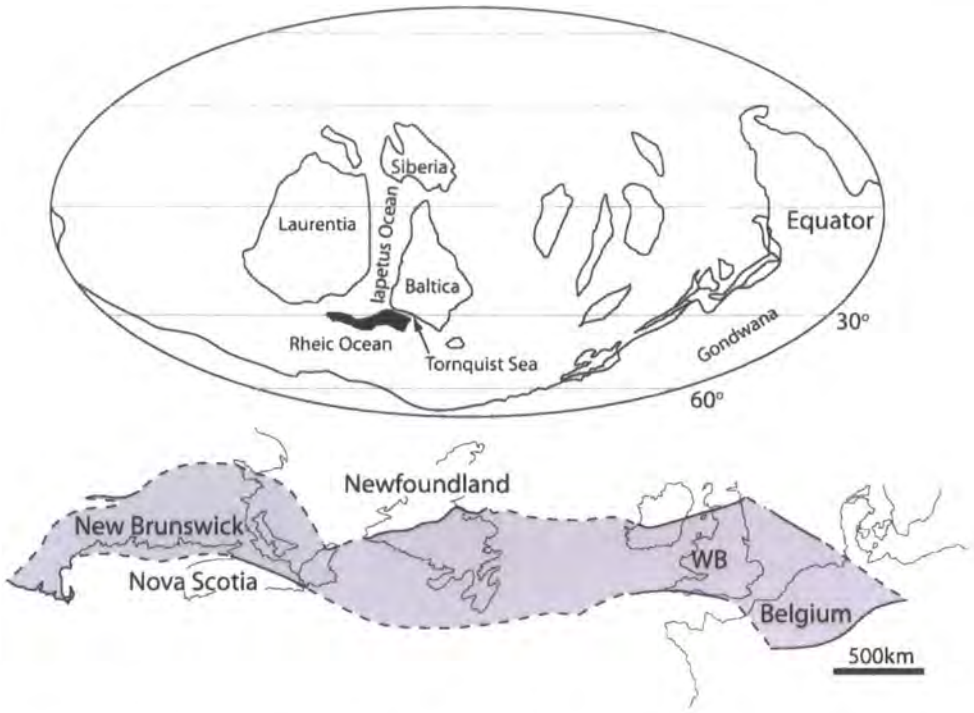

Figure 1.5: a) Palaeogeography of the late Katian and the position of Avalonia (in black). Avalonia lay at mid-latitudes between 32-45° south throughout the late Katian. b) Detailed palaeogeography of Avalonia showing position of the Welsh Basin (WB) relative to other modern Avlonian localities (from Cocks *et al.*, 1997).

the Tornquist Sea which closed as Avalonia drifted northwards (Figure 1.5). Avalonia was first recognized as a separate palaeocontinent by Cocks & Fortey (1982) on faunal grounds from which approximate latitudinal positions could be established as the palaeocontinent progressively moved into tropical latitudes from the Early Ordovician to the Silurian. By the late Katian, Avalonia was within close proximity to Laurentia and Baltica and by the Wenlock Avalonia as an individual palaeocontinent was below the limits of palaeomagnetic resolution (MacNiocaill, 2000).

Throughout the Late Ordovician, Avalonia was situated at mid-palaeolatitudes in the southern hemisphere. Vizan *et al.* (2003) summarized all palaeomagnetic work carried out from Avalonia from the Neoproterozoic to the Silurian. They calculated a palaeolatitude of 32°S $+11^{o}/-8.5^{o}$ for Avalonia during the late Katian (Ashgill, U-Pb zircon - badelleyite age 442 ± 3 Ma) from rocks sampled from the Midlands Minor Suite from Nuneaton, Central England. Other late Katian palaeolatitudes calculated for Avalonia are $34^{o} \pm 4^{o}$ from Dunn Point (Johnson & Van der Voo, 1990), $32^{o} \pm 12^{o}$ (Vizan *et al.*, 2003), $45^{o} \pm 7^{o}$ (Channell & McCabe, 1992) and 33°S (calculated using Point-tracker software at 440 Ma, www.scotese.com).

The exact timing of the collision of Avalonia and Baltica is uncertain but it is generally

accepted from faunal data and convergence of palaeomagnetic wander curves that subduction of the Baltica plate beneath Avalonia began in the Caradoc (Torsvik & Rehnström, 2003) and oblique soft docking of Avalonia and Baltica had taken place at about the Ordovician-Silurian boundary (Cocks & Torsvik, 2005; Torsvik & Rehnström, 2003). This does not imply a closure of the Tornquist sea but by the Hirnantian most palaeogeographic reconstructions do not show the existence of the Tornquist sea anymore. This is undoubtedly because of low sealevel coincident with the HGM and so it is reasonable to assume that prior to the Hirnantian there was still a body of water between Avalonia and Baltica through which ocean currents could move and flora and fauna disperse (see Figure 1.7).

1.2 History of research

A full appraisal of the entire history of geological and palaeontological research that has been conducted in the Cardigan and Llandovery areas is beyond the scope of an introduction and only the key developments that will allow an appreciation of how the science has progressed and those investigations pertinent to this study are outlined.

The thick, extensive Ordovician–Silurian rocks of the coastal region of Ceredigion, west Wales, were neglected in study while other classic regions such as north Wales and Llandovery received much attention during the 'Golden era' of geology in the mid-nineteenth century. Murchison (1839) commented on the 'vast unclassified heaps of greywackes' of the Palaeozoic deposits of the south-central Wales region and the maps produced by the British Geological Survey between 1845 and 1857 (Old Series sheets 40, 41, 57 and 58) only referred to areas 'dominated by argillaceous slates', 'grits' and 'sandstone' (Anketell, 1987). The earliest published description of the geology of the Cardigan district is by Keeping (1882) who collected *Dicellograptus morrisi* from the Dinas Island Formation and recognised that the stratigraphy south of Cardigan was older than the Landovery Aberystwyth grits thus providing the first subdivision of the rocks in the area into their correct chronostratigraphy. However, he placed the Yr Allt Formation at Llangranog within the Aberystwyth grit and considered it to be of Llandovery age but subsequent to this the base of the Llandovery has been redefined as the first appearance of *Akidograptus ascensus* marking the base of the *Akidograptus ascensus* Biozone (Melchin & Williams, 2000; Rong, 2006). The area immediately around Cardigan subsequently received attention from Latter (1925) and Challinor (1927). Hendriks (1926) provided the first detailed stratigraphy of the area around Llangranog which was subsequently revised by Anketell (1963). McCann (1990b) adopted Anketell's lithostratigraphy for the Ashgill of the Llangranog region as well as that proposed by Craig (1985) for the mottled mudstones between Cardigan and Tresaith. Most recently the British Geological Survey mapped the Cardigan and Llangranog sheets at 1:10000 scale (Cardigan

and Dinas Island sheet, Sheet 193, 2003 and the Llangranog sheet, Sheet 194, 2006) refining the lithostratigraphy to that adopted in this study.

A comprehensive review of the rich geological history of the Llandovery area is given by Cocks *et al.* (1984). The type area of the Llandovery was most recently remapped by the British Geological Survey in 2006. Prior to this, the region has been the subject of intense research, and still continues to attract attention from a historical point of view and for recognition of what the region still offers for understanding Lower Palaeozoic climate.

Murchison produced the first interpretations of the rocks of the Llandovery area in his work *The Silurian System* (1839) following work carried out between 1833 to 1835 but it was not until the the production of the British Geological Survey map of the area in 1857 that the terms Upper and Lower Llandovery were first used, the Lower Llandovery containing what is now recognized as the Katian and Hirnantian. In the original definition of the Ordovician, Lapworth (1879) defined the top of the Ordovician as being at the base of the Lower Llandovery demonstrating that this chronostratigraphy was by then a broadly accepted and convenient system. Evans (1906) recognized distinct facies differences between sections north and south of an anticline structure subsequently recognized by Strahan & Jones (1914) and interpreted this to be the region of maximum pre-Ashgill uplift and a possible topographic and tectonic control on basin sedimentation in the area. Evans (1906) provided a detailed account of the sedimentology and faunas found in Katian-age rocks of southern Wales (the '*Dicranograptus* Shales') but only briefly mentioned the units to the north as vaguely resembling the Redhill beds but more so Llandovery-age rocks of what he termed the Great Pale beds. The structure and stratigraphy of the early- to mid Katian Stage in the southern region was refined during mapping by the British Geological Survey in 1914.

Cocks *et al.* (1984) undertook a remapping study in the south western extent of Katian-Llandovery rocks between Llandovery and the Afon Sefin (Sefin river) south of Llandovery and the Crychan Forest area in the north and defined the Scrach Formation. A major advance during subsequent remapping of the Type Llandovery area by the British Geological Survey in 2005 was the subdivision the Scrach Formation into the Yr Allt, Ciliau, Cwm Cringlyn, Cwmclyd Sandstone and Garth House formations and the identification of a major unconformity at the base of the Cwmclyd Sandstone Formation. This unconformity is taken to indicate regional tectonic activity coupled with low eustatic sealevel during the Hirnantian glacial maximum (Schofield *et al.*, 2004). The current study forms the most recent biostratigraphical study and palaeoclimate synthesis of the Llandovery and Cardigan areas. /newpage

1.3 Setting the scene: Late Ordovician climate change

For much of the Ordovician the global climate was dominated by a greenhouse state with elevated atmospheric CO_2, as suggested by isotopic proxy data, and water vapor (Berner, 1994; Barnes, 2004; Herrmann *et al.*, 2004). Major transgressive events, occurring at the beginning of each of the stages of the Ordovician (Nielsen, 2004), and the combination of high sealevels and a warm climate produced, in general, wide tropical and warm temperate marine climate belts with sluggish ocean circulation and extensive marine anoxia (Barnes, 2004, , see Figure 1.6). However, the most striking changes in global ocean and climate reorganization came about towards the end of the Ordovician with the onset of the Late Ordovician icehouse in the mid-Katian (Caradoc), the subsequent Boda Event in the late-Katian (Cautleyan-Rawtheyan) and culminating in the Hirnantian glacial maximum.

The inception in the mid-Katian (Caradoc) of ice-house conditions, that may have persisted for some 30 Ma into the Lower Silurian (Berner, 1994; Berner & Kothavala, 2001; Tobin *et al.*, 2005; Saltzman & Young, 2005; Herrmann *et al.*, 2004; Page *et al.*, 2007), is supported by isotopic data and lithostratigraphic evidence (diamictites, tillites and glacial striae) from many parts of the world (see Page *et al.*, 2007, for a review). A positive $\delta^{13}C$ excursion peak from Nevada of *clingani* graptolite Biozone age, the Guttenberg Isotopic Carbon Excursion (GICE, Hatch *et al.*, 1987) was noted to be associated with synchronous positive $\delta^{18}O$ values (Tobin *et al.*, 2005; Shields *et al.*, 2003) and marine regression (Nielsen, 2004, , Figure 1.6). This event has also been recognized in Estonia (Baltoscandia, Meidla *et al.*, 1999) supporting its global extent. The development of a single ice-sheet at this time covering the southern palaeocontinent of Gondwana, is further indicated by climate modeling (Herrmann *et al.*, 2003, 2004, 2005) and continental configuration (Cocks, 2001, (Cocks & Torsvik, 2002), see Figure 1.6 inset).

Changes in global climate state occurred in two discrete stages from the beginning of glaciation in the mid-Katian until the glacial maximum in the Hirnantian (Armstrong, 2007), each stage being marked by a significant oceanographic reorganization and, in some cases, associated with distinct isotopic events. Firstly, following GICE, abrupt oxygenation of oceans at low-latitude (Sheehan, 2001; Armstrong & Coe, 1997), extensive burrow-mottled sediments and an absence of black shales in the lower mid-Katian (mid *linearis* Biozone in Scotland and Wales) was concurrent with marine regression (Page *et al.*, 2007; Vanmeirhaeghe, 2007; Nielsen, 2004) and a positive $\delta^{13}C_{carb}$ excursion of around 2 ‰ (recorded from Estonia, Kaljo *et al.*, 2007, ; see Figure 1.6). Secondly, migration of warm water low-latitude faunas took place during high sealevel (Nielsen, 2004; Ross & Ross, 1992) in the late Katian (Boucot *et al.*, 2003; Fortey & Cocks, 2005) marking a period of relative expansion of a warm climate conditions, the Boda Event of Fortey & Cocks (2005). A positive $\delta^{13}C_{carb}$ excursion of up

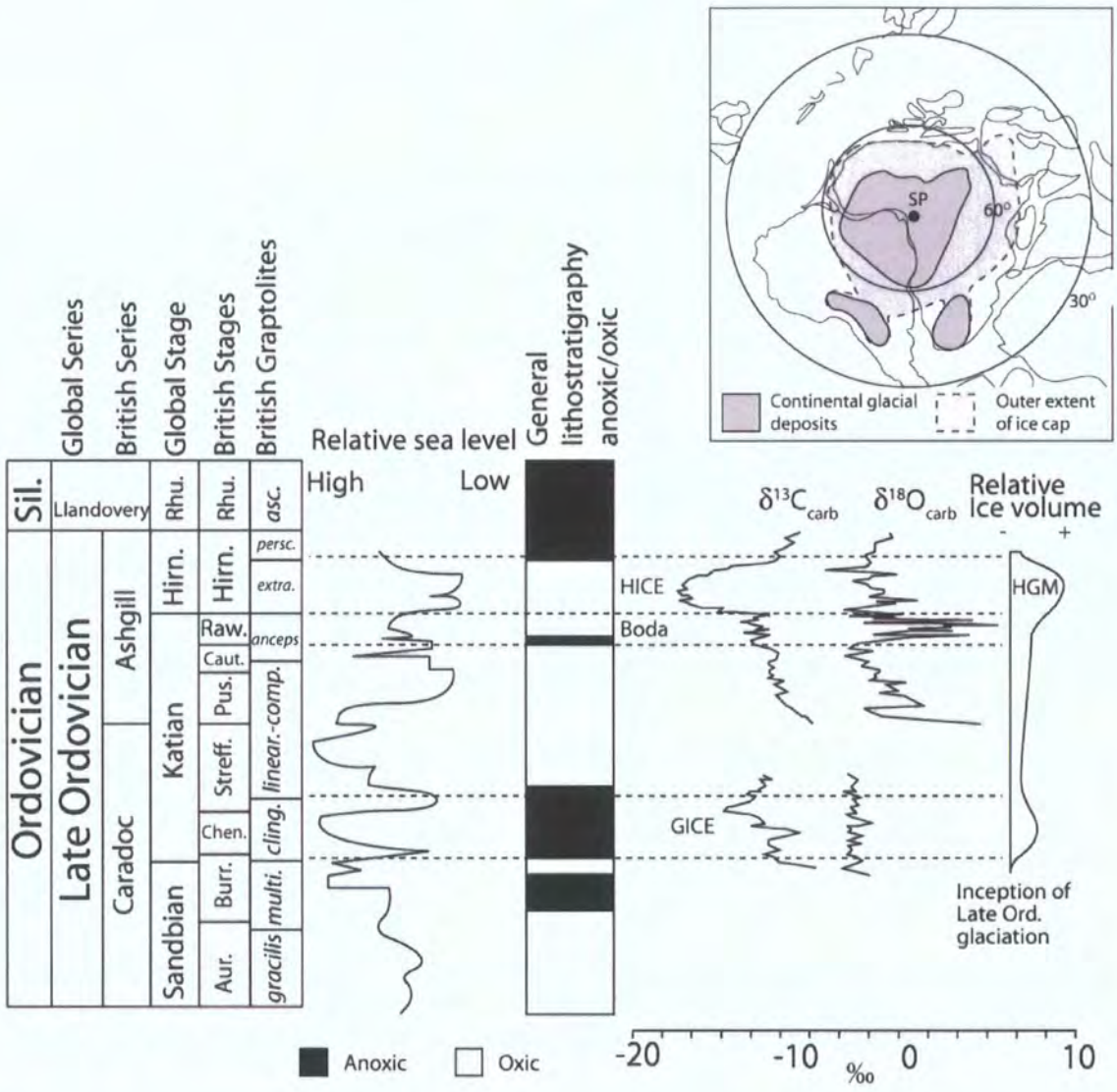

Figure 1.6: Late Ordovician sealevel (from Nielsen, 2004), general anoxic-oxic lithostratigraphy (after Page *et al.*, 2007) and $\delta^{13}C_{carb}$ and $\delta^{18}O_{carb}$ (from Saltzman & Young, 2005). Chronostratigraphic abbreviations: Aur.=Aurelucian, Burr.=Burrellian, Chen.=Cheneyan, Streff.=Streffordian, Pus.=Pusgillian, Caut.=Cautleyan, Raw.=Rawtheyan, Hirn.=Hirnantian, Rhu.=Rhuddanian. Biostratigraphic abbreviations: *multi.=multidens*, *cling.=clingani*, *linear.=linearis*, *comp.=complanatus*, *extra.=extraordinarius*, *persc.=persculptus*, *asc.=ascensus*.

to 3 ‰ occurred at this time (late Katian, Richmondian of North America, late Pirgu of Baltoscandia, see Armstrong *et al.* in review) in Nevada and Estonia alongside a negative $\delta^{18}O$ excursion of 10 ‰.

1.3.1 Oceanographic conditions during the Late Ordovician

The Caradoc saw the highest global sealevels in the entire Phanerozoic (Hallam, 1992) and fluctuating sealevels undoubtedly had an influence on ocean circulation patterns and global climate. Early attempts at reconstructing surface ocean currents employed a method of transcribing modern ocean circulation patterns onto Ordovician palaeogeographies (McKerrow & Scotese, 1990; Wilde, 1991). Whereas these reconstructions have not been refuted, Ordovician ocean circulation patterns are dependent on configuration of the Ordovician palaeocontinents and numerous palaeogeographic reconstructions have produced various circulation pattern models e.g. McKerrow & Scotese (1990); Wilde (1991); Barnes (2004); Herrmann *et al.* (2004). However, all models agree that in the northern hemisphere, which lacked large land masses north of the tropics, ocean circulation was zonal with the Panthalassic circumpolar current flowing eastwards uninhibited (Figure 1.7). In the southern hemisphere, ocean circulation was driven by low latitude evaporation and the subduction of mid-latitude saline waters, moderated by the position of the inter-tropical convergence zone (ITCZ) (Railsback *et al.*, 1990).

From the early recognition of the patterns documenting the terminal Ordovician glaciation soon came models of the processes and mechanisms causing changes in ocean circulation patterns and climate belt configuration. Berry & Wilde (1978) and Berry *et al.* (1991), for instance, used the distribution of graptolites around inferred upwelling zones in the Late Ordovician, to indicate the introduction of nutrients into coastal surface waters following the initiation of thermohaline circulation. It was subsequently suggested that the product of such a mechanism would have been the increased burial of organic carbon drawn from atmospheric CO_2 (the Monterey hypothesis) which in turn acted as the stimulus for glaciation with a lowered atmospheric pCO_2 (Armstrong & Coe, 1997; Brenchley *et al.*, 1994, 1995).

1.3.2 Climate belts in the Ordovician

The position and extent of the latitudinal global climate belts, the Intertropical Convergence Zone (ITCZ), the Sub-tropical High Pressure belt (STHP) and the Polar Front, determines ocean circulation patterns, trade wind strength and heat transport throughout the globe (Rind, 1998; Billups, 2005). Orbital variations in insolation cause the Hadley Cells to vary in intensity and size latitudinally and the latitudinal high-pressure (STHP) and low-pressure (ITCZ and Polar Front) belts to migrate north and south with orbital periodicity (Christiansen & Stouge, 1999; Perlmutter & Matthews, 1990; Rind, 1998).

For the Upper Ordovician Armstrong *et al.* (in revision) recognized distinct $\delta^{13}O_{calcite}$ populations in the middle Katian (late Caradoc, syn-GICE), upper Katian (Cautleyan-Rawtheyan) and Hirnantian, that match changes in $\delta^{13}O_{calcite}$ values in marine waters be-

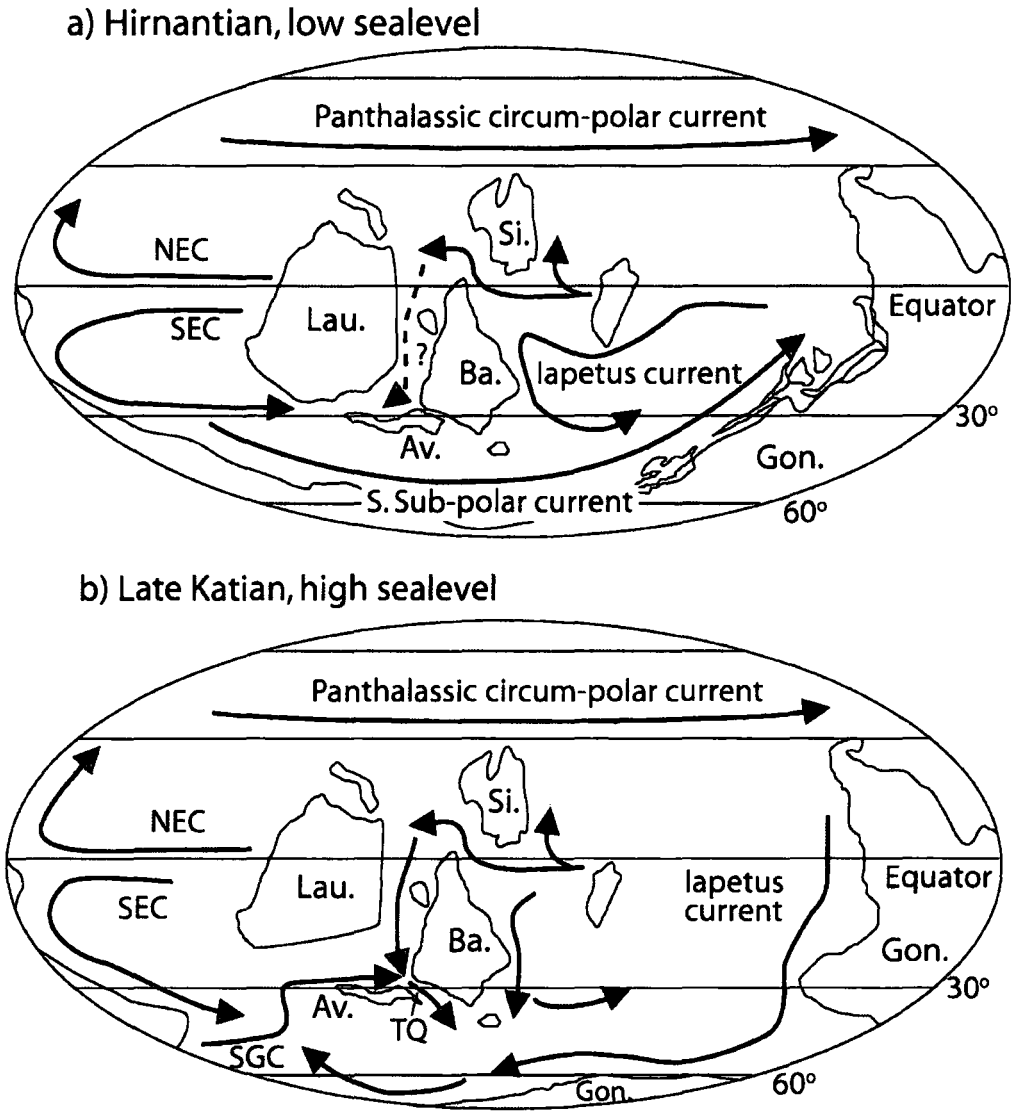

Figure 1.7: Late Katian and Hirnantian palaeogeography and ocean circulation for low sealevel (a) and high sealevel (b). Importantly, in the high sealevel scenario there is a current system flowing through the Tornquist Sea (TQ) and low-latitude water is brought to high southerly latitudes by the Iapetus current. Currents after Herrmann *et al.* (2004), palaeogeography after Cocks & Torsvik (2004). NEC=North equatorial current, SEC=South equatorial current, SGC=Southern Gondwana current, Lau.=Laurentia, Gon.=Gondwana, Ba.=Baltica, Si.=Siberia, Av.=Avalonia.

neath the present migrating ITCZ. They proposed that the ITCZ progressively moved northward in response to global cooling, from the beginning of the Late Ordovician glaciation in the mid-Katian (at GICE) to the Hirnantian (Figure 6.2). In particular, during the late Katian, an equatorial position of the ITCZ and convergent trade winds was conducive to transport of warm equatorial waters to high-latitudes, through entrainment in sub-tropical ocean gyres, resulting in a low meridional temperature gradient. This mechanism potentially explains the

Boda Event (Fortey & Cocks, 2005) as being the result of poleward redirection of warm water following climate belt rearrangement and is a hypothesis to be tested at mid-palaeolatitude settings.

Another important effect of the position of the climate belts that has been overlooked in Palaeozoic climate research is the position of prevailing global wind patterns relative to climate belt position. The zones of high and low pressure for the Ordovician proposed by Parrish (1982) are broadly confirmed by the GCM models of Herrmann *et al.* (2005) and so there is a basis for examining the regional and global effects of these wind configurations. For example, Torsvik & Rehnström (2003) interpreted the mid-latitude continent of Avalonia to have been south of the STHP beneath a zone of westerly winds during the Caradoc as a means to explain the distribution of the mid-Caradoc Kinnekulle bentonite from Sweden having been sourced from Avalonia, volcanic ash being blown eastwards from Avalonia towards Baltica. In addition to being fundamental in the reorganization of ocean currents, zonal wind intensity can induce coastal and open-ocean upwelling and increased productivity, where continental configuration is favorable. This is one potential means of sequestering large amounts of carbon in the oceans and in ocean sediment and as is yet, an untested hypothesis for the Late Ordovician.

Figure 1.8: Armstrong *et al.* (in revision) Inter-Tropical Convergence Zone (ITCZ) model. From the inception of glaciation, $\delta^{18}O$ curves for the upper Katian and Hirnantian exhibit coincident positive excursions at discrete stages up to the glacial maximum in the Hirnantian. Each excursion event is interpreted as representing the isotopic response of ocean water, a combination of regional and global factors, to the position of the ITCZ during its northward migration. Bi-x= Boda isotopic event. Place name abbreviations: A. C.=Arctic Canada; Est.=Estonia; Nev.=Nevada; W. B.=Welsh Basin. Ocean current abbreviations (solid arrows): EEC=Eastern Equatorial Current; NEC=Northern Equatorial Curent; PCPC=Panthalassic Counter-Polar Current; SEC=Southern Equatorial Current; SGC=South Gondwana Current. Open arrows = predominant wind direction

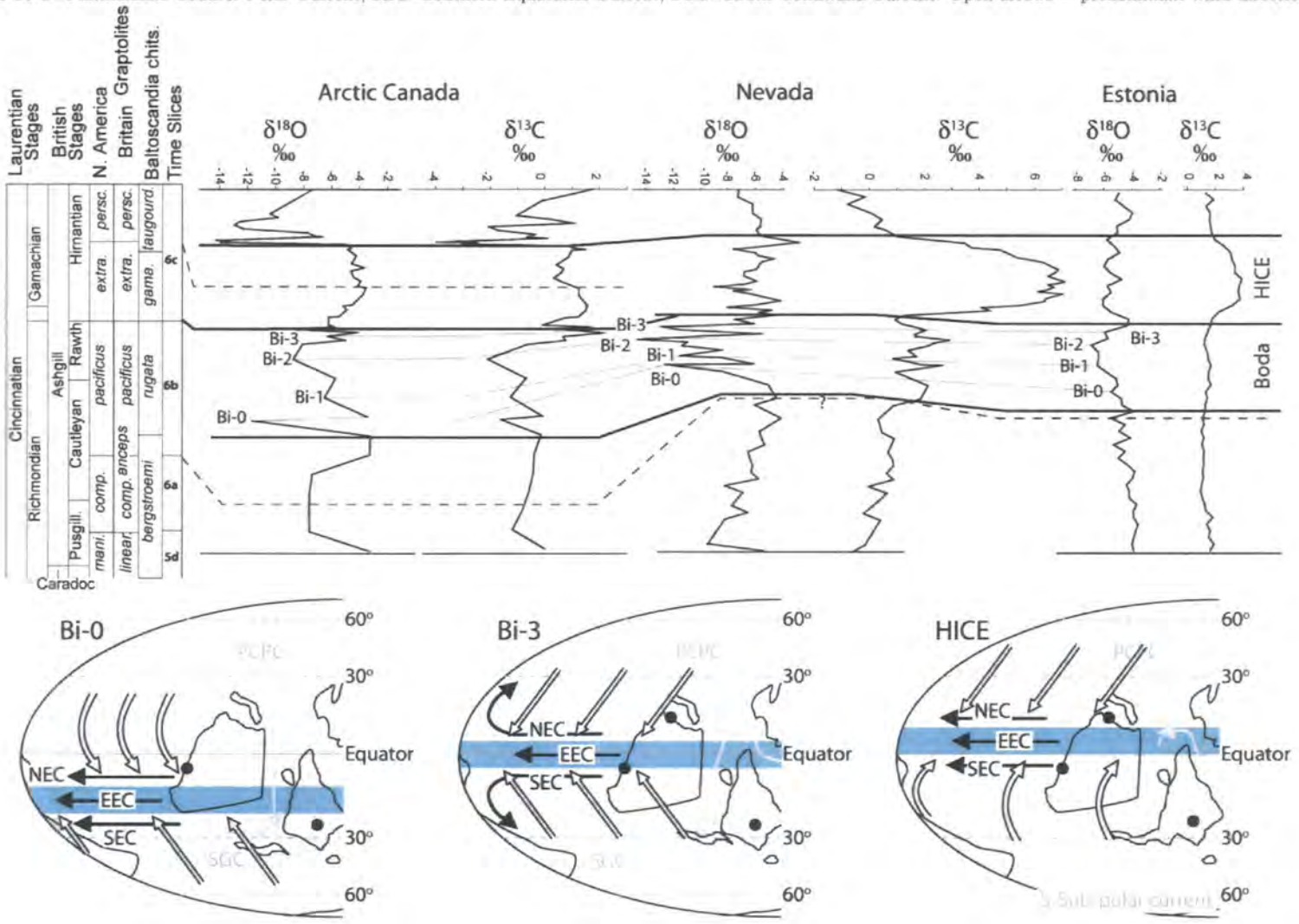

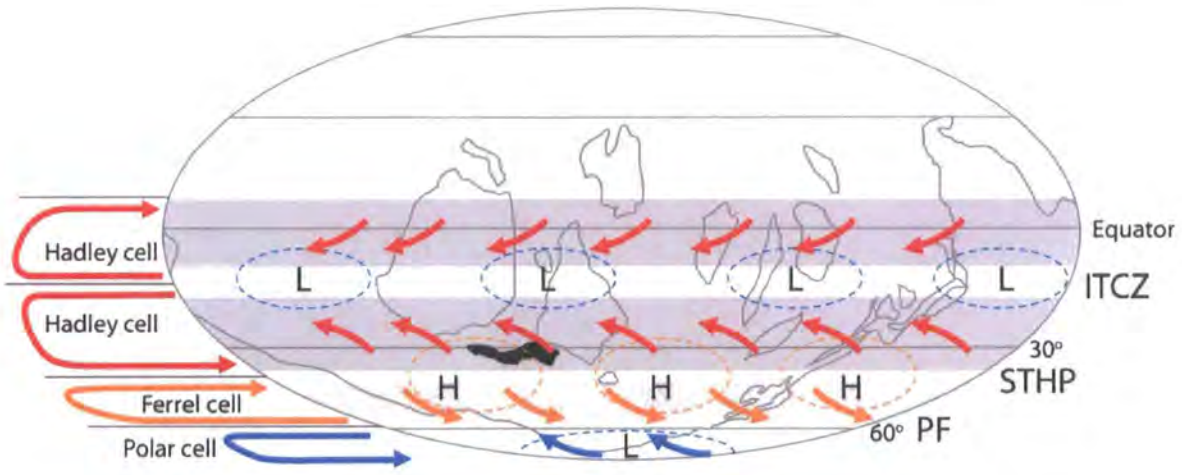

Figure 1.9: Configuration of Inter-Tropical Convergence Zone (ITCZ), Sub-Tropical High pressure belt (STHP) and Polar Front (PF) with high and low-pressure zones (after Parrish, 1982, ; Herrmann *et al.* (2004)) for the Late Ordovician. Predominant winds are shown (from Parrish, 1982). The climate belt configuration illustrated here mimics that of Bi-0 in the ITCZ model of Armstrong *et al.* (in review) with the ITCZ and STHP in a southerly position. Avalonia is highlighted in black. Palaeogeographic reconstruction after Cocks & Torsvik (2004) and www.scotese.com

1.4 The key Late Ordovician climate change events

1.4.1 The Boda Event: pre-glacial warming?

The Boda Event is regarded as being enigmatic because it potentially indicates a brief (Cautleyan–Rawtheyan, approximately 3 Myr) period of global warming in an otherwise deteriorating ice-house climate immediately prior to the Hirnantian glacial maximum. The effect of such an event could have significant effects on global carbon burial from flooding of continental shelves from melting polar ice and deposition of transgressive black shales (Page *et al.*, 2007). As such, it is critical to understand the consequences of this event on the ensuing Hirnantian glacial maximum i.e. the effect the Boda Event had on global CO_2 drawdown, and also the stresses the Boda Event may have placed on biota in the run-up to the Hirnantian mass extinction (Fortey & Cocks, 2005).

Indications of ameliorating climatic conditions during the Late Ordovician glaciation prior to the Hirnantian glacial maximum were first recognized by Boucot *et al.* (2003) from the migration in the mid-Ashgill of low-latitude Baltoscandian faunas into high-latitudes of Gondwana (the Mediterranean realm). Boucot *et al.* (2003) postulated that the cause of such a faunal shift may have been the establishment of a warm water gateway from low- to high-latitudes. Subsequently, Fortey & Cocks (2005) provided additional faunal data and noted increased endemism at low-latitudes during this time. The extensive deposition of high-

latitude warm-water carbonates, kaolinites and laterites also supported their hypothesis for a globally extensive warming event which they termed the 'Boda Event'. Further to this, Armstrong (2007) inferred from previously published ocean circulation and palaeogeographical data, the redirection of warm equatorial waters to high latitudes by the Southern Equatorial and Southern sub-polar current following the termination of the South Gondwana Current (Figure 1.7). This potentially provides a mechanism for the Boda Event. However, the Boda Event as a global warming episode was questioned by Cherns & Wheeley (2007) who interpreted the extensive limestones occurring at low- to high-latitudes during this interval as representing cool-water carbonates (Figure 1.10). In particular they interpreted cool-water limestones in a lower shelf ramp in the upper Katian (Cautleyan to Rawtheyan) of Wales as having formed during upwelling of cool water following initiation of thermohaline circulation at the onset of ice-house cooling. At the same time, shallow shelf waters were not affected by upwelling and warm water carbonates persisted in mid-ramp facies (Figure 1.10). Whether the Boda Event represents warming or cooling, the proliferation of carbonate deposition preceding the HGM has also been regarded as an important factor for long-term carbon sequestration, like the expansion of transgressive black shales, and the triggering of a glacial maximum (Villas *et al.*, 2002).

The work of Cherns & Wheeley (2007) is important for this study because it lays out a hypothesis for the first of the 'key issues' of Late Ordovician climate change; that mid-palaeolatitudes experienced cool-water conditions prior to the Hirnantian glaciation. The observations of Cherns & Wheeley (2007) is a key interpretation suggesting how mid-latitudes may responded to climate in the late Katian where the majority of faunal, lithostratigraphical and geochemical data for this interval is derived from low- or high-latitudes. The alternative, that mid-palaeolatitudes experienced warm climate conditions and warm water, conforms to the notion of the Boda Event *sensu* (Fortey & Cocks, 2005).

1.4.2 The Hirnantian glacial maximum

The Hirnantian glacial maximum represents the peak of glaciation in the Late Ordovician but its initiation and subsequent pacing are poorly understood because of uncertainty of atmospheric CO_2 levels at the time (Poussart *et al.*, 1999; Berner, 1994) and the length of the Hirnantian glacial maximum (straigraphic uncertainty; Sutcliffe *et al.*, 2000; Armstrong, 2007). Understanding this event is of paramount interest and importance because it is associated with one of the three Phanerozoic mass extinction events (Bambach *et al.*, 2004) and major palaeocecological change (Droser *et al.*, 2000; Finney *et al.*, 1999; Brenchley *et al.*, 1995; Owen & Robertson, 1995).

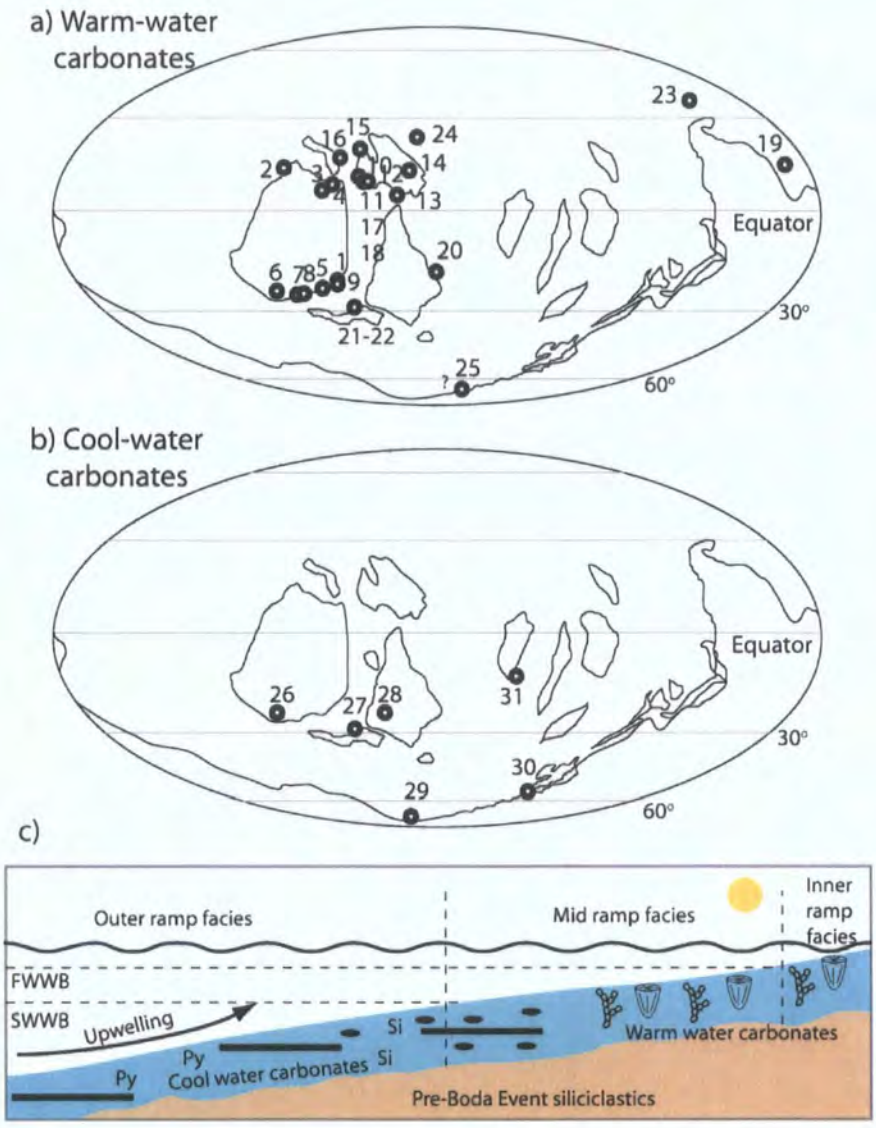

Figure 1.10: Distribution of warm-water (a) and cool-water (b) carbonates in the late Katian during the Boda Event. (c) Mid-latitude model of cool- and warm-water carbonate distribution during (redrawn from Cherns & Wheeley, 2007). Upwelling introduces cool water and nutrients into the outer ramp environments whilst warm-water carbonates with dasclydaceans and corals are deposited in shallow mid ramp facies. Warm-water carbonate distribution from Webby (2002) except 21 and 22. Cool-water carbonate distribution from Cherns & Wheeley (2007). 1=Anticosti Island, 2= Mackenzie Mountains, NW Canada, 3=Southampton Island, 4=Melville Peninsula, 5=S. Ontario, 6=Franklin & Baylor Mountains, Texas, 7=SE Indiana, 8=Central Kentucky, 9=Manitoulin Island, 10=Vaigach Island, 11=Pal-Khoi, 12=NW Urals, 13=Taimyr Peninsula, 14=Mankoka River, 15=Gorny Altai, 16=Sette-Dabhan and Verkhoyan ranges, Siberia, 17=Tas-Kayaktakh range, 18=Verkhoyan Range, NE. Russia, 19= New South Wales, Australia, 20= Kartaly-Ayat river, S. Urals, 21=Bryn Nicol Formation, Wales, 22=Robestan Wathen Limestone, Wales, UK, 23=SW Ordos Platform NW China, 24=Western Outer Mongolia, 25=Spain, 26=New Mexico & W. Texas, USA, 27=Sholeshook Limestone, Birdshill Limestone, Crûg Limestone, Wales, 28=Boda Limestone & Gotland, Sweden, W. Estonia, 29=Morroco, 30=Libya, 31=Kazakh terranes.

A major positive $\delta^{13}C_{carb}$ excursion, which is double-peaked at many locations (e.g. Dob's Linn, Arctic Canada) of between 2–7 ‰ and a positive $\delta^{18}O_{carb}$ excursion of 2–3 ‰ is recognized globally to occur with the HGM (Finney *et al.*, 1999; Marshall & Middleton, 1990; Saltzman & Young, 2005; Underwood *et al.*, 1997; Kaljo *et al.*, 2001, 2004; Brenchley *et al.*, 2003; Brenchley, 2004; Melchin & Holmden, 2006; Long, 1993; Schmitz & Bergström, 2007; Wang *et al.*, 1993). At low-latitudes however, the beginning of the excursion is in the late Katian (*pacificus* graptolite Biozone) in Laurentia and the *mirus* Biozone in China (Melchin & Holmden, 2006; Bergström *et al.*, 2006b; Saltzman & Young, 2005; Underwood *et al.*, 1997; Wang *et al.*, 1997, Figure 1.6), whereas at mid-latitudes (e.g. the palaeocontinent of Avalonia) the relative timing of isotopic perturbation and palaeoecological change of marine plankton at the HGM has not been defined. A mechanism for the Hirnantian $\delta^{13}C$ excursion that can be applied throughout the globe has also yet to be demonstrated. Proposed mechanisms include the increased burial of organic carbon matter during increased global productivity (Brenchley *et al.*, 1994) and increased weathering of carbonate (Kump *et al.*, 1999). Additionally, individual HICE records have been proposed to represent a combination of a global signal overprinted by by regional processes (Panchuk *et al.*, 2005).

The HGM took place in a climate when oxygen levels were lower than the present day, around 50% present atmospheric level (PAL), and pCO_2 was higher, estimated to have been anywhere from 8 to 18 * PAL (Berner, 1994, 2006). However, recent estimates of pCO_2 derived from biomarker $\delta^{13}C-org$ data from high-latitude late Hirnantian transgressive black shales suggests that pCO_2 levels may be much closer to present day values and are comparable with those of the pre-glacial Pliocene (Armstrong *et al.*, 2006). These recent figures have great implications for the way in which we interpret lithological data and the onset of the HGM (Crowley & Baum, 1995; Kump *et al.*, 1999; Poussart *et al.*, 1999). For example, would a (Boda) warming event be possible without high initial pCO_2 levels? Further to understanding the mechanisms for triggering the HGM, if pCO_2 were not as high as previously thought, the HGM may not be regarded as a unique glacial event but purely a manifestation of common conditions shared with other glacial episodes, such as the more recent Cenozoic glaciation (Armstrong, 2007).

Armstrong (2007) addressed this idea in detail and discussed consistency between the mechanisms of the Ordovician and Cenozoic glaciations. In summary, the crucial similarities in the triggering mechanism for the Late Ordovician and Cenozoic glaciations are:

1) *The ocean gateway trigger.* In the Cenozoic, besides the important effect of decreased atmospheric CO_2 levels, the development of the East Antarctic Ice Sheet and the Northern Hemisphere glaciation were both supplemented by plate tectonic reconfiguration, namely the closure of the Drake Passage in the Southern Hemisphere and the closure of the Central

Atlantic seaway in the Northern Hemisphere (Stoll, 2006). Such a process is interpreted for the Late Ordovician from high-resolution sealevel curves (Nielsen, 2004; Ross & Ross, 1992) and palaeocontinental reconstructions (Cocks, 2001; Cocks & Torsvik, 2002, 2004). The progressive closure of the Iapetus Ocean is envisaged to have displaced the circum-equatorial current into southerly latitudes redirecting warm water to higher latitudes (Armstrong, 2007). Further evidence for ocean current reorganization in the Mid-Ordovician comes from homogenization of Palaeozoic water mass ϵNd signatures (Keto & Jacobsen, 1987).

2) *The snow gun.* The establishment of warmer ocean currents that direct warm, moist air to high-latitudes was also essential to development of ice sheet growth within the continental interior for the Cenozoic glaciation (Tarling, 1978; Schnitker, 1980; Oglesby, 1989; Prentice & Matthews, 1991; Billups, 2005; Haug *et al.*, 2005). In the Late Ordovician, high evaporation rates at low-latitudes (Herrmann *et al.*, 2004) coupled with closure of an Iapetus ocean gateway and subsequent ocean current reorganization may have resulted in the poleward transport of warm, saline bottom water and moisture-laden air which, given favorable wind conditions and climate belt arrangement (Armstrong, 2007), could have blown onto Gondwana where it would fall as snow eventually leading to the accumulation of ice.

1.5 The importance of orbital forcing and insolation on glaciation and global warming

Patterns of ice sheet growth in both hemispheres correspond to insolation driven by Milankovitch-period orbital parameters (Naish *et al.*, 2001; Zachos *et al.*, 1996). Periods of heightened ice sheet sensitivity occur with high eccentricity (when the Earth's orbit is furthest from the sun), low obliquity (Earth's tilt is minimal) and aphelion during Austral summer, the point of orbit furthest away from the sun (Aber-Ouchi & Blatter, 1993; Birchfield *et al.*, 1982; Crowley *et al.*, 1994; Macqueda *et al.*, 1998). These conditions have a profound effect on ice volume, eustatic sealevel and mean isotopic composition of ocean water (Armstrong *et al.*, 2006; DeConto & Pollard, 2003). Also, variations in solar insolation with an eccentricity-modulated precession and obliquity period affect latitudinal temperature gradients and the intensity of atmospheric circulation patterns (e.g. Hadley and Walker cells) within latitudinal climate belts (Rind, 1998). The response time of these insolation-driven climate systems further determines the climate pattern at different latitudes in different parts of the world. For instance, monsoons and meridional temperature gradients respond rapidly to changes in global insolation whereas growth and decay of ice sheets lag behind the true insolation flux pattern (Ruddiman, 2003). However, the local or regional air temperature is controlled by ice sheet volume and so follows the delayed pattern of ice sheet growth rather than that of global insolation. Oceans also respond quickly to insolation-driven ice sheet processes and changes

in atmospheric CO_2 levels (at an obliquity period, Ruddiman, 2001) and so degassing of CO_2 from ice sheets may therefore be rapidly sequestered by the ocean producing a negative feedback mechanism for global warming (Kump *et al.*, 1999; Villas *et al.*, 2002; Page *et al.*, 2007).

In the northern Hemisphere at 0.9 Ma (the Mid-Pleistocene Transition), during the Cenozoic glaciation, a change from precession-obliquity-dominated to obliquity-eccentricity-dominated periods in ice sheet processes occurred at a critical ice sheet mass threshold (Imbrie *et al.*, 1993). This change perhaps came about through different response times of ocean-atmosphere processes. On a precession scale (23 000 yr) CO_2 and CH_4 maxima are thought to enhance ablation and drive an interglacial state, whereas ice sheet growth responds to a 41 000 yr obliquity feedback mechanism (mentioned above) driving the climate into a glacial state. Alternation of the intensity of the precession- and obliquity-driven processes from eccentricity amplitude modulation results in a 100 kyr signal once the ice sheet has achieved a mass whereby it can survive precession-induced ablation, as at the Mid-Pleistocene Transition.

The documentation of orbital forcing mechanisms in the Hirnantian further suggests commonality between the Cenozoic glaciation and HGM. Sutcliffe *et al.* (2000) suggested the HGM occurred in two advances and retreats and assumed, from modeled sensitivity of ice sheets (Poussart *et al.*, 1999), that each pulse represented a 100 kyr eccentricity-driven insolation cycle. However, Hirnantian time resolution is not refined enough to indicate an abrupt transition from precession-obliquity to eccentricity-dominated processes as in the Mid-Pleistocene transition. Orbital forcing processes have also been demonstrated for Hirnantian strata. For example, low-latitude evaporites from Australia exhibit ratios of cycles with frequencies at the precessional period (Williams, 1991) and Armstrong *et al.* (2005) contend that total organic carbon (TOC) content cycles of high-latitude black shales from Jordan represent obliquity-driven nutrient flux from a melting Gondwanan ice cap.

Another plausible mechanism besides insolation proposed for controlling climate-driven processes within the glacial maximum is the silicate weathering hypothesis (Sheehan, 2001). This proposes an atmospheric response to increased weathering during late Ordovician mountain building events (e.g. Taconic orogeny, collision of Avalonia with Baltica) thereby sequestering atmospheric CO_2. A consequence of this mechanism is that as ice sheets grew and covered the landmass, less rock was exposed and weathered and CO_2 levels were able to gradually rise again. However, numerical modeling of this mechanism (Kump *et al.*, 1999) is only able to replicate a fall in atmospheric CO_2 from around 5000ppm to 3000ppm, the predicted pCO_2-ice threshold (Kump *et al.*, 1999; Herrmann *et al.*, 2004; Royer, 2006), during the Hirnantian but this value is still far above CO_2 values associated with other cool events

throughout the Phanerozoic e.g. the Late Pliensbachian, Maastrictian and the Cenozoic glaciation (Royer, 2006).

Further identification and documentation of changes in burial of carbon that are coincident with glacial advance and retreat, as in the Hirnantian of Jordan (Armstrong *et al.*, 2005), forms a test for the hypothesis of orbital forcing controlling the pace of the HGM, particularly because models such as GEOCARB III (Berner & Kothavala, 2001) operate at timescales greater than those claimed by Sutcliffe *et al.* (2000). Organic carbon burial, in particular, may have been an important mechanism for CO_2 draw-down that contributed to the HGM (Brenchley *et al.*, 1995, 2003; Kump & Arthur, 1999) at a time of high pCO_2, when oceans may have been acidified and carbonate deposition was restricted (Page *et al.*, 2007). Crowley & Baum (1995), however, suggested that glaciation and high CO_2 could co-occur owing to the position of Gondwana over the south pole and that low-latitudes may not respond to short, sharp glaciations because of distance of separation from the centre of glaciation (Manabe & Broccoli, 1985), just as the Asian monsoons are not controlled by rhythms of northern hemisphere glaciation. But Cenozoic sites far from northern hemisphere glaciation centres have been demonstrated to respond to ice sheet processes, for instance from pollen records in New Zealand (Heusser & van de Geer, 1994) and from sea surface temperature data in the Southern Ocean (Hays, 1978). The presence of response to glaciation at mid-palaeolatitudes in the Late Ordovician would therefore further strengthen the argument for commonality in the Late Ordovician and Cenozoic glaciations.

1.6 Biostratigraphy, correlation and chitinozoans in the Late Ordovician of the Welsh Basin

Biostratigraphic correlation for the Late Ordovician between basin and shelf sections in the Cardigan and Llandovery regions is limited. The *linearis* graptolite biozone (of early- to mid-Katian age) has been identified from the Dinas Island Formation in exposures south of Cardigan (Williams *et al.*, 2003a) and correlates with the *spinifera* and *bergstroemi* chitinozoan biozones (Figure 1.11) which are also recorded from the same formation (Vandenbroucke *et al.*, 2008). The *linearis* Biozone has not been recorded from the Llandovery area (Schofield *et al.*, 2004). From the late Katian, the *anceps* graptolite biozone (Williams, 2001a,b) and the Hirnantian *persculptus* Biozone (Hendriks, 1926; Davies *et al.*, 1997) occur in the Cardigan and Llandovery regions providing good correlation. The *anceps* Biozone has also been recorded from laminated hemipelagites further north of the Llandovery and in the Cadair Idris district of Wales (Pugh, 1923). Besides these occurrences from inland exposures, dating in the Llandovery area has been limited to isolated studies of acritarchs and shelly faunas (Williams & Wright, 1981; Rushton, 1994; Davies *et al.*, 1997). Shelly faunas indicative of

late Katian (Rawtheyan) age (Rushton, 1994) and the Hirnantian *Hirnantia* fauna Williams & Wright (1981) have been recovered from shelfal deposits in the Llandovery region.

As it stands there is currently a lack of correlative tools to compare basin (Cardigan area) and shelfal (Llandovery area) sections in the Welsh Basin at this time, particularly in the late Katian and Hirnantian when sealevel was lower than in the early- to mid-Katian and facies heterogeneity was greater. The recent development of a chitinozoan biozonation scheme for the Late Ordovician for Avalonia (Figure 1.11, Vandenbroucke, 2008; Vandenbroucke & Vanmeirhaeghe, 2007) provides a potentially high-resolution means to refine correlation of lithostratigraphy between regions throughout the Welsh Basin in basin and shelf settings where other biostratigraphically useful fossil groups are scarce. Enhanced dating of lithostratigraphy between areas is also essential for comparing the response of basin and shelf to the climatic events studied herein and also for the response of the fauna to such events. Key biozonation schemes for the major palaeocontinents have been developed only since the late 1970s (e.g. Achab, 1978; Paris, 1981; Nõlvak & Grahn, 1993; Vandenbroucke, 2008) and have not been tested significantly against developing palaeoecological models for the Chitinozoa. They therefore cannot be said to have stood the 'test of time' in their application, especially considering that the established Ordovician biozonal groups, the graptolites and conodonts, and their respective biozonation schemes, are being viewed in a new light in the context of recent palaeoecological models (Zalasiewicz *et al.*, 1995; Williams *et al.*, 2003a; Armstrong & Owen, 2002a).

1.7 Problem identification, hypothesis formulation and aims

1.7.1 Problem identification

The discussion given above highlights key problems in our understanding of Late Ordovician climate change and for using the Welsh Basin to document climate change at this time:

1. Global climate change processes in the Late Ordovician have a sparse record from mid-latitudes. This is, in part, a sampling bias because of the relatively small preserved volume of rocks deposited in the mid-latitudes in the late Katian and Hirnantian (Figure 1.5).

2. It is uncertain if the Boda Event is a warm event (Boucot *et al.*, 2003; Fortey & Cocks, 2005) or a cool event (Cherns & Wheeley, 2007). As Armstrong (2007) states, any model for the onset of the HGM should take into account the effects of the Boda Event. Such effects could include sequestration of carbon (Brenchley *et al.*, 1994; Page *et al.*, 2007) and increasing sensitivity of the biota to the HGM (Fortey & Cocks, 2005).

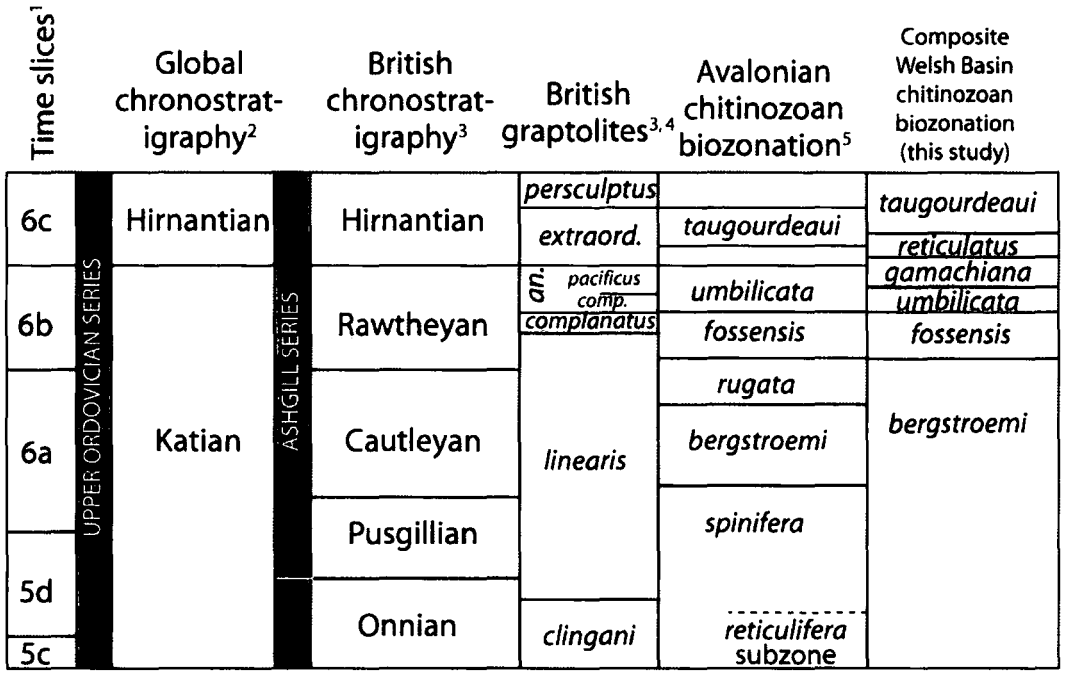

Figure 1.11: The current Avalonian chitinozoan biozonation scheme and correlation with British graptolite biozonation scheme and British chronostratigraphy. No chitinozoan biozone has yet been recognized for the lower part of the Hirnantian Stage. [1]Webby *et al.* (2004); [2]Bergström *et al.* (2006a); [3]Fortey *et al.* (2000); [4]Vandenbroucke (2008).

3. Numerous mechanisms are proposed for HICE. Some lack physical evidence (sequestration of large amounts of carbon during HICE; Brenchley *et al.*, 1994) and others which have not been tested against each other using empirical data (e.g. Kump *et al.*, 1999). HICE is also regarded by some as a product of regional processes (Panchuk *et al.*, 2005). HICE is used as a strong correlative tool and yet if regional effects can be demonstrated to affect HICE at various locations throughout the globe then its efficacy for chemostratigraphy is reduced.

4. There is currently no strong biostratigraphic correlation between basin and shelf in the upper Katian and Hirnantian of the Welsh Basin. This is essential if the Welsh Basin is to be used to test hypotheses for mechanisms of the Boda Event and the HGM.

5. Chitinozoan biostratigraphy is rapidly advancing without significant regard for the influences of their palaeoecology on biozonation schemes.

1.7.2 Hypothesis formulation

The product of this study will help to rectify the first problem, a lack of mid-latitude palaeoclimate data, and provide stimulus for investigation in other mid-latitude localities in the

late Ordovician.

Being situated on the northern margin of Avalonia during the Upper Ordovician, the Welsh Basin provides a suitable environment to address the problems and issues of climate change processes in the Late Ordovician discussed above from mid-latitudes, an area from data are currently sparse. The characteristics of these events expressed at mid-latitudes provides a test for the climate belt model of (Armstrong *et al.*, in revision). Confirmation of this model is a test of the Boda Event as a global warming event or simply the expression of climate belt and ocean current rearrangement during ongoing cooling in the Late Ordovician glaciation (problem 2). The climate belt model of Armstrong *et al.* (in press) is adopted as a key 'running' hypothesis throughout to be tested at mid-palaeolatitude in the Welsh Basin:

Hypothesis 1. Climate belt rearrangement is evident at mid-latitudes during the Boda Event (late Katian, Cautleyan-Rawtheyan).

This hypothesis leads to a set of predictions addressed in detail in Chapter 3. In summary, these are:

Prediction 1. Increased coastal upwelling in the Welsh Basin from repositioning of SE trade winds into mid-latitudes and directly over Avalonia.

Prediction 2. Deposition of phosphates and organic-rich black shales from increased productivity during upwelling along the northern margin of Avalonia during the Boda Event.

Prediction 3. Increased aridity at mid-latitudes.

These predictions are tested by identifying presence/absence of phosphatic-rich units and organic-rich units in the Welsh Basin coincident with the Boda Event and through the use of proxy data such as those indicative of upwelling and aridity. Given that the position of climate belts is controlled on orbital periods (Christiansen & Stouge, 1999; Perlmutter & Matthews, 1990; Rind, 1998), a further test on climate sensitivity at mid-palaeolatitudes, and for the possible influence of rearrangement of climate belts, is in the identification of orbital periodicity in basin deposits. This test is only applicable providing non-periodic influences such as tectonism can be ruled out as contributing to basin sedimentation (Chapter 5).

Problem three, that there is no single agreed mechanism for the HICE, is addressed by treating each proposed mechanism for the HICE as a hypothesis and testing predictions for each hypothesis by comparing carbon sequestration and isotopic records from basin and shelf sections:

Hypothesis 2. HICE is a product of increased productivity and carbon burial.

Prediction. Increased black shale and carbonate burial before or at the time of HICE.

Test. Presence/absence of black shale and carbonate burial at the time of HICE.

Hypothesis 3. Regional records of HICE can be obscured by a combination of regional isotopic signatures.

Prediction. Numerical modeling of carbon isotope systems in marine sediments (e.g. Kump *et al.*, 1999; Kump & Arthur, 1999) simulates the isotopic response using different parameters. Each simulation provides a prediction for the regional HICE isotope curve.

Test. Comparison of a regional HICE curve with simulated predictions.

The fourth problem, a lack of biostratigraphic correlation between basin and shelf sections in the late Katian and Hirnantian of the Welsh Basin, can be rectified by undertaking a study of the chitinozoan fauna in basin and shelf environments in rocks of this age. Such a study will provide the framework on which to begin subsequent investigations. It is necessary to pin point the age range of an event of interest in the rock record (e.g. Boda Event = late Katian, Cautleyan-Rawtheyan), before undertaking further analyses. Specifically for the Welsh Basin, the following hypothesis is put forward:

Hypothesis 4. The Welsh Basin, being part of Avalonia during the late Katian and Hirnantian, records the *spinifera*, *bergstroemi*, *rugata*, *fossensis*, *umbilicata* and *taugourdeaui* chitinozoan biozones following the chitinozoan biostratigraphic scheme for Avalonia of Vandenbroucke (2008).

Prediction. The chitinozoan biozones for the late Katian and Hirnantian of Avalonia will be recorded in the basin and shelf setting of the Cardigan and Llandovery areas.

Test. Undertake a chitinozoan biostratigraphical study in the Late Ordovician of the Cardigan and Llandovery areas.

In addition to this, the data base for a biozonation study also provides the means to test hypotheses for chitinozoan palaeoecology and the integrity of chitinozoan biozonation schemes (problem 5). I propose the following hypotheses to test with respect to this:

Hypothesis 5. Specific chitinozoan assemblages can be identified representing discrete biotopes.

Prediction. At any one time, there will have been discrete assemblages of chitinozoa in depth-controlled lithofacies.

Test. Analysis of chitinozoan distribution from different facies in basin to shelf environments.

Hypothesis 6. Some biotopes are sensitive to climate change.

Prediction 1. Shallow water biotope chitinozoans that occupy basin and shelf settings will be less sensitive to changes in climate than chitinozoans from shelf biotopes and deep water biotopes.

Prediction 2. The Boda Event and HGM will cause rearrangement of specific chitinozoan assemblages between basin and shelf in the Welsh Basin.

Test. Examination of data set of chitinozoan occurrences for different environments at different time intervals, before and after climatic event.

1.7.3 Aims and outcomes

The aims of this study are to conduct tests for the hypotheses given above. In doing so, the outcomes of this study will accept or reject the stated hypotheses. Five major practical outcomes of this work will be:

- A late Katian and Hirnantian geochemical, biological and sedimentological record from mid-palaeolatitudes.
- A chitinozoan biostratigraphical scheme for the late Katian and Hirnantian of the mid-southern Welsh Basin.
- A model for the effect of climate change and facies control on chitinozoan palaeoecology and biostratigraphic schemes.
- A chemostratigraphical scheme for the Hirnantian of the Welsh Basin.
- A numerical model that simulates the formation of the HICE under different conditions.

Chapter 2

Chitinozoan biostratigraphy in the Ashgill (Upper Katian) of the Welsh Basin.

Abstract

Here I present a chitinozoan biostratigraphical framework for the South Wales Ashgill succession. This is compared to that proposed by Vandenbroucke (2008) and Vandenbroucke & Vanmeirhaeghe (2007) who recognize six chitinozoan biozones with two subzones for the Upper Katian. However, this scheme has not yet been tested outside the type areas on which it was based. The chitinozoan biozonation in this project has also been developed alongside the British Geological Survey (BGS) Welsh mapping project, GeoCymru, to aide correlation between regions recently mapped on the Cardigan coast (Cardigan and Dinas Island, Sheet 193; Llangranog, Sheet 194) and in central south Wales (Builth Wells, Sheet 196; Llandovery, Sheet 213) between 2003 and 2006.

The current study indicates that four of the six Avalonian Ashgill chitinozoan biozones are recognized in the Welsh Basin; the *bergstroemi*, *fossensis*, *umbilicata* and *taugourdeaui* biozones. The Baltoscandian and Laurentian index taxon *Hercochitina gamachiana* is recorded for the first time in Avalonia and a new lower Hirnantian regional biozone, the *Belonechitina reticulatus* n. sp. Biozone is erected. The Cautleyan-Rawtheyan (late Katian) *rugata* Biozone was not recorded.

2.1 Introduction

The recent development of an integrated Upper Ordovician chitinozoan biozonation in British Avalonia (Vandenbroucke, 2008; Vandenbroucke & Vanmeirhaeghe, 2007), based on type areas for the British chronostratigraphic scheme (Fortey *et al.*, 1995, 2000), recognizes six

chitinozoan biozones with two subzones for the Ashgill (Upper Katian) and potentially provides a powerful tool for dating Upper Ordovician successions where graptolite preservation is not favorable. However, there still remain problems concerning calibration with graptolite and conodont-based stratigraphies, including local and global stratigraphic schemes (Vandenbroucke, 2008). As such, the applicability of the scheme, as it currently stands, outside the type areas on which it was based has not yet been tested. Here I present a regional biostratigraphic scheme from data on chitinozoan abundance and distribution for the Ashgill from a well-constrained basin - shelf section of the Cardigan and Llandovery regions of the Welsh Basin, UK and compare it to that proposed by Vandenbroucke (2008). This allows: 1) a test of reproducibility for new British Avalonia chitinozoan biostratigraphic scheme; and 2) a test of persistence of the scheme across different depositional environments (i.e. basin and shelf).

The development of a British Avalonia chitinozoan biostratigraphic scheme has come at an opportune time, coinciding with the re-mapping of regions of the Welsh Basin by the British Geological Survey (BGS, the GeoCymru project), which have historical importance. These include Cardigan (Keeping, 1882) and the type Llandovery region from which Murchison (1839) developed his Silurian System and Lapworth (1879) developed his tripartite classification of the Lower Palaeozoic. The chitinozoan biozonation presented herein therefore also aides regional correlation between regions recently mapped on the Cardigan coast (Cardigan and Dinas Island, Sheet 193; Llangranog, Sheet 194) and in central south Wales (Builth Wells, Sheet 196; Llandovery, Sheet 213) where graptolite occurrences are rare and chronostratigraphy is sometimes poorly constrained with respect to lithostratigraphy.

2.2 Palaeoenvironmental setting and lithostratigraphic framework

The Welsh Basin provides a nearly complete section through the Upper Katian (Ashgill) and Hirnantian in a slope-apron to muddy shelf depositional environment (Davies *et al.*, 1997). The line of demarcation between basin and shelf is approximated by the Llanwyrtyd Fault and Garth Fault systems in the Llandovery area

The oldest rocks exposed in the Cardigan-Llangranog coastline are from the Dinas Island Formation which contains the distinct dark anoxic Cwm Degwel Mudstone Member (up to 100m thick) in the upper part of the formation (Davies *et al.*, 2003).

Burrow-mottled oxic-dysoxic grey shales of the Nantmel Mudstones Formation abruptly overly the Cwm Degwel Mudstone Member and dominate the lithostratigraphy and the coastal cliffs in the Cardigan region and much of the lower lying country around Llandovery. This Formation is interrupted by four repeated dysoxic-anoxic organic-rich laminated

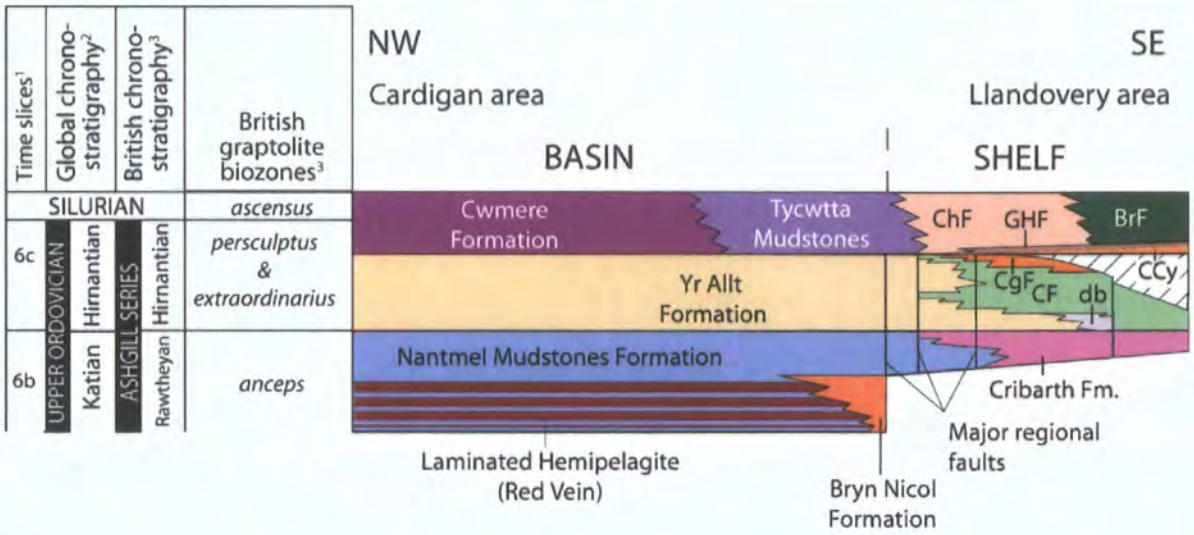

Figure 2.1: Lithostratigraphy between basin (Cardigan area) and shelf (Llandovery area). [1]Webby *et al.* (2004); [2]Bergström *et al.* (2006a); [3]Fortey *et al.* (2000). BrF=Bronydd Formation, db=disturbed beds (of Ciliau Formation), CCy=Cwm Clyd Sandstone Formation, CF=Ciliau Formation, CgF=Cwmcringlyn Formation, ChF=Chwefri Formation

hemipelagite (LH) units in the upper part of the Nantmel Mudstones Formation, the "Red Vein" (Pugh, 1923, Figure 4.3) and are numbered herein LH^0 (oldest) to LH^3 (youngest) following numbering convention of the British Geological survey for these units.

At the shelf-basin break in the Llandovery area, the Red Vein units interleave with localized debrites and shelly turbidites of the Bryn Nicol Formation. To the east, the mud-dominated Tridwr Formation was deposited in a mid- to outer-shelf environment and also interdigitates with the Nantmel Mudstones Formation (Schofield *et al.*, 2004). The shelfal Cribarth Formation locally overlies the Nantmel Mudstones Formation in the Llandovery area and is Rawtheyan in age.

In basin, the Hirnantian Stage is represented by the sandy Yr Allt Formation followed by the transgressive Cwmere Formation in the *persculptus* Biozone. In the shelf environment the stratigraphy is more complicated. The basal Hirnantian is represented by silty-muddy sediments of the Ciliau Formation, and is the shelfal facies equivalent of the Yr Allt Formation. The acme of the Hirnantian glaciation is recorded by deposition of sandy muds of the Cwm-Cringlyn Formation and is overlain by smooth, dark muds of the Garth House Formation. Lower Hirnantian beds are locally truncated by a disconformity which is immediately overlain by a transgressive conglomerate-sandstone Cwm Clyd Sandstone. The shelf equivalent of the Cwmere Formation are muddy, burrow-mottled sands of the Bronydd Formation and the Ystrad Walter Formation.

2.3 Graptolites and shelly fossils

Few graptolites have been recovered from the Ashgill of south-mid Wales but those that are present provide a key framework from which to compare a regional scheme with the British Avalonia chitinozoan biostratigraphic scheme of Vandenbroucke (2008).

In the Cwm Degwel Mudstone Member at the top of the Dinas Island Formation, Williams *et al.* (2003a) recorded probable *Climacograptus tubuliferus*, a proxy for the *Pleurograptus linearis* Biozone though *P. linearis* itself is not present.

The Nantmel Mudstones Formation is devoid of graptolites except for the anoxic laminated hemipelagite beds of the "Red Vein". Pugh (1923) assigned the type Red Vein locality in the Cadair Idris region to the *anceps* Biozone recovering the index taxon along with *Orthograptus truncatus* var. *abbreviatus* and *Climacograptus scalaris* var. *miserabilis*. The Red Vein in the Cardigan region contains a graptolite assemblage dominated by *Orthograptus abbreviatus* with rarer *'Climacograptus'* cf. *supernus* and *Normalograptus miserablis* and a dicellograptid fragment. This assemblage also suggests the upper part of the Nantmel Mudstones Formation lies in the *anceps* graptolite Biozone (Williams, 2001a,b) though the index taxon *Dicellograptus anceps* has not actually been recovered from the Cardigan region. Graptolites collected from the Red Vein in the Rhayader area, north of Llandovery, are similar to those from the Red Vein laminated hemipelagites on the coast (Williams, 2001a) and include *Orthograptus abbreviatus*, *Normalograptus miserabilis* and *Normalograptus* cf.*miserabilis* (Davies *et al.*, 1997) providing good correlation with the type Red Vein locality and with the Sholeshook Limestone in the Whitland area of south Wales (probable *anceps* Biozone age) which also yields *Orthograptus abbreviatus*) Zalasiewicz *et al.* (1995).

In the Llandovery area, Cocks *et al.* (1984) recovered graptolites from the Tridwr Formation that were no more diagnostic in age than the uppermost Ordovician. The Cribarth Formation at Garth Bank (SN 942 499) yielded *Orthograptus abbreviatus* (sample TJC 09-06-01) suggestive of the *anceps* Biozone whilst at Glasallt Farm, south of Llandovery, cf. *Normalograptus normalis* (J. Zalasiewicz *pers. comm.*) was collected during this study.

In the Hirnantian, the *extraordinarius* Biozone is not recognised, but the base of the *Normalograptus persculptus* Biozone is located in the Mottled Mudstone Member of the Cwmere Formation, and provides an important marker horizon throughout the Welsh Basin (Temple, 1988) [e.g. at Cerrig Gwinion Quarry (Blackett *et al.*, 2008) and Lynn Brianne (SN 816 493) whereas at Ystrad Walter the *persculptus* bands occur above the burrow-mottled Ystrad Walter Formation in the lower Chwefri Formation (J. Davies *pers. comm.*)]. The *persculptus* Biozone is recognized in the Cardigan region from occurrences of *Normalograptus persculptus* from the Mottled Mudstone Member at Traeth Y Ynys Lochtyn near Llangranog (Hendriks, 1926).

Infrequent graptolitic material was collected by Cocks *et al.* (1984) in the Lower Bronydd Formation including *Climacograptus normalis* from which they assigned an age no higher than the *acuminatus* Biozone.

As well as graptolite fauna, a shelly fauna collected from the Pen Derlwyn facies of the Bryn Nicol Formation has yielded a diverse fauna suggestive of a Rawtheyan age (Rushton, 1994). In addition to this, in the Llandovery region, a shelly '*Hirnantia* fauna' has been recorded by Williams & Wright (1981) from an ooidal component in the Ciliau Formation constraining the age of this shelfal sequence to the Hirnantian.

2.4 Biostratigraphic and chronostratigraphic framework

Vandenbroucke (2008) developed a chitinozoan biostratigraphy for the Upper Katian (Ashgill) from historical sections in the Anglo-Welsh area, including the Cautley District, Pus Gill, Greenscoe (Vandenbroucke *et al.*, 2005) and Whitland. Six chitinozoan biozones, with two subzones, have been recognized for the Upper Katian (Figure 2.2; Vandenbroucke, 2008):

The *Fungochitina spinifera* Biozone corresponds to the total range of the index fossil. In the Cardigan area it has previously tentatively been recognized in the *Dicranograptus*

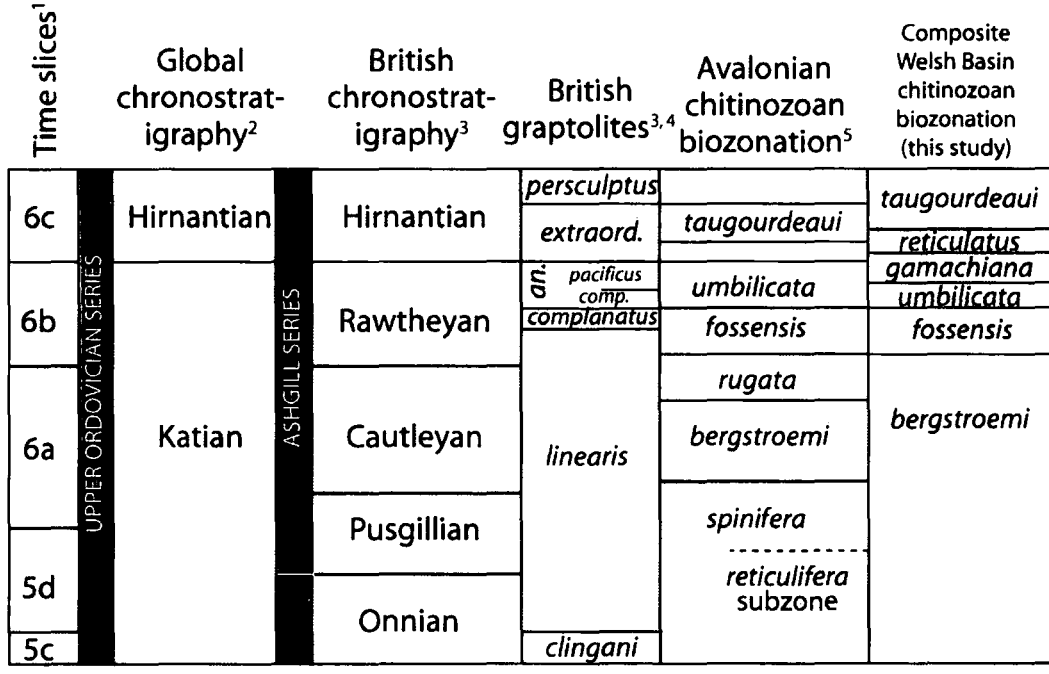

Figure 2.2: The current Avalonian chitinozoan biozonation scheme and correlation with British graptolite biozonation scheme and British chronostratigraphy. No biozone has yet been recognized for the lower part of the Hirnantian Stage. [1]Webby *et al.* (2004); [2]Cope (2007); [3]Fortey *et al.* (2000); [4]Rickards (2002); [5]Vandenbroucke (2008).

clingani (Vandenbroucke *et al.*, 2008) to *Pleurograptus linearis* Biozones (using the graptolite Biozonation scheme of Rickards, 2002) and is dated as middle Katian (Onnian to Pusgillian of the local British chronostratigraphy, Fortey *et al.* (2000), time slice 5d-6a of Webby (2004)). In Avalonia, *Saharochitina fungiformis* is taken as a proxy for the *F. spinifera* Biozone. Other important associated taxa corresponding to this biozone are *Lagenochitina baltica*, *Lagenochitina prussica*, *Belonechitina robusta*, *Spinachitina ? coronata* and *Conochitina ? incerta.*

The *Armoricochitina reticulifera* Subzone, defined by Nõlvak & Grahn (1993) in Baltoscandia, has been recognized in the Cardigan area associated with graptolites of the *Dicellograptus morrisi* Subzone of the *Dicranograptus clingani* Biozone.

The *Tanuchitina bergstroemi* Biozone in Avalonia is defined as corresponding to the first appearance datum (FAD) of *T. bergstroemi* to the first occurrence of *Conochitina rugata*, the index fossil of the overlying biozone. It corresponds to the *Pleurograptus linearis* Biozone in the Cardigan area (Vandenbroucke *et al.*, 2008) using the graptolite biostratigraphic scheme of Rickards (2002) and is dated as upper Katian (Cautleyan). *Belonechitina americana* is an associated taxon with this Biozone.

The *Conochitina rugata* Biozone in Avalonia is defined as the total range of the index fossil. It corresponds to the *C. rugata* Biozone in Baltoscandia (Nõlvak & Grahn, 1993) and is dated upper Katian (late Cautleyan to early Rawtheyan).

The *Spinachitina fossensis* is a partial range Biozone defined by the first appearance of *S. fossensis* to the first appearance of *Bursachitina umbilicata*, the overlying Biozone index taxon. It is dated as upper Katian (mid-Rawtheyan) and has been assigned to the *Pleurograptus linearis* Biozone in the Cautley district of northern England (Rickards, 2002). Associated chitinozoans are *Spinachitina penbryni*, *Belonechitina* sp. 8 Vandenbroucke, 2004 and *Spinachitina* sp. 4 Vandenbroucke, 2004 are associated taxa. This zone has been recorded from the Condroz inlier of Belgium (Vanmeirhaeghe & Verniers, 2004), but is not known outside Avalonia.

The *Bursachitina umbilicata* Biozone is defined as the total range of the index taxon *B. umbilicata.* It is endemic to Avalonia and has also been recorded from the Condroz inlier of Belgium (Vanmeirhaeghe & Verniers, 2004). It is of upper Katian (mid- to late-Rawtheyan) age.

The *Ancyrochitina merga* Subzone is defined in Avalonia as corresponding to the total range of the index fossil. This is the same definition as for the *A. merga* Subzone in northern Gondwana where it was first defined (Paris, 1990). *Euconochitina lepta* is an associated chitinozoan species.

The *Spinachitina taugourdeaui* Biozone is a partial range Biozone defined in Avalonia as it is in Baltoscandia (Nõlvak & Grahn, 1993), by the first appearance of *S. taugoudeaui* to the first appearance of *Conochitina scabra.* It was first recognized in Avalonia from the Hirnant Limestone in Wales (Vandenbroucke *et al.*, submitted) and is of Hirnantian age. An important characteristic taxon associated with this zone is *Belonchitina reticulatus* n sp. (described by Vandenbroucke (in press) and Vandenbroucke (2008) as *Belonechitina* sp. 11) which may serve as a correlative proxy taxon (Vandenbroucke, 2008).

2.5 Sampling and treatment

A total of 64 samples from localities representing a shelf to basin transect from the uppermost Caradoc through the entire Ashgill (mid - upper Katian) have been acquired. Localities were chosen on completeness of section (lack of faulting and cleavage), exposure and accessibility. Twenty-seven samples came from the Cardigan region, representative of the basin from the Cwm Degwel Mudstone Member (oldest), the Nantmel Mudstones (including the laminated hemipelagite Red Vein), the Yr Allt Formation and the Cwmere Formation (youngest; Figure 2.3).

Thirty-seven samples were collected from seven sections (Figures 2.4, 2.5, 2.6 and 2.7) in the Llandovery region from basin facies (Sugar Loaf Member, Tridwr Formation and Nantmel Mudstones Formation from outcrop and Yr Allt and Cwmere Formations from the Dolaucothi M8 core, Pumsaint), the shelf-break facies (Pen Derlwyn and Coed Ifan facies of the Bryn Nicol Formation) and the shelf environment (Cribarth Formation, Ciliau Formation, Cwmcringlyn Formation, Cwm Clyd Sandstone, Garth House Formation and Bronydd Formation; Figure 2.4). All sample localities are listed in Appendix II. Extraction of organic residues followed the procedure outlined by Paris (1981)

2.6 Results

2.6.1 Cardigan to Llangranog

A total of 678 chitinozoans were recovered from 27 samples from the coast section between Cwm Degwel, Cardigan and Traeth-yr-Ynys Lochtyn, Llangranog (Figure ??). Of these, 331 could not be identified at specific level. Abundance data for the Cardigan region is given in Table 2.1 and the range of recovered taxa is presented in Figure 2.8. The preservation of chitinozoans from the Cardigan-Llangranog coast section varies from poor, crushed and broken specimens typically found in oxic fractions of sediment to slightly worn 3-dimensional vesicles maintaining diagnostic features. The best material was recovered from the anoxic

units of the Red Vein (samples TJC D979, TJC D1015) and dark mudstones of the Yr Allt Formation at Llangranog (sampleS TJC D946 and TJC D1005).

2.6.2 Llandovery region

A total of 736 chitinozoans were collected from 37 samples (including the Bryn Nicol section and Dolaucithi M8 core) in the Llandovery region. Of these, 452 could not be identified to specific level. The numerical results for the Llandovery region are presented in Tables 2.2 and 2.3 and the chitinozoan ranges are plotted on a composite range chart for the Llandovery region constructed from the recent mapping survey conducted by the British Geological Survey in 2006 (Figure 2.9). Chitinozoan preservation is variable from section to section in this region. Multiple samples taken from the same formation along strike were noted to vary considerably in chitinozoan abundance and state of preservation. For example, in the Garth House Formation the majority of specimens from the Y-Grug - A40 road section are flattened (TJC D971, TJC D974) whereas from Garth Bank (TJC D976), the Garth House Formation Type locality, numerous and 3-dimensionally preserved chitinozoans from a diverse and interesting assemblage were recovered. Only one sample (sample TJC D951) from the Nantmel Mudstones Formation of the Sugar Loaf section (section A, Figure 2.4) was barren.

2.7 Biozonation

Five Ordovician biozones can be recognized in the Cardigan and Llandovery areas: four formerly known Avalonian biozones and one Laurentian biozone not previously recorded from Avalonia.

The lowest recognized biozone is the *Tanuchitina bergstroemi* Biozone, originally defined by Nõlvak & Grahn (1993) in Baltoscandia as corresponding to the total range of the index fossil. *T. bergstroemi* is recorded herein in the Cardigan area from samples TJC D946 (Gwbert) to TJC D943 (Pen y Craig). Samples stratigraphically lower did not yield any biostratigraphically useful chitinozoans. The associated taxon *Belonechitina americana* was recovered within the range of *T. bergstroemi* at Mwnt (sample TJC D941) and also much higher stratigraphically in the Yr Allt Formation (sample TJC D946). Neither *T. bergstroemi* nor the associated *B. americana* were recovered in the Llandovery area.

The overlying *rugata* Biozone is not recognized in the Welsh Basin but *C. rugata* was recorded in LH^0 (sample TJC D1015) in the *umbilicata* Biozone. *C. rugata* has been recorded from the *umbilicata* Biozone previously in the Cautley district of northern England by Vandenbroucke *et al.* (2005).

The *Spinachitina fossensis* Biozone. This biozone is recognized in both the Cardigan and Llandovery areas. In the former area the base is marked by the first appearance of *S.*

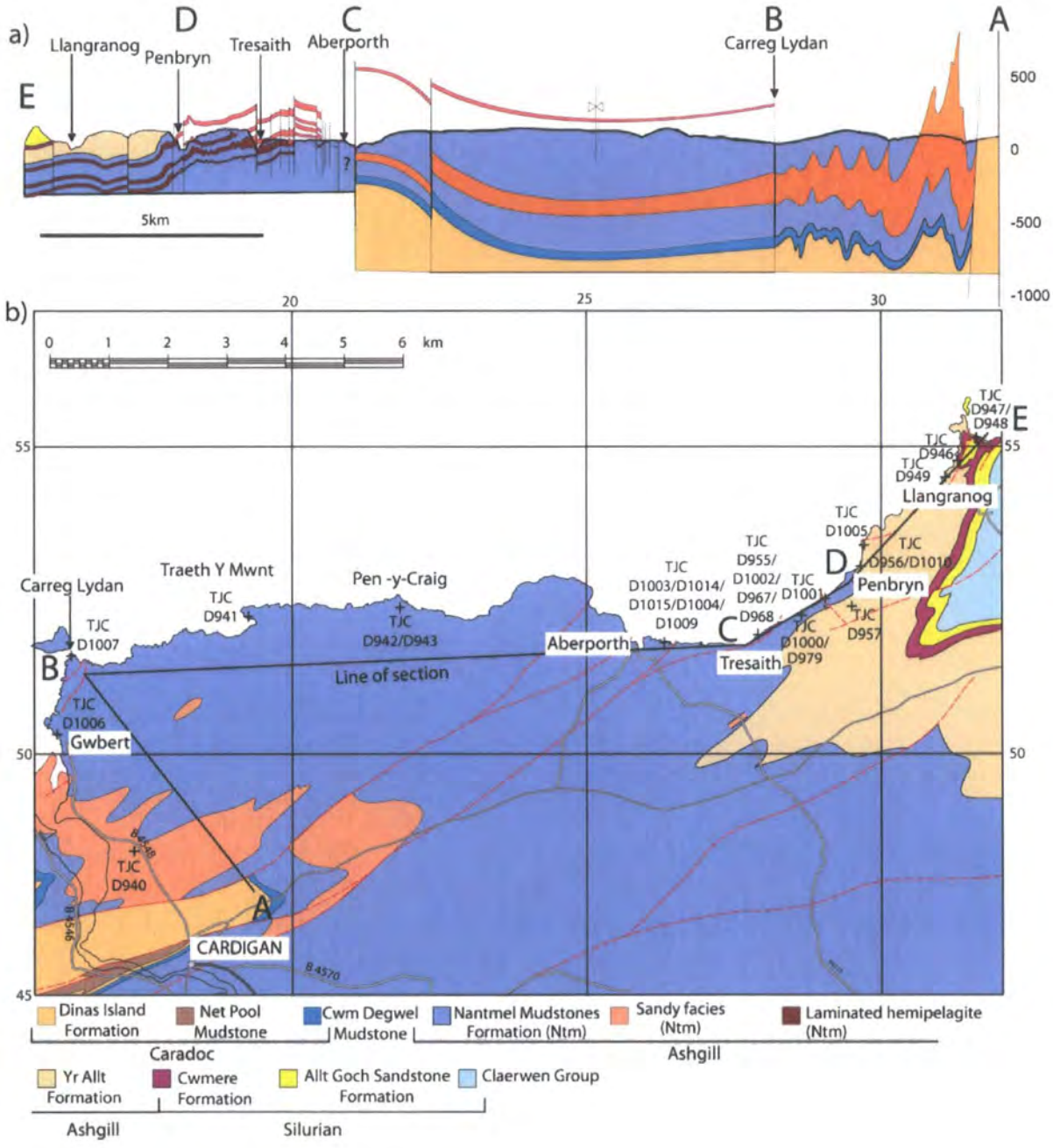

Figure 2.3: a) Elevation profile and cross-section of Cardigan-Llangranog coastal section demonstrating Upper Caradoc (Dinas Island Formation and Cwm Degwel Mudstone) and b) geology and chitinozoan sample locations

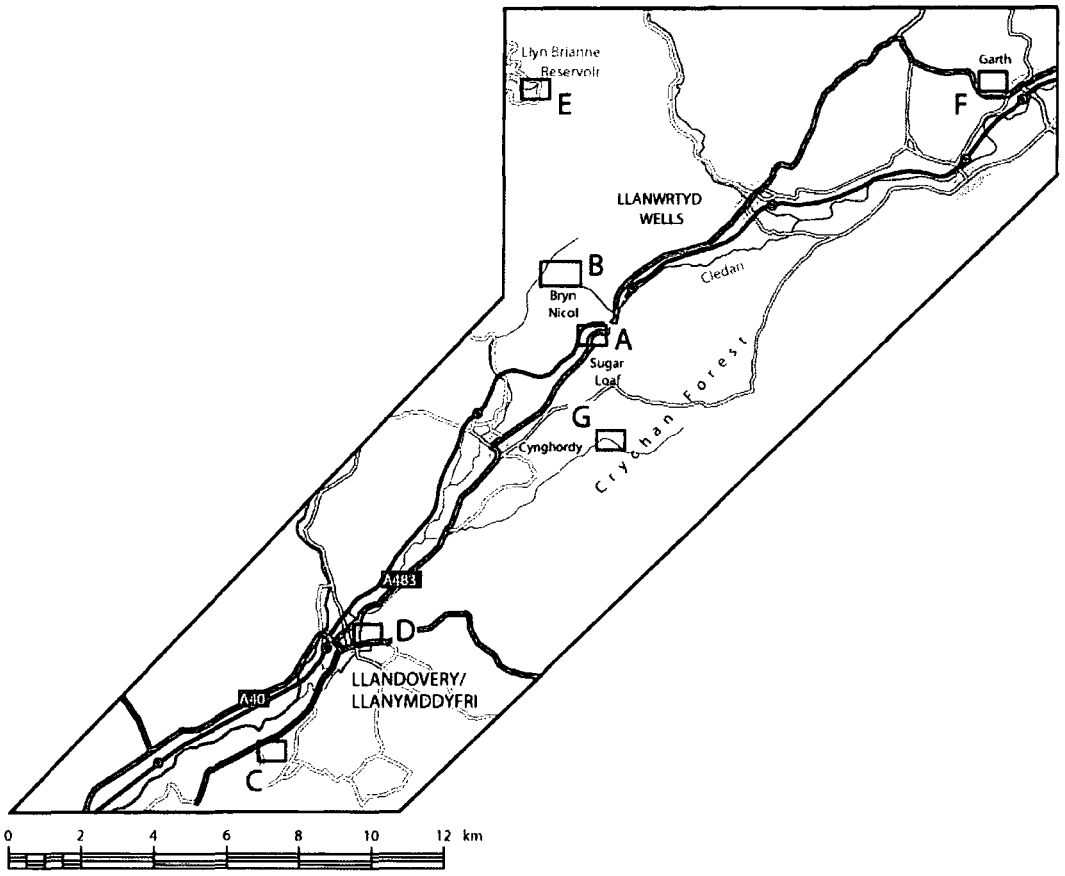

Figure 2.4: Sample sections for chitinozoan biostratigraphy in the Llandovery region. A = Sugar Loaf section, B = Bryn Nicol section, C = Glasallt Fawr, D = A40 road section, E = Llyn Brianne reservoir samples, F = Garth House Formation Type locality, G = Brynffo Forest section.

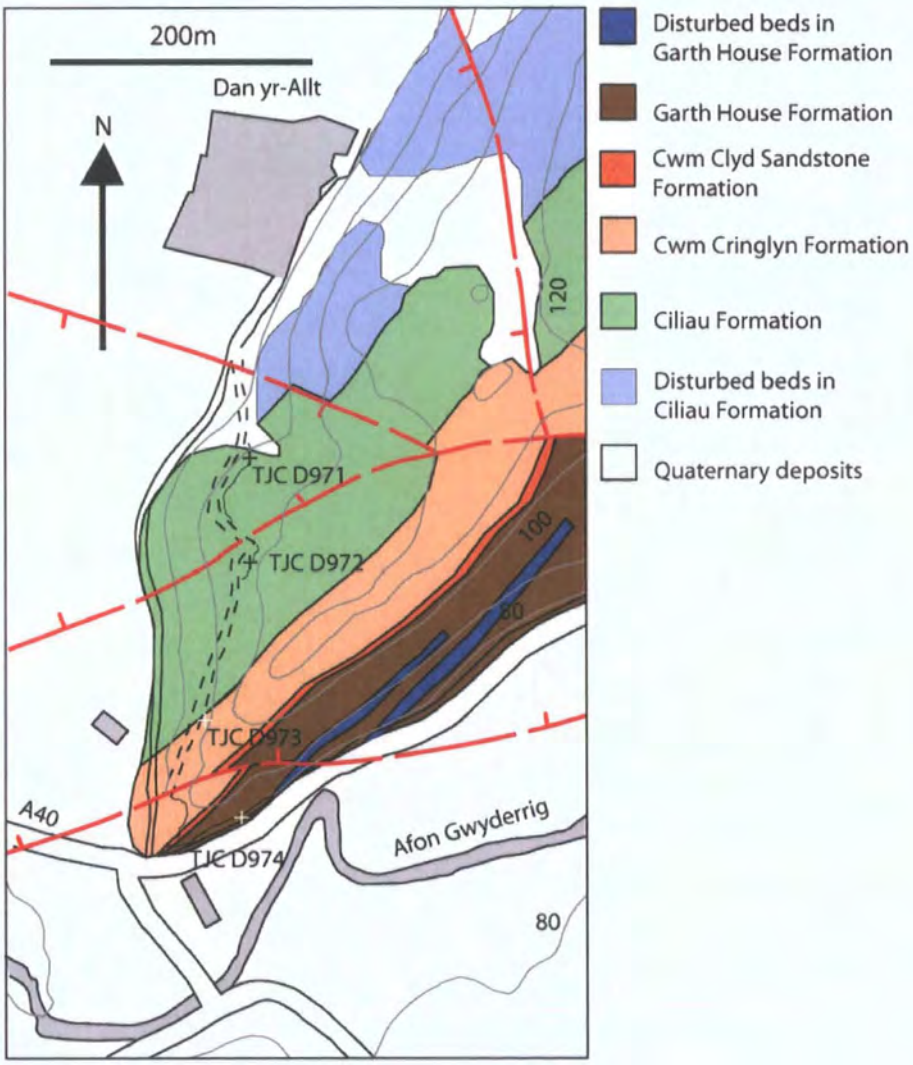

Figure 2.5: Geology of Dan–yr–allt and A40 road section, Llandovery (section D on Fig. 2.4). After BGS 1 : 50000 Geology Series, England and Wales Sheet 212, Llandovery *unpublished*

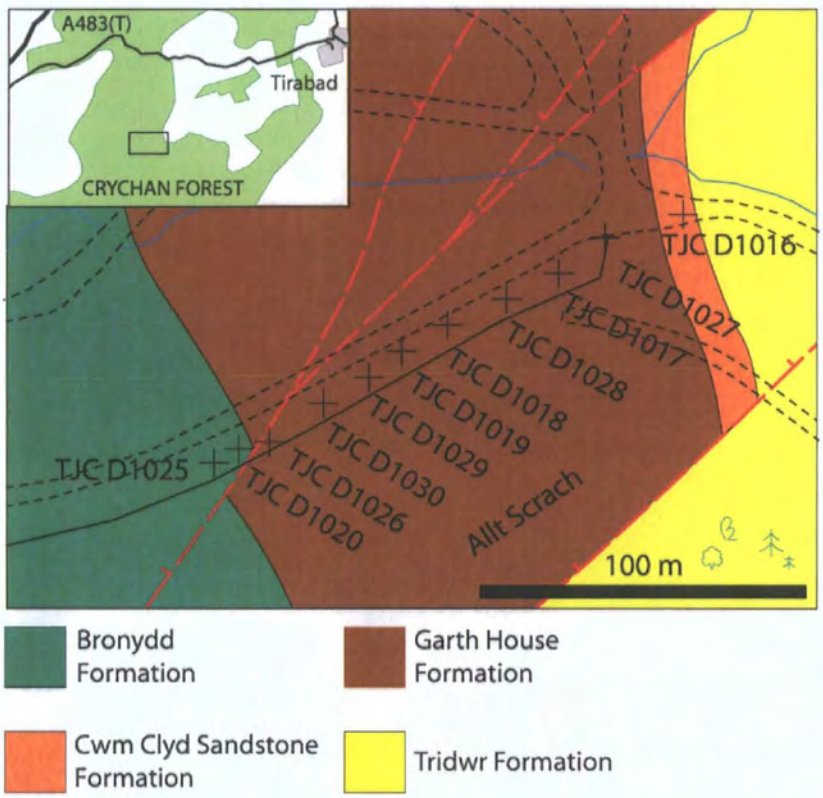

Figure 2.6: Geology of and sample localities from Crychan Forest (section G on Fig. 2.4). After BGS 1 : 50000 Geology Series, England and Wales Sheet 212, Llandovery *unpublished*

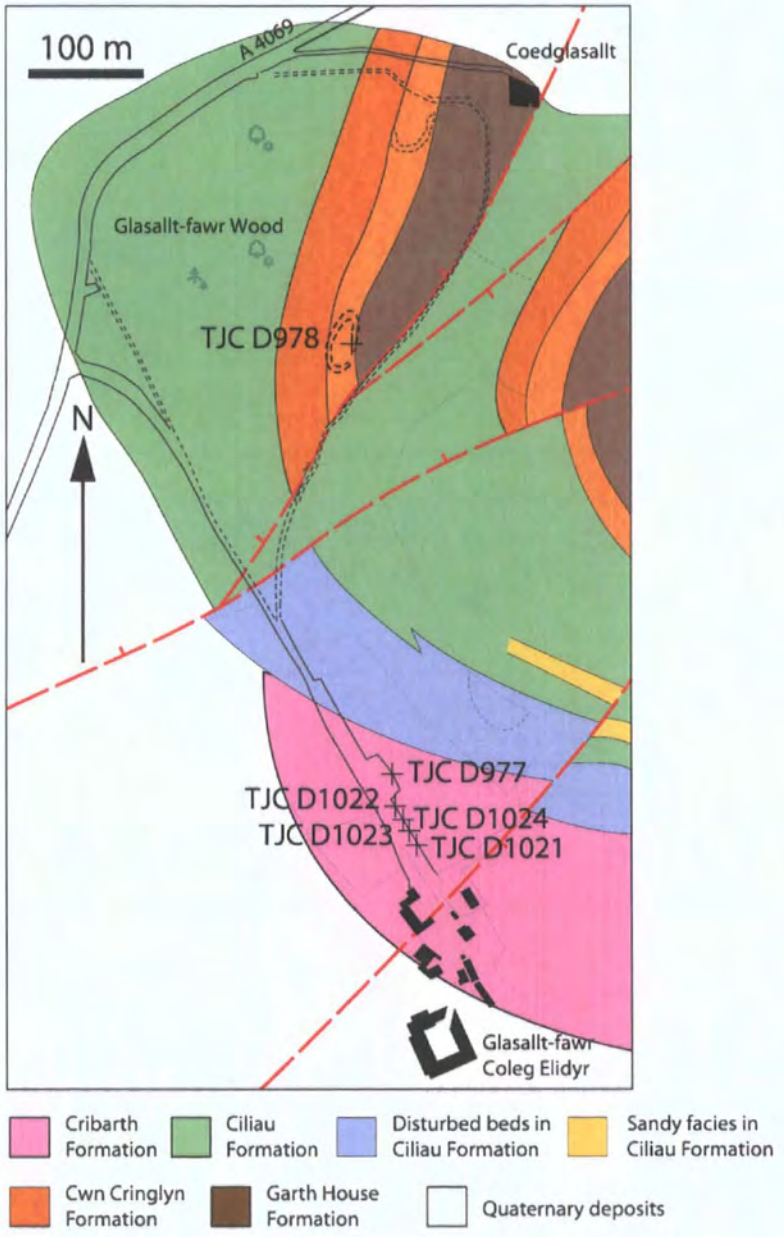

Figure 2.7: Geology of and sample localities from Glasallt Fawr, (section C on Fig. 2.4). After BGS 1 : 50000 Geology Series, England and Wales Sheet 212, Llandovery *unpublished*

fossensis in sample TJC D943 (Pen y Craig) and the top is marked by the first appearance of *Bursachitina umbilicata* from sample TJC D1013 (LH^0), the index taxon of the overlying biozone. In the Llandovery area, the first occurrence of *S. fossensis* is from sample TJC D958 in the Nantmel Mudstones Formation at Bryn Nicol. The top of this biozone was not recorded in the Llandovery area.

The *Bursachitina umbilicata* Biozone. This biozone is defined by the total range of the index taxon which in the Cardigan region is from sample TJC D1013 to TJC D1015 and is restricted to LH^0. This biozone is not recorded from the Llandovery region.

The *Hercochitina gamachiana* Biozone. This zone was first erected in Laurentia by Achab (1989) and subsequently recognized in Baltoscandia (Nõlvak, 1999) but was not recorded in Avalonia by Vandenbroucke (2008). It corresponds to the partial range of *Hercochitina gamachiana* between its first appearance and the appearance of *Spinachitina taugourdeaui* which is the index species of the succeeding biozone. In Baltoscandia, this corresponds to upper Pirgu (uppermost Rawtheyan, highest Katian) (Nõlvak, 1999) to lowest Hirnantian. *Hercochitina* cf. *gamachiana* was recovered in both the Cardigan and Llandovery areas. In the Cardigan area the FAD was from sample TJC D979 (Nantmel Mudstones Formation, LH^1) and in Llandovery from sample TJC D1023 (Cribarth Formation).

In the Welsh Basin *Belonechitina reticulatus* n. sp. has a restricted stratigraphical range. This biozone was not recognized in Avalonia by Vandenbroucke (2008) but the taxon was noted to have potential for biostratigraphic use. In the Hirnant Limestone Quarry in the Wye Valley it occurs with *Spinachitina taugourdeaui* and in Cerrig Gwinion Quarry, north of the Llandovery area, it occurs within the upper Yr Allt Formation below the *persculptus* graptolite bands (Vandenbroucke *et al.*, submitted). In the Cardigan area it ranges from the Lower Yr Allt Formation at Traeth Penbryn (sample TJC D1005), above the last appearance datum of *H. gamachiana*, to the upper Yr Allt Formation at Llangranog (sample TJC D946). It similarly has a restricted range in the Llandovery area from sample TJC D980 in the Yr Allt Formation of the Dolaucothi M8 borehole to the Cwm Clyd Sandstone from Glasallt Fawr Wood (sample TJC D978). Within the Welsh Basin, the partial range of *Belonechitina reticulatus* n. sp. defines a local range biozone corresponding to the FAD of *Belonechitina reticulatus* n. sp. to the FAD of *Spinachitina taugourdeaui*, the index taxon of the overlying biozone. It occurs between the *H. gamachiana* and *S. taugourdeaui* biozones constraining the age to early-Hirnantian to mid-Hirnantian.

The *Spinachitina taugourdeaui* Biozone. This biozone is recognized in the Llandovery area by the first appearance of *S. taugourdeaui* in sample TJC D976 (Garth House Formation, Garth House) and also occurs stratigraphically higher in the Garth House Formation in Brynffo Forest in sample TJC D1026, 2 m below the base of the overlying Bronydd Formation.

Table 2.1: Chitinozoan abundance for the Cardigan-Llangranog composite coast section. [1]Vanmeirhaeghe (2006), [2]Vandenbroucke (2005)

	TJC D953	TJC D940	TJC D1006	TJC D1007	TJC D941	TJC D942	TJC D943	TJC D1003	TJC D1004	TJC D1013-1014	TJC D1015	TJC D1009	TJC D1001	TJC D1000	TJC D979	TJC D955-1002	TJC D967	TJC D968	TJC D957	TJC D956	TJC D1010	TJC D1005	TJC D949	TJC D946	TJC D947	TJC D948
Cyathochitina campanulaeformis	–	–	–	–	–	–	–	–	–	–	–	–	–	–	8	–	–	–	–	1	–	–	–	3	–	–
Cyathochitina cf. *campanulaeformis*	–	–	–	–	–	–	–	–	–	–	–	–	–	5	–	–	–	–	–	–	2	–	1	3	–	–
Cyathochitina kuckersiana	–	–	–	–	–	–	–	–	–	–	–	–	–	–	–	–	–	–	–	–	–	–	–	2	–	–
Cyathochitina cf. *kuckersiana*	–	–	–	–	–	–	–	–	–	–	–	–	–	–	–	–	–	–	–	–	–	–	–	2	–	–
Cyathochitina calix	–	–	2	–	–	–	–	–	–	–	–	–	–	–	–	–	–	–	–	–	–	–	–	2	–	–
Cyathochitina cf. *reticulifera*	–	–	–	–	1	–	–	–	–	–	–	–	–	–	–	–	–	–	–	–	–	–	–	–	–	–
Cyathochitina sp.	5	–	–	–	–	–	–	–	–	–	–	–	–	8	–	–	–	–	–	–	–	–	–	3	–	–
Saharochitina cf. *fungiformis*	–	–	–	–	1	–	–	–	–	–	–	–	–	–	–	–	–	–	1	–	–	–	–	–	–	–
Saharochitina sp.	–	–	–	–	1	–	–	–	–	–	–	–	–	–	–	–	–	–	–	–	–	–	6	–	–	–
Tanuchitina bergstroemi	–	–	1	–	–	1	1?	–	–	–	–	–	–	–	–	–	–	–	–	–	–	–	–	–	–	–
Tanuchitina sp.	–	–	–	–	–	–	–	–	–	–	–	–	–	–	–	–	–	1	–	–	1	–	–	–	–	–
Hercochitina sp.	1	–	1	–	–	2	1	1	–	8	6	–	–	5	–	2	–	–	2	–	5	1	–	–	–	–
Hercochitina cf. *normalis*	–	–	–	–	–	–	–	–	–	–	–	–	–	1	10	2	2	–	–	–	–	–	–	–	–	
Hercochitina aff. *normalis*	–	–	–	–	–	–	–	–	–	–	–	–	–	–	6	–	–	–	–	–	1	–	–	–	–	–
Hercochitina cf. *seriespinosa*	–	–	–	–	–	–	–	–	–	–	–	–	–	–	2	–	–	–	–	1	–	–	–	–	–	–
Hercochitina aff. *seriespinosa*	–	–	–	–	–	–	–	–	–	–	–	–	–	–	11	–	–	–	–	–	–	–	–	–	–	–
Hercochitina cf. *crickmayi*	–	–	–	–	–	–	–	–	–	5	3	–	–	–	1	–	–	1	–	–	–	–	–	–	–	–
Hercochitina cf. *gamachiana*	–	–	–	–	–	–	–	–	–	–	–	–	–	–	1	–	–	–	–	2	–	–	–	–	–	–
Hercochitina minuta	–	–	–	–	–	–	1	–	–	–	–	–	–	–	–	–	–	1	–	–	–	–	–	–	–	–
Hercochitina sp. A[1]	–	–	–	–	–	–	–	–	–	–	–	–	–	–	–	–	–	–	–	–	2	–	–	2	–	–
Hercochitina cf. *grandispinosa*	–	–	–	–	–	–	6	–	–	–	–	–	–	–	–	–	–	–	–	–	–	–	–	–	–	–
Hercochitina turnbulli	–	–	–	–	–	–	–	–	–	–	1	–	–	–	–	–	–	–	–	–	–	–	–	–	–	–
Ancyrochitina sp.	–	–	–	–	–	–	–	–	–	–	–	–	–	–	–	–	2	–	1	–	–	–	–	1	–	–
Bursachitina umbilicata	–	–	–	–	–	–	–	–	–	16	7	–	–	–	–	–	–	–	–	–	–	–	–	–	–	–
Spinachitina penbryniensis	–	–	–	–	–	–	4	–	6	35	21	–	–	–	14	–	–	–	1	2	11	–	–	–	–	–
Spinachitina coronata	–	–	–	–	–	–	–	–	–	–	–	–	–	–	5	–	–	–	–	–	–	–	–	–	–	–
Spinachitina cf. *fossensis*	–	–	–	–	–	–	1	–	–	–	–	–	–	–	–	–	–	–	–	–	–	–	–	–	–	–
Spinachitina fossensis	–	–	–	–	–	–	2	–	–	–	–	–	–	–	1	–	–	–	–	–	–	–	–	–	–	–
Spinachitina cf. *bulmani*	–	–	–	–	–	–	–	1	–	1	–	–	–	–	–	–	–	–	–	–	–	–	–	–	–	–
Spinachitina sp. 2[2]	–	–	–	–	–	–	–	–	–	–	–	–	–	–	–	–	2	–	–	–	–	–	–	–	–	–
Spinachitina sp. A[2]	–	–	–	–	–	–	–	–	–	–	–	–	–	–	–	–	1	–	–	–	–	–	–	–	–	–
Spinachitina sp. 4[2]	–	–	–	–	–	–	–	–	–	–	–	–	–	–	1	–	–	–	–	–	–	–	–	–	–	–
Spinachitina sp.	–	–	1	–	–	–	1	–	–	–	3	1	–	–	–	–	1	–	1	–	–	–	–	1	–	–
Rhabdochitina gracilis	–	–	–	–	–	–	–	–	–	2	2	–	–	–	–	–	–	–	–	–	–	–	–	–	–	–
Conochitina rugata	–	–	–	–	–	–	–	–	–	–	1	–	–	–	–	–	–	–	–	–	–	–	–	–	–	–
Conochitina cf. *homoclaviformis*	–	–	–	–	–	–	–	–	–	–	–	–	–	–	–	–	–	1	–	–	1	–	–	2	–	–
Conochitina sp.	–	–	2	–	–	–	1	4	1	1	–	1	–	–	–	–	–	1	3	2	–	–	–	–	–	–
Belonechitina ceredigionensis	–	–	–	–	–	–	–	–	–	–	3	–	–	–	–	–	–	–	–	–	–	41	–	–	–	–
Belonechitina cf. *americana*	–	–	–	–	–	4	–	–	–	–	–	–	–	–	–	–	–	–	–	–	–	–	–	1	–	–
Belonechitina reticulatus	–	–	–	–	–	–	–	–	–	–	–	–	–	–	–	–	–	–	–	–	–	15	–	4	–	–
Belonechitina wessenbergensis	–	–	–	–	–	–	–	–	–	–	–	–	–	1	–	–	–	–	–	–	–	–	–	1	–	–
Belonechitina sp. 7[2]	1	–	–	–	–	–	–	–	–	–	–	–	–	–	–	–	–	–	–	–	–	–	–	–	–	–
Belonechitina sp. 12[2]	–	–	–	–	–	–	–	–	–	–	–	–	–	–	–	–	–	–	–	–	–	1	–	1	–	–
Belonechitina sp.	–	1	–	–	–	–	4	1	–	1	2	–	–	6	–	–	–	–	–	3	14	–	6	–	2	
Laufeldochitina lardeuxi	–	–	–	–	–	–	–	–	–	–	–	–	–	–	–	–	–	–	–	–	3	–	2	–	–	
Eisenackitina sp.	–	–	–	–	–	–	2	–	–	–	–	–	–	–	–	–	–	–	–	–	–	–	–	–	–	
Desmochitina cocca	–	–	–	–	–	–	–	–	–	–	–	–	–	–	–	–	–	–	–	–	–	–	5	–	–	
Desmochitina minor	–	1	–	–	–	–	–	–	–	–	–	–	–	–	–	–	–	–	–	–	–	–	3	5	5	
Chitinozoa indet.	15	–	11	–	2	4	93	6	11	7	16	–	1	10	–	–	2	1	–	8	9	9	2	1	3	–
Total number of chitinozoans	22	3	17	–	5	11	117	13	18	78	65	2	1	35	50	12	10	8	8	16	33	84	9	47	8	7
Amount of dissolved rock (g)	30	20.7	17.4	20.9	21.3	20.7	26.2	20.3	13.2	39.9	20.2	16.6	20.5	23.8	30.5	52	79.9	79.8	30	30	20.3	21	97.4	49.2	50.9	44.1

Table 2.2: Chitinozoan abundance from the Llandovery region composite section. [1]Vanmeirhaeghe (2006), [2]Vandenbroucke (2005)

	Sugar Loaf section		Bryn Nicol section						Cribarth Formation, Glasallt Fawr				
	TJC D952	TJC D950	TJC D1033	TJC D960	TJC D959	TJC D1032	TJC D1031	TJC D958	TJC D1021	TJC D1023	TJC D977	TJC D1024	TJC D1022
Hercochitina sp. 1[1]	–	–	–	–	–	–	–	–	–	–	4	–	1
Hercochitina aff. *seriespinosa*	–	1	–	3	–	1	–	–	–	–	–	–	–
Hercochitina cf. *seriespinosa*	–	–	–	–	–	–	–	–	–	–	1	–	–
Hercochitina aff. *normalis*	–	–	1	–	1	2	–	–	–	–	–	–	–
Hercochitina cf. *normalis*	–	–	–	–	–	–	–	1	–	–	–	–	–
Hercochitina cf. *crickmayi*	–	–	2	–	4	–	–	–	–	–	4	–	–
Hercochitina cf. *gamachiana*	–	–	–	–	–	–	–	–	–	–	–	1	–
Hercochitina sp.	2	4	7	3	24	–	5	1	1	–	4	1	–
Belonechitina ceredigionensis	–	–	–	–	–	–	–	–	–	1	–	–	–
Belonechitina capitata	–	–	–	–	–	–	–	–	1	–	4	–	–
Belonechitina sp. 7[2]	1	–	–	–	–	–	–	–	–	–	–	–	–
Belonechitina sp.	1	1	–	1	–	–	–	–	–	–	3	–	–
Cyathochitina campanulaeformis	1	–	–	2	–	–	–	–	–	–	–	1	–
Cyathochitina cf. *campanulaeformis*	–	–	8	14	–	–	–	–	–	–	–	–	–
Cyathochitina cf. *kuckersiana*	–	–	2	–	–	–	–	–	–	–	–	–	–
Cyathochitina calix	–	–	1	–	–	–	–	–	–	–	–	–	–
Cyathochitina sp.	–	1	2	–	1	–	3	3	–	1	1	1	–
Desmochitina erinacea	–	–	–	–	–	–	2	–	–	–	–	–	–
Desmochitina minor	–	–	–	1	–	–	–	–	–	2	–	–	–
Desmochitina cocca	–	2	–	–	–	–	–	–	–	–	–	–	–
Desmochitina sp.	1	–	–	–	–	–	–	–	–	–	–	–	–
Spinachitina fossensis	–	–	9	–	–	–	4	–	–	–	–	–	–
Spinachitina cf. *fossensis*	–	–	3	2	1	1	–	–	–	–	–	–	–
Spinachitina cf. *bulmani*	–	1	–	–	–	–	–	–	–	–	–	–	–
Spinachitina coronata	–	–	–	–	–	–	–	–	–	1	–	4	–
Spinachitina sp.	–	–	–	–	–	–	–	1	–	–	–	–	–
Laufeldochitina sp.	1	–	–	–	–	–	1	–	–	–	–	–	–
Tanuchitina sp.	–	–	–	–	1	–	–	2	–	–	–	–	–
Conochitina homoclaviformis	3	4	–	–	–	–	–	–	–	–	–	–	–
Conochitina sp. 1	1	3	–	–	–	–	–	–	–	1	2	–	–
Conochitina sp.	–	5	3	–	–	–	–	1	–	–	–	–	–
Ancyrochitina sp.	–	–	–	1	–	–	–	–	–	–	–	–	–
Saharochitina sp.	–	–	–	–	–	–	2	1	–	–	–	–	–
Chitinozoa indet.	2	20	3	8	10	4	7	–	2	1	1	–	–
Total number of chitinozoans	13	42	41	35	43	8	26	10	4	7	24	8	1
Amount of dissolved rock (g)	30	30	12.4	10	12	9	12.9	15	15.4	14.6	41.3	14.6	11.8

Table 2.3: Chitinozoan abundance of from the Llandovery region composite section. [1]Vanmeirhaeghe (2006), [2]Vandenbroucke (2005). LB='Smooth Mudstones', Llyn Brianne reservoir, GH=Garth House Formation, Garth House, CCy=Cwm Clyd Sandstone, Glasallt Fawr.

	A40 road section				LB	GH	CCy	Brynffo Forest section											Dolaucothi M8 core					
	TJC D971	TJC D972	TJC D973	TJC D974	TJC D975	TJC D976	TJC D978	TJC D1016	TJC D1027	TJC D1017	TJC D1028	TJC D1018	TJC D1019	TJC D1029	TJC D1030	TJC D1026	TJC D1020	TJC D1025	TJC D980	TJC D981	TJC D982	TJC D983	TJC D984	TJC D985
Hercochitina micracantha	–	–	–	–	–	–	1	–	–	–	–	–	–	–	–	–	–	–	1	–	–	–	–	–
Hercochitina aff. *seriespinosa*	–	–	–	–	–	–	–	–	–	–	–	–	–	–	–	–	–	–	6	–	–	–	–	–
Hercochitina sp.	–	1	–	–	–	1	1	–	–	–	–	–	–	–	–	–	–	–	–	–	–	–	–	–
Belonechitina reticulatus	–	–	–	–	–	–	1	–	–	–	–	–	–	–	–	–	–	–	6	–	–	–	–	–
Belonechitina ceredigionensis	–	–	–	–	–	1	–	–	–	–	–	–	–	–	–	–	–	–	–	–	–	–	–	–
Belonechitina wessenbergensis	–	1	–	1	–	1	–	–	–	–	–	–	–	–	–	–	–	–	–	–	–	–	–	–
Belonechitina capitata	–	–	–	–	–	2	–	–	–	–	–	–	–	–	–	–	–	–	–	–	–	–	–	–
Belonechitina sp. A[2]	–	–	–	–	–	2	–	–	–	–	–	–	–	–	–	–	–	–	–	–	–	–	–	–
Belonechitina sp. 12[2]	–	–	–	–	–	1	–	–	–	–	–	–	–	–	–	–	–	–	–	–	–	–	–	–
Belonechitina sp.	–	1	–	1	–	4	–	3	–	–	–	–	1	–	–	–	–	–	–	–	–	–	–	–
Lagenochitina cf. *ponceti*	–	–	–	–	–	–	–	–	–	–	–	–	–	–	–	–	1	–	–	–	–	–	–	–
Lagenochitina sp.	–	–	–	–	1	3	–	–	–	–	–	–	–	2	–	–	–	–	–	–	–	–	–	–
Cyathochitina campanulaeformis	–	1	–	–	–	4	–	1	2	–	–	–	–	–	–	–	–	–	–	–	–	–	–	–
Cyathochitina cf. *campanulaeformis*	–	–	1	–	–	–	–	–	–	–	–	–	–	1	–	–	–	–	4	–	–	–	10	8
Cyathochitina kuckersiana	–	–	–	–	–	3	–	–	–	–	–	–	–	–	–	2	–	–	–	–	–	–	–	–
Cyathochitina cf. *reticulifera*	–	–	–	–	–	1	–	–	–	–	–	–	–	–	–	–	–	–	–	–	–	–	–	–
Cyathochitina calix	–	–	–	–	–	2	–	2	–	–	–	–	–	–	–	–	–	–	–	–	–	–	–	–
Cyathochitina sp.	–	–	–	–	–	1	–	–	–	–	–	–	–	–	–	–	–	–	–	–	–	–	–	–
Desmochitina juglandiformis	–	–	–	–	–	4	–	–	–	–	–	–	–	3	–	–	–	1	–	–	–	–	–	–
Desmochitina erinacea	–	–	–	–	–	2	–	–	–	–	–	–	–	–	–	–	–	–	–	–	–	–	–	–
Desmochitina minor	–	–	–	–	–	–	–	21	–	–	1	–	1	9	3	7	–	3	–	–	–	–	–	–
Desmochitina cf. *minor*	–	–	–	–	–	–	–	–	–	–	–	–	–	–	–	–	–	2	–	–	–	–	–	–
Desmochitina cocca	–	–	–	–	–	1	–	1	–	–	–	–	–	–	–	–	–	–	–	–	–	–	–	–
Desmochitina sp.	–	–	–	–	1	1	1	5	2	–	–	–	–	–	5	12	3	4	–	–	–	–	–	–
Spinachitina taugourdeaui	–	–	–	–	–	6	–	–	–	–	–	–	–	–	–	1	–	–	–	–	–	–	–	–
Spinachitina sp. 4[2]	1	–	–	1	–	–	–	–	–	–	–	–	–	–	–	–	–	–	–	–	–	–	–	–
Spinachitina sp.	–	–	–	–	1	2	–	6	–	–	–	–	–	1	–	–	–	–	–	–	–	–	–	–
Laufeldochitina lardeuxi	–	–	–	–	–	4	–	–	–	–	–	–	–	–	–	–	–	–	–	–	–	–	–	–
Laufeldochitina sp.	–	–	–	–	–	–	–	–	–	–	–	–	–	–	–	–	–	1	–	–	–	–	–	–
Tanuchitina sp. A[1]	–	–	–	–	–	–	1	–	–	–	–	–	–	–	–	–	–	–	–	–	–	–	–	–
Tanuchitina sp.	–	–	2	–	–	2	–	2	–	–	–	–	–	–	–	–	1	–	–	–	–	–	–	–
Conochitina sp. 1	–	–	–	–	–	3	–	–	–	–	–	–	–	–	–	–	–	–	–	–	–	–	–	–
Bursachitina sp.	–	–	1	–	–	–	–	–	–	–	–	–	–	–	–	1	–	–	–	–	–	–	–	–
Eisenackitina inconspicua	–	–	–	–	–	2	–	–	–	–	–	–	–	–	–	–	–	–	–	–	–	–	–	–
Eisenackitina cf. *rhenana*	–	–	–	–	–	–	–	3	–	–	–	–	–	–	–	–	–	–	–	–	–	–	–	–
Eisenackitina sp.	–	–	–	–	–	–	–	–	–	–	–	–	–	–	–	1	–	–	–	–	–	–	–	–
Siphonochitina sp.	–	–	–	–	–	1	1	–	–	–	–	–	–	–	–	–	–	–	–	–	–	–	–	–
Ancyrochitina sp.	–	–	–	–	–	–	–	1	–	–	–	–	–	–	–	–	–	1	–	–	–	–	7	14
Ancyrochitina cf. *primitiva*	–	–	–	–	–	–	–	–	–	–	–	–	–	–	–	–	–	–	–	–	–	–	–	8
Chitinozoa indet.	14	3	1	5	11	151	7	6	–	–	2	–	–	–	–	1	–	2	–	–	–	5	3	1
Total number of chitinozoans	17	7	5	10	18	200	12	54	4	–	3	–	1	17	8	25	5	14	18	–	–	5	20	31
Amount of dissolved rock (g)	25.3	27.7	25.9	33	46.8	32.6	35.9	14.2	13.8	12.1	16.4	12.7	13.9	15.3	16.5	14.5	13.4	13.3	18.3	15.6	25.2	11.3	21.2	11.7

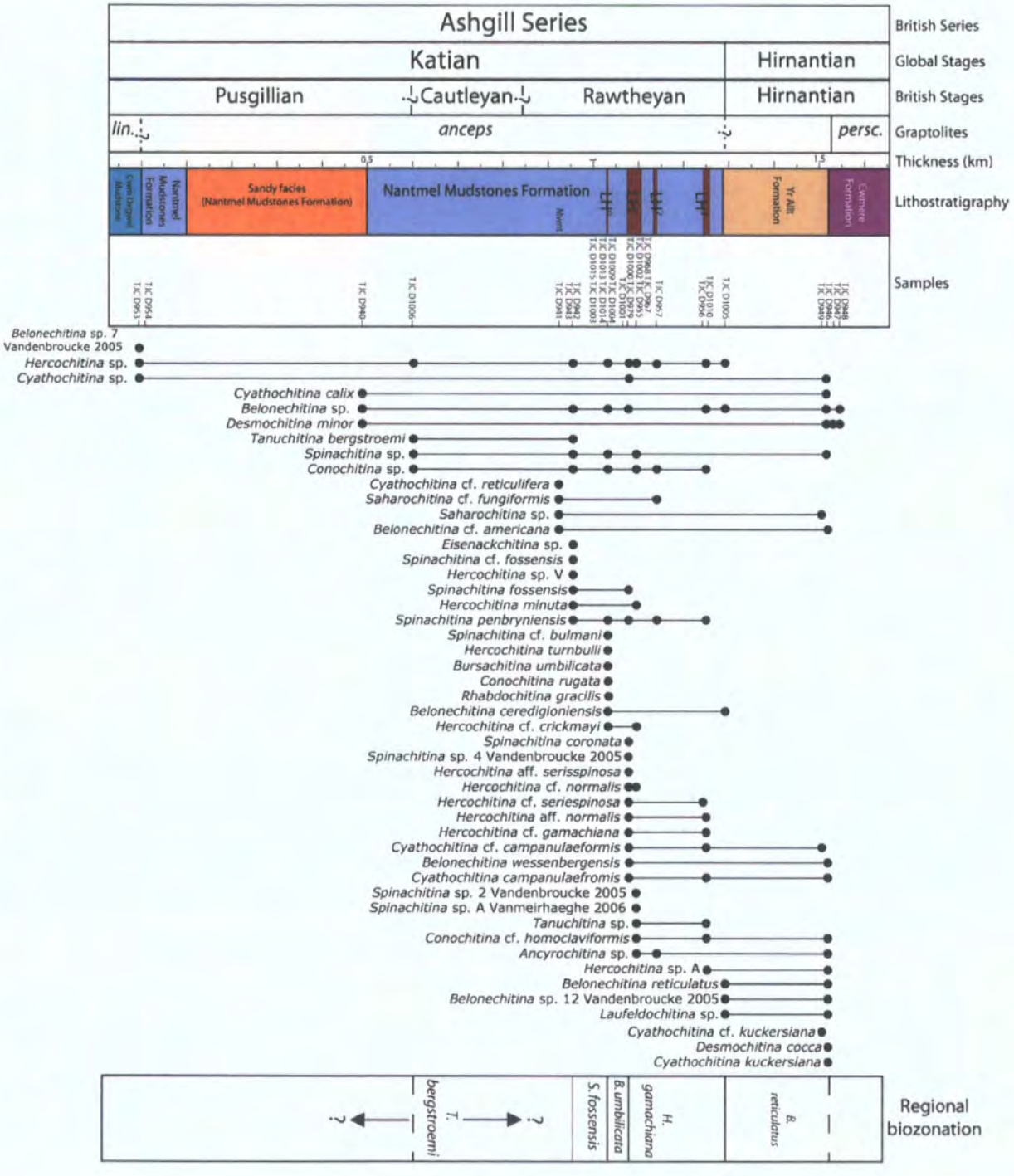

Figure 2.8: Range of Ashgill chitinozoan taxa in the Cardigan to Llangranog district and interpreted biozonation.

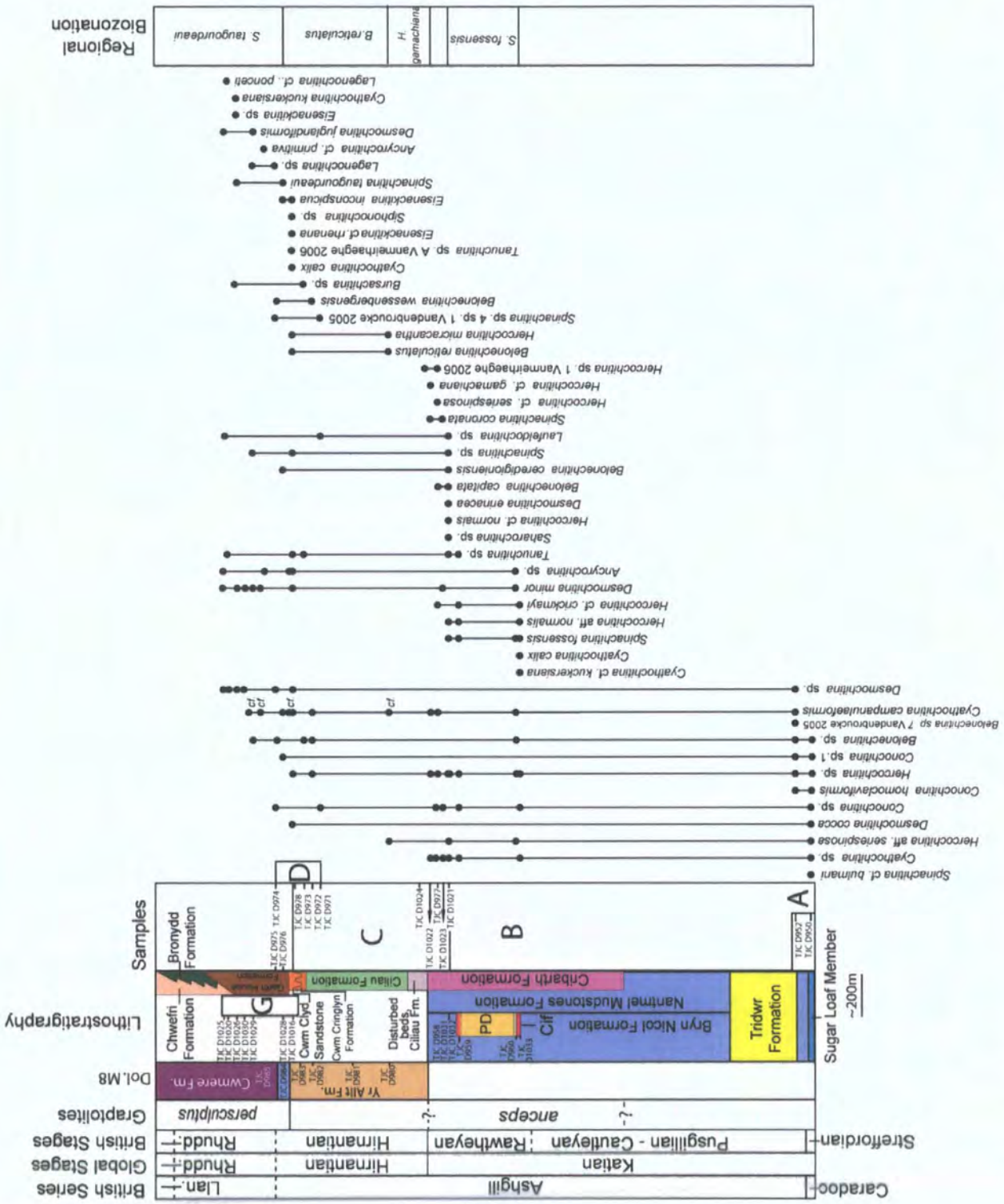

Figure 2.9: Chitinozoan ranges and interpreted chitinozoan Biozonation of the Upper Caradoc – Llandovery, Llandovery region.

2.8 Regional Correlation and Interpretation

The five recognized biozones in the Cardigan and Llandovery areas together allow good correlation between the two regions. The regional correlation interpretation is shown in Figure 2.10.

In the Cardigan area, the absence of the index taxon *Saharochitina spinifera* or associated taxa from the lowest Ashgill (mid-Katian) chitinozoan biozone and the appearance of *T. bergstroemi* at Gwbert implies that the *bergstroemi* Biozone ranges from the Cwm Yr Eglwys Mudstone Formation south of Cardigan at Frongoch (Vandenbroucke *et al.*, 2008) up into the Nantmel Mudstones Formation. This reinforces the proposal by Vandenbroucke *et al.* (2008) that the base of the Ashgill lies below the base of the Nantmel Mudstones Formation rather than at the boundary of the Dinas Island Formation - Nantmel Mudstones Formation as suggested by Fortey *et al.* (2000). The *Fungochitina spinifera* Biozone and *Tanuchitina bergstroemi* Biozone are not recognized in the Llandovery area and so no correlation can be made at this level. The lowest assemblage from the Sugar Loaf road section does not contain any taxa diagnostic of either of these two biozones.

The base of the *Spinachitina fossensis* Biozone in the Cardigan area, from bioturbated grey shales of the Nantmel Mudstones Formation at Pen-y-Craig, below the Red Vein LH units, correlates with the Llandovery area where the FAD of *S. fossensis* occurs above LH^2 in the Nantmel Mudstones Formation from the Bryn Nicol Formation type section. The stratigraphical offset of the FAD of *S. fossensis* between Cardigan and Llandovery implies either diachroneity of the biozone or diachroniety of the LH units. Ecological control on *S. fossensis* by the LH units is implicit in the former interpretation, whereas the latter interpretation favours the traditional view of isochronous chitinozoan biozones. Alternatively further sampling of the Nantmel Mudstones Formation lower than the LH units in the Llandovery area may reveal a lower FAD of *S. fossenis* and is a necessity before confirmation of either interpretation. *Spinachitina penbryniensis* n. sp., which is considered a key associated taxon of the *S. fossensis* Biozone (Vandenbroucke, 2005), is present with *S. fossenis* in the Cardigan area but not in the Llandovery area. In this study, it is noted that *Hercochitina* aff. *normalis* is a distinct taxon with *S. fossensis* in the Llandovery area but it does not occur in the Cardigan region until LH^1, after the *B. umbilicata* Biozone. This may be taken as tenuous evidence in support of diachroniety of the index taxon, *S. fossensis*, but assumes that *H.* aff. *normalis* was not influenced by the ecological constraints that affected *S. fossensis*, a situation that is plausible if chitinozoan assemblages were stratified into depth assemblages.

The chitinozoan fauna from the lower Cribarth Formation rocks includes taxa found in the *S. fossensis* and *Bursachitina umbilicata* Biozones in the Cardigan area and the Bryn Nicol section such as *Spinachitina coronata* and *Hercochitina crickmayi* as well as taxa exclusive to

this formation in the Welsh Basin such as *Hercochitina* sp. A *sensu* Vanmeirhaeghe (2006) and *Belonechitina capitata*. In addition to the chitinozoan fauna, a specimen of *Orthograptus abbreviatus* recovered from the Cribarth Formation at Garth Bank indicates an *anceps* Biozone age.

However, the base of the *Hercochitina gamachiana* Biozone is marked by the appearance of the index taxon in the upper Cribarth Formation at Glasallt Fawr in the Llandovery area and correlates with the FAD of *H. gamachiana* in the Cardigan region from the Nantmel Mudstones Formation LH^1. The presence of this biozone in both areas in the Nantmel Mudstones Formation and Cribarth Formation conforms with currently accepted lithostratigraphical placement of the base of the Hirnantian in the southwest Welsh Basin. On the Llangranog sheet of the Cardigan area (British Geological Survey Sheet 194) the uppermost Nantmel Mudstones Formation is mapped as Hirnantian but the base of the Stage is not defined. The appearance of *H. gamachiana* in LH^1 would place the base of the Hirnantian Stage in LH^1 itself or higher. In the Llandovery area, on the Builth Wells sheet (British Geological Survey Sheet 196) the Cribarth Formation is mapped as upper Rawtheyan. The chitinozoan age of the uppermost Cribarth Formation is reinforced by a shelly fauna recovered from the Penrhiwmoch Member of the Cribarth Formation at Glassallt Fawr which includes the trilobite *Brongniartella* cf. *robusta* which, according to Williams & Wright (1981), indicates a 'very high Rawtheyan age'.

The base of the newly-defined local *Belonechitina reticulatus* n. sp. Biozone is recorded from the Yr Allt Formation in the Cardigan and Llandovery areas allowing good correlation and dating the Yr Allt Formation as lower to middle Hirnantian. The last occurrence of *Belonchitina reticulatus* n. sp. before the FAD of *S. taugourdeaui* is from the Cwm Clyd Sandstone from Glasallt Fawr Wood in the Llandovery area.

The *Spinachitina taugourdeaui* Biozone is present in the Llandovery area and is marked by the first appearance of *S. taugourdeaui* in the Garth House Formation at Garth House. The index taxon was not recovered from the Cardigan area and so no correlation can be made.

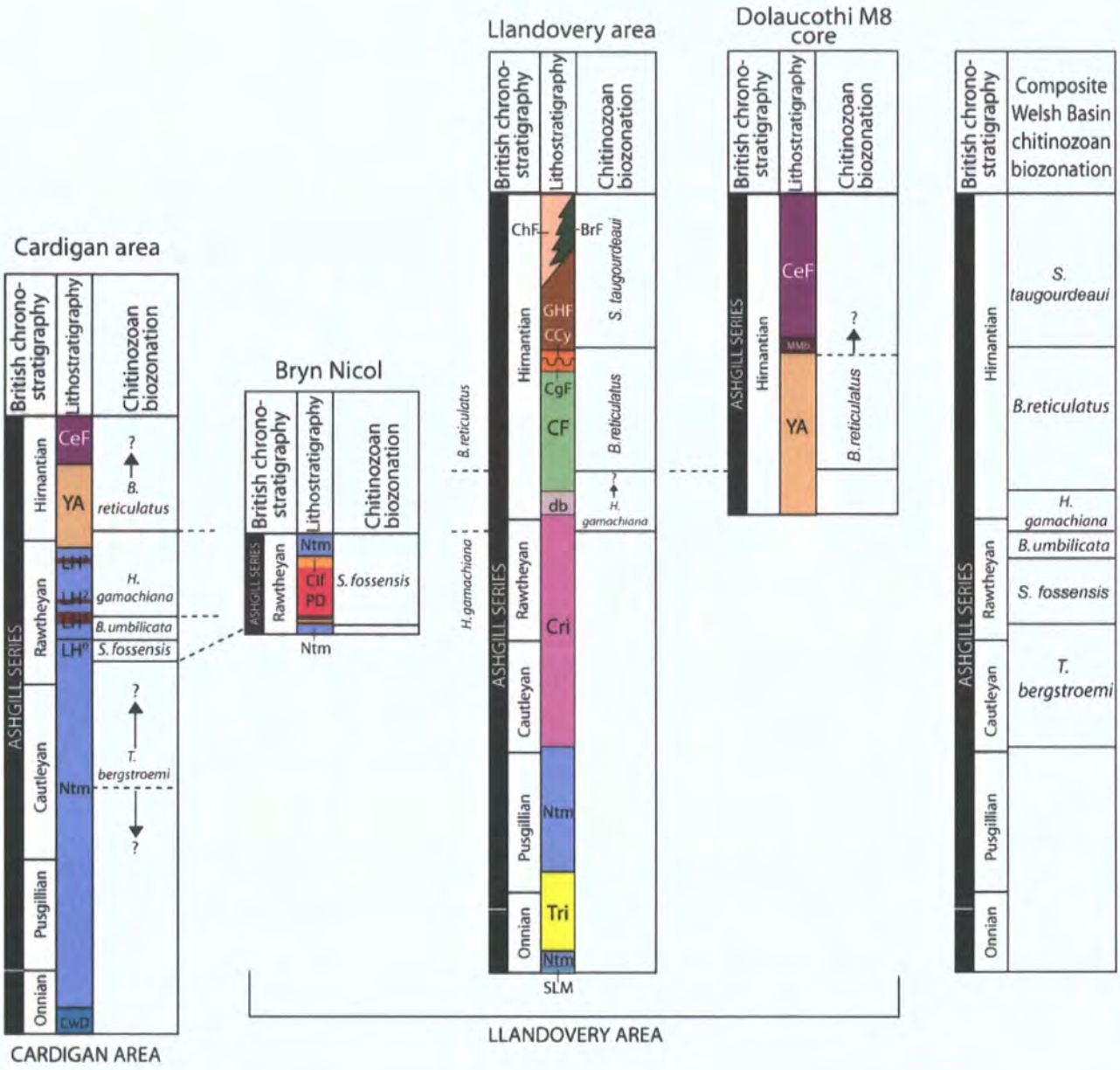

Figure 2.10: Correlation of regional chitinozoan biozones between sections in the Cardigan and Llandovery areas and composite chitinozoan biozonation scheme for the Upper Katian and Hirnantian Stages of the Welsh Basin. BrF = Bronydd Formation; CCy = Cwm Clyd Sandstone; CeF = Cwmere Formation; CF = Ciliau Formation; CgF = Cwmcringlyn Formation; ChF = Chwefri Formation; CIf = Coed Ifan facies of the Bryn Nicol Formation; Cri = Cribarth Formation; CwD = Cwm Degwel Mudstone Member; db = disturbed beds of the Ciliau Formation; GHF = Garth House Formation; LH^{0-3} = laminated hemipealgite units 0–3 of the Nantmel Mudstones Formation; Ntm = Nantmel Mudstones Formation; MMb = Mottled Mudstone Member of the Cwmere Formation; PD = Pen Derlwyn facies of the Bryn Nicol Formation; SLM = Sugar Loaf Member; Tri = Tridwr Formation and YA = Yr Allt Formation.

2.8.0.1 Correlation outside the Welsh Basin

Recognition of the *T. bergstroemi*, *S. fossenis*, *B. umbilicata* and *S. taugourdeaui* biozones allow direct correlation with other Avalonian sections in the Cautley District, the Wye Valley, Wales and in Belgium, where these biozones have been recognized (Vanmeirhaeghe & Verniers, 2004; Vanmeirhaeghe, 2006).

Outside Avalonia, the presence of the *T. bergstroemi* and *S. taugourdeaui* provide correlation with Baltoscandia whereas the *H. gamachiana* Biozone provides strong correlation with Laurentia and Baltoscandia. The *H. gamachiana* Biozone in Wales demonstrates further similarities of the Avalonian chitinozoan composition with that of Laurentia despite Vandenbroucke (2008) considering a Baltoscandian - Gondwanan signature to be dominant.

The *rugata* Biozone has not been identified in the Welsh Basin in the current study but has been recognized elsewhere in Avalonia, from the Cautley district in northern England (Vandenbroucke *et al.*, 2005) and the Condroz Inlier in Belgium (Vanmeirhaeghe & Verniers, 2004). The low sampling resolution in this study below the base of the *fossensis* Biozone in the Nantmel Mudstones Formation may be a likely cause for its absence.

Hercochitina cf. *crickmayi*, recorded from the Nantmel Mudstones Formation in the *umbilicata* Biozone in the Cardigan area and from the *S. fossensis* Biozone in the Llandovery area provides further support for correlation with the Avalonian *S. fossensis* Biozone with the upper Rawtheyan (Upper Katian) *H. crickmayi* Biozone of North America (Laurentia, Achab, 1989). *Hercochitina minuta*, recorded in this study in the *fossensis* Biozone, is also mentioned as being an associated taxon of the *Tanuchitina anticostiensis* Biozone which underlies the *crickmayi* Biozone (Achab, 1977a). Within the *T. anticostensis* Biozone, *H. minuta* is succeeded by *Hercochitina normalis*, each taxon defining a subzone. In the Cardigan - Llangranog region, *H.* cf. *normalis* is reported above *H. minuta* in the *umbilicata* Biozone implying that if the presence of these two taxa do represent a direct correlation with the Laurentian zonation scheme, then the *anticostiensis–crickmayi* Biozones may span the *fossensis–umbilicata* Biozones in Avalonia. The late Rawtheyan (Upper Katian) *Ancyrochitina merga* Biozone, reported from Gondwana, Laurentia and Avalonia, is not recognized in the Welsh Basin.

Correlation of the lower Hirnantian within Avalonia and to other palaeocontinents has been inhibited by the lack of a consistent discrete range-defining taxon. Vandenbroucke (in press) and Vandenbroucke & Vanmeirhaeghe (2007) recognized that *Cyathochitina* spp. and *Ancyrochitina* spp. become abundant in the Upper Ordovician and Lower Silurian and demonstrated this from analysis of samples taken from Cerrig Gwynion Quarry. This pattern is also reported from the Llandovery sections in this study (Figure 2.9, Table 2.3) but these taxa are either long-ranging (*Cyathochitina* spp.) or too poorly preserved (*Ancyrochitina*

spp.) to be utilized for biostratigraphical purposes. Vandenbroucke (2008) recognized that *Belonchitina reticulatus* n. sp. may prove a worthy regional zone fossil if more assemblages could be recovered from other Hirnantian horizons. This species was recovered by Vandenbroucke (2005) and Vandenbroucke *et al.* (2005) from Hirnantian sections in the Cautley district, UK, the Hirnant Limestone member of the Welsh Basin and from the Brabant Massif in Belgium (Vanmeirhaeghe, 2006) alongside *Spinachitina taugourdeaui* and reinforces the restricted range of this species within Avalonia. The present study confirms the suitability of this taxon for correlative purposes within Avalonia but it was not recovered alongside *S. taugourdeaui.* At the time of writing no occurrences of *Belonechitina reticulatus* n. sp. are known outside Avalonia.

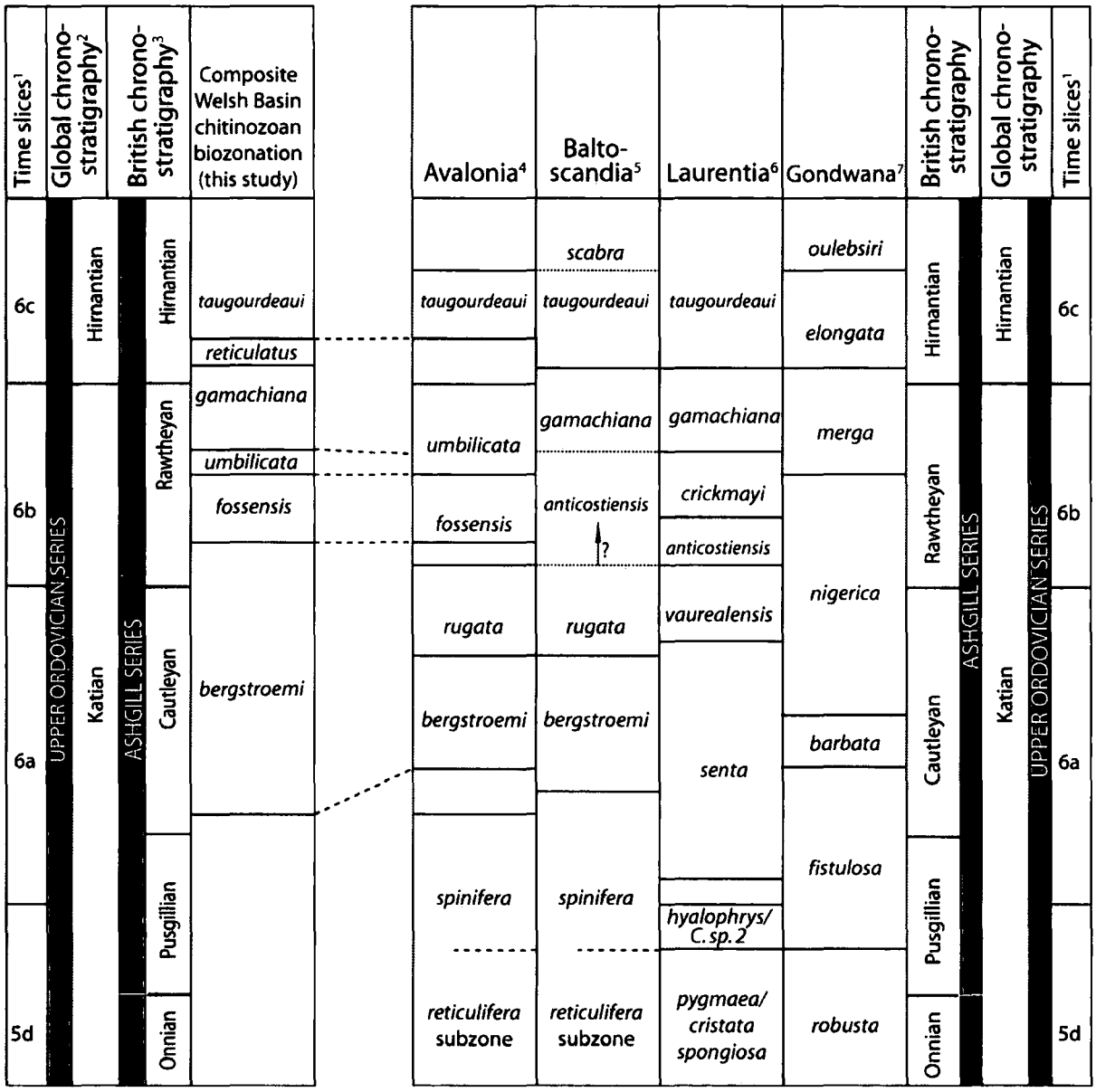

Figure 2.11: Correlation of the Welsh Basin chitinozoan biozonation scheme with those of Avalonia, Baltoscandia, Gondwana and Laurentia. In this study the *rugata* Biozone is not recognized in the Welsh Basin. [1]Webby *et al.* (2004); [2]Bergström *et al.* (2006a); [3]Fortey *et al.* (2000); [4]Vandenbroucke (2008); [5]Nõlvak (1999); [6]Soufiane & Achab (2000); Achab (1978); [7]Paris (1990).

2.9 Conclusions

A regional chitinozoan biozonation scheme has been developed that identifies the Avalonian *Tanuchitina bergstroemi*, *Spinachitina fossensis*, *Bursacitina umbilicata* and *Spinachitina taugourdeaui* Biozones in the Upper Katian of the the Welsh Basin and provides confirmation of the recently erected Avalonian chitinozoan biozonation scheme of Vandenbroucke (2008). The oldest biozone reported in this study is the *Tanuchitina bergstroemi* Biozone, the *Fungochitina spinifera* Biozone is not identified in the Nantmel Mudstones Formation in the Cardigan and Llandovery areas, and implies that the base of the Ashgill (Mid-Katian) is lower than the lithostratigraphic boundary marking the onset of basin oxygenation (the Dinas Island Formation–Nantmel Mudstones Formation boundary), as proposed by Vandenbroucke *et al.* (2008). The *Conochitina rugata* Biozone, which overlies the *T. bergstroemi* Biozone, is not recognized in the Welsh Basin in this study. Higher in the lithostratigraphy, the presence of the *H. gamachiana* Biozone allows correlation with Laurentian and Baltoscandia and demonstrates that the base of the Hirnantian Stage is within the upper Nantmel Mudstones Formation in the Cardigan area and in the upper Cribarth Formation in the Llandovery area.

A new regional biozone, the *Belonechitina reticulatus* n. sp. Biozone, has been defined and is of lower to mid Hirnantian age. This new biozone enables correlation between other Avalonian sections in the Anglo-Welsh region and in Belgium.

The high degree of correlation between the Cardigan area, representing a basin depositional environment, and the Llandovery area, predominantly representing a shelf-break to shelf depositional environment, demonstrates the applicability of the chitinozoan biozonation scheme between different palaeoecological environments. However, distinct differences are observed as in the case of the lithostratigraphical position of the base of the *S. fossensis* Biozone, which in the Llandovery area is higher than in the Cardigan area and likely implies palaeoecological constraints on the taxa employed in the Avalonian biozonation scheme.

2.10 Chitinozoan systematics

In the following systematic discussion of the taxa recovered in this study, the chitinozoan classification scheme of Paris *et al.* (1999a) is adopted whereby genera and species are identified on diagnostic characters of vesicle shape and surface ornamentation. The taxa are presented in the same order as Paris *et al.* (1999a) following his suprageneric classification system. The terms used to describe chitinozoan vesicle shape and ornamentation are those proposed by Paris *et al.* (1999a) (see Figure 2.12).

When considered appropriate, open nomenclature has been used following the scheme of Bengston (1988). Uncertainty of an identified species is given by the prefixes "?", "cf." and "aff.", where "?" indicates uncertain identification of the species on grounds of poor preservation or small assemblage yields, "cf." indicates a provisional identification when diagnostic characters are lacking but, for example, the shape is identical, and "aff." indicates that the taxon is superficially similar to a known species and is used to relate a new undescribed species to an existing species.

Species in open nomenclature are used when a separate taxon is identified that does not relate to an existing species. In this study, capital roman numerals are used to identify such species in order to avoid confusion with species placed open nomenclature from previous studies using either a numerical suffix or a captial roman alphabet suffix. In addition, when a species in open nomenclature from a previous study is recognized, the previous author is recognized following the species using *sensu* e.g. *Hercochitina* sp. 1 *sensu* Vanmeirhaeghe (2006).

The recent increase in work on Avalonian chitinozoa over the past ten years has identified many new taxa that remain unpublished and in open nomenclature. This study does not intend to contribute to this growing list of *nomen nuda* and so the number of taxa that are placed in open nomenclature has been kept to a minimum. Where taxa do not warrant separate open nomenclature species classification, mostly on preservational grounds, but whose occurrence is noteworthy, figured taxa have been identified with the suffix -sp. indet.

All biometric data are given in μm and the following chamber dimensions have been measured on each specimen where preservation permits: following abbreviations in Paris *et al.* (1999a)

L: total chamber length

Dp: maximal diameter

Dc: diameter of the neck at the flexure (if present)

L:Dp: ratio of L to Dp

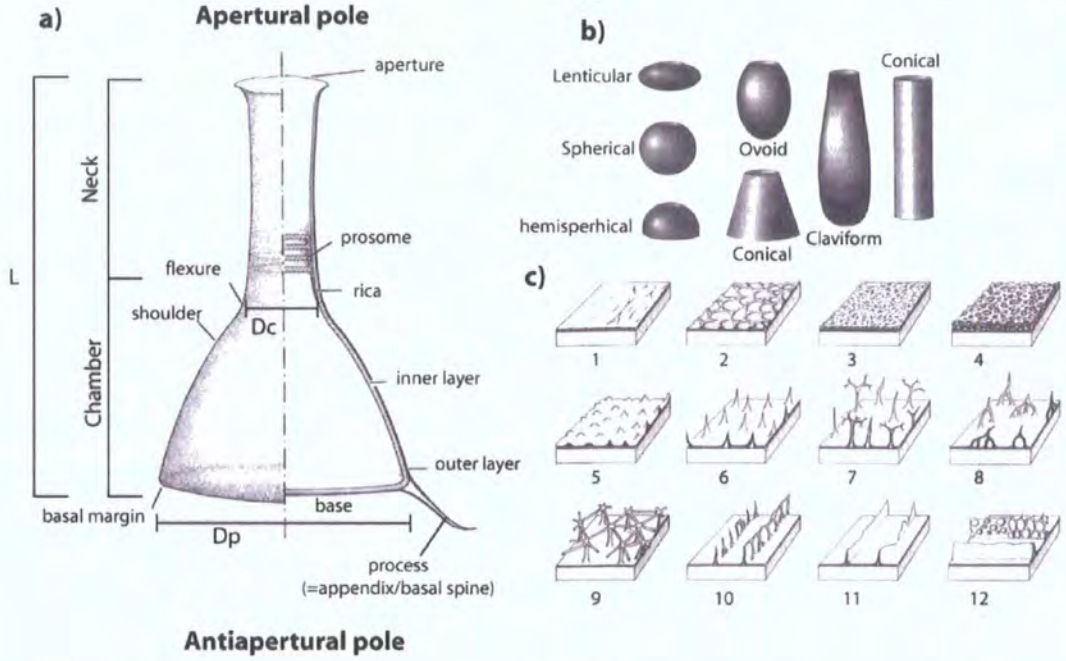

Figure 2.12: a) Morphological features and measured dimensions of a typical Spinachitinid chitinozoan; b) basic chamber shape silhouettes of chitinozoans; c) different types of ornamentation of the chitinozoan vesicle wall. 1. Smooth, scabrate; vermiculate, 2. Foveolate; 3. Felt-like; 4. Spongy; 5. Verucate (granules, tubercules and/or cones less than $2\mu m$ high); 6. Simple spines; 7. Simple and branched spines; 8. Bi-and multi-rooted spines; 9. Mesh-like structure; 10. Crests with vertical rows of free or connected spines; 11. Crests of web-like to discontinuous membranes; Complete or perforated/reticulated carina. Stippled = inner layer; black = outer layer. (From Paris *et al.*, 1999a).

N: number of chitinozoans used in calculation.

For each metric, the maximum, mean and minimum values are given when $N > 3$. When $N < 3$, the metrics are given in decreasing value. Figures given in brackets following a sample number for "*Material*" or in a plate caption refers to the unique specimen number for that specimen in the sample.

Biometric data for flattened specimens have not been corrected.

See Appendix C for details of sample number localities.

Incertae sedis group Chitinozoa Eisenack, 1931
Order Prosomatifera Eisenack, 1972
Family Conochitinidae Eisenack 1931, emend. Paris, 1981
Subfamily Conochitininae Paris, 1981
Genus *Conochitina* Eisenack, 1931 emend. Paris et al., 1999

Diagnosis Conochitinidae with a conical to claviform glabrous chamber provided with a mucron.

Conochitina cf. *homoclaviformis* Bouché, 1965
Pl. 5.11-12; Pl. 6.4; Pl. 11.5; Pl. 15.4

Material: 11 specimens; 1 specimen from sample TJC D968, Nantmel Mudstones Formation, LH^1; 2 specimens from sample TJC D979, Nantmel Mudstones Formation, LH^1; 1 specimen from sample TJC D1010, Nantmel Mudstones Formation, LH^3, Traeth Penbryn; 2 specimens from sample TJC D946, Yr Allt Formation, Llangranog; 3 specimens from sample TJC D950, Sugar Loaf Member, A40 road section; 4 specimens from sample TJC D952 Tridwr Formation, Sugar Loaf road section, Llandovery region.
Dimensions: Yr Allt Llangranog: L: 270-225-180, Dp: 100-88-75, Dc: 70-63-55, L/Dp: 2.7-2.5-2.4; Llandovery region: $L : 239 - 210 - 171\mu m, Dp : 139 - 98 - 70\mu m, Dc : 59 - 56 - 53\mu m, L/Dp : 2.8 - 2.1 - 1.6, (N = 3)$.
Description: A smooth, reasonably large claviform chitinozoan with a rounded basal margin which is sometimes secondarily flattened. The rounded basal margin often bears a circular basal scar resembling a mucron with a few smaller concentric scars anti-aperture-wards of the largest one
Discussion: The specimens recovered are very close to the holotype and only differ by having no evident circular basal scar. They are considerably shorter than *Rhabdochitina ?gracilis* and have, in some specimens, a maximum width (Dp) greater than $100\mu m$. *Rhabdochitina magna* Eisenack (1931) is longer and does not have such a rounded basal margin. This species is easily distinguished from *Conochitina* sp. I by the broad, convex base. The recovered specimens are also smaller than the holotype but are within the range of morphological variation.

Conochitina rugata Nõlvak, 1980 *nomen nudum*

Material: 1 specimen from sample TJC D1015, LH^0, Aberporth, Cardigan region.
Dimensions: $L : 190\mu m, Dp : 45\mu m, Dc : 30\mu m, L/Dp : 4.2$.

Description: *nomen nudum*(freely after Vandenbroucke (2005)) A cylindro-conical species of *Conochitina* with a small but well-developed mucron and closely-spaced longitudinal linear structures on the vesicle wall, hardly elevated above the test.
Discussion: The specimen recovered possesses the characteristic surface ornamentation of *Conochitina rugata* figured in Nõlvak & Grahn (1993) but is shorter and a mucron is not as clearly visible or well-developed.

Conochitina sp. I
Pl. 11.3-4

Material: 7 specimens; 1 specimen from sample TJC D950, Sugar Loaf Member, Sugar Loaf road section; 3 specimens from sample TJC D952, Tridwr Formation, Sugar Loaf road section; 3 specimens from sample TJC D976, Garth House Formation, Garth Bank, Llandovery region.
Dimensions: Llandovery region: $L: 170-138-113\mu m, Dp: 78-71-58\mu m, Dc: 80-70-57\mu m, L/Dp: 2.6-2.0-1.5$.
Description: A *Conochitina* species distinguished by cylindrical flanks and a flat to concave base with a rounded basal margin.
Discussion: Specimens assigned to this species were all incomplete and identified by the characteristic shape of the base and straight walls. Only specimens with a flat to slightly convex base were included in this species.

Genus *Rhabdochitina* Eisenack, 1931

Diagnosis: Conochitinidae with glabrous elongated cylindrical vesicle.

Rhabdochitina gracilis Eisenack, 1962
Pl. 3.10

Material: 4 specimens; 2 specimens from sample TJC D1015, 2 specimens from sample TJC D1014, LH^0, Aberporth, Cardigan region.
Dimensions: $L: 370-353-340\mu m, Dp: 75-74-70\mu m, Dc: 60-48-40\mu m, L/Dp: 4.9-4.8-4.5, (N=4)$.
Description: A slightly conical *Rhabdochitina* species with a an indistinct flexure and a neck

approximately half the width of the base.

Discussion: Some specimens are shorter than the holotype because the neck is broken off. They are assigned to *R. gracilis* on account of having Dp $< 100\mu m$ which distinguishes them from *R. magna*. A mucron is not well developed in any of the specimens.

Subfamily Tanuchitininae Paris, 1981

Genus *Laufeldochitina* Paris, 1981

Diagnosis: Conochitinidae with a claviform, glabrous chamber and a complete, flaring membranous carina, below the margin.

Laufeldochitina lardeuxi Paris, 1981

Pl. 9.1-2; Pl. 16.2-4

Material: 9 specimens; 3 specimens from sample TJC D1005, Yr Allt Formation, Traeth Penbryn; 2 specimens from sample TJC D946, Yr Allt Formation, Llangranog, Cardigan region; 4 specimens from sample TJC D976, Garth House Formation, Garth Bank, Llandovery region.

Dimensions: Cardigan region: $L : 350 - 238 - 140\mu m, Dp : 80 - 68 - 45\mu m, Dc : 80 - 61 - 30\mu m, L/Dp : 4.4 - 3.4 - 3.0, (N = 4)$; Llandovery region; $L : 272 - 184 - 135\mu m, Dp : 117 - 81 - 59\mu m, Dc : 59 - 54 - 51\mu m, L/Dp : 3.3 - 2.3 - 1.2, (N = 4)$.

Description: A moderately long species of *Laufeldochitina* with a distinctly claviform chamber and a thin neck approximately one quarter the total chamber length. The base is ornamented with a short, flaring carina and a wrinkled wall around the basal margin. See also holotype description in (Paris, 1981).

Discussion: This species is easily recognised by the short carina and claviform chamber. The L/Dp in most specimens is between 2.5 and 4.0, those with a lower value representing broken vesicles. The neck is frequently broken or missing. This species is identical to *Laufeldochitina* sp. indet figured by Vanmeirhaeghe (2006) (Plate 13.12, Appendix II, p.83).

Genus *Tanuchitina* Jansonius, 1964
emend. Paris, Grahn, Nestor and Lakova, 1999

Diagnosis: Conochitinidae with a cylindrical chamber and a complete membranous carina below the margin.

Tanuchitina bergstroemi Laufeld 1967
Pl. 2.9-10

Material: 3 (+1?) specimens; 1 specimen from sample TJC D1006, Nantmel Mudstones Formation, Gwbert; 1 specimen from sample TJC D942, Nantmel Mudstones Formation, Pen-y-Craig; 1 (+1?) specimen from sample TJC D943, Nantmel Mudstones Formation, Pen-y-Craig, Cardigan region.

Dimensions: $L : 371 - 192 - 96\mu m, Dp : 77 - 65 - 57\mu m, Dc : 45 - 40 - 36\mu m, L/Dp : 3.0 - 2.8 - 1.7, (N = 4)$.

Description: See holotype description by Laufeld (1967), pp. 343, Pl. 14, Fig. 34.

Discussion: The specimens are well preserved and resemble the holotype. A single specimen from sample TJC D943 is only partly preserved. Vandenbroucke *et al.* (2008) only recovered partial specimens from the Cardigan region but the material here is considered complete enough to warrant a firm identification.

Stratigraphical remark: Vandenbroucke *et al.* (2008) determined, from fragmentary specimens, the first appearance datum of *Tanuchitina ?bergstroemi* to lie within the Dinas Island Formation, below the base of the Nantmel Mudstones Formation. From the first appearance datum of accessory species of the *Saharochitina ?fungiformis* Biozone recorded by Vandenbroucke *et al.* (2008) below the Nantmel Mudstones Formation and the definite appearance of *Tanuchitina bergstroemi* recorded herein above that horizon, it is considered here that the base of the Nantmel Mudstones Formation lies within the *spinifera* Biozone not within the *bergstroemi* Biozone.

Tanuchitina sp. A *sensu* Vanmeirhaeghe 2006

Material: 1 specimen from sample TJC D978, Cwm Clyd Sandstone Member, Glasallt Fawr, Llandovery region.

Dimensions: $L : 136\mu m, Dp : 59\mu m, Dc : 46\mu m, L/Dp : 2.3$.

Description: This species is a long *Tanuchitina* species with a wide base and a short, continuous carina. The vesicle flanks are claviform with a very weak flexure and no shoulder. The neck is approximately half the maximum width (Dp)and one third he total vesicle length.

Discussion: Vanmeirhaeghe (2006) recorded this taxon to be present in the Lessines borehole from the Fauquez Formation, Brabant Massif, Belgium, but provided no description. It has

a wide base relative to other *Tanuchitina* species and the specimen recovered is smaller than those figured in Vanmeirhaeghe (2006) ($L: 400-352-300\mu m, Dp: 110-101-95\mu m, Dc: 90-64-65\mu m$.

Subfamily Spinachitininae Paris, 1981

Genus *Spinachitina* Schallreuter 1963 emend. Paris *et al.* (1999a)

Diagnosis: Conochitinidae with a conical to cylindrical chamber bearing a crown of processes.

Spinachitina penbryniensis n. sp.

Pl. 2.1; Pl. 5.1-7

Conochitina aff. *bulmani* Achab (1977b).

Spinachitina cf. *coronta* Vandenbroucke *et al.* (2003)

Spinachitina ?bulmani sensu Achab, 1977 Vandenbroucke *et al.* (2005).

Derivatio nominis: From the hamlet of Penbryn, Ceredigion, Wales were the type assemblage was recovered.

Material: 94 specimens; 4 specimens from sample TJC D943, Pen-y-Craig, Nantmel Mudstones Formation; 34 specimens from samples TJC D1013-1014, LH^0, 240cm on log 1, Aberporth; 21 specimens from sample TJC D1015, LH^0, 340cm on log 1, Aberporth; 15 specimens from sample TJC D979, LH^1, Traeth Penbryn; 1 specimen from sample TJC D957, LH^2, Traeth Penbryn, 2 specimens from sample TJC D956, LH^3 oxic-anoxic boundary oxic facies, Traeth Penbryn; 11 specimens from sample TJC D1010, LH^3, Traeth Penbryn. All samples from the Cardigan region.

Holotype: Plate 5.1

Holotype dimensions: $L: 300\mu m, Dp: 62\mu m, Dc: 39\mu m$.

Type stratum: Laminated hemipelagite horizon 1 (LH^1), Nantmel Mudstones Formation, Traeth Penbryn, Ceridigion, Wales.

Paratype: Plate 2.1 *Dimensions*: LH^0 and LH^1 material: $L: 366-183-90\mu m, Dp: 100-65-45\mu m, Dc: 85-44-20\mu m, L/Dp: 5.8-2.9-1.5$.

Diagnosis: A *Spinachitina* species with a long neck approximately the same length as the claviform vesicle chamber and a chamber base surrounded by short, coniform spines directed ante-aperturewards.

Description: The chamber base is very slightly convex and the basal edge sharp with a crown of short simple, coniform spines up to $4\mu m$ pointing anti-apeturewards. The neck is thinnest

at the flexure which is inconspicuous and the width of the neck at the apeture (Dc) is 66−75% the width of the base. The neck wall thins towards the aperture and in the best preserved specimens, flares outwards. The vesicle surface is smooth.

Discussion: This form differs considerably from *S. bulmani* in being almost three times longer; the length of *S. bulmani* being between 100-200 μm (Jansonius, 1964). Also, *S. bulmani* may possess multipode spines whereas those of *S. penbryniensis* are distinctly coniform. It does not have the distinct flexure towards the base of the vesicle that *S. coronata* possesses and the conical shape of the chamber is less well defined and maximum L/Dp is greater than *S. coronata* (= 4.2).

Remarks: The long, thin fragile neck is frequently broken off specimens but it is still recognisable from the claviform chamber and short, downward-pointing spines e.g. Plate 5.4, 5.7.

Spinachitina coronata (Eisenack, 1931)

Pl. 4.11-12; Pl. 14.11-12

Material: 5 specimens from sample TJC D979, LH[1], Traeth Penbryn, Cardigan region; 1 specimen from sample TJC D1023, 4 specimens from sample TJC D1024, Cribarth Formation, Glasallt Fawr, Llandovery area.

Dimensions: Cardigan material: $L : 340 - 309 - 263\mu m, Dp : 71 - 64 - 59\mu m, Dc : 57 - 48 - 38\mu m, L/Dp : 5.3 - 4.9 - 4.4, (N = 5)$, Llandovery

Material: $L : 256 - 180 - 127\mu m, Dp : 99 - 81 - 61\mu m, Dc : 67 - 51 - 32\mu m\ L/Dp : 3.1 - 2.2 - 1.4, (N = 4)$.

Description: See holotype description in Eisenack (1931) and further description and discussion in Grahn (1982).

Discussion: Material recovered resembles material figured by Vandenbroucke (2005). The holotype of Eisenack (1931) lacks a basal constriction, however, the neotype (Eisenack, 1962) does and subsequent authors have included material lacking a basal constriction e.g. cf. Nõlvak (1980)

Spinachitina taugourdeaui (Eisenack, 1968)

Pl. 16.5-8

Material: 6 specimens from sample TJC D976, Garth House Formation, Garth Bank; 1 specimen from sample TJC D1026, Garth House Formation, Brynffo Forest Section, Llandovery region.

Dimensions: L : $328 - 176 - 123\mu m$, Dp : $154 - 88 - 59\mu m$, Dc : $83 - 47 - 32\mu m$, L/Dp : $2.5 - 2.0 - 1.5$.

Description: See holotype description in Eisenack (1968).

Discussion: Specimens of *S. taugourdeaui* possess granular surface ornamentation distinguishing them from *Spinachitina fragilis*, the index taxon of the overlying Llandovery biozone.

Spinachitina cf. *bulmani* (Jansonius, 1964)

Pl. 11.8; Pl. 12.10

Material: 7 specimens; 1 specimen from sample TJC D1013, Nantmel Mudstones Formation, LH^0, Aberporth; 1 specimen from sample TJC D1003, Nantmel Mudstones Formation, Aberporth; 1 specimen from sample TJC D952, Tridwr Formation, Sugar Loaf road section; 1 specimen from sample TJC D959, Bryn Nicol Formation; 1 specimen from sample TJC D1033, Bryn Nicol Formation, Llandovery area.

Dimensions: L : $181 - 163 - 139\mu m$, Dp : $106 - 89 - 68\mu m$, Dc : $72 - 56 - 41\mu m$.

Description: See holotype description in Jansonius (1964).

Discussion: The specimens resemble the holotype well in shape and size but because the neck and spines are frequently broken off or worn, a certain identification is not possible and these specimens are kept in open nomenclature.

Spinachitina sp. 2 *sensu* Vandenbroucke (2005)

Pl. 4.4

Material: 2 specimens from sample TJC D967, Nantmel Mudstones Formation, LH^1, Traeth Penbryn.

Dimensions: L : $166 - 89\mu m$, Dp : $80 - 51\mu m$, Dc : $39 - 28\mu m$ (N=2).

Description: A species of *Spinachitina* with a cylindro-conical chamber, an inconspicuous flexure and a minor constriction immediately aperture-wards of the base. The base is rounded to slightly conical and the basal edge also rounded. The remains of a crown of spines is present around the basal edge which appear to be continuous with vertically-aligned ridges around

the basal edge.

Discussion: The specimens from this study differ from specimens recovered by Vandenbroucke (2005) by lacking slightly convex flanks. They are similar to *Spinachitina bulmani* recorded by Vanmeirhaeghe (2006) from the Sart-Bernard Member (Vitrival-Bruyre Formation) from Belgium but have a more rounded base and basal edge.

Spinachitina sp. 4 *sensu* Vandenbroucke (2005)

Pl. 4.8

Material: 1 specimen from sample TJC D979(106).

Dimensions: $L : 103\mu m, Dp : 103\mu m, Dc75\mu m, L/Dp : 1$.

Description: *Spinachitina* species with L/Dp close to 1, a cylindro-conical chamber and a short neck. Possesses a slightly flared basal edge and the crown of basal spines appear to be positioned slightly aperturewards of the base.

Remark: The one recovered specimen is well preserved save for a slightly broken basal edge but preserving short, multipode basal spines.

Spinachitina sp. A *sensu* Vanmeirhaeghe (2006)

Pl. 4.5

Material: 1 specimen from sample TJC D967, Nantmel Mudstones Formation, LH[1], Traeth Penbryn.

Dimensions: $L : 166\mu m, Dp : 54\mu m, Dc : 28\mu m$

Description: A species of *Spinachitina* with longitudinally-elongated basal spines. It bears vague vertical ridges exaggerated towards the base. The base is concave.

Discussion: The specimen recovered is 3-dimensionally preserved and possesses all the features described by Vanmeirhaeghe (2006). *Conochitina suecica* (Grahn, 1982) has a less conspicuous flexure and a convex, rounded base.

Spinachitina fossensis Vanmeirhaeghe & Verniers 2004

Pl. 4.9-10; Pl. 13.2-4;13-14

Material: 17 specimens; 2 specimens from sample TJC D979(66, 85), LH^1, Traeth Penbryn; 2 specimens from sample TJC D943 (93, 70) Nantmel Mudstones Formation oxic facies, Pen-y-Craig; 13 specimens from samples TJC D1031 and TJC D1033, Bryn Nicol Formation, Llandovery region.
Dimensions: LH^1, Traeth Penbryn; $L: 155-121\mu m, Dp: 73-72\mu m, Dc: 50-43\mu m, L/Dp: 2.1-1.7$; Pen-y-Craig; $L: 123-163\mu m, Dp: 61-77\mu m, Dc: 25-52\mu m, L/Dp: 2.0-2.1$; Bryn Nicol Formation; $L: 157\mu m, Dp: 83\mu m, Dc: 47\mu m, L/Dp: 1.89 (N = 12)$
Description: See holotype description in Vanmeirhaeghe & Verniers (2004).
Discussion: This eponymous biozonal taxon extends into the *Bursachitina umbilicata* Biozone as it does in the Cautley area, UK.

Spinachitina cf. *fossensis* Vanmeirhaeghe & Verniers 2004
Pl. 2.2-5; Pl. 3.9; Pl. 12.6,7

Material: 6 specimens; 1 specimen from sample TJC D943 Nantmel Mudstones Formation, oxic facies, Pen-y-Craig; 1 specimen from sample TJC D1032, 5 specimens from sample TJC D960, 2 specimens from sample TJC D1033, all from the Bryn Nicol Formation, Llandovery region.
Dimensions: Cardigan region: $L: 240-165-110\mu m, Dp: 90-72-56\mu m, Dc: 63-41-50\mu m, L/Dp: 3.4-2.3-1.5 (N = 18)$
Description: See holotype description in Vanmeirhaeghe & Verniers (2004).
Discussion: These specimens possess a poorly preserved crown of spines or basal spines necessitating placement in open nomenclature.

Genus *Hercochitina* Jansonius, 1964

Diagnosis: Conochitinidae with a conical chamber and distinct

Hercochitina cf. *crickmayi* Jansonius, 1964
Pl. 3.3-5; Pl. 4.18; Pl. 13.6-7; Pl. 14.8

Material: 18 specimens; 2 specimens from sample TJC D1014; 3 specimens from sample TJC D1015; 3 specimens from sample TJC D1013, all from Nantmel Mudstones Formation, LH^0, Aberporth; 1 specimen from sample TJC D979, Nantmel Mudstones Formation, LH^0,

Traeth Penbryn; 1 specimen from sample TJC D968, Nantmel Mudstones Formation, burrow-mottled mudstone, Traeth Penbryn; 3 specimens from sample TJC D959, 2 specimens from sample TJC D1033, Bryn Nicol Formation, Llandovery area; 4 specimens from sample TJC D977, Cribarth Formation, Glasallt Fawr, Llandovery area.

Dimensions: LH^0: L : $240 - 169 - 110\mu m$, Dp : $85 - 72 - 60\mu m$, Dc : $55 - 49 - 45\mu m$; LH^1: L : $189\mu m$, Dp : $56\mu m$, Dc : $48\mu m$; Bryn Nicol: L : $152 - 138 - 118\mu m$, Dp, $90 - 83 - 77\mu m$, Dc, $63 - 56 - 49\mu m$, L/Dp : $1.9 - 1.7 - 1.5$.

Description: A long, conical *Hercochitina* species with indistinct longitudinal ridges on the vesicle surface. Distinct simple spines are present around the base. See also holotype description in Jansonius (1964).

Discussion: The specimens recovered resemble the holotype in overall shape but the longitudinal ridges are not as distinct as on the holotype material or material figured by Achab (1977b). It is not possible to determine if the basal edge possesses aboral ridges or fusing spines like the holotype material, most likely from abrasion and so the specimens are kept in open nomenclature.

Hercochitina cf. *turnbulli* Jenkins, 1969

Pl. 3.6

Material: 1 specimen from sample TJC D1015(8), Nantmel Mudstones Formation, (LH^0), Aberporth.

Dimensions: L : $170\mu m$, Dp : $110\mu m$, Dc : $60\mu m$, L/Dp : 1.5.

Description: A *Hercochitina* species with a conical chamber with rounded flanks. The neck is broken off but the flexure is apparent. Indistinct longitudinal spines are present on the chamber wall.

Discussion: The recovered specimen resembles the shape of holotype but does not posses the distinct slender λ-spines. With only one specimen recovered and moderate preservation, the species is kept in open nomenclature.

Hercochitina aff. *normalis* Achab, 1977a

Pl. 4.20; Pl. 7.1; Pl. 12.11; Pl. 13.8

Material: 10 specimens; 5 specimens from sample TJC D979, Nantmel Mudstones Formation, LH^1, Traeth Penbryn; 1 specimen from sample TJC D1010, LH^3, Traeth Penbryn; 2 specimens from sample TJC D1032, 1 specimen from sample TJC D959, 1 specimen from sample sample TJC D1033, both from Bryn Nicol Formation, Llandovery region.
Dimensions: LH^1: $L: 133-163-172\mu m$; $Dp: 78-92-95\mu m$; $Dc: 43-48-61\mu m$; $LH^3: L: 100\mu m$; $Dp: 85\mu m$; $Dc: 40\mu m$; $BrynNicol: L: 133-124-107\mu m$; $Dp: 73-72.6-72\mu m$; $Dc: 45-44-41\mu m$.
Description: A moderate sized hercochitinid with a conical vesicle with straight neck and a distinct constriction oral-wards of the basal edge. The vesicle walls are straight to slightly convex with a narrow shoulder. An obvious thickening of the ridges at the rounded basal edge forms an obvious crown of spines. The surface of the vesicle is ornamented with short wavy longitundinally-arranged ridges up to $20\mu m$ long that do not anastomose.
Discussion: This species superficially resembles *Hercochitina normalis* Achab (1977a) but the distinct constriction close to the base warrants segregation as a separate species. The flanks are also straighter than *Hercochitina* aff. *seriespinosa* and *Hercochitina* cf. *crickmayi*.

Hercochitina cf. *normalis* Achab, 1977a
Pl. 5.14-15

Material: 16 specimens; 10 specimens from sample TJC D955, 2 specimens from sample TJC D967, 1 specimen from TJC D979, from Nantmel Mudstones Formation, (LH^1), Traeth Penbryn; 2 specimens from sample TJC D968, Nantmel Mudstones Formation oxic facies between LH^1 and LH^2; 1 specimen from sample TJC D958, Bryn Nicol Formation, Llandovery area.
Dimensions: LH^1: $L: 153-145-141\mu m, Dp: 96-79-71\mu m, Dc: 52-48-43\mu m, L/Dp: 2.0-1.9-1.5(N=5)$; Nantmel Mudstones Formation burrow-mottled mudstone: $L: 162-124\mu m, Dc: 103-70\mu m, Dp: 60-40\mu m, L/Dp: 1.8-1.6(N=2)$.
Description: See holotype description in Achab (1977a).
Discussion: The size and shape of the material fits well with the holotype assemblage. Because much of the material is worn and some broken, and the vertical ridge surface ornamentation is reduced, most probably from erosion, this taxon is kept in open nomenclature.

Hercochitina aff. *seriespinosa* (Jenkins, 1969)
Pl. 4.16; Pl. 5.9-10; Pl. 11.7

Material: 18 specimens; 12 specimens from sample TJC D979, Nantmel Mudstones Formation, LH[1], Traeth Penbryn; 1 specimen from sample TJC D952, Tridwr Formation, Sugar Loaf Road section, Llandovery; 3 specimens from sample TJC D960, Bryn Nicol Formation; 1 specimen from sample TJC D1032, Bryn Nicol Formation, Llandovery; 1 specimen from sample TJC D980, Yr Allt Formation, Dolaucithi M8 borehole.
Dimensions: LH[1] Traeth Penbryn: L : $181 - 159 - 124\mu m, Dp$: $113 - 101 - 73\mu m, Dc$: $80 - 65 - 43\mu m, L/Dp$: $2.1 - 1.6 - 1.2(N = 9)$.
Description: A conical form with rounded flanks and a rounded basal edge. The basal edge is ornamented with a crown of thickened ridges and the vesicle surface is ornamented with ridges, granules and ridges composed of granules.
Discussion: The flexure is less conspicuous than on *Hercochitina* cf. *normalis* and *Hercochitina* cf. *seriespinosa*. A rounded basal edge also distinguishes this form from *Hercochitnia seriespinosa* and *Hercochitina* cf. *seriespinosa*.

Hercochitina cf. *seriespinosa* (Jenkins, 1969)
Pl. 4.19; Pl.7.9 Pl. 12.12

Material: 1 specimen from sample TJC D979, Nantmel Mudstones Formation, (LH[1]), Traeth Penbryn; 1 specimen from sample TJC 956, Nantmel Mudstones Formation, LH[3], Traeth Penbryn; 1 specimen from sample TJC D959, Bryn Nicol Formation, Llandovery area.
Dimensions: LH[1]: L : $161 - 141\mu m, Dp$: $98 - 73\mu m, Dc54 - 44\mu m$.
Description: See holotype description in Jenkins (1969).
Discussion: The Cardigan specimens are broken yet close to the shape of the holotype. The ornamentation is poorly preserved not allowing certain identification of the species.

Hercochitina cf. *gamachiana* (Achab, 1978)
Pl. 7.8; Pl. 14.10

Material: 1 specimen from sample TJC D979(93), Nantmel Mudstones Formation, LH[1], Traeth Penbryn; 2 specimens from sample TJC D956, Nantmel Mudstones Formation, LH[3]

oxic-anoxic boundary, burrow-mottled mudstones, Traeth Penbryn; 1 specimen from sample TJC D1033(40), Bryn Nicol Formation, Llandovery region; 1 specimen from sample TJC D1024(1), Cribarth Formation, Llandovery region.

Dimensions: LH[1]: L : 135μm, Dp : 91μm, Dc : 50μm, L : Dp1.5; Nantmel Mudstones Formation oxic facies: L : 161μm, Dp : 71μm, Dc : 45μm; Cribarth Formation: L : 156μm, Dp : 86μm, Dc : 61μm.

Description: See holotype description in Achab (1978).

Discussion: The shape and size of the specimens remind of *Hercochitina gamachiana*, most notably the strong, aligned crests but the basal edge is more rounded. This species was originally described as *Conochitina gamachiana* Achab, 1978 and subsequently moved to the genus *Belonechitina*. Following revision of chitinozoa systematics by Paris *et al.* (1999a), this species fits into the genus *Hercochitina*.

Hercochitina minuta Achab, 1977a

Pl. 2.6; Pl. 6.1

Material: 2 specimens; 1 specimen from sample TJC D943(30, Nantmel Mudstones Formation, oxic facies, Pen-y-Craig; 1 specimen from sample TJC D968(19), Nantmel Mudstones Formation LH[1] anoxic-oxic boundary, oxic facies, Traeth Penbryn.

Dimensions: Pen-y-Craig: L : 153μm, Dp : 51μm, Dc : 44μm, L/Dp3.0; $TraethPenbryn$: L : 95μm, Dp : 69μm, Dc : 46μm.

Description: See holotype description in Achab (1977a).

Discussion: The specimens recovered have only vague surface ornamentation, straight-convex sides, narrow shoulder and a weak flexure. The neck of the specimen from Traeth Penbryn is also slightly concave.

Hercochitina sp. 1. *sensu* Vanmeirhaeghe (2006)

Pl. 4.3; Pl. 14.4-7

Material: 1 specimen from sample TJC D967, Nantmel Mudstones Formation, LH[1], Traeth Penbryn; 4 specimens from sample TJC D977, Cribarth Formation, Glasallt Fawr, Llandovery.

Dimensions: LH[1] Traeth Penbryn: L : 177μm, Dp : 55μm, Dc : 28μm; $GlasalltFawr$: L :

$269 - 200 - 127\mu m, Dp : 90 - 74 - 52\mu m, Dc : 93 - 70 - 47\mu m.$

Description: A long, conical species of *Hercochitina* with straight flanks. It has a moderate flexure between the chamber and neck forming a narrow shoulder. The neck is approximately equal in length to the chamber but around 50% narrower. The basal edge is clearly defined yet rounded and the base is characteristically convex with a pronounced mucron. The surface texture in the specimens recovered is believed to be worn but consists of thin vertically-aligned crests that thicken towards the basal edge where they may form raised crest-like spines.

Discussion: This species is similar in form to *Hercochitina* Type 1 but much longer and has a longer neck. The obvious mucron reminds of specimens of *Conochitina ?incerta* (cf. Vandenbroucke, 2005) which have similar shape but lack any texture from missing outer layer.

Hercochitina sp. A.

Pl. 6.3; Pl. 7.6

Material: 4 specimens; 2 specimens from sample TJC D946, Yr Allt Formation, Llangranog; 2 specimens from sample TJC D1010, Nantmel Mudstones Formation, LH^3, Traeth Penbryn.

Dimensions: Llangranog: $L : 115 - 108 - 100\mu m, Dp : 80 - 75 - 70\mu m, Dc : 45 - 45 - 45\mu m, L/Dp : 1.6 - 1.5 - 1.3\mu m$; Nantmel Mudstones Formation oxic facies: $L : 95\mu m, Dp : 69\mu m, Dc : 46\mu m$. LH^3: $L : 210 - 170\mu m, Dp : 100 - 90\mu m, Dc : 60 - 50\mu m, L/Dp : 2.1 - 1.9(N = 2)$

Description: *Hercochitina* with a conical chamber bearing well-defined isolated vertical ridges. The walls are convex with a distinct flexure separating the chamber from neck forming a broad shoulder. The neck is long and tapers outwards aperturewards and at the aperture it is typically over half the width of the base of the chamber. The base is flat and concave with a sub-rounded basal edge.

Discussion: This is a long, slender form, like *H. crickmayi* but differs in having convex walls and a broad shoulder and lacks distinct spines around the base. It differs from *H. micracantha* in having a longer neck.

Hercochitina cf. *grandispinosa* Achab, 1977a

Material: 7 specimens from sample TJC D943, Nantmel Mudstones Formation.

Dimensions: $L : 156 - 132 - 109\mu m, Dp : 57 - 51 - 41\mu m, Dc : 50 - 42 - 33\mu m, L/Dp :$

2.8 – 2.6 – 2.1

Description: A species of *Hercochitina* with a claviform chamber widest at one third of the total chamber length from the base. It has a short neck that is approximately one third of the total length. Simple short longitudinal ridges are present along the entire length of the vesicle and get thicker towards the base. The basal margin is rounded and bears spines that are continuations of thick ridges.

Discussion Resembles some specimens of *H. grandispinosa* figured by Achab (1977a) though, being worn, the true structure of the longitudinally aligned ridges cannot be confidently discerned. The vesicle is more claviform than true *H. grandispinosa* and is closer to a form intermediate between *H. spinetum* and *H. crickmayi* as described and figured in Melchin & Legault (1985).

Subfamily Belonechitinae Paris, 1981

Genus *Belonechitina* Jansonius, 1964

Diagnosis: Conochitinidae with a conical chamber and randomly distributed spines.

Belonechitina micracantha (Eisenack, 1931)

Material: 1 specimen from sample TJC D978(1), Cwm Clyd Sandstone Member, Glasallt Fawr Wood, Llandovery region; 1 specimen from sample TJC 980, Yr Allt Formation, Dolaucothi M8 borehole.

Dimensions: Cwm Clyd Sandstone: $L : 131\mu m, Dp : 84\mu m, Dc : 46\mu m$.

Description: See holotype description in Eisenack (1931).

Discussion: Vandenbroucke (2005) noted that only specimens with a proper conical chamber shape should be assigned to this species.

Belonechitina ceredigionensis n. sp.

Pl. 3.1; Pl. 8.1-4, 13-15

Belonechitina aff. *brittanica* Vandenbroucke (in press)

Derivatio nominis: From the Welsh county, and former kingdom, of Ceredigion, west Wales, UK, from where the type assemblage was recovered.

Material: 44 specimens: 41 specimens from sample TJC-D1005, Lower Yr Allt Formation, Traeth Penbryn; 3 specimens from sample TJC D1015, Nantmel Mudstones Formation, LH^0, Aberporth,.

Dimensions: Traeth Penbryn: $L : 280 - 212 - 120\mu m, Dp : 100 - 85 - 60\mu m, Dc : 85 - 64 - 30\mu m, L/Dp : 3.9, 2.5 - 1.5.$; Aberporth: $L : 175 - 165 - 155\mu m, Dp : 70 - 60 - 50\mu m, Dc : 45 - 38 - 35\mu m, L/Dp : 3.1 - 2.8 - 2.4.$;

Holotype: Plate 7.1 (sample TJC D1005-20, British Geological Survey).

Holotype dimensions: $L : 250\mu m, Dp : 90\mu m, Dc : 70\mu m, L/Dp : 2.8$.

Type stratum: Yr Allt Formation, Traeth Penbryn, Near Penbryn, Ceredigion, Wales, UK.

emphDiagnosis: A species of *Belonechitina* with a claviform test and slightly ovoid chamber with maximum thickness at half the chamber length. The test is ornamented with simple coniform and λ-shaped spines that are larger and more dense around the basal margin.

Description: The chamber has a rounded basal margin and a concave base bearing a basal scar *c.* 5 μm in diameter. The neck is conical with a weak flexure. The distribution of spines is generally sparse, except around the base, and decreases in density aperturewards. A circular mucron-like structure may be present in the centre of the base.

Discussion: This species has a more ovoid chamber and is considerably larger than *Belonechitina brittanica* (L: 150 μm, Dp: 60 μm, Dc: 45 μm). Some of the simple coniform spines may in fact be broken λ-shaped spines. *Belonechitina robusta* and *Belonechitina chydea* both have a more conical chamber and the latter does not possess λ-shaped spines. This species differs from *Belonechitina capitata* in lacking a constriction around the base and a more even covering of spines.

Belonechitina cf. *americana* Taugourdeau, 1965

Pl. 2.12-13; Pl. 18.15

Material: 5 specimens; 4 specimens from sample TJC D942, Nantmel Mudstones Formation, oxic facies, Pen-y-Craig; 1 specimen from sample TJC D946, Yr Allt Formation, Llangranog, Cardigan region.

Dimensions: Nantmel Mudstones Formation: $L : 184 - 167 - 132\mu m, Dp : 71 - 67 - 64, Dc : 62 - 53 - 49\mu m, L/Dp : 2.7 - 2.5 - 2.0$,; Yr Allt Formation: $L : 210\mu m, Dp : 80\mu m, Dc : 65\mu m$.

Description: A species of *Belonechitina* with poorly differentiated, short neck and straight to slightly convex sides. The test is covered in simple spines that may be more dense around the basal margin. See also holotype description in Taugourdeau (1965) and description in Achab (1977b).

Discussion: The slightly convex flanks distinguish this species from *Belonechitina micracantha* (see discussion in Vandenbroucke, 2005) though those with straighter flanks very closely resemble material figured by Vandenbroucke (2005). No spines with double bases were observed as in material figured by Achab (1977b) and because of such poor preservation of surface ornamentation this species is placed in open nomenclature.

Belonechitina wessenbergensis (Eisenack, 1959)
Pl. 9.4; Pl. 15.3; Pl. 16.12

Material: 5 specimens; 1 specimen from sample TJC D1000, Nantmel Mudstones Formation, Traeth Penbryn, Cardigan area; 1 specimen from sample TJC D946, Yr Allt Formation, Traeth Yr Yscland, Llangranog, Cardian region; 1 specimen from sample TJC D972, Ciliau Formation, 1 specimen from sample TJC D974, Garth House Formation, both A40 road section, Llandovery; 1 specimen from sample TJC D976, Garth House Formation, Garth Bank, Llandovery area.

Dimensions: Cardigan material: $L : 130\mu m, Dp : 80\mu m, Dc : 65\mu m$; Llandovery material: $L : 135 - 123.6 - 117, Dp : 99 - 89 - 77, Dc : 59 - 56 - 52$.

Description: See description of holotype in Eisenack (1959)

Discussion: Both elongate and compact forms described by Eisenack (1959) (*forma elongata* and *brevis*) are included in this species.

Belonechitina sp. A *sensu* Vandenbroucke *et al.* (2004)

Material: 2 specimens from sample TJC D976, Garth House Formation, Garth Bank, Llandovery region.

Dimensions: $L : 251 - 184\mu m, Dp : 103 - 100\mu m, Dc : 51 - 51\mu m$.

Description: See description in Vandenbroucke *et al.* (2004).

Discussion: This form differs clearly from *Belonechitina micracantha* in having rounded flanks so that the widest point of the vesicle (Dp) is around one third of the total vesicle length from the base (Vandenbroucke, 2005). The specimens reported in this study fit well with the description given in Vandenbroucke *et al.* (2004).

Belonechitina cf. *capitata* (Eisenack, 1962)

Pl. 14.1-3

Material: 5 specimens; 1 specimen from sample TJC D1021, 4 specimens from sample TJC D977, both from the Cribarth Formation, Glasallt Fawr, Llandovery area. *Dimensions*: Llandovery region: $L : 251 - 233 - 206\mu m, Dp : 87 - 78 - 71\mu m, Dc : 73 - 57 - 46, L/Dp : 3.5 - 2.8 - 2.7$.

Description: See holotype description in Eisenack (1962).

Discussion: Differs from *Belonechitina capitata* by having ornamentation covering the entire vesicle surface and being shorter. There is some resemblance to the eroded surface ornamentation of *Angochitina multiplex* Schallreuter (1963) but is easily distinguished by shape. *B.* cf. *capitata* in the present study has a distinct restriction above the basal margin and a 'flared' basal edge unlike the holotype and is also shorter (holotype length = 366 μm) due to incomplete specimens. The specimens differ from *Belonechitina* sp. 6 (Vandenbroucke, 2005; Vandenbroucke *et al.*, 2005) in having larger, more distinct spines covering the entire vesicle surface and lacking a granular vesicle ornamentation.

Belonechitina sp. 7 *sensu* Vandenbroucke (2005)

Pl. 1.4

Material: 2 specimens; 1 poorly preserved specimen from sample TJC D953, Cwm Degwel Mudstone Member, Cwm Degwel, Cardigan area; 1 specimen from sample TJC D950, Sugar Loaf Member, Llandovery area.

Dimensions: $L : 140\mu m, Dp : 70\mu m, Dc :?, L/Dp : 2.0$.

Description: Claviform to slightly conical *Belonechitina* species with big, conical, blunt, spines, evenly distributed over the vesicle surface. There is a smooth transition from chamber to neck, and no shoulders are present. When distinguishable, the neck is short. The basal margin is slightly rounded. The maximum width is found more or less half way along the chamber.

Discussion: The specimens recovered are poorly preserved but possess both the general shape and characteristic large blunt spines of this *Belonechitina* species but because the upper region of the vesicle is missing, it is not possible to determine the characteristics of the neck.

Belonechitina reticulatus n. sp.

Pl. 9.5-7; 14-15

Belonechitina sp. 11 Vandenbroucke (2005)

Belonechitina sp. 11 Vanmeirhaeghe (2006)

Belonechitina sp. 11 Vandenbroucke *et al.* (submitted)

Deravatio nominis: From the latin *reticulum* meaning a fine network referring to the vesicle ornamentation.

Material: 21 specimens; 15 specimens from sample TJC-D1005, Lower Yr Allt Formation, Traeth Penbryn; 4 specimens from sample TJC D946, Yr Allt Formation, Llangranog, Cardigan region; 1 specimen from sample TJC D976, Garth House Formation, Garth Bank, Llandovery region; 1 specimen from sample TJC D980, Yr Allt Formation, Dolaucothi M8 core.

Dimensions: D1005, Yr Allt Formation, Traeth Penbryn: $L : 285 - 202 - 150\mu m, Dp : 120 - 96 - 80\mu m, Dc : 90 - 67 - 50\mu m, L/Dp : 2.4 - 2.1 - 1.9.(N = 15)$ D946 Yr Allt Formation, Llangranog: $L : 170 - 160 - 145\mu m, Dp : 80 - 70 - 60\mu m, Dc : 55 - 45 - 40\mu m$; Yr Allt Formation, Dolaucothi M8 core: $L : 187\mu m, Dp : 54\mu m, Dc : 52\mu m$.

Holotype: Plate 9.5 sample TJC D946-12 (British Geological Survey).

Holotype dimensions: L: 199 μm, Dp: 84 μm, Dc: 67 μm, L/Dp: 2.97.

Type stratum: Yr Allt Formation, Taeth Yr Yscland, near Llangranog, Ceredigion, west Wales, UK.

Diagnosis: A *Belonechitina* species with a claviform to steeply conical chamber and a short cylindrical neck. The vesicle wall entirely is covered by densely distributed thin coni or small spines, which may be bi-rooted and interlinking, giving characteristic a mesh-like appearance.

Description: The base is flat and the basal margin is rounded.

Discussion: This *Belonechitina* species differs from *B. robusta* in possessing interlinked spines rather than isolated λ-shaped spines. The surface ornamentation is similar to that of *Belonechitina punctata* but *B. punctata* is more claviform and has a broadly rounded base.

Belonechitina sp. 12 *sensu* Vandenbroucke (2005)

Pl. 9.13; 9.16

Material: 4 specimens; 1 specimen from Yr Allt Formation, Traeth Penbryn (TJC D1005-57), 3 specimens from sample TJC D946, Yr Allt Formation, Traeth Yr Yscland; 1 specimen from sample TJC D976, Garth House Formation, Garth Bank, Llandovery area.

Dimensions: L : $205 - 153 - 90\mu m, Dp$: $91 - 85 - 70\mu m, Dc$: $75 - 54 - 40\mu m, L/Dp$: $2.2 - 1.9 - 1.1$.

Description: A claviform *Belonechitina* species with a gentle flexure, no shoulders, little difference between Dp and Dc, a rounded base, carrying quite large, multipode and λ-shaped spines with anastomosed tops. The ornamentation is best developed on the chamber wall (Vandenbroucke, 2005).

Discussion: *Belonechitina* sp. 12 is narrower than *B. punctata* Paris (1981) and has straighter flanks lacking shoulders. *Belonechitina* sp. indet *sensu* Vanmeirhaeghe (2006) (Appendix 1, plate 14 (3) p.85) is most likely *Belonechitina* sp. 12. The specimens recovered here are more claviform than *B. robusta*. *Belonechitina* sp. 12 differs from *B. reticulatus* n. sp. in having simpler spines and a rounded base. This chitinozoan is similar to *Conochitina* sp. 2 *sensu* Achab (1987) in shape and possessing spines and cones around the base of the vesicle but is smaller in all dimensions.

Family Lagenochitinidae Eisenack (1931) emend. Paris (1981)

Subfamily Lagenochitininae Paris (1981)

Genus *Lagenochitina* Eisenack, 1931

emend. Paris, Grahn, Nestor and Lakova, 1999

Diagnosis: Lagenochitinidae with an ovoid to cylindrical glabrous chamber.

Lagenochitina cf. *ponceti* Rauscher, 1973

Pl. 15.12

Material: 2 specimens; 1 specimen from sample TJC D1020(2), Bronydd Formation, Brynffo Forest; 1 specimen from sample TJC D976, Garth House Formation, Garth Bank, Llandovery region.

Dimensions: L : $259 - 129\mu m, Dp$: $82 - 80\mu m, Dc$: $53 - 41\mu m, L/Dp$: $3.16 - 1.6$.

Description: A species of *Lagenochitina* with an ovoid chamber and a conical neck separated by a distinct flexure. The neck is approximately the same length as the chamber. The surface of the vesicle is verrucate covered in small, simple indistinct spines. See also holotype description in Paris (1981).

Discussion: The specimen recovered differ from *Lagenochitina ponceti* in having a verrucate vesicle surface.

Genus *Saharochitina* Paris *et al.* 1999

Diagnosis: Lagenochitinidae with a glabrous conical to lenticular chamber.

Saharochitina cf. *fungiformis* (Eisenack, 1931)
Pl. 1.2; Pl. 6.6

Material: 2 specimens: 1 specimen from sample TJC D941, Nantmel Mudstones Formation, Traeth y Mwnt; 1 specimen from sample TJC D957, Nantmel Mudstones Formation, LH^2, Traeth Penbryn, Cardigan region.
Dimensions: L : $129 - 92 - 65\mu m, Dp$: $70 - 59 - 53\mu m, Dc$: $38 - 28 - 21\mu m, L/Dp$: $1.9 - 1.5 - 1.2, (N = 5)$.
Description: See holotype description in Eisenack (1931).
Discussion: The recovered specimens partially lack a clear vesicle wall from poor preservation. *Fungochitina* possess granular to spiny surface ornamentation > 2 μm long whereas *Ancyrochitina* spp. possess a crown of spines around the basal edge.

Subfamily Cyathochitininae Paris (1981)
Genus *Cyathochitina* Eisenack (1955) emend. Paris *et al.* (1999a)

Diagnosis: Lagenochitinidae with a conical to hemispherical glabrous chamber and a complete membranous carina on a sharp margin.

Cyathochitina calix (Eisenack, 1931)
Pl. 1.7; Pl. 8.8; Pl. 15.9

Material: 2 specimens from sample TJC D956(17,27) Yr Allt Formation, Llangranog; 1 specimen from sample TJC D940, sandy facies, Nantmel Mudstones Formation, Cardigan region; 2 specimens from sample TJC D976, Garth House Formation, Garth Bank; 2 specimens from sample TJC D1016, Cwm Clyd Sandston Member, Brynffo Forest section, Llandovery area; 1 specimen from sample TJC D1033, Bryn Nicol Formation, Llandovery area.
Dimensions: Cardigian region L : $180 - 170 - 160\mu m, Dp$: $75 - 73 - 10\mu m, Dc$: $50 - 48 - 45\mu m, L/Dp$: $2.6 - 2.4 - 2.1.(N = 3)$ Llandovery region: L : $182 - 158 - 132\mu m, Dp$: $102 - 90 - 79\mu m, Dc$: $53 - 50 - 47\mu m, (N = 3)$
Description: See holotype description in Eisenack (1931).

Cyathochitina campanulaeformis Eisenack, 1962
Pl. 4.13-14; Pl. 8.8; Pl. 9.11; Pl. 12.2-3; Pl. 17.9

Material: 3 specimens from sample TJC D946, Yr Allt Formation, Llangranog; 8 specimens from sample TJC D979, LH^1, Nantmel Mudstones Formation, Tresaith, Cardigan region; 1 specimen from sample TJC D950, Sugar Loaf Member, Sugar Loaf road section; 1 specimen from sample TJC D972, Cilau Formation, A40 road section; 4 specimens from sample TJC D976, Garth House Formation, Garth Bank, 1 specimen from sample TJC D1015, Cwm Clyd Sandstone Member, Brynffo Forest section; 2 specimens from sample TJC D1027, Garth House Formation, Brynffo Forest section, Llandovery area.
Dimensions: Yr Allt, Llangranog: $L : 250 - 193 - 120\mu m, Dp : 120 - 106 - 85\mu m, Dc : 60 - 54 - 45\mu m, L/Dp : 2 - 1.8 - 1.2$; Nantmel Mudstones Formation, LH^1: $L : 277 - 208 - 139\mu m, Dp : 182 - 144 - 108\mu m, Dc : 86 - 65 - 52\mu m, L/Dp : 2 - 1.5 - 0.9.$; Llandovery area: $L : 189 - 145 - 132\mu m, Dp : 171 - 115 - 89\mu m, Dc : 57 - 52 - 46, L/Dp : 1.6 - 1.3 - 0.9$.
Description: See holotype description by Eisenack (1931) and neotype description by Eisenack (1962).
Comment: Those specimens with a L/Dp close to 1 are incomplete or slightly broken.

Cyathochitina cf. *campanulaeformis* Eisenack, 1962
Pl. 1.3; Pl. 12.1; Pl. 18.10-12

Material: 57 specimens; 5 specimens from sample TJC D1000. LH^1 oxic-anoxic boundary, Nantmel Mudstones Formation, oxic facies; 3 specimens from sample TJC D946, Yr Allt Formation, Llangranog, Cardigan region; 2 specimens from sample TJC D1010, LH^3, Traeth Penbryn; 1 specimen from sample TJC D949, Yr Allt Formation, Llangranog, Cardigian area: 14 specimens from sample TJC D960, 8 specimens from sample TJC D1033, Bryn Nicol Formation, 1 specimen from sample TJC D1024, Cribarth Formation, Glasallt Fawr; 1 specimen from sample TJC D1029, Garth House Formation, Brynffo Forest section; 1 specimen from sample TJC D973, Cwm Cringlyn Formation, A40 road section; 4 specimens from sample TJC D980, 10 specimens from sample TJC D984, 8 specimens from sample TJC D985, Dolaucothi M8 core, Llandovery area.
Dimensions: Cardigan area $L : 204 - 153 - 90\mu m, Dp : 152 - 114 - 80\mu m, Dc : 77 - 53 - 30\mu m, L/Dp : 1.9 - 1.3 - 0.9, (N = 7)$; Llandovery area: $L : 165 - 138 - 92\mu m, Dp : 170 - 126 - 97\mu m, Dc : 75 - 51 - 42, L/Dp : 1.6 - 1.1 - 0.7.(N = 18)$

Description: See holotype description by Eisenack (1931) and neotype description by Eisenack (1962).

Discussion: Imperfectly preserved specimens of *Cyathochitina campanulaeformis* are placed in this species. Dimension measurements may appear somewhat smaller than for *Cyathochitina campanulaeformis* due to broken vesicles.

Cyathochitina kuckersiana (Eisenack, 1934)

Pl. 8.10; Pl. 9.3; Pl. 15.10; Pl. 17.10

Material: 9 specimens; 2 specimens from sample TJC D946(6,24), Yr Allt Formation, Llangranog, Cardigan region; 3 secimens from sample TJC D976, Garth House Formation, Garth Bank; 2 specimens from sample TJC D1026, Garth House Formation, Brynffo Forest section; 2 specimens from sample TJC D1033, Bryn Nicol Formation, Llandovery region.

Dimensions: Yr Allt, Llangranog: $L : 160 - 120 - 80\mu m, Dp : 170 - 128 - 85\mu m, Dc : 60 - 55 - 50\mu m, L/Dp : 0.9 - 0.9 - 0.9.$; Llandovery region: $L : 199 - 129 - 45\mu m, Dp : 170 - 128 - 107\mu m, Dc : 71 - 47 - 30\mu m, L/Dp : 1.4 - 1.0 - 0.4.(N = 8)$

Description: See holotype description by Eisenack (1934).

Dicsussion: The specimens possess a well preserved, wide wrinkled carina diagnostic of this species.

Cyathochitina cf. *kuckersiana* (Eisenack, 1934)

Pl. 13.5

Material: 2 specimens from sample TJC D946, Yr Allt Formation, Llangranog, Cardigan region.

Dimensions: $L : 160 - 130\mu m, Dp : 170 - 90\mu m, Dc : 60 - 45\mu m, L/Dp : 2.8 - 1.4$.

Description: See holotype description in Eisenack (1934)

Discussion: Specimens with a broken carina can resemble *C. campanulaeformis.*

Cyathochitina cf. *reticulifera* Grahn, 1981

Pl. 15.11

Material: 2 specimens; 1 specimen from sample TJC D941, Nantmel Mudstones Formation, Mwnt, Cardigan region; 1 specimen from sample TJC D976, Garth House Formation, Garth Bank, Llandovery region.

Dimensions: $L : 161\mu m, Dp : 126\mu m, Dc : 61\mu m, L/Dp : 1.3$.

Description: See holotype description by Grahn (1981).

Discussion: Due to the poor preservation of these specimens, this species is kept in open nomenclature.

Subfamily Ancyrochitininae Paris (1981)
Genus *Ancyrochitina* Eisenack (1955)

Diagnosis: Lagenochitinidae with a lenticular to conical chamber bearing a crown of nonanastomosed hollow processes on the margin.

Ancyrochitina cf. *primitiva* Eisenack (1964)
Pl. 18.6-9

Material: 8 specimens from sample TJC D985, Cwmere Formation, Dolaucothi M8 core, Llandovery region.
Dimensions: L : $155 - 125 - 82\mu m, Dp$: $70 - 65 - 55\mu m, Dc38 - 28 - 19\mu m, L/Dp$: $2.2 - 1.9 - 1.3$.
Description: An *Ancyrochitina* species with a lenticular chamber and a sharp flexure defining the base of a long neck that flares aperturewards. The base is rounded and carries a set of simple spines around the basal edge. See also holotype description in Eisenack (1964).
Discussion: *Ancyrochitina ancyrea* has a similar shape but has branching spines. *Ancyrochitina merga* Jenkins, 1970 has a broader and less-rounded base.

Order Operculatifera Eisenack, 1931
Family Desmochitinidae Eisenack, 1931, emend. Paris, 1981
Subfamily Desmochitininae Paris, 1981
Genus *Bursachitina* Taugourdeau, 1966

Diagnosis: Glabrous Desmochitinidae with a conical chamber.

Bursachitina umbilicata Vandenbroucke *et al.* (2005)
Pl. 3.7-8; 3.16

Material: 23 specimens; 16 specimens from sample TJC D1014 and TJC D1013, 7 specimens from sample TJC D1015, Nantmel Mudstones Formation, LH^0, Aberporth.
Dimensions: L : $120 - 95 - 75\mu m, Dp$: $80 - 66 - 60\mu m, Dc$: $65 - 44 - 35\mu m, (N = 16)$
Description: See holotype description by Vandenbroucke *et al.* (2005).
Discussion: The specimens match the diagnosis and description given by Vandenbroucke *et al.* (2005). Some specimens appear to only have one ring on the umbilicus though this was observed on some specimens by Vandenbroucke *et al.* (2005) in the holotype assemblage. The granular wall diagnostic of this *Bursachitina* species is noted on the majority of the recovered

specimens.

Genus *Desmochitina* Eisenack, 1931

Diagnosis: Desmochitinidae with an ovoid, glabrous chamber.

Desmochitina cocca Eisenack, 1931
Pl. 8.5; Pl. 11.6

Material: 4 specimens from sample TJC-D946, Yr Allt Formation, Llangranog, Cardigan region; 2 specimens from sample TJC D952, Tridwr Formation, Sugar Loaf road section; 1 specimen from sample TJC D976, Garth House Formation, Garth Bank; 1 specimen from sample TJC D1016, Cwm Clyd Sandstone Member, Brynffo Forest section, Llandovery region.
Dimensions: Cardigan region: L : $145 - 114 - 80\mu m, Dp$: $115 - 103 - 85\mu m, Dc$: $70 - 56 - 50\mu m, L/Dp$: $1.3 - 1.1 - 0.9, (N = 5)$; Llandovery region: L : $168 - 123 - 98\mu m, Dp$: $134 - 97 - 77\mu m, Dc$: $46 - 42 - 38\mu m, L/Dp$: $1.3 - 1.27 - 1.25, (N = 4)$.
Description: See holotype description in Eisenack (1931)

Desmochitina minor Eisenack, 1931
Pl. 1.6; Pl. 8.6-7; Pl. 13.11; Pl. 17.1

Material: 64 specimens; 1 specimen from sample TJC D940, Nantmel Mudstones Formation sandy facies; 3 specimens from sample TJC-D946, Yr Allt Formation, Llangranog; 5 specimens from sample TJC D947, Cwmere Formation, '*persculptus* band', Llangranog, Cardigan region; 2 specimens from sample TJC D1023, Cribarth Formation, Glasallt Fawr; 21 specimens from sample TJC D1016, Cwm Clyd Sandstone Member; 1 specimen from sample TJC D1028; 1 specimen from sample TJC D1019, 9 specimens from sample TJC D1029, 3 specimens from sample TJC D1030, 7 specimens from sample TJC D1026, Garth House Formation; 5 specimens from sample TJC D1025, Bronydd Formation, all from the Brynffo Forest section; 1 specimen from sample TJC D960, Bryn Nicol Formation, Landovery region.
Dimensions: Cardigan region: L : $138 - 119 - 80\mu m, Dp$: $133 - 98 - 75\mu m, L/Dp$: $1.4 - 1.2 - 1, (N = 9)$; Llandovery region: L : $171 - 117 - 76\mu m, Dp$: $164 - 107 - 53\mu m, L/Dp$: $1.5 - 1.1 - 0.7, (N = 44)$.

Description: See holotype description in Eisenack (1931).
Discussion: *Desmochitina* species are diagnosed by their surface texture. The ornamentation of *Desmochitina minor* is variable from foveolate to vermiform and may constitute more than one species (Vandenbroucke, 2005).

Desmochitina erinacea Eisenack, 1931
Pl. 12.5; Pl. 15.13

Material: 3 specimens; 2 specimens from sample TJC D976, Garth House Formation, Garth Bank; 1 specimen from sample TJC D960, Bryn Nicol Formation, Llandovery region.
Dimensions: $L: 95-92-85\mu m, Dp: 97-87-75\mu m, L/Dp: 1.3-1.0-0.9, (N=3)$.
Description: A *Desmochitina* species with a spherical to ovoid chamber with spiny ornamentation covering the entire test. The aperture is slightly flaring.
Discussion: Specimens with short ($<3\mu m$; see Laufeld, 1967) spines are restricted to *D. erinacea*. *Desmochitina minor* with a pronounced granulated surface may sometimes be confused with *Desmochitina erinacea*.

Desmochitina juglandiformis Laufeld, 1967
Pl. 15.14-15; Pl. 17.2

Material: 8 specimens; 4 specimens from sample TJC D976, Garth House Formation, Garth Bank; 3 specimens from sample TJC D1029, Garth House Formation; 1 specimen from sample TJC D1025, Bronydd Formation, Brynffo Forest section, Llandovery region.
Dimensions: $L: 147-98-76\mu m, Dp: 129-93-71\mu m, L/Dp: 1.3-1.1-0.9, (N=8)$.
Description: See holotype description in Laufeld (1967).
Discussion: The specimens are identical to the holotype, in particular, they possess the long, conical operculum with membranous flange and an outer wrinkled membranous surface texture.

Genus: *Eisenackitina* Jansonius, 1964

Diagnosis: Desmochitinidae with an ovoid chamber and randomly-distributed spiny ornamentation.

Eisenackitina inconspicua Vandenbroucke *et al.* (2004)
Pl. 16.9; Pl. 17.5

Material: 3 specimens: 2 specimens from sample TJC D976, Garth House Formation, Garth Bank; 1 specimen from sample TJC D1016, Cwm Clyd Sandstone Member, Brynffo Forest section, Llandovery region.
Dimensions: $L: 137-119\mu m, Dp: 77-76\mu m, Dc: 54-40\mu m, L/Dp: 1.8-1.5., (N=2)$
Description: See holotype description in Vandenbroucke *et al.* (2004).

Eisenackitina cf. *rhenana* Eisenack, 1939
Pl. 17.3-4

Material: 2 specimens from sample TJC D1016, Cym Clyd Sandstone Member, Brynffo Forest section.
Dimensions: $L: 128-107\mu m, Dp: 76-67\mu m, Dp: 56-51\mu m, L/Dp: 1.9-1.4.$
Description: See holotype description in Eisenack (1939).
Discussion: The specimens recovered are tentatively assigned to this species as flattening distorts the flanks and the diagnostic 'S'-shaped walls are difficult to distinguish.

Plate 1. Chitinozoans from Cwm Degwel to Mwnt, Cwm Degwel Formation - Nantmel Mudstones Formation, oxic facies. L, Dp, Dc. All dimensions in microns. Abbreviations following Paris (1981): L= total length, Dp=chamber diameter, Dc=diameter of oral tube.

1. *Sphaerochitina* sp. indet (116, 42, 33; TJC D941-6).
2. *Saharochitina* cf. *fungiformis.* (72, 57, 28; TJC D941-2).
3. *Cyathochitina* cf. *campanulaeformis* (69, 96, 25; TJC D953-12).
4. *Belonechitina* ?sp. 7 (143, 70, -; TJC D953-18).
5. *Hercochitina* sp. indet (155, 58, -; TJC D953-29).
6. *Desmochitina minor* (101, 106, 31; TJC D940-2).
7. *Cyathochitina calix* (202, 82, 48; TJC D940-1).
8. *Tanuchitina ?bergstroemi* (201, 65, 39; TJC 1006-12).
9. Detail of carina of 8, ×1419.

Plate 2.1: Chitinozoans from Cwm Degwel to Mwnt, Cwm Degwel Formation - Nantmel Mudstones Formation, oxic facies.

Plate 2. Chitinozoans from Mwnt to Aberporth, Nantmel Mudstones Formation, oxic facies. L, Dp, Dc. All dimensions in microns. Abbreviations following Paris (1981): L= total length, Dp=chamber diameter, Dc=diameter of oral tube.

1. *Spinachitina penbryniensis* n. sp. (300, 62, 39; TJC D943-18).
2. *Spinachitina* cf. *fossensis* (123, 61, 25; TJC D943-92).
3. *Spinachitina* cf. *fossensis* (163, 77, 52; TJC D943-93).
4. *Spinachitina* cf. *fossensis* (96, 57, 40; TJC D943-97).
5. *Spinachitina* cf. *fossensis* (98, 59, 39; TJC D943-70).
6. *Hercochitina minuta* (101, 60, 47; TJC D943-30).
7. *Hercochitina* aff. *grandispina* (156, 57, 43; TJC D943-11).
8. *Hercochitina* aff. *grandispina*(139, 50, 36; TJC D943-22).
9. *Tanuchitina bergstroemi* (371, 77, 45; TJC D942-8).
10. *Tanuchitina ?bergstroemi* (152, 48, 30; TJC D943-55).
11. *Hercochitina* sp. indet. (192, 73, 45; TJC D942-3).
12. *Belonechitina ?americana* (132, 64, 49; TJC D942-13).
13. *Belonechitina ?americana* (164, 78, 49; TJC D-943-91).
14. Detail of basal edge of 7 showing thickened vertical ridge ornamentation ×1868.
15. Detail of basal margin of 6 showing vertical ridge ornamentation ×1469.

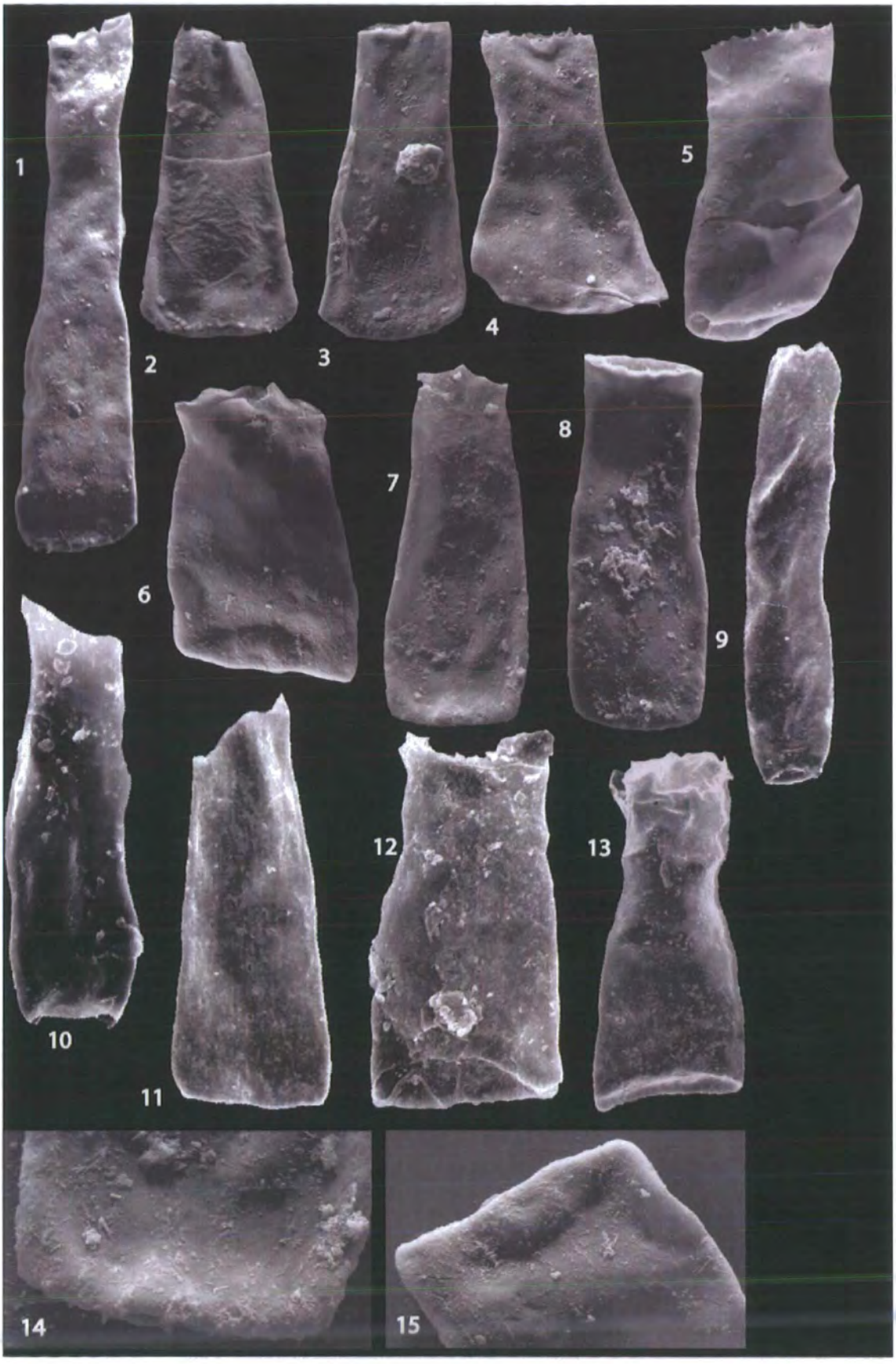

Plate 2.2: Chitinozoans from Mwnt to Aberporth, Nantmel Mudstones Formation, oxic facies.

Plate 3. Chitinozoans from laminated hemipelagite 0 (LH^0), Nantmel Mudstones Formation, Aberporth. L, Dp, Dc. All dimensions in microns. Abbreviations following Paris (1981): L= total length, Dp=chamber diameter, Dc=diameter of oral tube.

1. *Belonechitina ceredigionensis* (155, 50, 35: TJC D1015-St1-13)
2. Detail of base of 1.
3. *Hercochitina* cf. *crickmayi* (170, 75, 50; TJC D1015-St1-22).
4. *Hercochitina* cf. *crickmayi* (240, 85, 55; TJC D1013-27).
5. *Hercochitina* cf. *crickmayi* (175, 70, 45; TJC D1013-40).
6. *Hercochitina ?turnbulli* (170, 110, 60; TJC D1015-St2-8).
7. *Bursachitina umbilicata* (75, 75, 55; TJC D1015-St2-13).
8. *Bursachitina umbilicata* (105, 70, 45; TJC D1013-8).
9. *Spinachitina* cf. *fossensis* (145, 85, 55; TJC D1013-23).
10. *Rhabdochitina ?gracilis* (340, 70, 40; TJC D1015-St1-3).
11. *Hercochitina* spp. (150, 95, 50; TJC D1013-22).
12. *Spinachitina* cf. *fossensis* (180, 65, 40; TJC D1013-16).
13. *Hercochitina* spp. (190, 60, 35; TJC D1013-18).
14. *Belonechitina* spp. (240, 80, 70; TJC D1013-1).
15. Detail of base of 4, ×4500.
16. Detail of umbilicus of 8, ×1600.

Plate 2.3: Chitinozoans from laminated hemipelagite 0 (LH^0), Nantmel Mudstones Formation, Aberporth.

Plate 4. Chitinozoans from the laminated hemipelagite 1 (LH^1), Nantmel Mudstones Formation, Traeth Penbryn. L, Dp, Dc. All dimensions in microns. Abbreviations following Paris (1981): L= total length, Dp=chamber diameter, Dc=diameter of oral tube.

1. *Ancyrochitina* sp. (139, 116, 48; TJC D967-2).
2. *Ancyrochitina* sp. (95, 56, 28; TJC D967-8).
3. *Hercochitina* sp. 1 *sensu* Vanmeirhaeghe (2006) (177, 55, 28; TJC D967-1).
4. *Spinachitina* sp. 2 *sensu* Vandenbroucke (2005) (166, 80, 39; TJC D967-5).
5. *Spinachitina* sp. A *sensu* Vanmeirhaeghe (2006) (166, 54, 28; TJC D967-3).
6. *Spinachitina* sp. 2 *sensu* Vandenbroucke (2005) (89, 51, 28; TJC D967-4)
7. *Hercochitina* sp. (122, 77, 41; TJC D967-6).
8. *Spinachitina* sp. 4 *sensu* Vandenbroucke (2005) (103, 103, 75; TJC D979-106).
9. *Spinachitia fossensis* (121, 72, 50; TJC D979-66).
10. *Spinachitia fossensis* (155, 73, 43; TJC D979-85).
11. *Spinachitina coronata* (310, 59, 51; TJC D979-25).
12. *Spinachitina coronata* (263, 60, 38; TJC D979-73).
13. *Cyathochitina campanulaeformis* (239, 127, 59; TJC D979-61).
14. *Cyathochitina campanulaeformis* (139, 145, 58; TJC D979-193).
15. *Cyathochitina* sp. indet (130, 90, 52; TJC D979-58).
16. *Hercochitina* aff. *gamachiana* (135, 91, 50; TJC D979-92).
17. *Hercochitina* sp. indet. (135, 98, 54; TJC D979-127).
18. *Hercochitina* cf. *crickmayi* (189, 56, 48; TJC D979-59).
19. *Hercochitina* cf. *seriespinosa* (175, 100, 65; TJC D979-41).
20. *Hercochitina* aff. *normalis* (153, 77, 53; TJC D979-18).

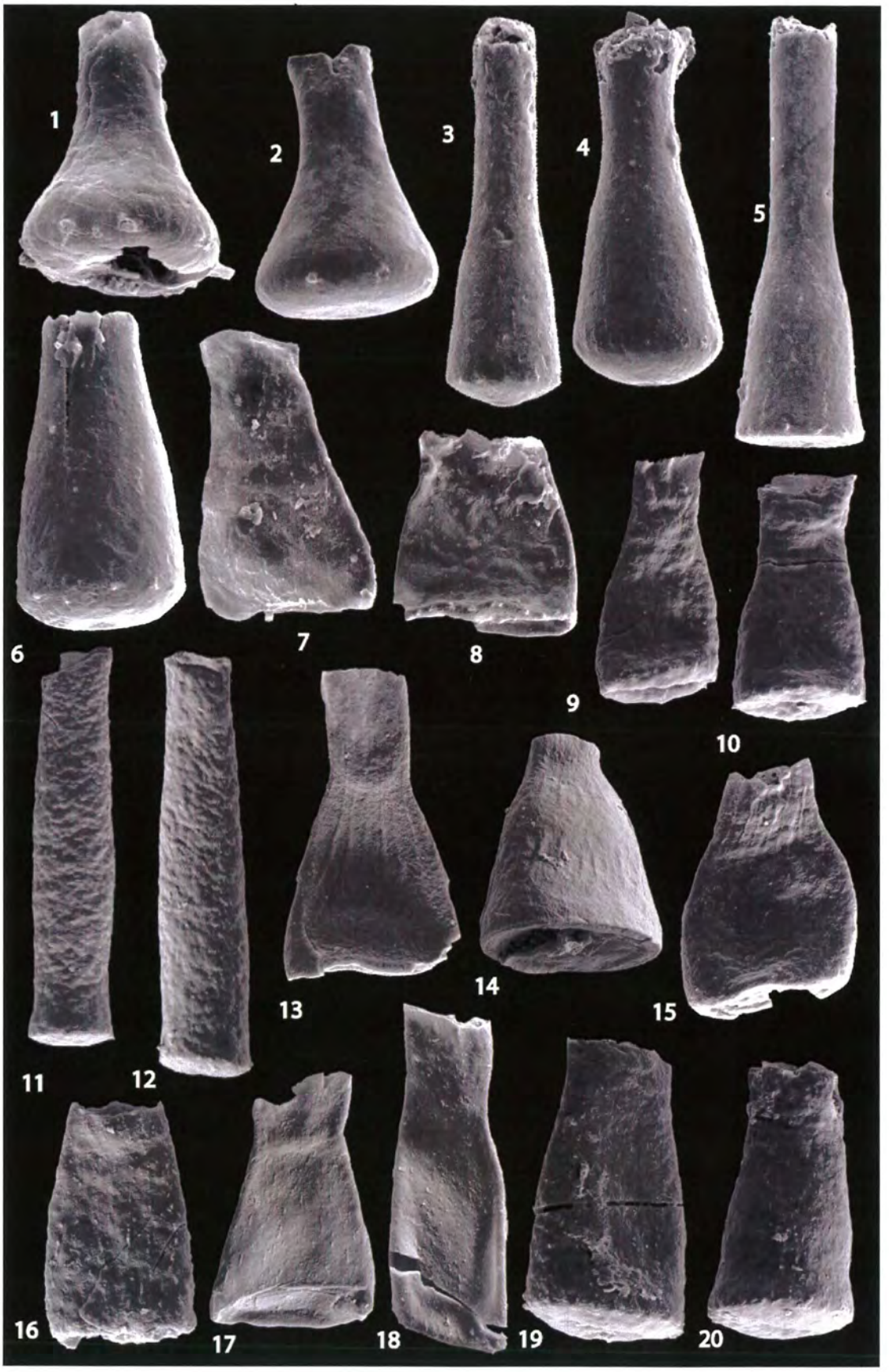

Plate 2.4: Chitinozoans from the laminated hemipelagite 1(LH^1), Nantmel Mudstones Formation, Traeth Penbryn.

Plate 5. Chitinozoans from laminated hemipelagite 1 (LH^1) anoxic facies and oxic facies between LH^1 and LH^2, Nantmel Mudstones Formation, Traeth Penbryn. L, Dp, Dc. All dimensions in microns. Abbreviations following Paris (1981): L= total length, Dp=chamber diameter, Dc=diameter of oral tube.

1. *Spinachitina penbryniensis* n. sp. holotype (280, 60, 40; TJC D1013-19).
2. *Spinachitina penbryniensis* n. sp. (366, 56, 40; TJC D979-117).
3. *Spinachitina penbryniensis* n. sp. (263, 56, 44; TJC D979-74).
4. *Spinachitina penbryniensis* n. sp. (258, 56, 40; TJC D979-53).
5. *Spinachitina penbryniensis* n. sp. (324, 73, 51; TJC D979-22).
6. Detail of basal edge of 4 .
7. Detail of spines on basal edge of 2 ×1672.
8. *Ancyrochitina* spp. (106, 64, 22; TJC D979-105).
9. *Hercochitina* aff. *seriespinosa* (126, 79, 40; TJC D979-143).
10. *Hercochitina* aff. *seriespinosa* (161, 98, 54; TJC D979-21).
11. *Conochitina homoclaviformis* (260, 97, 67; TJC D979-109).
12. *Conochitina homoclaviformis*(204, 59, 43: TJC D979-30).
13. *Hercochitina* sp. indet (162, 75, 43; TJC D955-2).
14. *Hercochitina* cf. *normalis* (141, 96, 52; TJC D955-38).
15. *Hercochitina* cf. *normalis* (153, 73, 44; TJC D955-7).

Plate 2.5: Chitinozoans from laminated hemipelagite 1 (LH^1) anoxic facies and oxic facies between LH^1 and LH^2, Nantmel Mudstones Formation, Traeth Penbryn.

Plate 6. Chitinozoans from oxic facies between LH^1 and LH^2 and from LH^2, Nantmel Mudstones Formation, Traeth Penbryn. L, Dp, Dc. All dimensions in microns. Abbreviations following Paris (1981): L= total length, Dp=chamber diameter, Dc=diameter of oral tube.

1. *Hercochitina ?minuta* (95, 69, 46; TJC D968-19) oxic facies.
2. *Tanuchitina* sp. (136, 54, -; TJC D968-25).
3. *Hercochitina* sp. A (207, 94, 50; TJC D968).
4. *Conochitina* sp. indet (186, 93, -; TJC D968-22).
5. *Conochitina homoclaviformis* (128, 52, 39; TJC D968-20).
6. *Saharochitina* cf. *fungiformis* (65, 56, 27; TJC D957-5).
7. *Spinachitina* sp. (113, 66, 18; TJC D957-65).
8. *Conochitina* sp. indet (146, 68, 58; TJC D957-12).
9. *Hercochitina* sp. indet. (162, 54, 31; TJC D957-60).
10. *Hercochitina* sp. indet. (151, 53, 40; TJC D957-61).

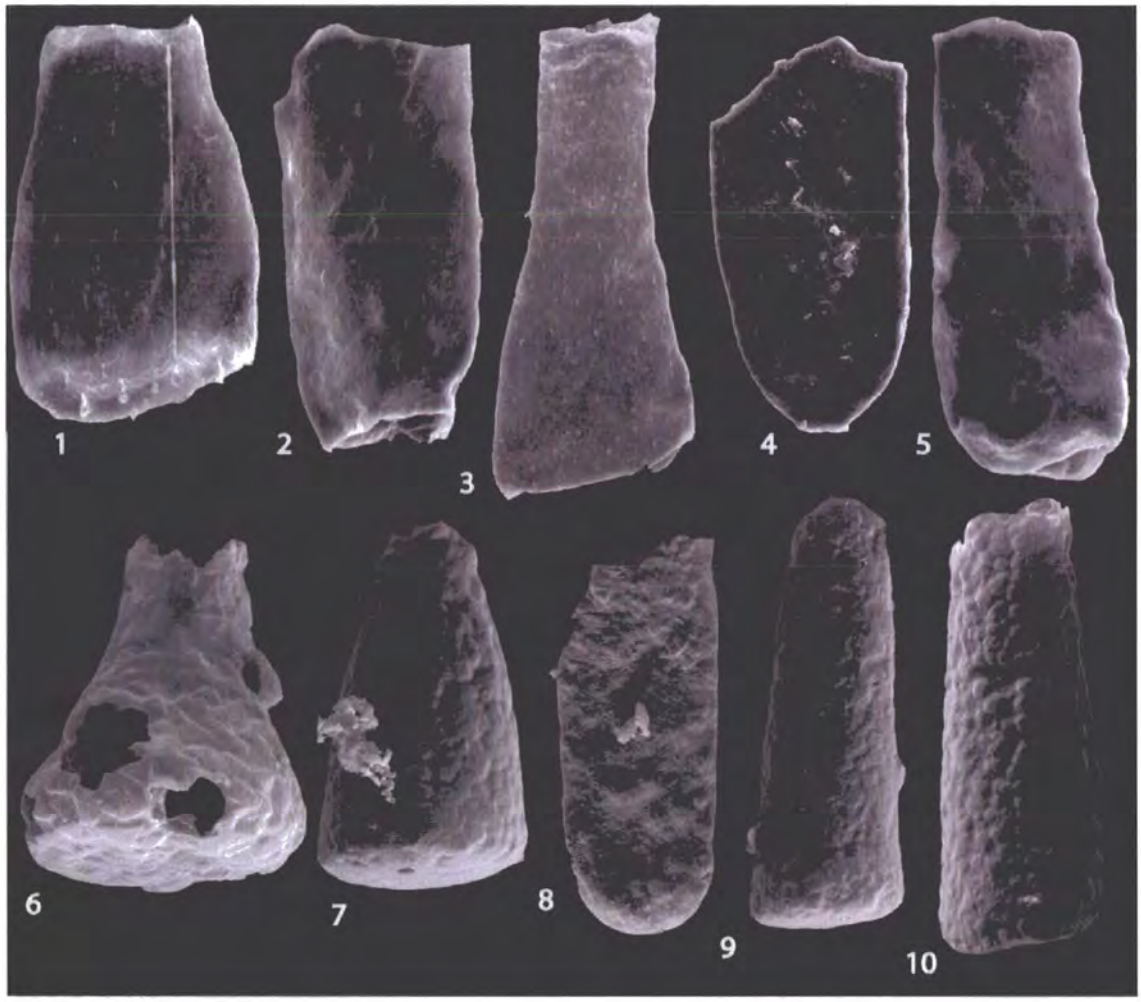

Plate 2.6: Chitinozoans from oxic facies between LH^1 and LH^2 and from LH^2, Nantmel Mudstones Formation, Traeth Penbryn.

Plate 7. Chitinozoans from laminated hemipelagite 3 (LH^3), Nantmel Mudstones Formation, Traeth Penbryn. L, Dp, Dc. All dimensions in microns. Abbreviations following Paris (1981): L= total length, Dp=chamber diameter, Dc=diameter of oral tube.

1. *Hercochitina* aff. *normalis* (100, 85, 40; TJC D1010-11).
2. *Spinachitina coronata* (160, 60, 40; TJC D1010-19).
3. *Tanuchitina* sp. (190, 75, 65; TJC D1010-18).
4. *Ancyrochitina* sp. (95, 70, 20; TJC D1010-22).
5. *Conochitina* sp. (200, 60, 40; TJC D1010-1).
6. *Hercochitina* sp. A (210, 100, 60; TJC 1010-2).
7. *Spinachitina* aff. *penbryniensis* (145, 30, 50; TJC D1010-35).
8. *Hercochitina* cf. *gamachiana* (161, 71, 45; TJC D956-22).
9. *Hercochitina* sp. II (98, 64, 59; TJC D959-21).
10. Detail of basal margin of 7 illustrating spines above basal edge, ×2200.

Plate 2.7: Chitinozoans from laminated hemipelagite 3 (LH^3), Nantmel Mudstones Formation, Traeth Penbryn.

Plate 8. Chitinozoans from the Yr Allt Formation, Llangranog. L, Dp, Dc. All dimensions in microns. Abbreviations following Paris (1981): L= total length, Dp=chamber diameter, Dc=diameter of oral tube.

1. *Belonechitina ceredigionensis* n. sp. (250, 90, 70; TJC D1005-20).
2. *Belonechitina ceredigionensis* n. sp. (180, 80, 60; TJC D1005-38).
3. *Belonechitina ceredigionensis* n. sp. (250, 80, 70; TJC D1005-65).
4. *Belonechitina ceredigionensis* n. sp. (270, 70, 60; TJC D1005-1).
5. *Desmochitina cocca* (120, 110, 50: TJC D946-39).
6. *Desmochitina minor* (95, 85, 35: TJC D946-1).
7. *Desmochtina minor* (105, 75, 50: TJC D946-3).
8. *Cyathochitina campanulaeformis* (120, 100, 50; TJC D946-29).
9. *Cyathochitina calix* (160, 75, 45; TJC D946-17).
10. *Cyathochitina kuckersiana* (160, 170, 60; TJC D946-24).
11. *Hercochitina* cf. *seriespinosa* (100, 80,45; TJC D946-36).
12. *Laufeldochitina sp.* (190, 65, 30; TJC D946-32).
13. *Belonechitina ceredigionensis* n. sp. Detail of basal edge of 1 showing simple dense simple spines becoming smaller up vesicle, ×950.
14. *Belonechitina ceredigionensis* n. sp. Detail of basal edge of 4, ×1200.
15. *Belonechitina ceredigionensis* n. sp. Detail of base of 4 showing simple spines and ?mucron structure, ×1400.

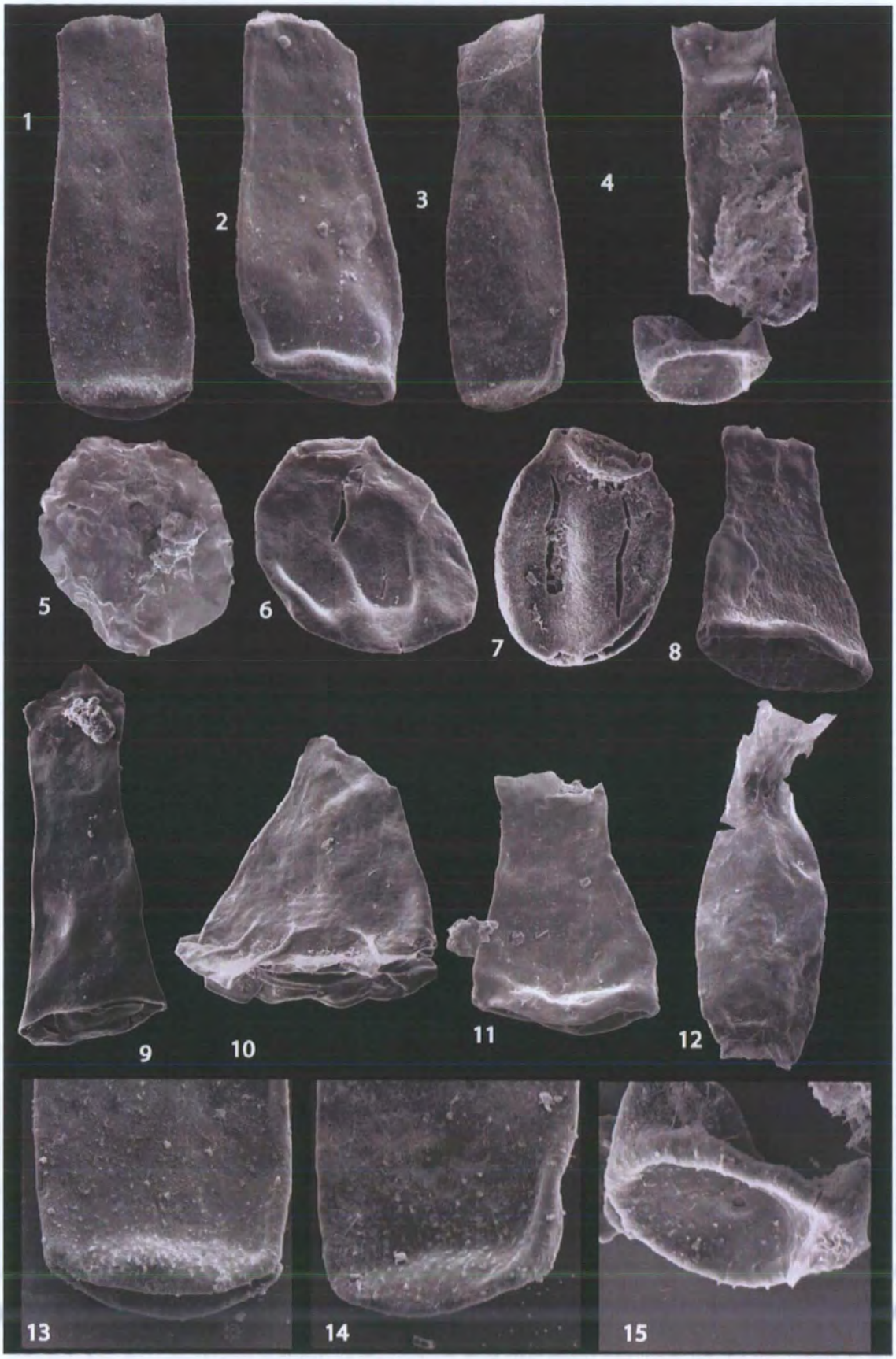

Plate 2.8: Chitinozoans from the Yr Allt Formation, Llangranog.

Plate 9. Chitinozoans from the Yr Allt Formation, Llangranog. L, Dp, Dc. All dimensions in microns. Abbreviations following Paris (1981): L= total length, Dp=chamber diameter, Dc=diameter of oral tube.

1. *Laufeldochitina lardeuxi* (174, 41, 52?; TJC D946-19).
2. *Laufeldochitina lardeuxi* (161, 57, 46; TJC D946-50).
3. *Cyathochitina kuckersiana* (105, 111, 57; TJC D946-26).
4. *Belonechitina ?wessenbergensis* (115, 74, 51; TJC D946-31).
5. *Belonechitina reticulatus* n. sp. (199, 84, 67; TJC D946-12).
6. *Belonechitina reticulatus* n. sp. (148, 81, 60?; TJC D946-29).
7. *Belonechitina reticulatus* n. sp. (163, 63, 34; TJC D946-45).
8. *Belonechitina* sp. (127, 70, 51; TJC D946-11).
9. *Belonechitina* sp. (119, 61, 49; TJC D946-15).
10. *Spinachitina* sp. (149, 80, 42; TJC D946-17).
11. *Spinachitina* sp. (99, 56, 34?; TJC D946-29).
12. *Cyathochitina campanulaeformis* (149, 80, 42; TJC D946-9).
13. *Belonechitina* sp. 12 *sensu* Vandenbroucke, 2005 (189, 54, 44; TJC D946-22).
14. *Belonechitina reticulatus* n. sp. Detail of surface of 5 showing 'lacy mesh-work' texture, ×1568.
15. *Belonechitina reticulatus* n. sp. Detail of surface texture of 7, ×4978.
16. Detail of surface spines of 13, ×3576.

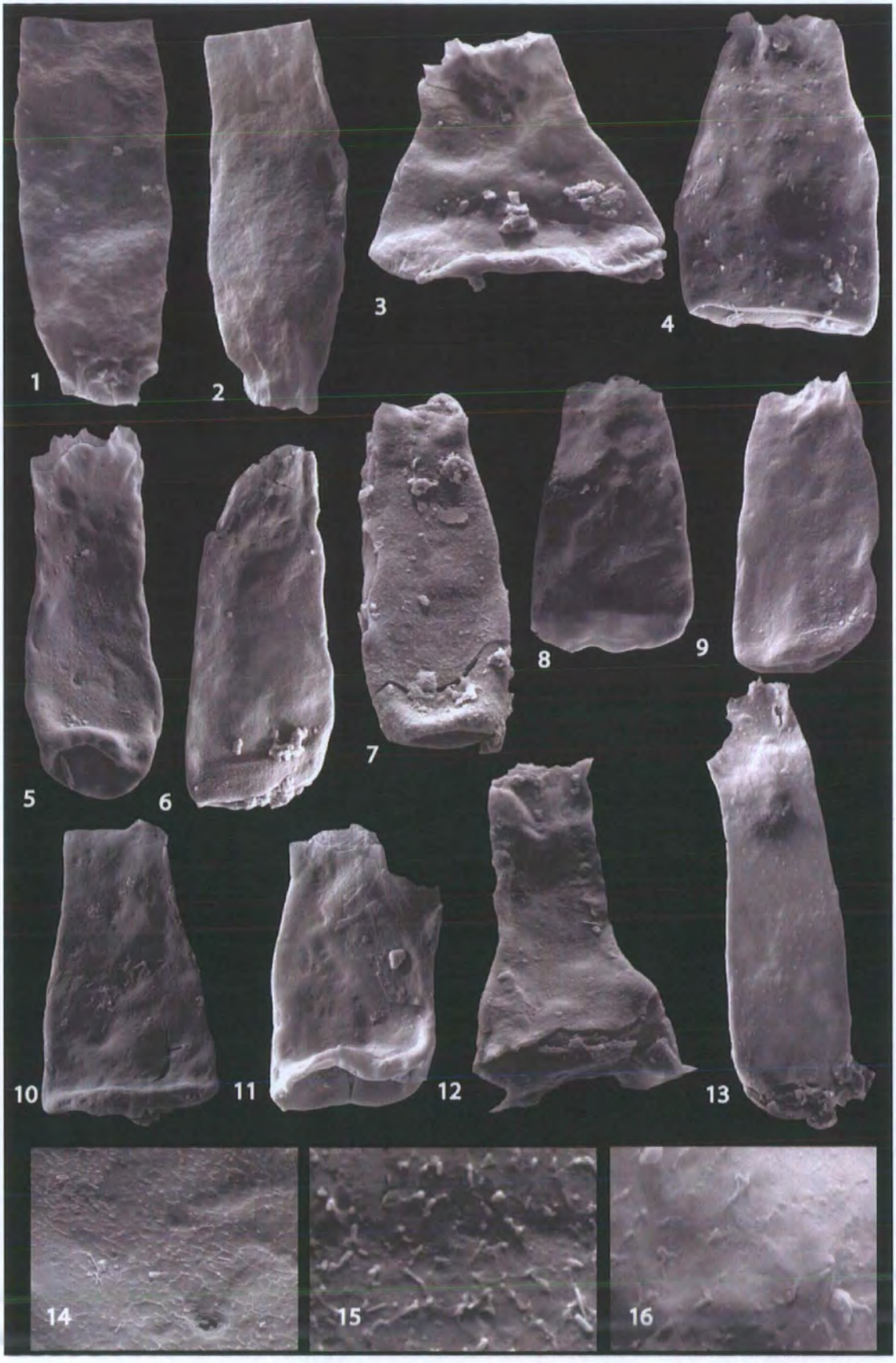

Plate 2.9: Chitinozoans from the Yr Allt Formation, Llangranog.

Plate 10. Chitinozoans from the Yr Allt Formation and Cwmere Formation, Llangranog. L, Dp, Dc. All dimensions in microns. Abbreviations following Paris (1981): L= total length, Dp=chamber diameter, Dc=diameter of oral tube.

1. *Saharochitina* sp. indet. (50, 56, 27; TJC D949-6).
2. *Saharochitina* sp. indet. (78, 53, 38; TJC D949-9).
3. *Saharochitina* sp. indet. (129, 54, 19; TJC D949-11).
4. *Saharochitina* sp. indet. (105, 50, 20; TJC D949-8).
5. *Belonechitina* sp. indet (171, 81, 53; TJC D948-23).
6. *Desmochitina minor* (100, 128, 53; TJC D947-22). Obliquely flattened specimen. Aperture evident as diagonal line to right of centre.
7. *Desmochitina minor* (118, 64, -; TJC D947-24).

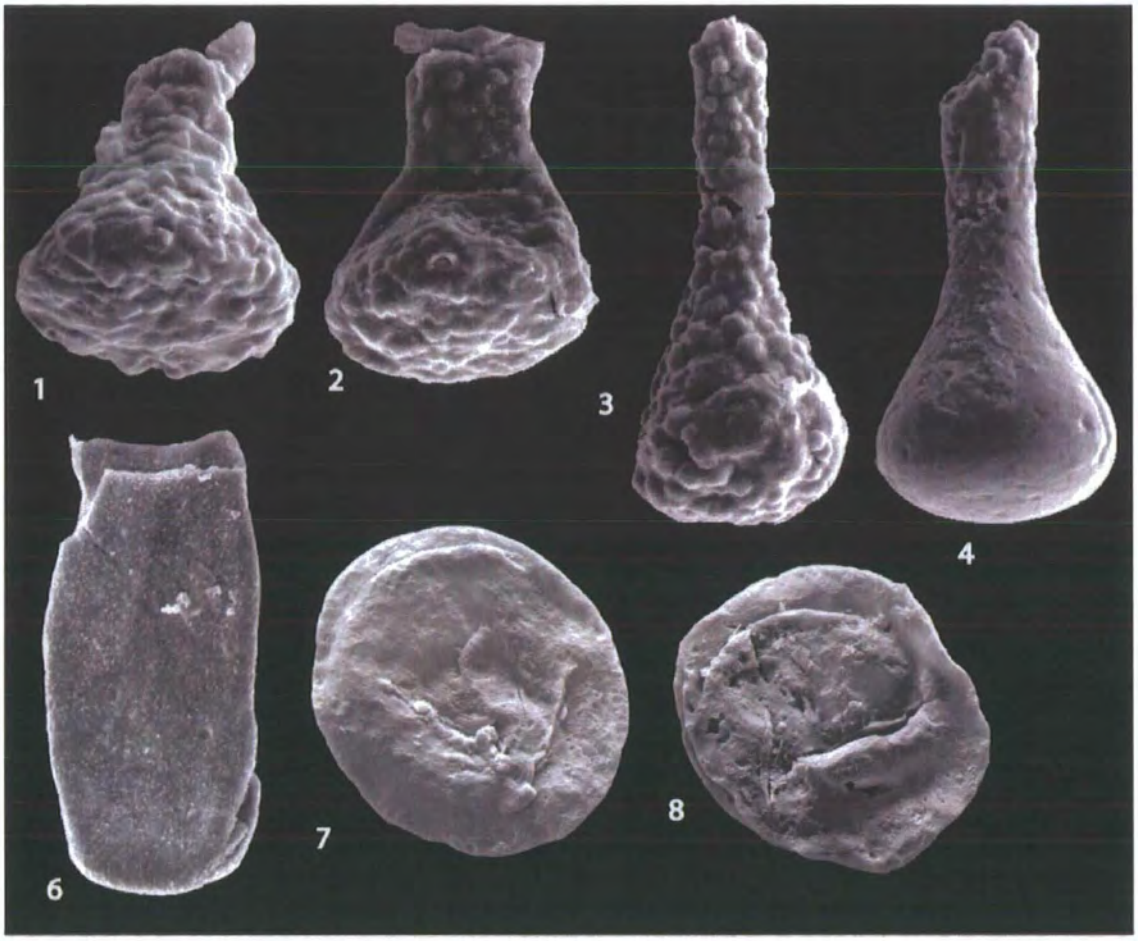

Plate 2.10: Chitinozoans from the Yr Allt Formation and Cwmere Formation, Llangranog.

Plate 11. Chitinozoans from the Sugar Loaf road cutting section; Sugarloaf Member, Nantmel Mudstones Formation and Tridwr Formation. L, Dp, Dc. All dimensions in microns. Abbreviations following Paris (1981): L= total length, Dp=chamber diameter, Dc=diameter of oral tube.

1. *Belonechitina* sp. 7 *sensu* (Vandenbroucke, 2005) (245, 82, 62; TJC D950-12).
2. *Laufeldocitina* sp. indet. (128, 78, ?; TJC D950-2).
3. *Conochitina* sp. I fragment (187?, 99, ?; TJC D950-5).
4. *Conochitina* sp. I fragment (144?, 78, 72?; TJC D952-27).
5. *Conochitina homoclaviformis* (239, 85, 59; TJC D952-1).
6. *Desmochitina cocca* (117, 93, 38; TJC D952-42).
7. *Hercochitina* aff. *seriespinosa* (139, 68, 41; TJC D952-38).
8. *Spinachitina* cf. *bulmani* (104, 73, 41; TJC D952-16).
9. Detail of 1,×2496.
10. Detail of 2, ×1387.

Plate 2.11: Chitinozoans from the Sugar Loaf road cutting section; Sugarloaf Member, Nantmel Mudstones Formation and Tridwr Formation.

Plate 12. Chitinozoans from laminated hemipelagite, Nantmel Mudstones Formation, Bryn Nicol Type section. L, Dp, Dc. All dimensions in microns. Abbreviations following Paris (1981): L= total length, Dp=chamber diameter, Dc=diameter of oral tube.

1. *Cyathochitina* cf. *campanulaeformis* (100, 125, 55; TJC D960-22).
2. *Cyathochitina campanulaeformis* (120, 110, 55; TJC D960-17).
3. *Cyathochitina campanulaeformis* (180, 160, 60; TJC D960-21).
4. *Ancyrochitina* sp. (115, 75, 40; TJC D960-4).
5. *Desmochitina erinacea* (85, 90, 50; TJC D960-23).
6. *Spinachitina* cf. *fossensis* (95, 70, 40; TJC D960-2).
7. *Spinachitina* cf. *bulmani* (105, 75, 45; TJC D960-7).
8. *Hercochitina* sp. (145, 65, 40; TJC D960-15).
9. *Saharochitina* sp. indet. (101, 67, 32; TJC D958-20).
10. *Spinachitina* cf. *bulmani* (142, 79, 53; TJC D959-29).
11. *Hercochitina* aff. *normalis* (151, 85, 63; TJC D959-26).
12. *Hercochitina* cf. *seriespinosa* (145, 78, 49; TJC D959-39).
13. Detail of basal edge of 10 showing projecting spines from basal spines, ×1542.
14. *Hercochitina* sp. indet (159, 102, 58; TJC D959-28).
15. *Hercochitina* sp. indet (152, 90, 58; TJC D959-34).

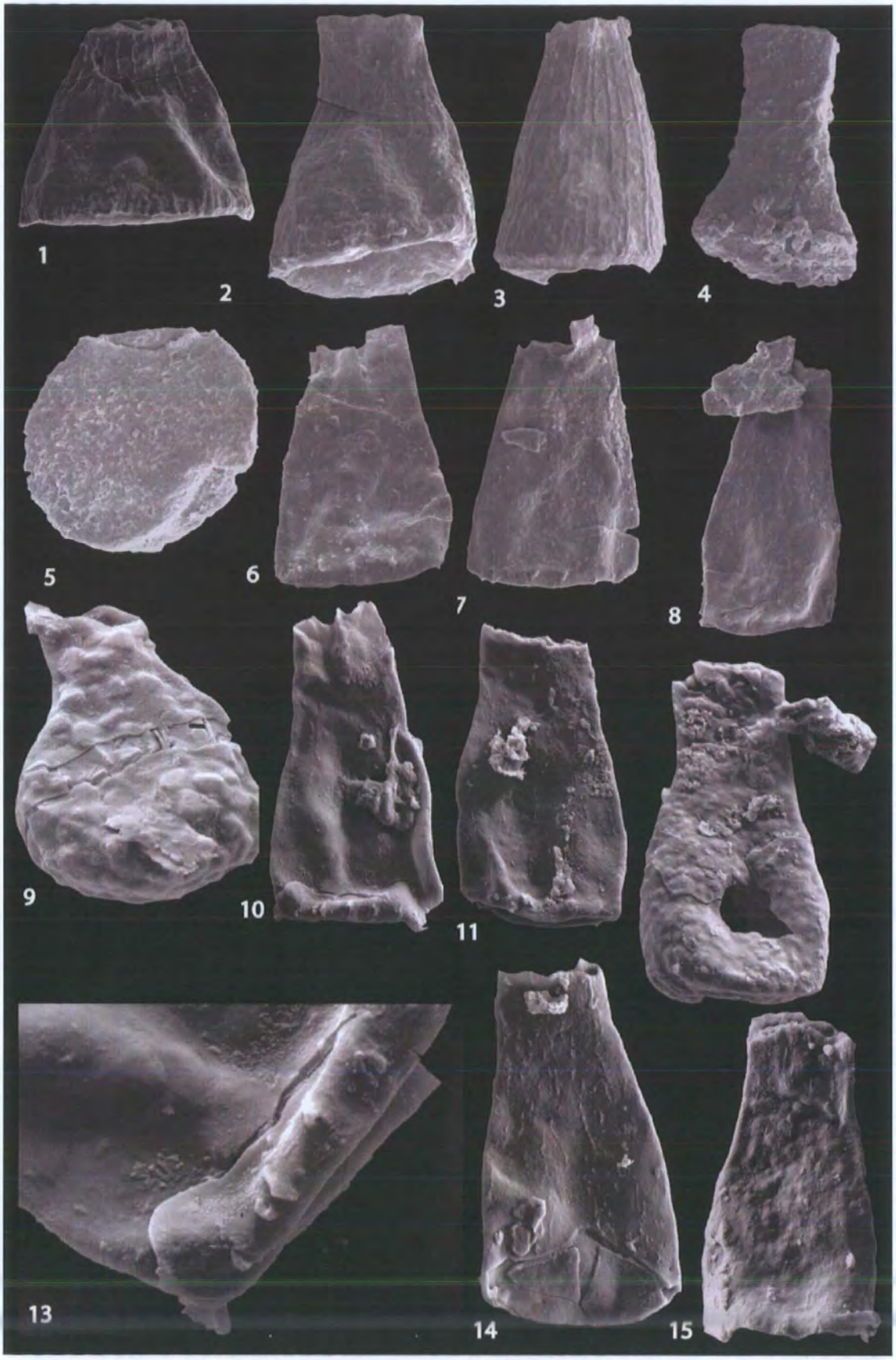

Plate 2.12: Chitinozoans from laminated hemipelagite, Nantmel Mudstones Formation, Bryn Nicol Type section.

Plate 13. Chitinozoans from Nantmel Mudstones Formation, Pen Derlwyn facies and Coed Ifan facies, Bryn Nicol Type section, Llandovery region. L, Dp, Dc. All dimensions in microns. Abbreviations following Paris (1981): L= total length, Dp=chamber diameter, Dc=diameter of oral tube.

1. *Laufeldochitina* sp. indet. (302, 78, 59; TJC D1031-3).
2. *Spinachitina fossensis* (143, 76, 38; TJC D1033-4).
3. *Spinachitina fossensis* (99, 78, 44; TJC D1033-30).
4. *Spinachitina fossensis* (154, 77, 38; TJC D1033-39).
5. *Cyathochitina* cf. *kuckersiana* (186, 132, 30; TJC D1033-36).
6. *Hercochitina* cf. *crickmayi* (121, 70, 33; TJC D1033-20).
7. *Hercochitina* cf. *crickmayi* (166, 86, 46; TJC D1033-33).
8. *Hercochitina* aff.*normalis* (133, 73, 41; TJC D1032-6).
9. *Ancyrochitina* sp. indet. (67, 76, 34; TJC D1031-12).
10. *Saharochitina* sp. indet. (73, 69, 33; TJC D1031-2).
11. *Desmochitina minor* (76, 57, 27 and 81, 53, 32; TJC D1031-7, 8).
12. Detail of basal copula of 1, ×1088.
13. Detail of apertural crown of 2, ×2052.
14. Detail of basal edge showing basal spines of 4, ×1455.

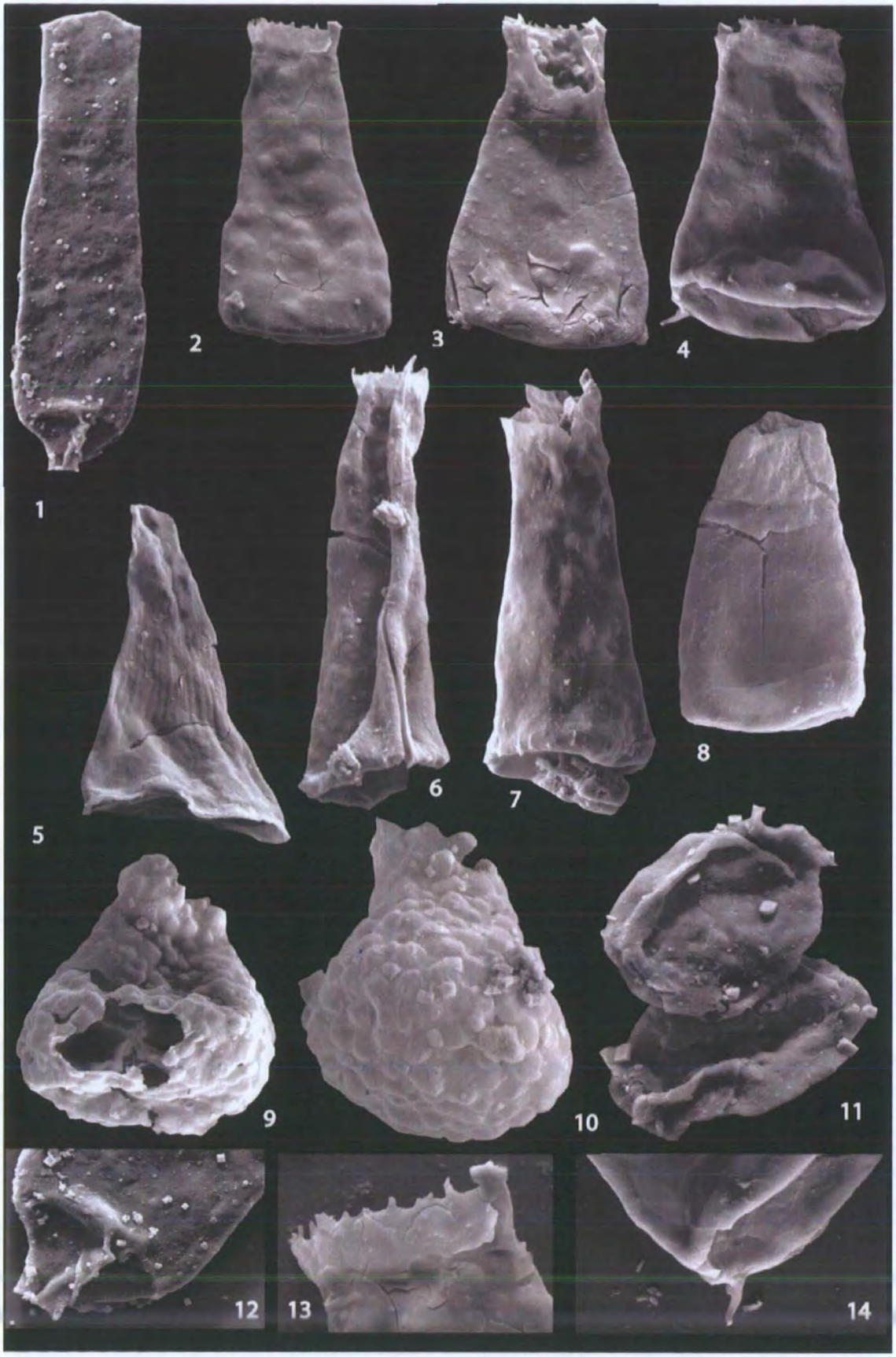

Plate 2.13: Chitinozoans from Nantmel Mudstones Formation, Pen Derlwyn facies and Coed Ifan facies, Bryn Nicol Type section, Llandovery region.

Plate 14. Chitinozoans from the Cribarth Formation, Glasallt Fawr, Rawtheyan (late Katian). L, Dp, Dc. All dimensions in microns. Abbreviations following Paris (1981): L= total length, Dp=chamber diameter, Dc=diameter of oral tube.

1. *Belonechitina ?capitata* (251, 87, 73: TJC D977-50).
2. *Belonechitina ?capitata* (236, 78, 56; TJC D977-4).
3. *Belonechitina ?capitata* (206, 74, 46; TJC D977-17).
4. *Hercochitina* sp. 1 *sensu* Vanmeirhaeghe (2006) (213, 71, 39; TJC D977-52).
5. *Hercochitina* sp. 1 *sensu* Vanmeirhaeghe (2006) (127?, 84, ?; TJC D977-42).
6. *Hercochitina* sp. 1 *sensu* Vanmeirhaeghe (2006) (189, 52, 38; TJC D977-57).
7. *Hercochitina* sp. 1 *sensu* Vanmeirhaeghe (2006) (127, 61, 32; TJC D1024-7).
8. *Hercochitina* cf. *crickmayi* (183, 58, 49; TJC D977-53).
9. *Belonechitina ?robusta* (150, 63, 36; TJC D1023-4).
10. *Hercochitina* cf. *gamachiana* (156, 86, 61; TJC D1024-1).
11. *Spinachitina coronata* (266, 81, 58; TJC D1024-2).
12. *Spinachitina coronata* (143?, 99, 67?; TJC D1024-6).
13. Detail of cones around basal edge of 9, ×2095.
14. Detail of basal spines of 11, ×2327.
15. Detail of 4 showing λ-shaped spines, ×1904.

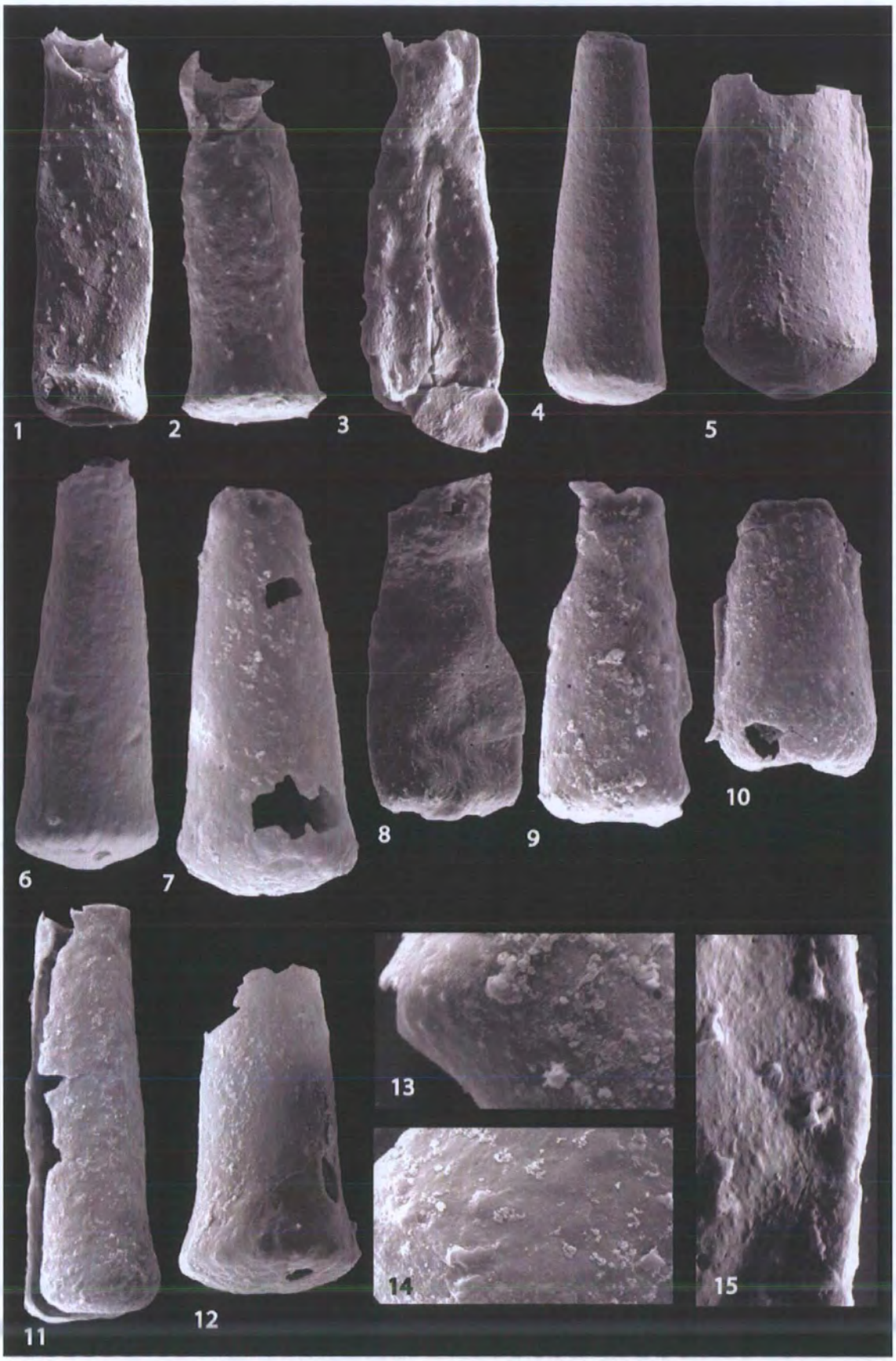

Plate 2.14: Chitinozoans from the Cribarth Formation, Glasallt Fawr, Rawtheyan (late Katian).

Plate 15. Chitinozoans from the Ciliau Formation, Garth House Formation and Yr Allt Formation, Garth House, Llandovery and Llyn Brianne, Llandovery region. L, Dp, Dc. All dimensions in microns. Abbreviations following Paris (1981): L= total length, Dp=chamber diameter, Dc=diameter of oral tube.

1. *Laufeldochitina* sp. (101?, 71, ?; TJC D971-40).
2. *Spinachitina* sp. (94, 78, 37; TJC D971-20).
3. *Belonechitina* cf. *wessenbergensis* (119?, 77, 57?; TJC D974-1).
4. *Conochitina* ? *homoclaviformis* (143?, 89, ?; TJC D974-11).
5. *Lagenochitina* sp. indet (122?, 64, ?; TJC D975-19).
6. *Spinachitina* sp. indet (122, 80, 46; TJC D975-15).
7. *Spinachitina* sp. indet (106, 66, 30; TJC D975-21).
8. *Bursachitina* sp. indet (195, 101, 74; TJC D976-195).
9. *Cyathochitina calix* (180, 159, 79; TJC D976-180).
10. *Cyathochitina kuckersiana* (160, 170, 71TJC D976-149).
11. *Cyathochitina* cf. *reticulatusfera* (161, 126, 61; TJC D976-125).
12. *Lagenochitnia* cf. *ponceti* (259, 82, 53; TJC D976-45).
13. *Desmochitina erinacea* (95, 75, 58; TJC D976-133).
14. *Desmochitina juglandiformis* (92, 90, 45; TJC D976-213).
15. *Desmochitina juglandiformis* chain.

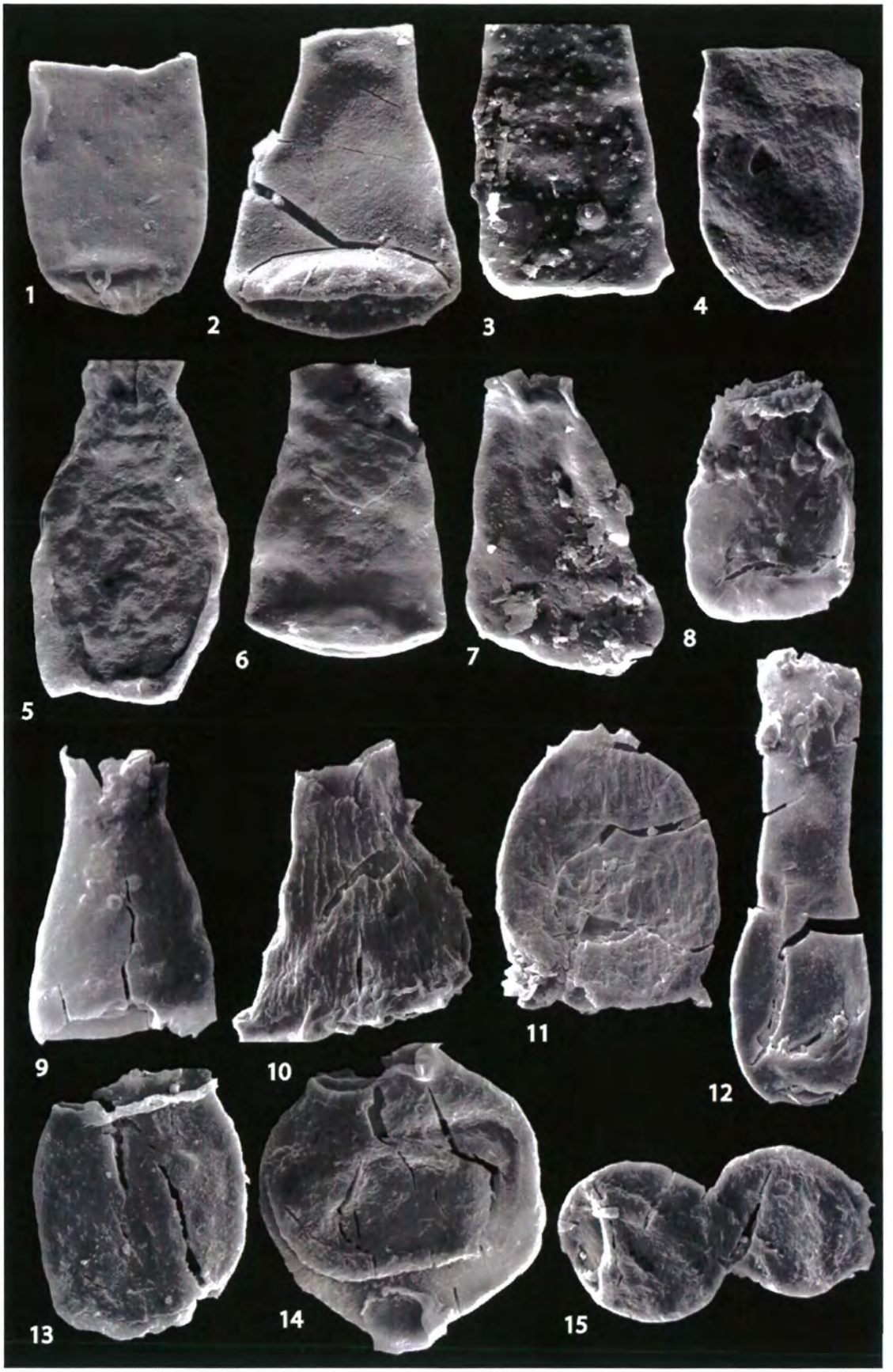

Plate 2.15: Chitinozoans from the Ciliau Formation, Garth House Formation and Yr Allt Formation, Garth House, Llandovery and Llyn Brianne, Llandovery region.

Plate 16. Chitinozoans from the Garth House Formation, Garth Bank, Llandovery region. L, Dp, Dc. All dimensions in microns. Abbreviations following Paris (1981): L= total length, Dp=chamber diameter, Dc=diameter of oral tube.

1. *Siphonochitina* sp. indet. (193, 54, 36; TJC D976-16).
2. *Laufeldochitina* sp. I (272, 82, 59; TJC D976-11).
3. *Laufeldochitina* sp. I (141?, 59, 52?; TJC D976-46).
4. *Laufeldochitina* sp. I (135?, 117, ?; TJC D976-4).
5. *Spinachitina taugourdeaui* (163, 81, 47; TJC D976-183).
6. *Spinachitina taugourdeaui* (123, 59, 32; TJC D976-184).
7. *Spinachitina taugourdeaui* (140, 72, 37; TJC D976-138)
8. *Spinachitina taugourdeaui* (306, 90, 60; TJC D976-205).
9. Detail of carina of 2. Scale = $50\mu m$.
10. Detail of siphon of 1. Scale = $20\mu m$.
11. *Eisenackitina inconspicua* (119, 77, 40; TJC D976-171).
12. *Belonchitin* cf. *wessenbergensis* (117, 92, 52; TJC D976-86).
13. *Belonechitina* sp. A *sensu* Vandenbroucke (2005) 2005 (251, 103, 51; TJC D976-14).

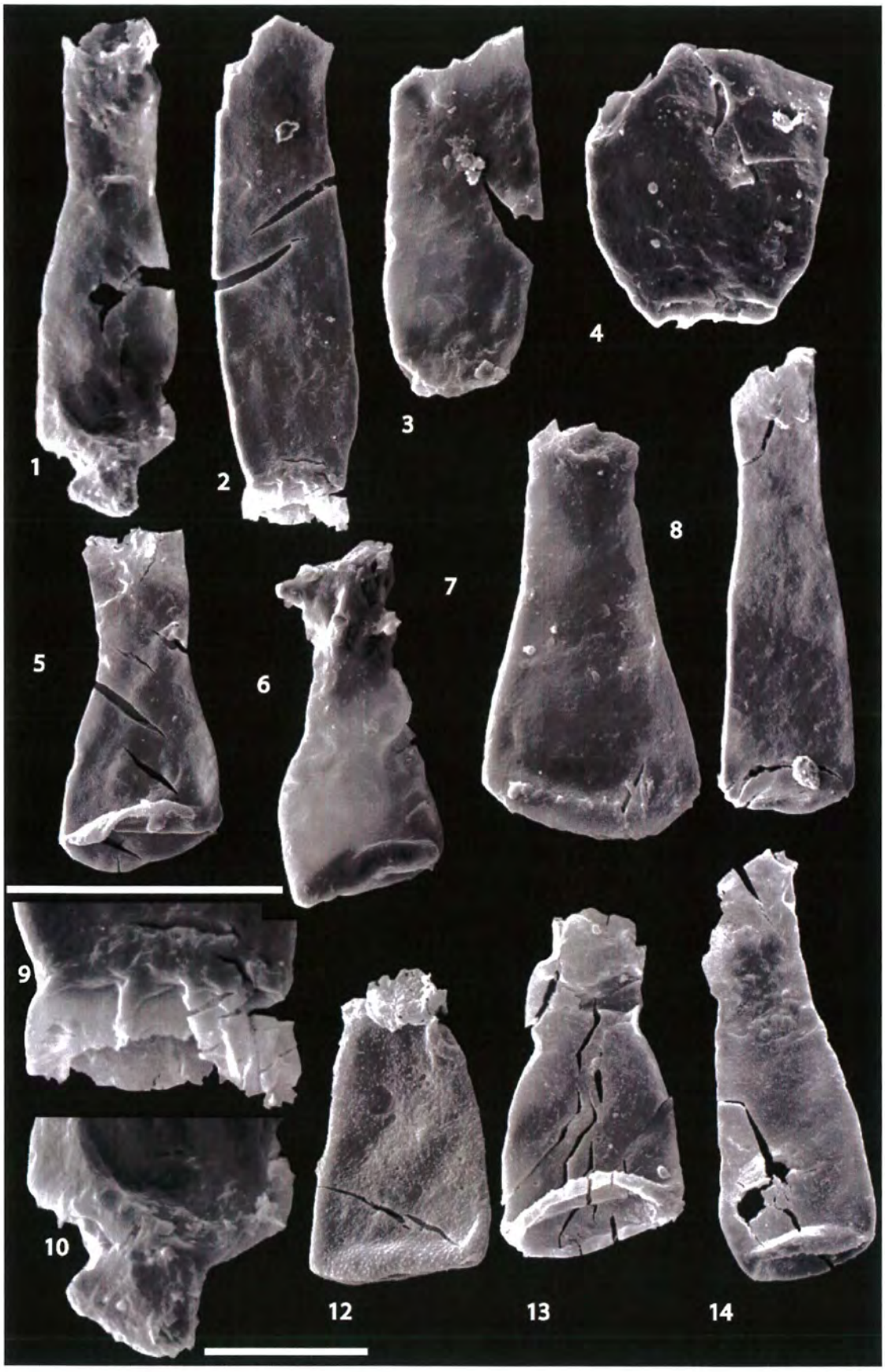

Plate 2.16: Chitinozoans from the Garth House Formation, Garth Bank, Llandovery region.

Plate 17. Chitinozoans from the Brynffo Forest section: Cwm Clyd Sandstone Member, Garth House Formation and Bronydd Formation, Llandovery region. L, Dp, Dc. All dimensions in microns. Abbreviations following Paris (1981): L= total length, Dp=chamber diameter, Dc=diameter of oral tube.

1. *Desmochitina minor* (113, 76, 43; TJC D1016-27).
2. *Desmochitina juglandiformis* (90, 81,?; TJC D1029-8).
3. *Eisenackitina* cf. *rhenana* (107, 76, 56; TJC D1016-17).
4. *Eisenackitina* cf. *rhenana* (137, 76, 54; TJC D1016-29).
5. *Eisenackitina inconspicua* (128, 67, 51; TJC D1016-4).
6. *Laufeldochitina* sp. indet. (165?, 73, 56?; TJC D1016i-6).
7. *Spinachitina* sp. indet. (115, 71, 39; TJC D1016-25).
8. *Lagenochitina* sp. indet. (149, 77, 42; TJC D1029-14).
9. *Cyathochitina campanulaeformis* (134, 136, 46; TJC D1027-2).
10. *Cyathochitina kuckersiana* (157, 171, 56; TJC D1027-157, 171, 56).
11. *Ancyrochitina* sp. indet. (109, 34, 17; TJC D1025-13).
12. *Spinachitina* sp. indet. (124, 82, 45; TJC D1026-15).
13. Detail of granular surface texture of 4, ×2460.
14. Detail of diminished carina and base of 6, ×1809.
15. Detail of basal spines of 12, ×1955.

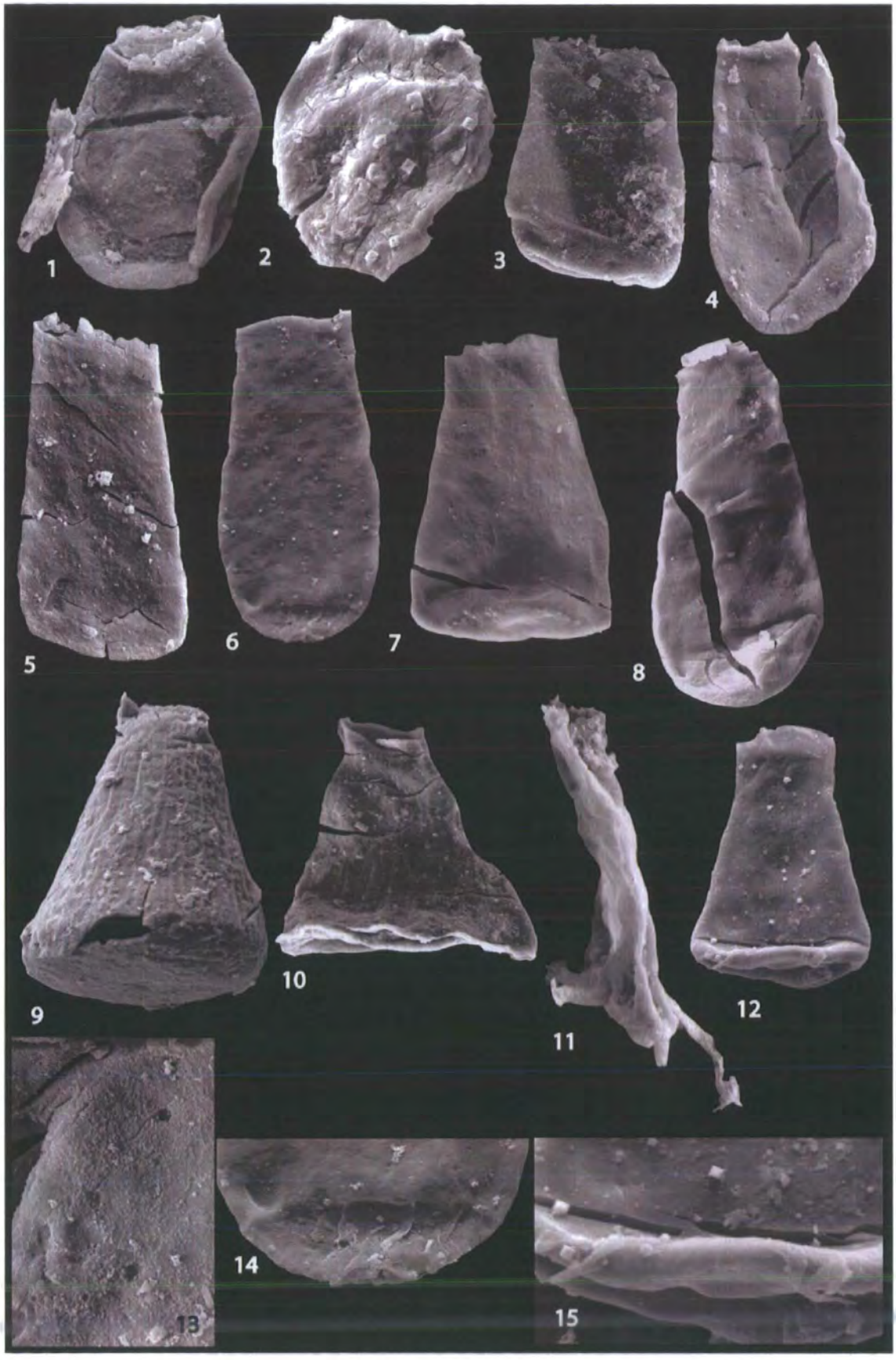

Plate 2.17: Chitinozoans from the Brynffo Forest section: Cwm Clyd Sandstone Member, Garth House Formation and Bronydd Formation, Llandovery region.

Plate 18. Chitinozoans from Dolaucothi M8 core, Yr Allt Formation, Mottled Mudstone Member and Cwmere Formation, Llandovery region. L, Dp, Dc. All dimensions in microns. Abbreviations following Paris (1981): L= total length, Dp=chamber diameter, Dc=diameter of oral tube.

1. *Ancyrochitina* sp. indet. (108, 56, 29; TJC D984-1).
2. *Ancyrochitina* sp. indet. (107, 60, 23; TJC D984-3).
3. *Ancyrochitina* sp. indet. (77, 57, 29; TJC D984-19).
4. *Ancyrochitina* sp. indet. (109, 62, 21; TJC D984-14).
5. *Ancyrochitina* sp. indet. (?, 72, 31; TJC D984-12).
6. *Ancyrochitina* cf. *primitiva* (82, 64, 19; TJC D985-16).
7. *Ancyrochitina* cf. *primitiva* (146, 66, 28; TJC D985-18).
8. *Ancyrochitina* cf. *primitiva* (99, 64, 22; TJC D985-9).
9. *Ancyrochitina* cf. *primitiva* (138, 64, 38; TJC D985-15).
10. *Cyathochitina* cf. *campanulaeformis* (133, 150, 55; TJC D985-9).
11. *Cyathochitina* cf. *campanulaeformis* (144, 129, 59; TJC D986-5).
12. *Cyathochitina* cf. *campanulaeformis* (147, 170, 50; TJC D985-15).
13. *Spinachitina* sp. indet. (99, 98, ?; TJC D980-7).
14. Detail of 13 showing vertical basal ridges forming short spines, ×1000.
15. *Belonechitina ?americana* (145, 60, 47; TJC D985-10).

Plate 2.18: Chitinozoans from Dolaucothi M8 core, Yr Allt Formation, Mottled Mudstone Member and Cwmere Formation, Llandovery region.

Chapter 3

Organic-carbon deposition and costal upwelling at mid-latitude during the Upper Ordovician (late Katian): a case study from the Welsh Basin, UK.

Acknowledgement note This chapter has been submitted and accepted to the journal Palaeogeography, Palaeoclimatology, Palaeoecology for publication with Dr H. A. Armstrong, Mr D. Maloney, Drs J. Davies, D. Wilson and A. W. Owen as co-authors. Maloney collected and contributed trace fossil data as part of an MSci thesis, Armstrong contributed suggestions and comments on organization and structure of the manuscript, Davies and Wilson provided valuable assistance in the field and Owen contributed helpful comments and proof-reading of the manuscript.

Abstract

A lack of stratigraphical, sedimentological and geochemical data for sediment accumulation rates and indicators of productivity and anoxia means that causative models for ancient black shales are largely inferred from modern settings. Coastal upwelling has been suggested as a general hypothesis for Ordovician black shale deposition within the Iapetus Ocean, but has not been directly tested. Despite anchizone metamorphism we utilize a suite of geological and geochemical environmental proxy data (TOC wt%, $\delta^{13}C_{org}$, Ba/Al, P) to elucidate the mechanism for the origin of a single grey-black shale cycle within the upper Katian succession of the Welsh Basin. Here we interpret organic carbon (OC)-rich deposition to be suggestive of a period of high photic productivity (higher TOC wt%), with ^{12}C and Ba enrichment, comparable to high productivity events in modern coastal upwelling systems. Productivity proxy values are consistent with those from margins where sedimentation rates are high (e.g.

Gulf of California). Inter-bedded grey shales have low TOC wt% more positive $\delta^{13}C_{org}$ and marginally lower Ba and are interpreted as low productivity events. *Thalassinoides*, *Planolites* and *Chondrites* ichnofacies indicate changing seafloor oxygen levels. These show predominantly dysoxic conditions even during the deposition of OC-poor grey shales. During an OC-rich laminated hemipelagite event, oxygen levels declined at the sea floor before the deposition of the OC-rich layers. Full anoxia was established early on in the deposition of OC-rich layers and the return to more oxic conditions was rapid though fluctuating and coincident with the return of grey shale deposition. This pattern suggests OC accumulation at the seafloor resulted from a complex interaction of productivity and preservation. None of the widely used trace element redox proxies are reliable in anchizone metamorphic rocks. Climate sensitive detrital proxies (K/Al and Ti/Al) indicate arid-temperate conditions in the basin hinterland during the deposition of the OC-rich layers. The Welsh Basin was situated on the southern margin of the Iapetus Ocean in (30°S) beneath the prevailing SE trade winds. We interpret the occurrence of OC-rich laminated hemipelagite events to represent the intensification of upwelling, prior to the Hirnantian glaciation, possibly having resulted from a strengthening of the trade winds, associated with stepped changes in ice volume, and a more arid local climate.

3.1 Introduction

Black shales provide important records of climate and atmosphere-ocean interactions. The Early Palaeozoic oceans differed from the Mesozoic and younger oceans because they experienced a mild greenhouse climate (Yapp & Poths, 1992; Berner, 1994; Berner & Kothavala, 2001) and were prone to permanent anoxia (Leggett, 1980). However, black shales deposited in the Early Palaeozoic potentially provide a detailed record of climate processes provided the mechanisms for their formation can be constrained. Under such different climatic conditions it is necessary to determine whether the processes that formed Mesozoic to modern ocean black shales are also applicable to Palaeozoic black shales. Processes for black shale formation can typically be considered to be the product of increased productivity or enhanced preservation (see Tyson, 1995, for a review). Increasing productivity has been explained by: 1) increasing continental runoff (the Runoff model e.g. Beckmann *et al.*, 2005; Bjerrum *et al.*, 2006), dominant at tropical latitudes, whereby increased continental runoff introduces nutrients, increases productivity and organic carbon (OC) export. Weathering regime proxies (K/Al, Ti/Al) have recently demonstrated that fresh-water and detrital input into basins is important for the formation of oxygen minima and the burial of carbon e.g. the Cretaceous Ivorian Basin (Beckmann *et al.*, 2005; Bjerrum *et al.*, 2006; Sobarzo *et al.*, 2007). Along the

upwelling margin of Chile, high freshwater input suppresses upwelling through the formation of a salinity stratified layer during wetter periods resulting in lower oxygen values at depth (Sobarzo *et al.*, 2007). 2) increased oceanic/coastal upwelling (the Upwelling model e.g. Parrish, 1982; Hay & Brock, 1992; Pope & Steffen, 2003) dominant at mid- to high latitudes in trade wind zones. Mechanisms for increasing preservation include: 1) the Transgressive model, whereby transgression introduces additional nutrients and expansion of the deep ocean oxygen minimum zone (OMZ) during sealevel rise promotes OC preservation in high productivity shelf environments (Leggett, 1980), 2) restricted circulation, either global thermohaline circulation or regional circulation such as in a restricted basin, and, 3) increased burial efficiency of OC during increased sedimentation rate (Canfield, 1989).

The Transgressive model with unrestricted oceans may explain thick black shales in Lower Palaeozoic basins (Leggett, 1980; Page *et al.*, 2007) but does not explain variation in productivity within black shale successions, and in fact assumes it to be effectively constant (Berry & Wilde, 1978, p. 271; Legget, 1980, p. 150). For example, the upper Katian (Rawtheyan - Hirnantian British Stages) succession of Dob's Linn, Scotland, located on the northern margin of the Iapetus Ocean contains thin (<30 cm thick) black shale units alternating with grey shale. These have been inferred to have been deposited at a time of increased productivity (Armstrong & Coe, 1997) and global eustatic, glacially-induced regression when the Iapetus Ocean was much narrower and likely more restricted than has been previously considered (Armstrong & Owen, 2002b). Two oceanic events have been recognized in the Dob's Linn succession (Fig. 3.1). The first, in the mid Katian (Streffordian-Pusgillian boundary), is the sudden change from anoxic to oxic conditions and the replacement of black with grey shales. This has been interpreted as the onset of glacially-induced thermohaline circulation (Armstrong & Coe, 1997). The second is the re-appearance of discrete black shale units within predominantly grey shales during the upper Katian (*anceps* graptolite Biozone), and was considered indicative of climatically-forced, Monterey-type processes reflecting upwelling (Armstrong & Coe, 1997). Similar lithological events in the Welsh Basin are potentially contemporaneous with those at Dob's Linn (i.e. they are of mid Katian and *anceps* Biozone age respectively) and may demonstrate that oceanic peturbations were Iapetus Ocean-wide, possibly reflecting fundamental changes in the climate-ocean system before the onset of glaciation

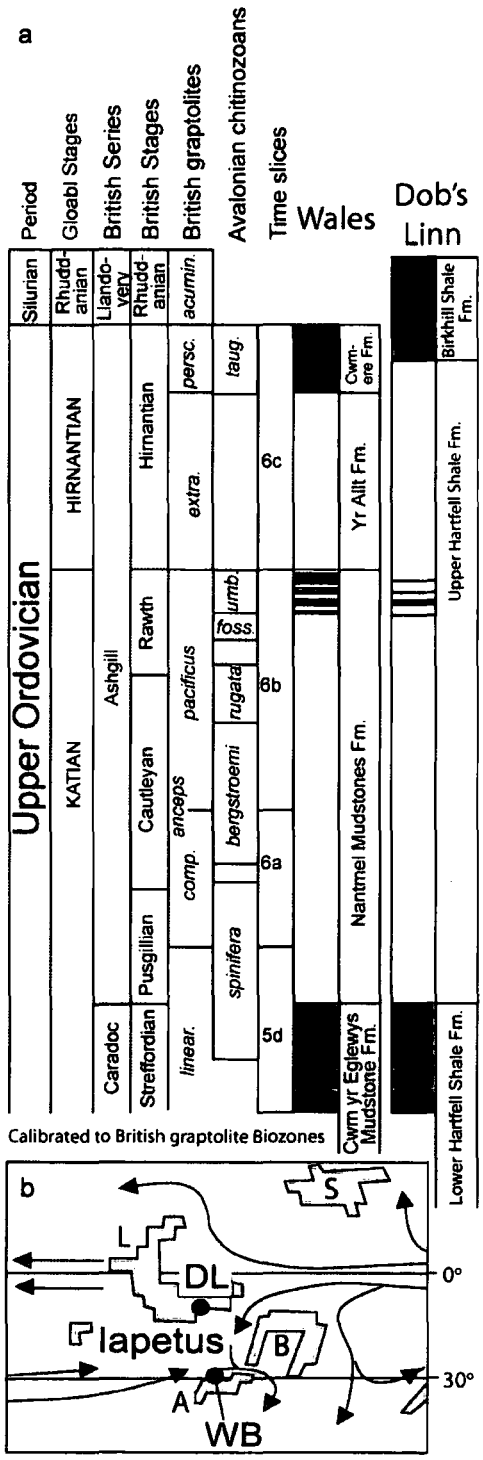

Figure 3.1: Stratigraphic chart (a) showing possible correlation between the sections at Dob's Linn (International boundary stratotype for the base of the Silurian System), lithostratigraphy and graptolite biostratigraphy for Dob's Linn after Underwood *et al.* (1997); Armstrong & Coe (1997); Melchin *et al.* (2003). (b) Palaeogeographic map of the Iapetus Ocean during the Late Ordovician (based on Herrmann *et al.* (2005)). This shows the distribution of the major continental land masses (L = Laurentia, S = Siberia, B = Baltica, A = Avalonia, DL = Dob's Linn, WB = Welsh Basin) and major surface currents (solid arrows).

Oceanic upwelling has been inferred from lower Katian (mid-Caradoc) radiolarian cherts along the Iapetus Ocean margin from Laurentia (Pope & Steffen, 2003) and in Wales from the presence of phosphorites and radiolarites (e.g. Cave, 1965). The latter were compared to phosphorites forming today at shelf-slope depths off the California coast and attributed to climatic factors reflecting an absence of currents and strong offshore winds or basin restriction from the presence of a bathymetric barrier (Cave, 1965).

In this case study we use a suite of proxy data to test an upwelling mechanism for an upper Katian black shale unit within the Welsh Basin. Despite anchizone facies metamorphism, it has been possible to reconstruct plausible palaeo-environmental conditions during deposition from proxy data. Coastal upwelling is the preferred cause of organic carbon (OC) enrichment of the sediments, and could have been driven by changes in the strength of the prevailing trade winds. Given the limitations of the extent and fidelity of the data, other possible mechanisms are: 1) increased anoxia and, 2) marine transgression. The upwelling hypothesis, however, is consistent with known patterns of Late Ordovician climate change associated with the developing Hirnantian glaciation.

3.2 Regional Geology of the Ordovician of the Welsh Basin

Two major changes in oceanography can be identified in the Welsh Basin during: 1) the mid-Katian (late Caradoc to early Ashgill) in the *linearis* - *complanatus* graptolite biozones (*spinifera* chitinozoan biozone) and, 2) in the late Katian *anceps* graptolite biozone (*umbilicata-gamachiana* chitinozoan biozones). At the first event, anoxic conditions were terminated and the succession changes to predominantly burrow-mottled lithofacies. These burrow-mottled grey shale units have been mapped regionally as the Nantmel Mudstones Formation (Davies *et al.* (2003); Fig. 3.2). During the late Katian a return to black shale deposition is recognized (the "Red Vein") comprising distinctive alternating black laminated and grey burrow- mottled siltstone and mudstones. The cause of this later change in lithofacies is unknown and is the focus of this paper.

The Red Vein (Fig. 3.2) crops out from the Cadair Idris region in the north, south to Rhayader and Builth Wells regions and further west around Newcastle Emlyn and north of Cardigan (British Geological Survey Llangranog 1:50 000 scale Sheet number 194; 2003). This distinctive unit was first recognized in the Cadair Idris area by Pugh (1923) and named on account of oxidation of the abundant iron sulphide it contains. Three separate OC-rich laminated units have previously been recognized in the Rhayader, Builth Wells and Llangranog regions (Davies *et al.*, 1997; Schofield *et al.*, 2004; Davies *et al.*, 2006) and interpreted as laminated hemipelagites (LH, Davies *et al.*, 1997). They consist of thin alternating laminae of dark grey, OC-rich and medium grey OC-poor mudstone.

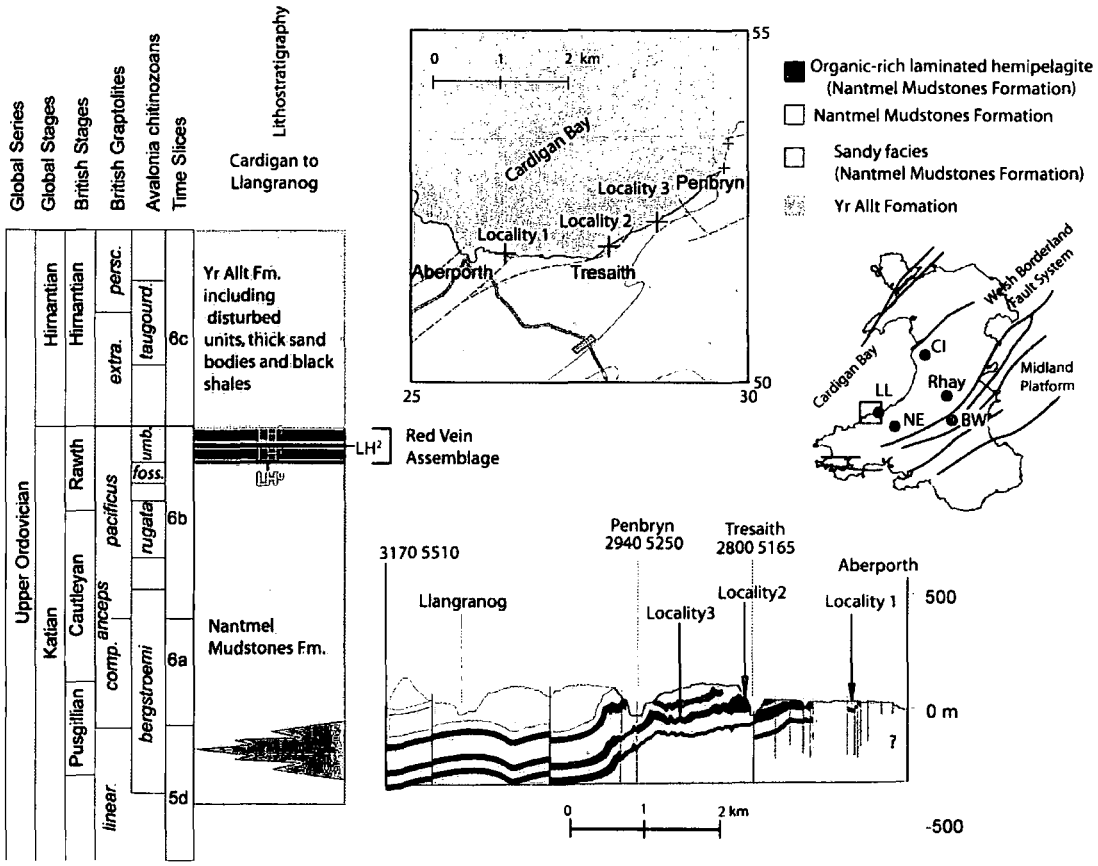

Figure 3.2: Regional Geology of the late Katian of the Cardigan-Llangranog region, southwest Wales, UK. Abbreviations on regional location map BW = Builth Wells, CI = Cadair Idris, LL = Llangranog, NE = Newcastle Emlyn, Rhay = Rhayader. Chronostratigraphy from Fortey *et al.* (2000) and Webby *et al.* (2004), chitinozoan biozonation from Vandenbroucke & Vanmeirhaeghe (2007), graptolite biozonation and Time slices from Webby *et al.* (2004), lithostratigraphy from Davies *et al.* (2003).

The LH units in the Llangranog region range in thickness from between 10-36 m. Laminated OC-rich layers after 1.4 m above the base of LH^0 contain abundant pyrite framboids and small nodules up to 1 mm in length alongside finely-disseminated pyrite. The OC-rich laminated horizons are composed of a fine clay matrix and angular quartz grains up to 0.25 mm and fine, platy muscovite and chlorite grains up to 0.175 mm long. The medium grey OC-poor mudstone component of the LH units occasionally contains thin fining-up sequences from silt to mudstone and occasional very thin (< 2 mm) fine-grained sand and are interpreted as hemiturbidites (Stow & Wetzl, 1987) deposited in a slope-apron system (Schofield *et al.*, 2004). Within the LH, the absence of significant grain-size variations between the OC-poor grey mudstones and OC-rich units suggest the increase in OC content of the sediment was independent of factors affecting sediment supply though precise measures of sedimentation

rate in ancient basin settings are difficult to measure (Wignall, 1994).

On regional maps of these areas the laminated hemipelagite units are termed lh'-lh"' (British Geological Survey Rhayader 1:50 000 scale Sheet numbers 178 and 179; 1997, British Geological Survey Builth Wells 1:50 000 scale Sheet number 196; 2004, British Geological Survey Llangranog 1:50 000 scale Sheet number 194; 2006). Herein, lh are capitalized and referred to numerically (e.g. LH^1) to avoid confusion between the letter 'l' and the number '1' and to prevent inconsistency in labelling. In the Llangranog region, an older LH horizon has been recognized in this study and, following the British Geological Survey numbering convention for these units, has been named LH^0.

The LH units are interbedded with grey burrow-mottled fine-grained sandstones, siltstones and mudstones up to 25 m thick that have been interpreted as fine grained distal turbidites resulting from periodic influx of coarser material (Davies *et al.*, 2003; Schofield *et al.*, 2004). They are hereafter referred to the OC-poor lithofacies.

Phosphatic nodules up to 1 m in length and phosphate horizons up to 10 cm thick are present in both the organic-rich and organic-poor facies. Diffuse fine-grained phosphatic layers up to 10 mm thick are more frequent in the LH units and less common in the OC-poor lithofacies. In the OC-poor lithofacies they occur in the light-grey silty mud layers.

The thermal history of the Ordovician of the Welsh Basin has been elucidated from illite crystallinity (Fettes *et al.*, 1985; Robinson & Bevins, 1986; Bevins & Robinson, 1988; Roberts *et al.*, 1996). These data indicate a regional record of diagenetic to epizone facies metamorphism. The Nantmel Mudstones Formation adjacent to the study area (British Geological Survey 1:50000 Sheet 193, Cardigan and Dinas Island) is of low anchizone grade. Darriwillian - lower Katian aged shales immediately south of Cardigan, have experienced late diagenetic to epizone temperatures (200-300°C; Lev *et al.*, 2008) indicating burial to *c.* 4-6km using a regional geothermal gradient of *c.* 50°C/km (Bevins & Merriman, 1988; Bottrell *et al.*, 1990; Roberts *et al.*, 1991).

3.3 Methods and materials

The best sections through the Red Vein are exposed in cliff sections along the coast of Cardigan Bay (Fig. 3.2). Accessibility is difficult in places and sections that allow safe access to the LH units and interbedded OC-poor lithofacies have been selected: LH^0 is accessible at Aberporth (SN 625 515), the base of LH^1 is exposed at Tresaith (SN 280 516) and the upper boundary of LH^1 crops out and is easily reached at Traeth Penbryn (SN 289 522) (see Fig. 3.2). The same sections for trace fossil analysis and geochemical analysis could not be used for reasons of access. All trace fossil data were collected from LH^0 at Aberporth (SN 625 515, Locality 1), two sections spanning the lower and upper parts of LH^0 are conflated

to a single composite section (Fig. 3.5). This 6.4 m-thick section was sub-sampled over six 40 cm intervals, each separated by approximately 1 m.

Geochemical samples were collected from two 5 m thick sections spanning both the upper and lower boundaries of LH^1. The lower boundary was collected at Tresaith (SN 280 516) and the upper boundary at Traeth Penbryn (SN 289 522, Localities 2 and 3 respectively, see Fig. 3.2). Samples for trace element analysis were taken through LH^1 from organic-rich horizons at 20 cm intervals. There is no evidence at the sampling sites of secondary mineralization and all samples were prepared from specimens with no surface alteration or fracturing. Powders were then drilled from samples using a tungsten carbide drill bit to homogenize and reduce matrix effects. Matrix effects were considered negligible due to the fine-grained nature of the samples. Sub-samples were taken for trace element and stable isotopic analysis. Sample digestion was carried out using HF-$HN0_3$ standard acid digestion techniques for ICP-MS following the procedure of Ottley *et al.* (2003). A Perkin Elmer-Sciex Elan 6000 ICP-MS used in conjunction with a Cetac Direct Injection Nebuliser and a Cetac Aridius Desolvating Nebuliser was used for analysis of trace elements. The machine was calibrated using international rock standards W2, BHV01, AGV1, Be-N, NBS688 and BIR-1 and shale standards ScO-1, MAG-1 and SGR-1 were also used for initial comparison of sample shale values. All samples were analysed over three separate runs and reproducibility throughout runs was monitored using SGR-1 (see Table D.1). Relative standard deviation (σ/mean$\times$100) was less than 11% in all runs. Internal precision for individual analyses was greater than 95%. Normalisation to Al is a standard procedure for comparing element proportions, particularly where organic matter content is variable (e.g., Tribovillard *et al.*, 2005). Certain elements e.g. Ni are traditionally plotted against other detrital indicators e.g. Co.

Spot samples for $\delta^{13}C_{org}$ and TOC wt% were also collected from eleven other localities representative of OC-poor facies below, between and above LH units and from LH^0, LH^2 and LH^3 (Table 3.2, Fig. 3.3). All $\delta^{13}C_{org}$ and TOC % measurements were made on a Thermo Finnigan MAT 253 Stable Isotope Mass spectrometer at Durham University, Department of Earth Sciences. TOC wt% analysis of samples from 779.5-794.5 cm from the base of LH^1 were conducted at Newcastle University Department of Civil Engineering and Geosciences using Rock Eval (6) Pyrolysis. $Urea_2$, CH-7 and CH-6 standards were used for machine calibration and standard deviation was less than 0.15 ‰ for all standards. Carbon isotope ratios were expressed in the standard delta (δ) notation in per mil (‰) against the internationally accepted standard notation, Vienna Peedee Belemnite (VPDB). Analytical reproducibility of replicate samples using this method was better than 0.4‰.

Table 3.1: Reproducibility and error data for all shale ICP-MS runs using shale standard SGR-1. Each run included both OC-rich and OC-poor samples. Al, K, Ti and Mn in wt% oxide, all other elements in ppm.

	Run-1, n=2			Run-2, n=7			Run-3, n-2		
	Mean	StDev	RSD%	Mean	StDev	RSD%	Mean	StDev	RSD%
Al	6.1	0.15	2.47	6.92	0.5	7.2	18.66	1.37	7.36
K	1.57	0.03	1.71	1.63	0.07	4.48	2.24	0.0	0.22
Ti	0.24	0.01	3.85	0.24	0.01	2.60	0.26	0.02	7.18
V	120.56	3.88	3.22	121.82	2.70	2.22	124.12	7.81	6.29
Cr	29.62	0.34	1.16	33.31	0.95	2.85	33.60	1.87	5.56
Mn	0.03	0.00	0.00	0.03	0.00	2.43	0.03	0.00	4.29
Co	11.35	0.29	2.52	11.87	0.19	1.63	12.39	0.39	3.12
Ni	25.69	0.52	2.01	31.10	0.70	2.25	31.62	1.23	3.90
Cu	60.60	0.44	0.72	60.73	0.53	0.87	63.84	1.91	3.00
Ba	299.63	1.89	0.63	295.20	8.16	2.77	263.07	8.72	3.32
Th	4.65	0.14	3.04	4.61	0.12	2.50	4.38	0.24	5.56
U	5.17	0.03	0.67	5.09	0.11	2.14	4.68	0.28	6.05

3.3.1 Redox proxies

Trace fossils - The application of analysis of trace fossil assemblages and the degree of bioturbation has proven a strong tool for determining fluctuations in sediment and basin oxygenation e.g. Ekdale & Mason (1988); Savrda & Bottjer (1994); Savrda (1995); Löwemark *et al.* (2004). Ichnogenera presence-absence, burrow diameter and bioturbation index data were collected in line with standard procedures (Savrda & Bottjer, 1994; Savrda, 1995; Löwemark *et al.*, 2004) at centimetre-resolution.

Trace elements The biological pump heavily influences the cycling, concentration and residence times of the redox-sensitive and sulphide-forming trace elements (Cu, Cr, Ni, V, Cd, Mo and U; Tribovillard *et al.*, 2005). These elements form sulphides and complex with organic matter under reducing conditions. OC-rich sediments are therefore typically enriched in these metals (De La Rocha, 2004; Tribovillard *et al.*, 2005, and references therein).

However some of these elements show significant mobility during late diagenesis to low grade metamorphic conditions. For example, at these grades V becomes mobile and complexes with illite (Peacor *et al.*, 2000) rendering the frequently used redox proxies V/(V+Ni) and V/Cr as unreliable. Uranium is also mobilized and enriched, whilst Th is depleted during the formation of illite at low metamorphic grades (Hannigan & Basu, 1998). Nickel, however, has been regarded as a reliable redox proxy in organic-rich shales (Jones and Manning, 1994) and has not been demonstrated to be mobile during low metamorphism. We therefore use

Ni/Co (Dypvik, 1984) and Ni/Al (Tribovillard *et al.*, 2005) ratios as an indicator of redox conditions in this study.

3.3.2 Productivity proxies

$\delta^{13}C_{org}$ The $\delta^{13}C_{org}$ values of sedimentary organic matter are controlled by a number of factors including organic matter composition and cell growth rates (for a review see Freeman, 2001; Maslin & Swann, 2005, and references therein). In the open ocean, sedimentary organic matter is derived from marine and terrestrial sources. In pre-Devonian time there was no extensive terrestrial vegetation (Peters-Kottig *et al.*, 2006) and organic matter in Ordovician rocks can therefore be considered entirely marine in origin. Cell growth rates cannot be constrained in ancient samples. Bulk sediment $\delta^{13}C_{org}$ values are therefore only considered indicative of shifts in mean oceanic isotopic composition.

$\delta^{13}C_{org}$ values have been shown to yield an unaltered environmental signal in greenschist facies rocks at Dob's Linn (Underwood *et al.*, 1997) and are therefore considered primary oceanic values in this study. Nineteen $\delta^{13}C_{org}$ samples were taken through the LH^1. One whole rock sample from each of the remaining three laminated hemipelagite units (LH^0, LH^2 and LH^3) was taken for $\delta^{13}C_{org}$ as well as nine samples taken from OC-poor lithofacies below, between and above the LH units (Table 3.2).

Total organic carbon (TOC wt%) TOC wt% is known to correlate with more direct measures of photosynthetic primary productivity such as total chlorophyll-a or total steryl chlorine esters (Nara *et al.*, 2005) and organic mass accumulation rate (Tyson, 1995; Vilinski & Domack, 1998; Twichell *et al.*, 2002; Kuypers *et al.*, 2002, 2004; Meyers & Arnaboldi, 2005) and may therefore be suitable as a proxy for productivity when supported by other proxy data (e.g. Ba). The burial efficiency of carbon is controlled by oxygen level and burial rate (for example, Wignall, 1994; ?) and is therefore only likely to be representative of productivity when these two factors can unambiguously be shown to be constant. Thirty-five TOC samples were measured through the OC-poor - LH^1 - OC-poor section at Tresaith-Penbryn and, like $\delta^{13}C_{org}$, one whole rock sample from each of the remaining three laminated hemipelagite units (LH^0, LH^2 and LH^3) was measured for TOC wt% as well as nine samples taken from OC-poor facies below, between and above the LH units (Table 3.2).

Trace elements The strong correlation between Ba and organic matter in marine sediments has led Ba values to be used to infer past export production (De La Rocha, 2004). Dysoxic conditions are characterized by relatively low Ba concentrations (<500 ppm), increased Cd and U (Prakash Babu *et al.*, 2002). Though frequently used as a palaeoproductivity indicator, Ba has been found to be associated with sapropels formed in euxinic basins

(Brumsack, 2006). In these environments, Ba is highly mobile and precipitates as barium-sulphides. Ba is thus an unreliable indicator of productivity if euxinia can be demonstrated (Shimmield, 1992; Prakash Babu *et al.*, 2002). Ba is typically measured as a ratio against Th which is taken to represent terrigenous detrital input (Shimmield, 1992). Due to the mobility of Th in low grade metamorphic rocks we have normalized to Al which is also considered to be a detrital indicator (Tribovillard *et al.*, 2005). We also plot raw Ba abundance (ppm) to test if an increase in Ba/Al is the product of decreasing Al.

3.3.3 Climate sensitive detrital input proxies, K/Al and Ti/Al

K and Al are mainly confined to the fine-grained aluminosilicate fraction, clay minerals and feldspars. Kaolinite which is rich in Al forms by intense chemical weathering under humid conditions whereas illites, which are rich in K, form under less humid weathering conditions (Beckmann *et al.*, 2005; Tribovillard *et al.*, 2005). Ti is concentrated in heavy minerals and is often transported as part of the wind blown detritus, considered indicative of weathering in arid environments. The K /Al ratios are therefore used as a proxy of temperate to humid weathering and, similarly, Ti/Al may be regarded as a proxy for arid to humid weathering (Yarincik *et al.*, 2000).

3.4 Results

3.4.1 Productivity proxies: TOC wt%,$\delta^{13}C_{org}$, Ba/Al

TOC values are higher during deposition of the organic-rich laminated hemipelagite unit LH^1. The maximum TOC value of 0.61 wt% in LH^1 occurs 822.9 cm and 832.5 cm in the measured section (mean value for LH^1 = 0.42 wt%) whereas the minimum for OC-poor oxic facies is 0.14 wt% at -80 cm (mean value for measured section = 0.31 wt%, minimum for entire coast section = 0.08 wt% at Pen y Craig, SN 221 252, Fig. 3.3). Hydrocarbon source rocks typically have >10 wt% TOC (Tyson, 1995). A weak negative correlation occurs between TOC wt% and $\delta^{13}C_{org}$ (r^2=0.4), high TOC wt% values correspond to more negative $\delta^{13}C_{org}$ values (Figures 3.4, 3.6 a).

For LH^1 at Tresaith, the mean $\delta^{13}C_{org}$ value is -31.6 ‰ (n=14) and in the OC-poor units, the $\delta^{13}C_{org}$ mean is -30.7 ‰ (n=5).

The more limited data from the other LH units suggest the LH lithofacies is associated with a negative $\delta^{13}C_{org}$ excursion of approximately 1 ‰ (Fig. 3.3). $\delta^{13}C_{org}$ values for each LH unit are between -30.5 ‰ (LH^1) and -31.9 ‰ (LH^3, mean for all LH units = -31.55 ‰) compared to a mean value of -30.25 ‰ for all OC-poor samples.

$\delta^{13}C_{org}$ values from the OC-poor lithofacies vary by up to 2.85 ‰ and exhibit an overall negative trend from the base of the measured section at Gwbert Hotel (SN 160 509) from

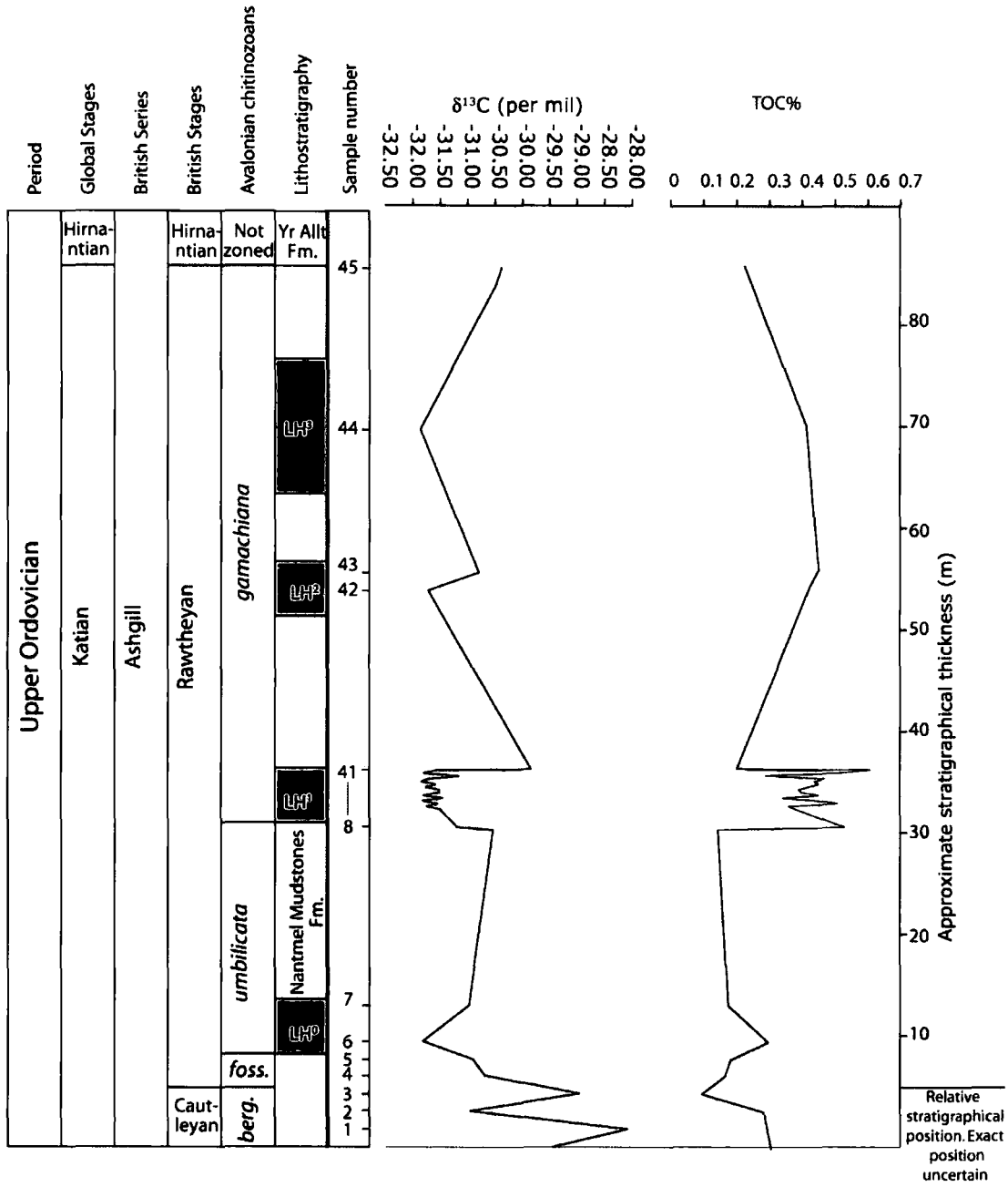

Figure 3.3: Composite stratigraphical chart showing variations in $\delta^{13}C_{org}$ and TOC % profile throughout the upper Katian (Cautleyan-Rawtheyan, Upper Ordovician) of the Cardigan-Penbryn coastal section, Welsh Basin (SN 161 500 to SN 296-530). See Table 3.2 for details of precise sample locations.

-28.10 ‰ to -30.50 ‰ at the highest OC-poor lithofacies above LH^3 (SN 296 530, Fig. 3.3, Table 3.2).

[p]

Table 3.2: $\delta^{13}C_{org}$ and TOC wt% for Cardigan coast line, Ceredigion, Wales. Samples are listed from stratigraphically lowest (oldest) to highest (youngest), see Figure 3.3 for stratigraphical plot of this data.

Sample no.	Locality	$\delta^{13}C_{org}$ ‰	TOC %
1	Gwbert Hotel (SN 161 500)	-29.46	0.29
2	Carreg Lydan (SN 162 513)	-28.1	0.28
3	Mwnt (SN 192 519)	-30.95	0.27
4	Pen-y-Craig (SN 218 523)	-28.97	0.08
5	Aberporth (SN 258 515)	-30.70	0.15
6	LH^0 lower boundary, subsection 3 (SN 625 515)	-30.91	0.17
7	LH^0 2m, subsection 3 (SN 625 515)	-31.83	0.28
8	LH^0 upper boundary, subsection 6 (SN 625 515)	-30.98	0.16
9	LH^1 -80 cm from base of LH^1, Tresaith (SN 280 516)	-30.5	0.14
10	LH^1 -40 cm from base of LH^1, Tresaith (SN 280 516)	-31.16	0.53
11	LH^1 280 cm from base of LH^1, Tresaith (SN 280 516)	-31.47	0.38
12	LH^1 320 cm from base of LH^1, Tresaith (SN 280 516)	-31.71	0.36
13	LH^1 360 cm from base of LH^1, Tresaith (SN 280 516)	-31.51	0.51
14	LH^1 400 cm from base of LH^1, Tresaith (SN 280 516)	-31.78	0.45
15	LH^1 440 cm from base of LH^1, Tresaith (SN 280 516)	-31.42	0.34
16	LH^1 480 cm from base of LH^1, Tresaith (SN 280 516)	-31.77	0.45
17	LH^1 520 cm from base of LH^1, Tresaith (SN 280 516)	-31.48	0.40
18	LH^1 560 cm from base of LH^1, Traeth Penbryn (SN 289 522)	-31.48	0.39
19	LH^1 600 cm from base of LH^1, Traeth Penbryn (SN 289 522)	-31.73	0.42
20	LH^1 640 cm from base of LH^1, Traeth Penbryn (SN 289 522)	-31.53	0.45
21	LH^1 680 cm from base of LH^1, Traeth Penbryn (SN 289 522)	-31.81	0.44
22	LH^1 720 cm from base of LH^1, Traeth Penbryn (SN 289 522)	-31.69	0.47
23	LH^1 760 cm from base of LH^1, Traeth Penbryn (SN 289 522)	-31.12	0.29
24	LH^1 800 cm from base of LH^1, Traeth Penbryn (SN 289 522)	-31.77	0.51
25	LH^1 822.9 cm from base of LH^1, Traeth Penbryn (SN 289 522)	-	0.61
26	LH^1 823.5 cm from base of LH^1, Traeth Penbryn (SN 289 522)	-	0.61
27	LH^1 824 cm from base of LH^1, Traeth Penbryn (SN 289 522)	-	0.524
28	LH^1 824.8 cm from base of LH^1, Traeth Penbryn (SN 289 522)	-	0.255
29	LH^1 825.9 cm from base of LH^1, Traeth Penbryn (SN 289 522)	-31.52	0.258
30	LH^1 826.4 cm from base of LH^1, Traeth Penbryn (SN 289 522)	-	0.522
31	LH^1 826.9 cm from base of LH^1, Traeth Penbryn (SN 289 522)	-	0.281
33	LH^1 827.5 cm from base of LH^1, Traeth Penbryn (SN 289 522)	-	0.604
33	LH^1 828 cm from base of LH^1, Traeth Penbryn (SN 289 522)	-	0.469
34	LH^1 830 cm from base of LH^1, Traeth Penbryn (SN 289 522)	-	0.322
35	LH^1 830.5 cm from base of LH^1, Traeth Penbryn (SN 289 522)	-	0.226

continued on next page

Table 3.2: *continued*

Sample no.	Locality	$\delta^{13}C_{org}$ ‰	TOC %
36	LH^1 831.6 cm from base of LH^1, Traeth Penbryn (SN 289 522)	-30.3	0.324
37	LH^1 832.5 cm from base of LH^1, Traeth Penbryn (SN 289 522)	-	0.267
38	LH^1 833.3 cm from base of LH^1, Traeth Penbryn (SN 289 522)	-	0.255
39	LH^1 833.8 cm from base of LH^1, Traeth Penbryn (SN 289 522)	-	0.313
40	LH^1 835.3 cm from base of LH^1, Traeth Penbryn (SN 289 522)	-	0.3
41	LH^1 836.9 cm from base of LH^1, Traeth Penbryn (SN 289 522)	-	0.275
42	LH^1 837.9 cm from base of LH^1, Traeth Penbryn (SN 289 522)	-	0.255
43	LH^1 842.4 cm from base of LH^1, Traeth Penbryn (SN 289 522)	-29.8	0.2
44	LH^2 (SN 293 523)	-31.73	0.41
45	LH^3 lower boundary, org.-poor facies (SN 296 528)	-30.8	0.44
46	LH^3 lower boundary org.-rich facies (SN 296 528)	-31.87	0.40
47	Highest Nantmel Mudstones Formation (SN 296 530)	-30.50	0.24

Table 3.3: *f*- and *t*-test statistics for Ba/Al and Ba (ppm) through LH^1, Traeth Penbryn. Both the means and variances for Ba/Al and Ba (ppm) are significantly different at α=0.05 between OC-poor and OC-rich units.

	OC-poor Mean	LH^1 Mean	t-stat	t-crit 2-tail	OC-poor Var.	LH^1 Var.	f-stat	f crit. 1-tail
Ba/Al	5.1×10^{-3}	5.4×10^{-3}	-2.33	± 2.03	3.55×10^{-7}	7.31×10^{-8}	4.85	1.76
Ba (ppm)	601.5	653.2	-2.5	± 2.0	6405.9	7978.3	0.8	0.55

Ba/Al values in OC-rich facies vary between 2.5 $\times10^{-3}$ to 3.1 $\times10^{-3}$ and the mean is higher (mean = 2.8 $\times10^{-3}$) than the mean for OC-poor facies (min. = 1.8 $\times10^{-3}$, max. = 4.0 $\times10^{-3}$, mean = 2.7 $\times10^{-3}$). Values remain relatively constant through the lower 140 cm of LH^1. There is an abrupt decrease from 3.0 $\times10^{-3}$ to 2.7 $\times10^{-3}$ at 140 cm (Fig. 3.4). Throughout the entire section, Ba/Al ratios and Ba values for samples from OC-poor lithofacies are statistically lower than in the OC-rich lithofacies (Table 3.3) and the correlation between Ba with Al is good (r^2=0.6; Fig. 3.6 b). There is no apparent correlation between Ba/Al and TOC (Fig. 3.6 c).

3.4.2 Redox proxies

Trace fossils Sub-sections 1 to 4 (Fig. 3.5) represent a transect through LH^0 at Aberporth (SN 625 515). Changing burrow diameter reflects changing ichnogeneric content through the section. *Thalassinoides* is not recorded in the LH^0 section but is present with *Planolites* and *Chondrites* elsewhere in the OC-poor lithofacies where bioturbation index (BI) and maximum burrow diameter are high (BI = 4, max. burrow diameter = $\geq$ 5mm).

Thalassinoides, *Planolites* and *Chondrites* dominate the burrow mottling of the sediment up to 2.8 m below the base of LH^0. At 2.8 m below the base of LH^0 *Thalassinoides* disappears

entirely and *Planolites* and *Chondrites* only are present with BI $\leq$ 4 and maximum burrow diameter $\leq$ 6 mm (sub-sections 1 to 3; Fig. 3.5). At 4.2 m above the base of the section (0 cm in sub-section 4, Fig. 3.5) *Chondrites* is the only ichnotaxon present and BI and burrow diameter are correspondingly low (BI = $\leq$ 2, max. burrow diameter $\leq$ 2 mm). Between 20 to 38 cm in sub-section 4 and between 22 cm and 38 cm in sub-section 5 strata are devoid of trace fossils. Also, between the top of sub-section 4 and the bottom of sub-section 5, no burrowing infauna are recorded. At the top of sub-section 5 (1.42 m below the top of LH^0 Aberporth section 2; Fig. 3.5) *Planolites* is found again corresponding with an increase in burrow diameters and BI (BI = $\leq$ 4, max. burrow diameter = 3mm).

Geochemical redox proxies; Ni/Co Ni values in LH^1 vary from 10.32 to 92.25 ppm and are typical for those reported from Phanerozoic shales deposited beneath upwelling systems (average shale = 68 ppm Brumsack, 1989; McCann, 1990a; Temple & Cave, 1992; Warnnig & Brumsack, 2000; Boening *et al.*, 2004; Borchers *et al.*, 2005; Brumsack, 2006, see Table 3.4). Values for samples at 780 cm and 780.75 cm above the base of the LH^1 section at Penbryn are anomalously low (10.32 and 14.24 respectively). Ni/Co values fall between 1.37 and 6.69 (mean = 2.88), the mean value for OC-rich LH^1 is 2.61 (1.36 to 3.89) whilst values in the OC-poor facies range have a mean of 3.28 (1.91 to 6.69). Crossing the base of the LH^1, Ni/Co values fall abruptly to 1.03 (Fig. 3.4). Through LH^1 values rise towards the centre (up to 3.31) and then decline towards the upper boundary. At 2.5 cm below the top of the LH^1, Ni/Co values fall to 1.4. In the base of the overlying OC-poor lithofacies this value rises abruptly to 6.7.

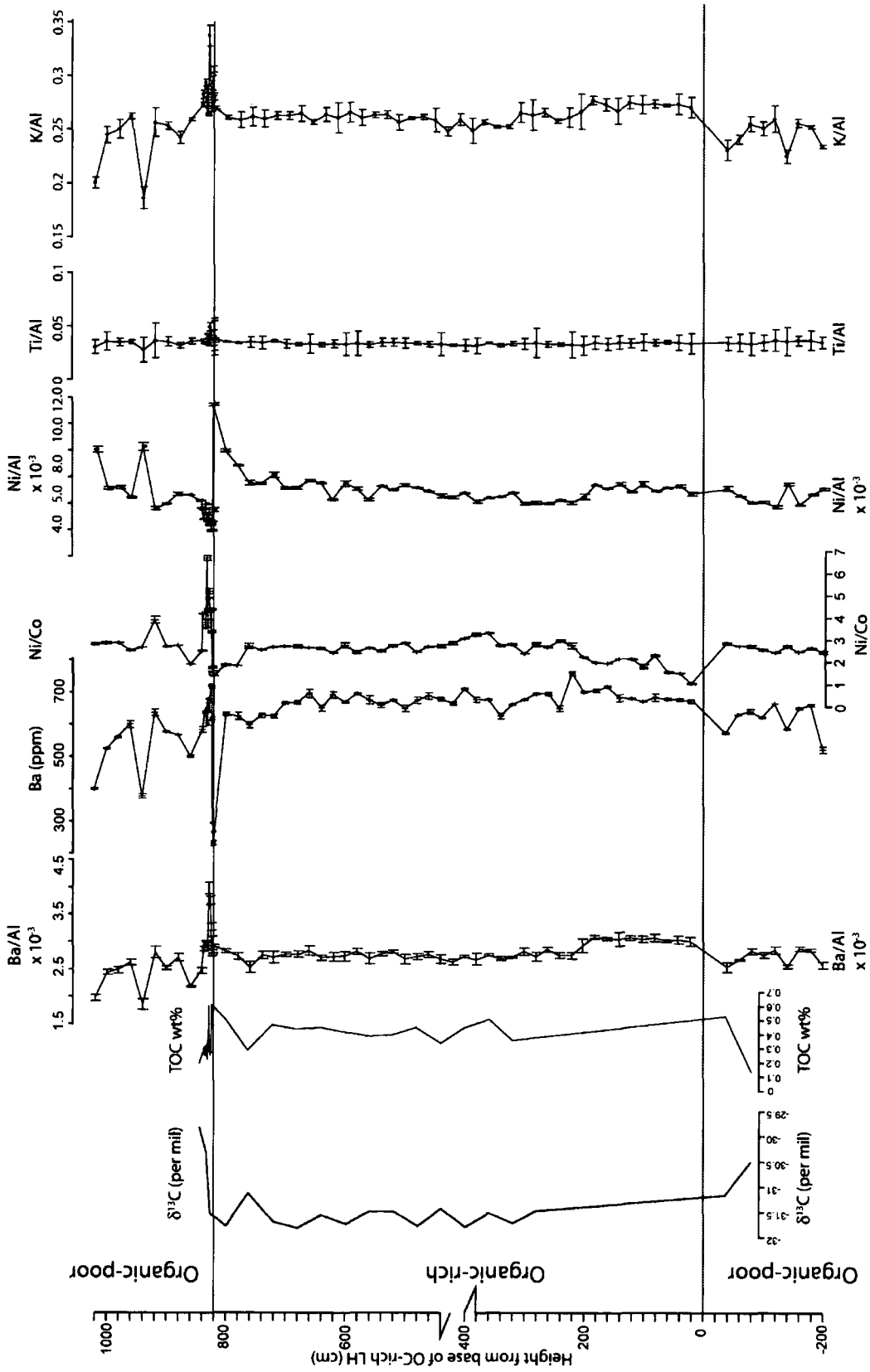

Figure 3.4: Geochemical proxy data plotted against stratigraphical height above base of LH[1], Traeth Penbryn. Error bars represent 1-σ.

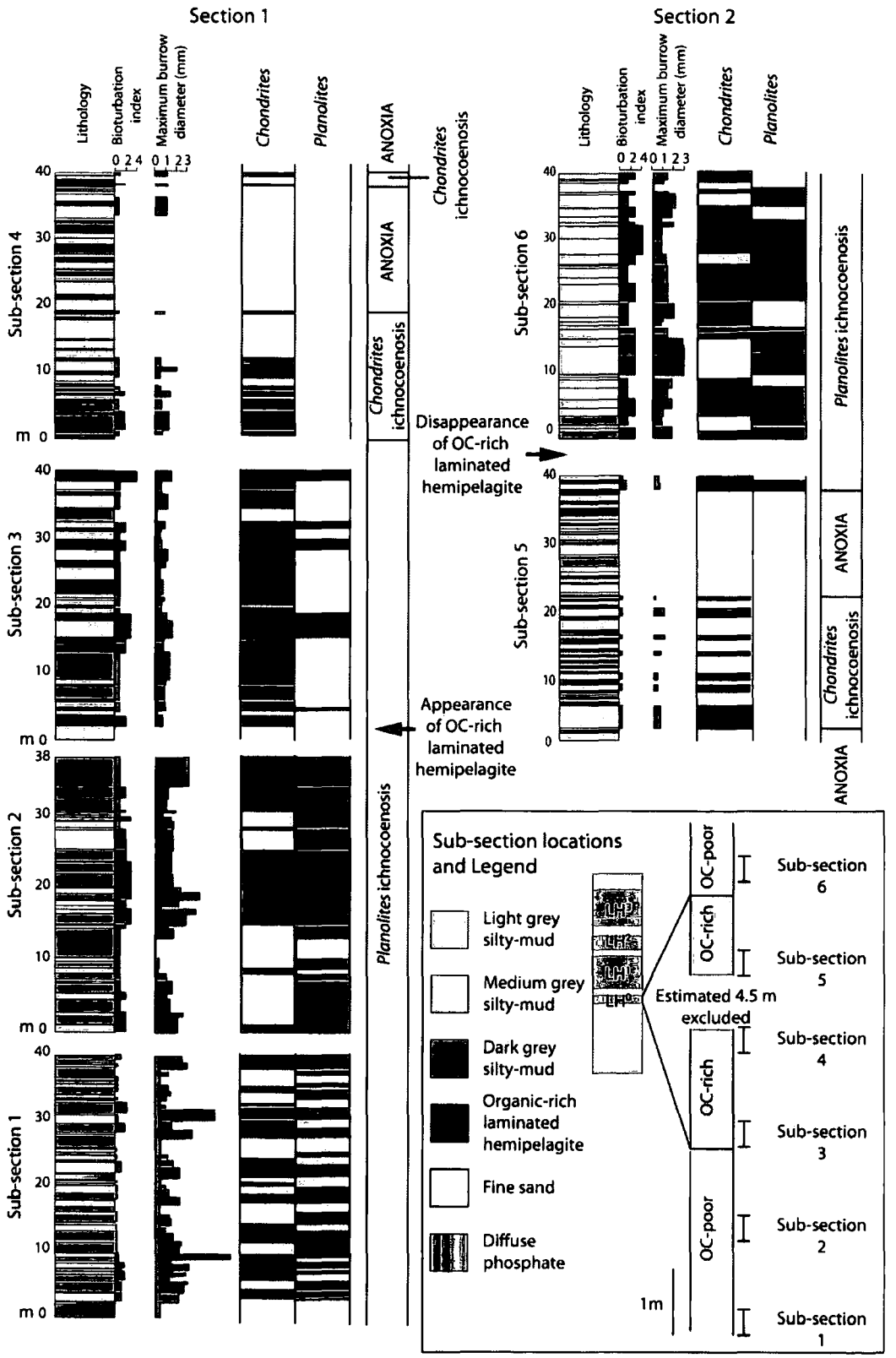

Figure 3.5: Ichnofaunal responses to organic-rich sedimentation and development of anoxia at OC-rich unit LH^0, Aberporth. See text in section 3.3 for details of sampling location.

Table 3.4: Trace metal values for modern and Welsh Ordovician OC-rich black shales. Al, K, Ti and Mn in wt% oxide, all other elements in ppm. [1]Boening *et al.* (2004), [2]Borchers *et al.* (2005), [3]Brumsack (1989), [4]Warnnig & Brumsack (2000), [5]Temple & Cave (1992), [6]McCann (1990a), [7]Brumsack (2006).

	Average shale[2]	Peru margin[1]	Namibia mud lens[2]	Gulf of California[3]	Nod Glas, Caradoc, Wales[4]	Modern turbidites[2]	Modern abyssal clays[2]	Tresaith, Wales 1[6]	Tresaith, Wales 2[6]	Black Sea Unit 1[7]	Black Sea Unit 2[7]
Al	16.7	8.9	2.38	8.91	7.69	17.19	14.52	23.4	23.6	6.66	8.86
K	3.8	1.53	0.58	1.66	1.18	2.99	2.28	3.75	3.78	1.26	2.67
Ti	0.78	0.41	0.16	0.39	0.42	0.71	0.7	1.11	1.03	0.28	0.35
Ni	68	74	46	38	208	53.06	47.83	41	74	57	110
Ba	580	314	324	566	228	1427	558.9	558	658	604	1171

Ni/Al values show a different pattern to Ni/Co. Values vary between 0.1 $\times 10^{-3}$ to 11.4 $\times 10^{-4}$ (mean = 4.7 1.1 $\times 10^{-4}$) throughout the same section (Fig. 3.4) whereas in the OC-poor facies values vary from 2.3 $\times 10^{-4}$ to 8.0 $\times 10^{-4}$ (mean = 4.2 $\times 10^{-4}$). In the OC-rich facies values range from 1.9 $\times 10^{-4}$ to 11.4 $\times 10^{-4}$ (mean = 5.0 $\times 10^{-4}$). At the base of LH[1], Ni/Al values increase by 1.0 $\times 10^{-4}$ (4.0 $\times 10^{-4}$ to 5.0 $\times 10^{-4}$). Values gradually rise to a maximum of 10.0 $\times 10^{-4}$ at the OC-rich - OC-poor boundary at 779.5 cm after which they decrease. In the OC-poor facies, values rise again fluctuating between 8.0 $\times 10^{-4}$ (920 cm) and 3.0 $\times 10^{-4}$ (800 cm). Ni shows a good positive correlation with Co (r^2 = 0.6; Fig. 3.7 a), however, Ni is only weakly correlated with Al (r^2 = 0.2; Fig. 3.7 b) and TOC wt% (r^2=0.2; Fig. 3.7 c).

3.4.3 Weathering regime proxies, K/Al. Ti/Al

During organic-rich sedimentation K/Al values increase by 0.007 (max. = 0.294, min. = 0.248, OC-rich LH mean = 0.264, OC-poor lithofacies mean = 0.258) whereas Ti/Al values do not vary significantly throughout the section (max. = 0.040, min. = 0.032, OC-rich mean = 0.034, OC-poor lithofacies mean = 0.035). Peak values of 0.21 and 0.049 for K/Al and Ti/Al respectively are observed just within the OC-poor lithofacies at 828.25 cm (Fig. 3.4). Both the means and variances for K/Al are significantly different at α=0.05 between OC-poor and OC-rich lithofacies. For Ti/Al, only the variance is significantly at α=0.05 between OC-poor and OC-rich lithofacies is different (Table 3.5).

Table 3.5: *f*- and *t*-test statistics for K/Al and Ti/Al through LH[1], Traeth Penbryn. Both the means and variances for K/Al are significantly different at α=0.05 between OC-poor and OC-rich units. For Ti/Al, only the variance is significantly at α=0.05 between OC-poor and OC-rich units is different.

	OC-poor Mean	LH[1] Mean	t-stat	t-crit 2-tail	OC-poor Var.	LH[1] Var.	f-stat	f crit. 1-tail
K/Al	0.16	0.17	-2.11	± 1.67	0.2×10^{-3}	0.005	7.39	1.75
Ti/Al	0.045	0.044	1.81	± 2.05	1.08×10^{-5}	4.72×10^{-6}	2.29	1.75

!h]

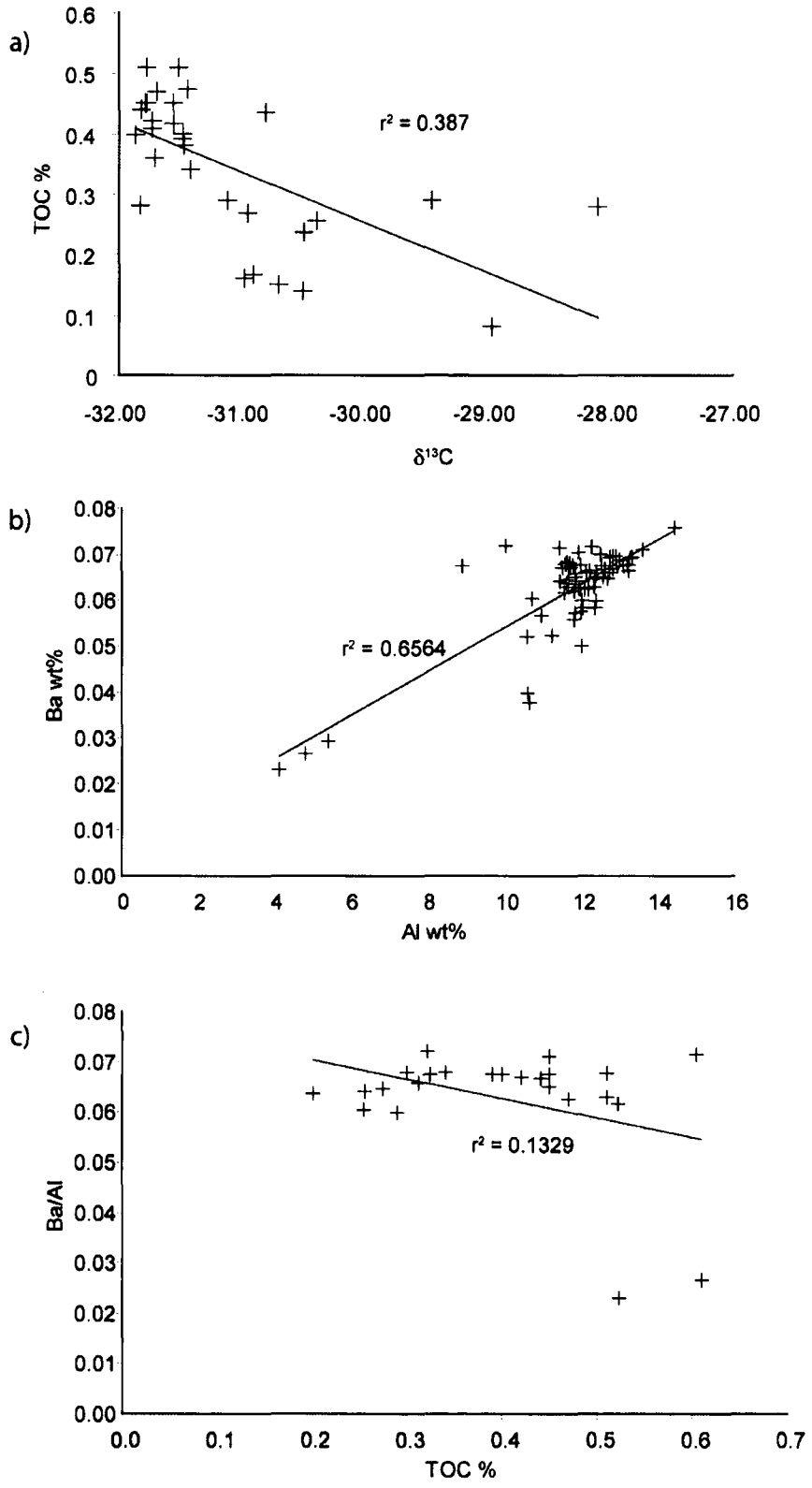

Figure 3.6: Cross-plots for a) TOC wt% vs. $\delta^{13}C_{org}$, b) Ba vs. Al and c) Ba/Al vs. TOC wt%.

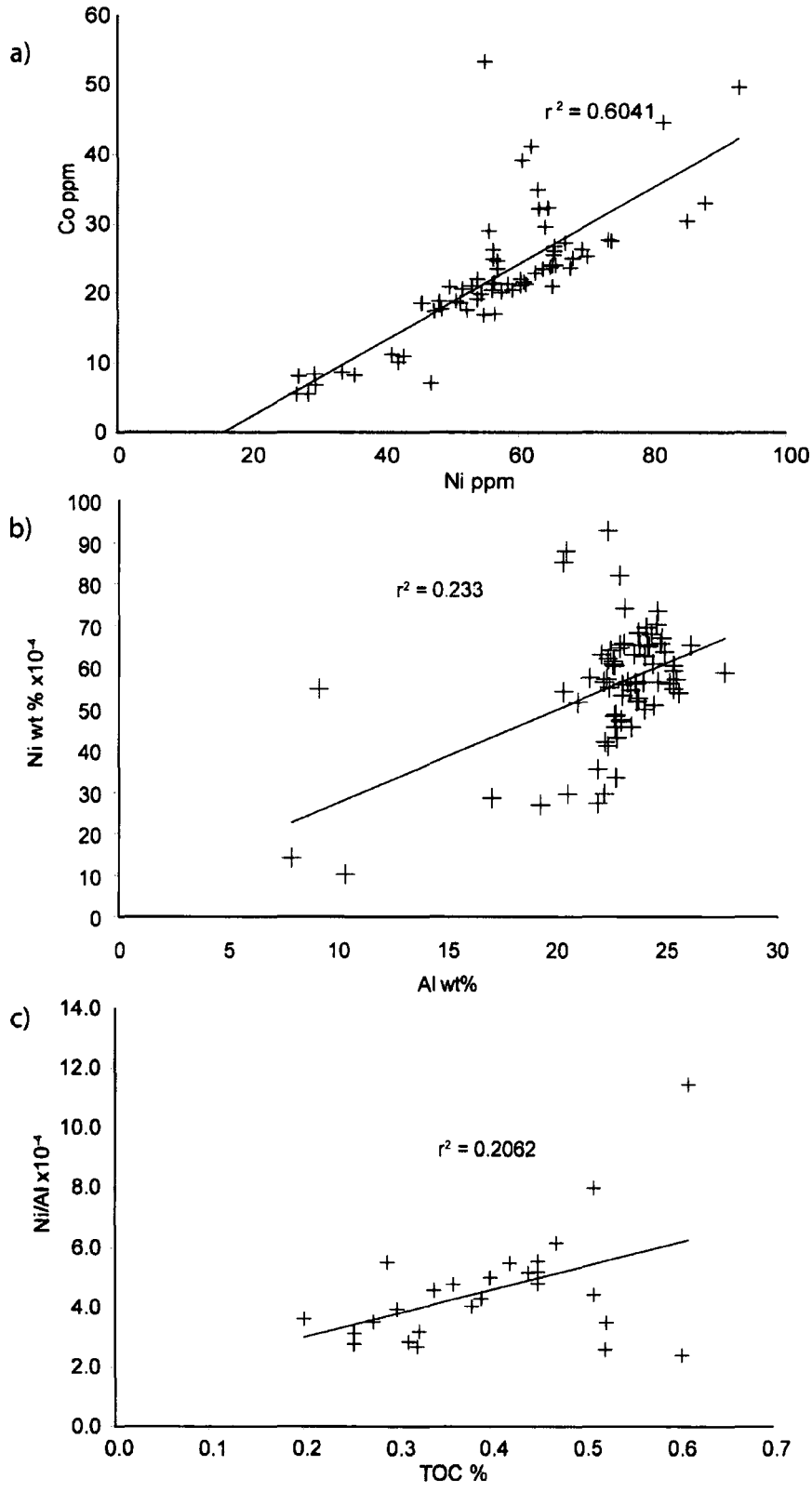

Figure 3.7: Cross-plots for a) Co vs. Ni, b) Ni vs Al and c) Ni/Al vs. TOC wt%

3.5 Preservation and productivity during deposition of OC-rich laminated hemipelagite

3.5.1 Synchroneity of productivity, preservation and redox

The trace fossil associations throughout LH^0 can be related to published models for biofacies and ichnofacies responses in deteriorating oxygen environments (Rhoads & Morse, 1971; Sageman *et al.*, 1991) and can be used to investigate relative timing of anoxia and LH deposition. Three distinct biofacies were recognized in the Rhoads & Morse (1971) model: anaerobic, dysaerobic and aerobic, each defined by a specific fauna and characteristic sedimentary fabrics. Sageman *et al.* (1991) defined seven biofacies corresponding to different levels of oxygenation. Level 1 and 2 indicate anaerobic conditions, level 2-6 dysaerobic conditions and level 7 aerobic conditions (Fig. 3.8).

The presence and absence of the three dominant ichnotaxa through LH^0 allows the recognition of three distinct ichnocoenoses that correspond to the biofacies levels described by Sageman *et al.* (1991): 1) *Thalassinoides* ichnocoenosis (biofacies level 6+), 2) *Planolites* ichnocoenosis (biofacies level 4-5), and 3) *Chondrites* ichnocoenosis (biofacies level 3). Oxy-

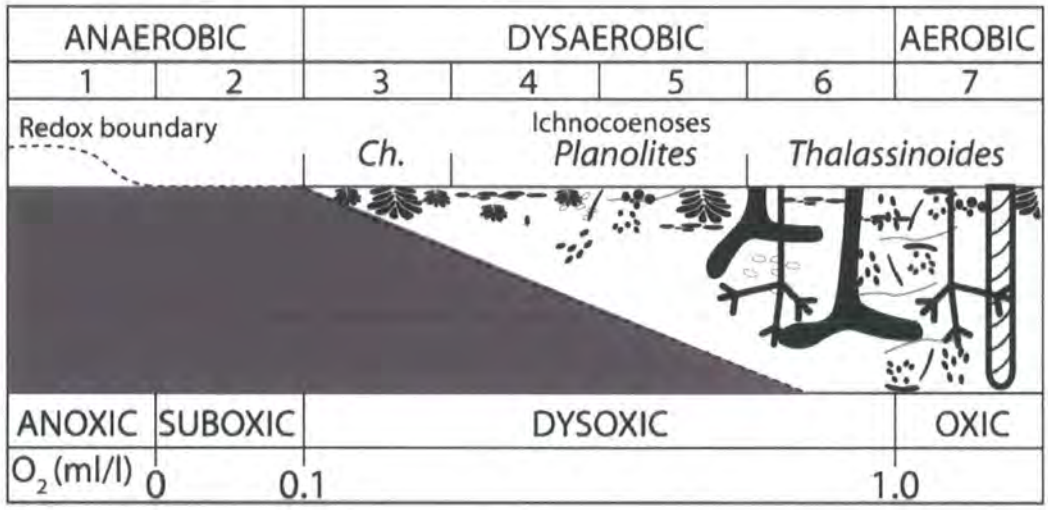

Figure 3.8: Infaunal biofacies model of Arthur & Sageman (1994). Level 1 reflects anaerobic conditions both above and below the SWI, with laminated sediments, the highest levels of preserved TOC and no evidence of benthic metazoans. At level 2 micro-burrowing disturbs the sedimentary laminae. Level 3 includes small deposit feeding pioneer ichnotaxa such as *Chondrites* or *Planolites*. Level 4 is characterized by an increase in the size and density of *Planolites* and *Chondrites* burrows, but no additional ichnotaxa. At level 5 more complex feeding traces such as *Zoophycos* and *Teichichnus* are found. Level 6 is indicated by the appearance of sediment-dwelling ichnotaxa ("domichnia") such as *Thalassinoides*. Above level 6 all groups included produce high-diversity assemblages. The *Chondrites*, *Planolites* and *Thalassinoides* ichnocoenoses present in the OC-poor sediments and the transition to OC-rich sediments represent infaunal biofacies levels 3-4. Interpreted oxygen levels at base of diagram (also from Arthur & Sageman, 1994) correspond to biofacies as shown.

gen depletion was initiated prior to the appearance of macroscopic OC, indicated by the disappearance of *Thalassinoides*, and declined gradually to fully anoxic conditions 1.4m into the event. In the upper part of LH^0, O_2 levels fluctuated between dysoxic (*Chondrites* ichnocoenosis, biofacies level 3) and fully anoxic conditions. O_2 levels rise through into the overlying OC-poor shales reaching levels close to the dysoxic-oxic boundary as marked by the reestablishment of *Thalassinoides*. Ichnocoenosis boundaries do not coincide with the boundaries of the LH suggesting OC burial flux/increased productivity and redox were not synchronous.

During the deposition of LH^1 we observe, 1) higher TOC WT% values which correspond to more negative $\delta^{13}C_{org}$ values when compared to the OC-poor lithofacies, 2) an increase in the inorganic productivity proxy Ba/Al and, 3) Ba values in OC-rich facies are higher than those for OC-poor facies (except samples at 7.84, 9.14 and 10.31 cm), 4) Ba values are variable (231 to 758 ppm) though are comparable to values recorded in modern upwelling systems e.g. Peru margin and Baja, California (see Table 3.4) but less than values from euxinic basins e.g. Black Sea (1171 ppm; Brumsack, 2006).

These patterns may suggest an increased productivity signal at the appearance of LH^1, however, because Ba values can be obscured by either euxinic conditions (Brumsack, 2006) or diagenesis (Milodowski & Zalasiewicz, 1991), it is possible our signal is obscured. Changes in productivity at the transition from OC-poor lithofacies to OC-rich LH are the most significant because this boundary represents a definite change in OC-burial and/or productivity. The trace fossil redox data from LH^0 suggest that euxinic conditions were not achieved (in LH^0 at least) until after 1.8 m across the OC-poor lithofacies - OC-rich boundary. Ba can be considered reliable up until this point in terms of diagenesis only if similar behaviour in redox is assumed for LH^1. A similar pattern in redox to LH^0 may be applicable for LH^1 by inference from Ba values which decrease approximately 2 m into the OC-rich event when oxygenation is inferred to become euxinic and Ba becomes mobile (Fig. 3.4). Where Ba values subsequently increase dramatically at the OC-rich to OC-poor boundary, may possibly reflect a 'barite-front' (Arndt *et al.*, 2006; Brumsack, 2006), a zone of precipitation of barium sulphate at a redox boundary following mobilization of Ba under euxinic conditions.

Bulk $\delta^{13}C_{org}$ data suggest LH^1 contains more negative $\delta^{13}C_{org}$ values than the OC-poor units. We consider this pattern is not attributed to changes in redox because sedimentary data and experimental data studies demonstrate greater depletion of $^{13}C_{org}$ in aerobic environments (Lehmann *et al.*, 2002). The difference in carbon isotope depletion between diagenesis in an aerobic and anaerobic environment is only 0.16 ‰ (-1.81 ‰ and -1.65 ‰ respectively, Lehmann *et al.*, 2002).The selective loss of different compounds with different reactivities and ^{13}C values during the decay of organic matter can account for minor shifts

in the $^{13}C_{org}$ of marine sediments (Freeman, 2001). However, for algal-dominated organic matter, such as in the Ordovician oceans, this effect is less than 1 ‰ (Freeman, 2001). Our values are greater than those expected from a change in redox environment and from loss of different compounds during diagenesis but consistent with increased burial of ^{12}C-enriched carbon. Also, the appearance of OC-rich LH is coincident with a decrease in $\delta^{13}C_{org}$ and not with the change in redox inferred in LH^1 from the trace fossil distribution of LH^0.

3.6 Stability of trace metal proxies

Both the values and patterns of Ni do not correspond to the sequence of redox conditions shown by the trace fossils. Indeed, during the deposition of LH^1, Ni/Co values are indicative of fully oxic conditions and during OC-poor they indicate dysoxia (Table 3.6). It is therefore clear that Ni and Co concentrations have been altered during late diagenesis and/or low-grade metamorphism and that the trace metals were mobile and can no longer be used as a redox proxy in the studied rocks.

On the other hand, we are confident of the reliability of the Ba values as a productivity proxy because of its enrichment in the OC-rich facies relative to the Rare Earth elements (REE, La-Yb). The REE have elsewhere been demonstrated to be mobile between turbidite beds and anoxic hemipelagites (Milodowski & Zalasiewicz, 1991) but REE in the measured transect of LH^1 are not enriched or depleted relative to OC-poor facies (Fig. 3.9) indicating either no remobilization, remobilization only on a small scale (e.g. cm-dm) or equal loss/gain of REE in each facies.

3.7 The origin of the Welsh Basin OC-rich laminated hemipelagites

The Runoff model predicts a decrease in products produced under arid weathering conditions (K relative to Al) and an increase in fluvial input indicated by higher Ti relative to Al and K. Though not of the same magnitude as previous studies utilizing these proxies (e.g. Beckmann *et al.*, 2005), we record higher K/Al values and constant Ti/Al values during deposition of LH^1 suggesting Avalonia experienced a relative increase in arid weathering conditions at this time with less fluvial input, making the means to produce a salinity-stratified basin from increased continental freshwater runoff unlikely.

Table 3.6: End-member values for trace element ratios for depositional redox conditions, Ni/Co. [1] (Jones & Manning, 1994).

	Oxic	Dysoxic	Suboxic-Anoxic	Euxinic
Ni/Co[1]	<5.00	5.00 - 7.00	>7.00	

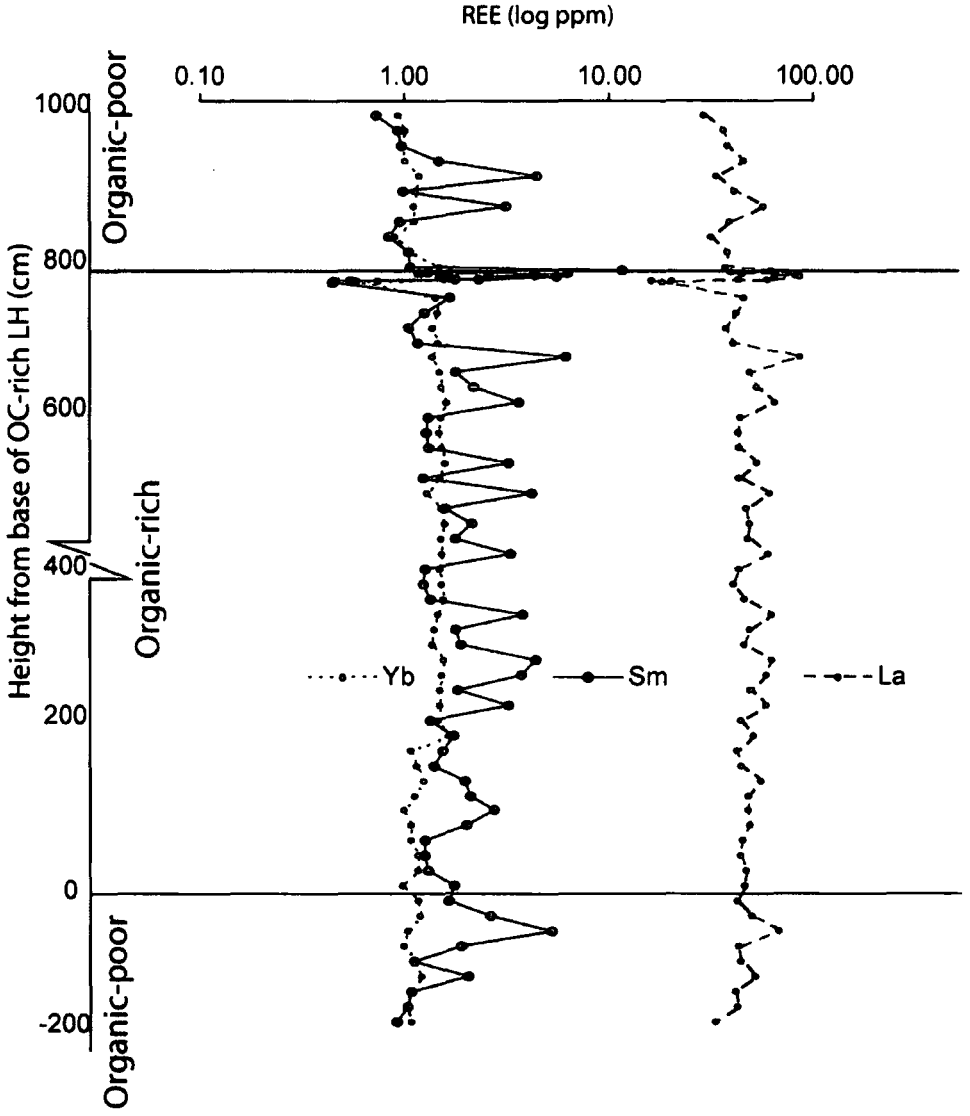

Figure 3.9: Light, middle and heavy Rare Earth Elements (La, Sm, Yb) plotted against stratigraphical height above base of LH[1], Traeth Penbryn. Sample points are scaled to maximum error.

The slightly lower K/Al values found in OC-poor facies indicate a relatively more humid climate with higher fluvial input but not significant to develop salinity stratification. As the majority of the late Katian Welsh Basin deposits are represented by the OC-poor burrow-mottled facies, we propose a more humid climate prevailed for much of the late Katian prior to the deposition of the Red Vein.

Transgressive shales are formed during relative sealevel rise, a concomitant rise in nutrients/productivity and an upwards expansion of the OMZ leading to increased preservation potential (Wignall, 1991). There are inconsistencies between the Transgressive model and

proxy data for the Welsh Basin LH[1]. The transgressive black shale model of Page *et al.* (2007) is essentially a glacioeustatic variant of the Runoff model, i.e. high nutrient input and productivity from glacial meltwater with associated sealevel rise. The stability of our Ti/Al ratio data throughout the OC-poor-LH-OC-poor transitions preclude increased runoff, as previously mentioned. An alternative transgressive black shale model, the 'Expanding puddle model' (Wignall, 1991) involves expansion of the OMZ as sealevel rises. However, in the productivity model, sealevel rise alone would only expand the OMZ and raise the pycnocline if accompanied by increased productivity and oxidation of organic matter which is not implied from sealevel rise. Implicit in the Transgressive model is increased preservation of OC (the Preservation model) from decreased thermohaline circulation and ensuing stagnation of the oceans and/or basin. Such a scenario could occur during global warming and melting of polar ice which has not been demonstrated during deposition of the LH. However, the approximately contemporaneous pre-Hirnantian Boda Event (Fortey & Cocks, 2005) has been described as a global warming event from faunal migrations but has in turn been refuted by Cherns & Wheeley (2007) on the grounds of increased global distribution of cool-water carbonates of Boda Event age.

The relative sealevel curve for the Welsh basin (Woodcock, 1990) is of too low a resolution to determine whether sealevel was rising during the *anceps* Biozone. An absence of grain-size changes during the Red Vein suggests sealevel was invariant at the resolution of our study.

In upwelling systems ^{12}C-enriched CO_2 derived from ^{13}C-depleted recycled organic matter is continually replaced from depth (Pancost *et al.*, 1999; Peeters *et al.*, 2002), therefore the supply of ^{12}C is effectively limitless in an open system that has high OC preservation such as an ocean with permanent deep water anoxia (Leggett, 1980). Sequestration of this depleted carbon into the marine phyoplankton through photosynthesis will result in sedimentary organic matter that is similarly depleted (Pancost *et al.*, 1999). Further to this, in modern lacustrine (e.g. Hollander & McKenzie, 1991) and marine environments (e.g. Freeman & Hayes, 1992; Goericke, 1994; Goericke *et al.*, 1994; Hofmann *et al.*, 2000), $\delta^{13}C_{org}$ has been shown to decrease as the concentration of dissolved CO_2 [CO_{2aq}] in surface waters increases and as productivity increases. We therefore interpret $\delta^{13}C_{org}$ in the current setting in terms of a proxy for upwelling intensity as reported from modern upwelling analogues (e.g. Pancost *et al.*, 1999). Finally, as recognized by Cave (1965), the presence of phosphate nodules throughout the succession in both OC-rich LH and OC-poor sediments could also be a further indication of nutrient-rich upwelling and the stabilisation of the redox boundary (see also Ingall *et al.*, 1993). Phosphorites have a limited occurrence at the present day, in particular being confined to zones of upwelling along west-facing continental margins (e.g. the Peru margin and S. Africa; Ingall *et al.*, 1993).

The LH unit analysed for inorganic and organic productivity proxies herein (LH^1), in light of redox data from LH^0, is thus interpreted to represent a period of higher productivity with increased organic carbon flux to the seafloor. The amount of marine organic carbon produced in the photic zone in the modern oceans is dependent largely on nutrient availability in surface waters (Berger *et al.*, 1989; Jahnke, 1990). We suggest coastal upwelling continually recycled bio-limiting nutrients (P, Ba) from depth and ^{12}C-enriched CO_{2aq}. The elevated Ba levels and negative $\delta^{13}C_{org}$ values observed in LH^1 are consistent with being the product of increased productivity from upwelling (Fig. 3.10 a, c). During these periods of high productivity, increased oxidative respiration of organic matter resulted in: 1) the seafloor becoming increasingly oxygen depleted and, 2) an upwards expansion of the OMZ. Organic-poor shales were deposited during periods of decreased productivity and organic carbon flux and a return to more oxygenated seafloor ensued (Fig. 3.10 b).

Coastal upwelling intensity can vary with a number of factors, but the most important of these is the strength of the offshore winds (Hay & Brock, 1992). During the late Katian, global atmospheric circulation models (Parrish, 1982) and palaeocontinental configurations (Herrmann *et al.*, 2004) infer that the Welsh Basin could have been located beneath the zone of southwesterly prevailing trade winds on a northwestwards facing coast (Fig. 3.11). We hypothesize that the cyclic nature of black shale deposition in the Red Vein reflects the changing intensity of the upwelling system in response to the changing strength of the offshore trade winds (see also Cave, 1965).

At the present day the strength of the trade winds is related to the intensity of the Hadley cell and is related to changes in equatorial high pressure. During the Plio-Pleistocene, the position and intensity of the Hadley circulation (and associated trade winds) varied with changes in ice volume and solar insolation respectively (Rind, 1998; Ruddiman, 2000), the Hadley cell moving polewards during periods of glacial retreat and reduced latitudinal temperature gradient. The intensification of coastal upwelling in the Welsh Basin and Iapetus Ocean from Hadley cell and trade wind position, prior to the Hirnantian glacial maximum, may therefore reflect latitudinal movement of the Hadley cell during an increase (northward movement of the Hadley cell) or decrease (southward movement of the Hadley cell) in the size of the Upper Ordovician ice sheet, depending on where the Hadley cell was initially positioned relative to Avalonia. Subsequent short-term cyclic patterns of increased upwelling (possibly represented by LH^0-LH^3) could reflect orbitally-moderated changes in solar insolation and ice volume.

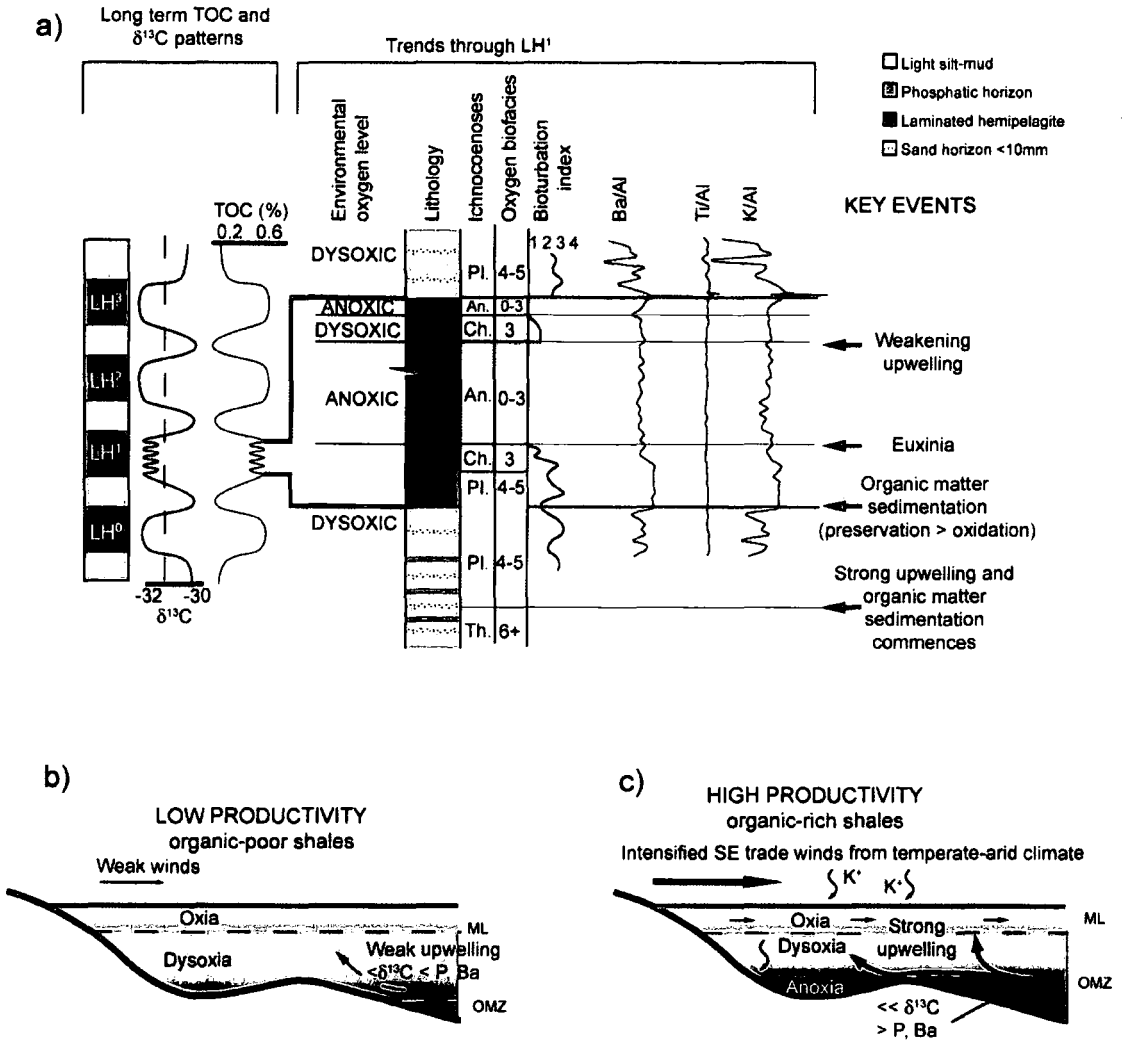

Figure 3.10: Summary of all proxies during deposition of LH^1 (a) Together, all proxies demonstrate that upwelling and oxygen deterioration commenced prior to the deposition of the LH event. Falling oxygen conditions were relatively gradual until euxinia was established whilst oxygen recovery was rapid yet fluctuated and occurred prior to the cessation of LH deposition. (b) Low productivity conditions were typified by weak upwelling and a depressed OMZ whereas high productivity conditions (c) occurred during high wind stress and increased upwelling that recycled nutrients and ^{12}C-enriched OC. ML = mixed layer.

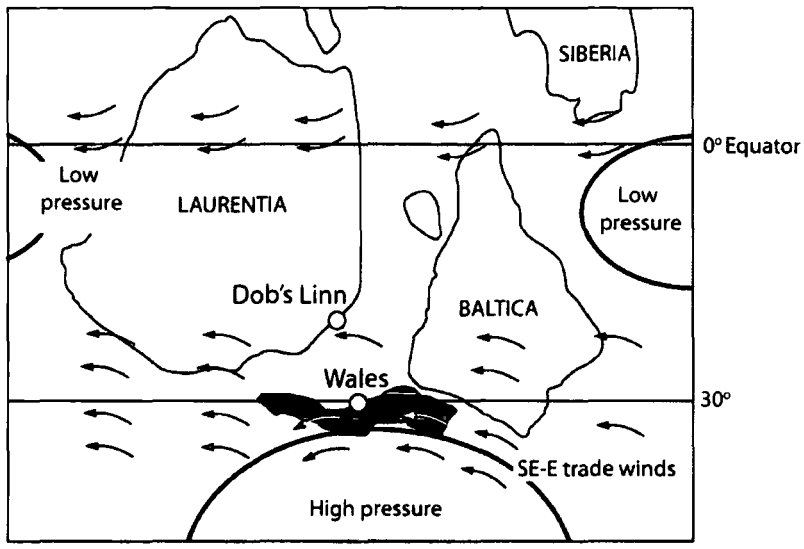

Figure 3.11: (a) Inferred trade wind positions and directions (from Parrish, 1982) over Avalonia. Palaeogeography adapted from Herrmann *et al.* (2004). (b) Detailed palaeogeography of the northern margin of Avalonia in the British Isles (after Woodcock & Strachan (2000)) and inferred position and direction of upwelling.

3.8 Conclusions

The fine grained siliciclastic rocks of the Welsh Basin record an evolving sequence of events during the transition from Ordovician greenhouse to icehouse climate states. We postulate that the proxy records from one OC-rich laminated hemipelagite unit (LH^1) presented herein indicate short-lived, cyclic enhanced coastal upwelling and surface organic productivity along the southern Iapetus margin. Increased upwelling and productivity could have been induced by increased wind stress from the intensification of coast-parallel to offshore SE trade winds. Higher productivity and OC supply to the deep ocean would likely have resulted in a rise in the position of the OMZ, which breached the semi-restricted Welsh Basin, in response to increased oxygen depletion of the water column. We hypothesize that black shale deposition may have been controlled by complex climate-ocean-biosphere interactions possibly reflecting responses to ice volume changes during the developing end-Ordovician glaciation. Replication of these results from other OC-rich units of similar age in the Welsh Basin (e.g. LH^0, LH^2 and LH^3) is necessary to further support this interpretation. Metamorphism to anchizone metamorphic facies reduces the number of ocean-environment proxies that can be used to elucidate palaeoenvironmental conditions. We consider the productivity proxies, Ba/Al, TOC %, $\delta^{13}C_{org}$ and the climate-sensitive detrital input proxies K/Al and Ti/Al to be robust and could be widely applied in the slate grade rocks commonly found in orogenic belts.

Chapter 4

Chitinozoan biotopes and biozone diachroneity.

Abstract

Correspondence analysis and unconstrained seriation have allowed the identification of four depth-facies biotopes for Chitinozoa from the Upper Katian–Hirnantian (Upper Ordovician) of Avalonia. These are: 1) an open ocean shallow-water epipelagic biotope including *Cyathochitina campanulaeformis*; 2) an open ocean middle-depth mesopelagic biotope comprising *Hercochitina* and *Spinachitina*; 3) an open ocean deep-water meso-bathypelagic biotope characterized by *Bursachitina umbilicata*; and 4) a shelf biotope containing predominantly *Desmochitina*. The taxonomic composition of the open ocean middle-depth mesopelagic biotope changes from one dominated by *Hercochitina* and *Spinachitina* in the pre-Hirnantian glacial maximum of the Upper Katian to one comprising *Ancyrochitina* in the Hirnantian post-glacial transgression. The distribution of the deep-water meso-bathypelagic biotope and the shelf biotope is affected by basin hydrography and sea level respectively. During upwelling along the southern margin of Iapetus, development of an expanding oxygen minimum zone displace deep-water taxa into the semi-restricted Welsh Basin. With sea level fall, taxa from the shelf biotope expand into the shallower basin. Origination of biostratigraphically useful taxa in such segregated environments restricts their distribution to periods of climatic and environmental change. Gradual change in climate and, hence, distribution of important biozone taxa, leads to diachroneity of chitinozoan biozones.

4.1 Introduction

Chitinozoans are microfossils of unknown biological affinity and little is known about their palaeoecology. They are relatively large and abundant in a wide variety of Ordovician marine

environments and commonly occur in graptolite-rich sediments but also persist where graptolites are absent. It has been postulated that they are the egg-cases of an unknown soft-bodied metazoan creature and have been used to document the biodiversification of their unknown producers, chitinozoophores (Paris *et al.*, 1999a; Nõlvak, 1999; Webby *et al.*, 2004). However, we have no direct understanding of the palaeoecology of the chitinozoophore and rely on inferences from comparisons of chitinozoan biofacies with lithofacies.

Unlike graptolites, for which many distribution and environmental models have been developed (see Cooper *et al.*, 1991, for a review), only a handful of studies have addressed similar problems for the Chitinozoa (Staplin, 1961; Jenkins, 1969, 1970; Urban & Kline, 1970; Laufeld, 1974; Miller, 1982; Grahn, 1982; Al-ameri, 1983; Bergström & Grahn, 1985; Grahn & Miller, 1986; Paris, 1996; Dorning *et al.*, 2006; Achab & Paris, 2007). The majority of these have been pattern-based studies documenting chitinozoan assemblages from particular lithofacies and have not been used in conjunction with any climate or hydrospheric models (i.e. changing latitudinal temperature gradient, water column oxygenation and sea level change).

It is generally agreed from the presence of abundant Chitinozoa in a wide variety of sediment types, including anoxic black shales, that the Chitinozoa were pelagic (Paris, 1981; Miller, 1982; Paris, 1996; Achab *et al.*, 1997; Armstrong & Brasier, 2005) and as such their dispersal, at a regional level at least, renders them biostratigraphically useful. However, chitinozoan provinciality in the Ordovician was high (Paris *et al.*, 2004) suggesting that they may have possessed a more environment-specific mode of life than graptolites, or that there was greater ecological barriers/gradients in the Ordovician oceans. Recently erected regional chitinozoan biozonation schemes (e.g. Paris, 1990; Nõlvak & Grahn, 1993; Nõlvak, 1999; Soufiane & Achab, 2000; Vandenbroucke, 2008) may therefore be marred to a certain extent by the uncertainty of how the chitinozoans were distributed in water masses and responded to changes in environmental gradients. This study addresses this area of uncertainty by testing a graptolite depth-facies model with chitinozoans.

4.1.1 Graptolite distribution models environmental gradients

Graptolites are, perhaps, the most suitable palaeoecological analogy to Chitinozoa (Achab & Paris, 2007; Cooper *et al.*, 2004). They inhabited a variety of pelagic environments, were generally wide-ranging and susceptible to oceanographic changes. In the early Palaeozoic, ecological constraints on graptolites have been suggested to be similar to those acting on modern plankton indicating that similar palaeoecological controls operated in the Palaeozoic (i.e. ocean current distribution, latitudinal temperature gradient, depth distribution and shelf–open ocean water mass partitioning, the continental boundary effect; see Cooper *et al.*,

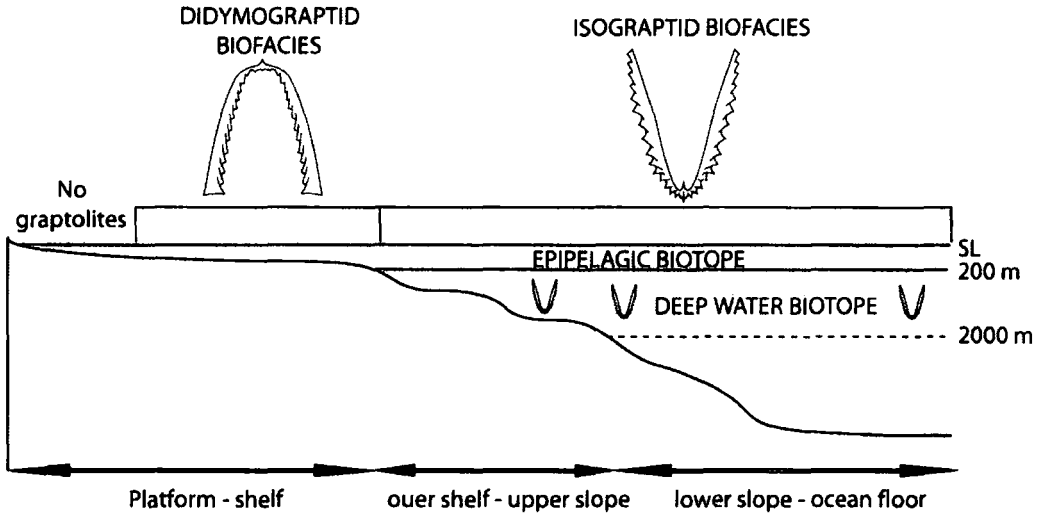

Figure 4.1: Graptolite depth biotopes and biofacies (after Cooper *et al.*, 1991). Both the epipelagic and deep water biotopes containing the didymograptid and isograptid biofacies resepectively are recognized in the latitudinally-controlled Pacific and Atlantic graptolite provinces.

1991, for a review of these processes in a graptolitic context). All of these controls have been proposed to be plausible for graptolite distribution for given scenarios, indicating that it is likely they are not mutually exclusive for graptolite dispersal.

In one case, the distribution of provincial graptolite faunas is interpreted as following the course of ocean currents with distinctive assemblages forming in gyre zones (Cooper *et al.*, 1991). Alternatively, Williams *et al.* (2003a) demonstrated the continental boundary effect in the Caradoc of the southern Welsh Basin, with an 'open marine biotope' assemblage dominated by *Orthograptus* spp. and an overlying *Normalograptus*-dominated 'inshore marine biotope'. They attributed the changes in graptolite faunas between the two environments to be the product of changing global sealevel alone. Furthermore, Finney *et al.* (2007) essentially demonstrated the same pattern for Laurentian graptolites but they further proposed that orthograptids were abundant in the denitrifying upwelling oxygen minimum zone (OMZ) during sealevel highstand and were replaced by normalograptids during glacio-eustatic sealevel fall in the Hirnantian. During post-glacial eustatic sealevel rise, reestablishment of the OMZ and extinction of the orthograptids, the normalograptids rapidly recolonized and diversified in the upwelling zone ecological niche left by the orthograptid biotope.

Finally, latitudinal gradient control has also been proposed for graptolites (Skevington, 1974). The 'Pacific' fauna of Skevington (1974) is characteristic of low-latitudes (30°N–30°S) and included such elements as *Phyllograptus typus*, whereas the 'Atlantic' fauna includes taxa such as *Didymograptus murchisoni* and *Azygograptus suecicus* and is prevalent at higher latitudes. However, the generality of this interpretation has been questioned by Mu *et al.*

(1979) in favor of a bathymetric distribution model which they suggested from the occurrence of each fauna in distinct depth-related facies at similar latitudes in China. Fortey & Cocks (1986) and Cooper *et al.* (1991) extended the concept of depth distribution in graptolites by recognizing an epipelagic biotope and a meso-bathypelagic biotope. From this, they defined the diverse deep water 'isograptid' biofacies which contained predominantly gracile forms and elements of both epipelagic and meso-bathypelaic graptolites, and an epipelagic, shelf-dominated 'didymograptid' biofacies. Additionally, it was noted that a water mass specific inshore biotope existed containing essentially pendent didymograptids (Figure 4.1).

These processes affecting graptolite distribution acted on different timescales. The response time of graptolite assemblages and their distribution to some of these environmental gradients (e.g. depth and/or temperature) may have been rapid (Zalasiewicz *et al.*, 1995) and may be climatic rather than tectonically controlled (e.g. current redistribution from geographical reconfiguration). Unlike graptolites, Chitinozoa have been reported from most types of Ordovician marine sediments (Webby *et al.*, 2004) and have minimal dependence on lithology. Despite the greater lithofacies dependency of graptolites than Chitinozoa, the principles of shelf and open ocean biotopes and depth zonation form a starting point to investigate and test chitinozoan palaeoecology.

4.2 A model for Chitinozoa

Rather than considering the relationship between chitinozoans and lithofacies alone, this study tests the hypothesis that Chitinozoa were depth stratified and environment specific as a response to changing basin hydrography. From the Welsh Basin, UK, presence-absence data of chitinozoan taxa in basin and shelf environments during perturbations in basin hydrography (i.e. development of basin anoxia and sealevel fall and rise), it is possible to establish the distribution of assemblages and to trace their movements during reorganization of water mass structure. Vertical migration of conodont biofacies related to the ocygen minimum zone (OMZ), for instance, has been demonstrated during upwelling along the southern Iapetus margin in the Upper Katian (Armstrong & Owen, 2002a). If chitinozoan assemblages were not depth stratified or environment specific, it is predicted that their distribution will be little affected by changes in hydrography such as upwelling (Figure 4.2). In the case of rejecting the null hypothesis of chitinozoan depth homogeneity, the appearance of key chitinozoan biozones may reflect, in part, displacement of index taxa into different environments. Such a mechanism could produce diachroneity of the first appearance datum of an index taxon throughout a basin and corrupt a biostratigraphical signal.

In the following discussion I adopt the terminology of Cooper *et al.* (1991): *biotope* is the area and depth zone (i.e. ecospace) occupied by a particular living fauna or flora, and

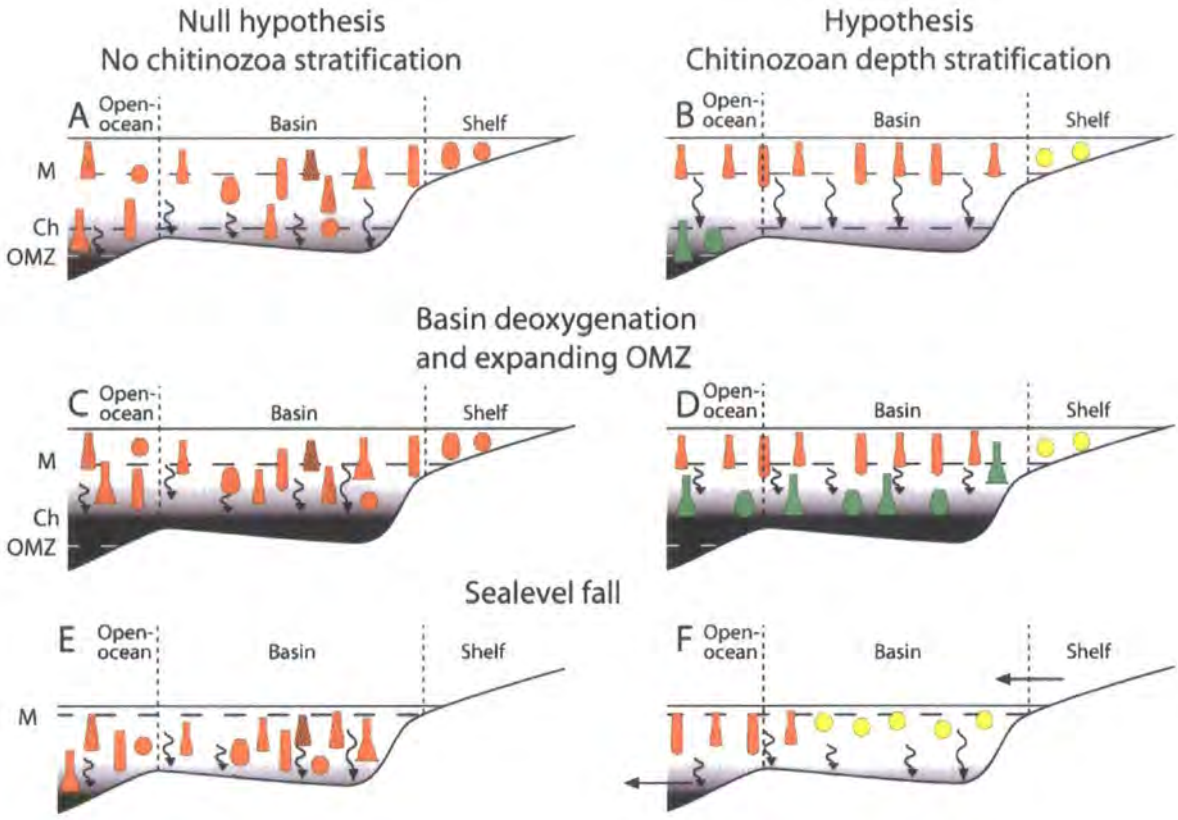

Figure 4.2: Chitinozoan depth stratification hypothesis. With no depth stratification, a given chitinozoan assemblage (orange figures) occupies a range of environments and the assemblage preserved (indicated by wavy arrows, representing deposition of chitinozoans) in basin or shelf sediment is not affected by changes in basin hydrography e.g. deoxygenation, or by sealevel fall (A, C and E). Where assemblages are depth and/or environment specific (orange, green and yellow figures in B), a change in basin oxygenation, for instance, may displace a deep water assemblage (green figures) into the basin and, if extreme, the shelf (D). During sealevel fall a shelf-specific assemblage (yellow figures) may be displaced into the basin environment (indicated by horizontal arrow) to coexist with an epipelagic assemblage (orange figures) while the deep-water assemblage is excluded from the basin (indicated by horizontal arrow, F). M=mixed layer, Ch=chemocline, OMZ=oxygen minimum zone. [1]Webby *et al.* (2004).

biofacies is a stratigraphic unit characterized by its fossil content. *Assemblage* is used to refer to the organisms inhabiting any individual biotope at a given time.

4.3 Palaeoenvironmental setting and hydrospheric model

The Upper Katian (Ashgill) and Hirnantian of the southern Welsh Basin, UK, provides a near complete record of deposition in both a basin and shelf mud-dominated slope-apron environment (Davies *et al.*, 1997). At this time, the Welsh Basin lay on the northern margin of Avalonia at mid-latitudes (MacNiocaill, 2000; Verniers *et al.*, 2002) and was semi-restricted,

bound to the east by the emergent Midland Platform with bathymetric barriers to the west (the Irish Sea Platform) and the south (Fishguard-Preseli Hills) (Woodcock & Strachan, 2000). Correlation between the basin (Cardigan area, west Wales) and shelf (Llandovery area, south central Wales) using both Chitinozoa and graptolites is robust (Figure 4.3 a).

In the upper Katian (Rawtheyan) *umbilicata* and *gamachiana* chitinozoan Biozones (*anceps* graptolite Biozone), deposition of four cyclical organic-rich laminated hemipelagites occurred in the basin environment punctuating a background of burrow-mottled mudstones (Nantmel Mudstones Formation). I interpret this distinct facies as an invigorated period of upwelling along the northern Avalonian coastline during relative warm climate when sealevel was high and climate belt configurations were favorable (Challands et al., *in review*; Armstrong et al., *in review*, see Figure 4.3 b). During upwelling an intense OMZ developed, associated with the deposition of organic-rich and phosphate-rich sediments (Figure 4.3 b). These organic-rich events are not expressed in the shelf environment which is composed of bioturbated muddy sands (Cribarth Formation). The shelf-basin break was bound by several faults active during the late Katian and comprises coarse sands and debris flows that interdigitate with the burrow-mottled basin mudstones (Bryn Nicol Formation).

During the Hirnantian, heterogeneity of lithofacies in the shelf environment was greater than in the basin and possibly reflects the greater sensitivity of this environment to the effects of climatically-driven changes in sediment supply and sealevel associated with the Hirnantian glacial maximum. It is not known whether coastal upwelling was active during this time in the southern Iapetus margin but upwelling from increased thermohaline circulation is envisaged to have been operating (Armstrong & Coe, 1997). Both basin and shelf environments were dominated by sand-rich deposition during this time (Yr Allt Formations, Ciliau Formation, Cwmcringlyn Formation) until subsequent warming and deglacial transgression in the Upper Hirnantian *persculptus* graptolite Biozone (*taugourdeaui* chitinozoan Biozone) which brought about deposition of transgressive organic-rich mudstones (Garth House Formation, Cwmere Formation, Figure 4.3 a).

4.4 Previous chitinozoan palaeoecology models

One of the earliest palaeoecological interpretations for Chitinozoa (Collinson & Schwalb, 1955) suggested that they were planktic from their wide occurrence in a variety of rock types. However, facies restriction on chitinozoan communities was subsequently demonstrated for the Devonian by Staplin (1961) who realized that the abundance of Chitinozoa was directly proportional to the amount of calcium carbonate in the rocks they were extracted from. Chitinozoans were found to be more abundant in fine-grained siliciclastic rocks. This observation was also made by Urban & Kline (1970) and Laufeld (1974) for Silurian chitinozoans from

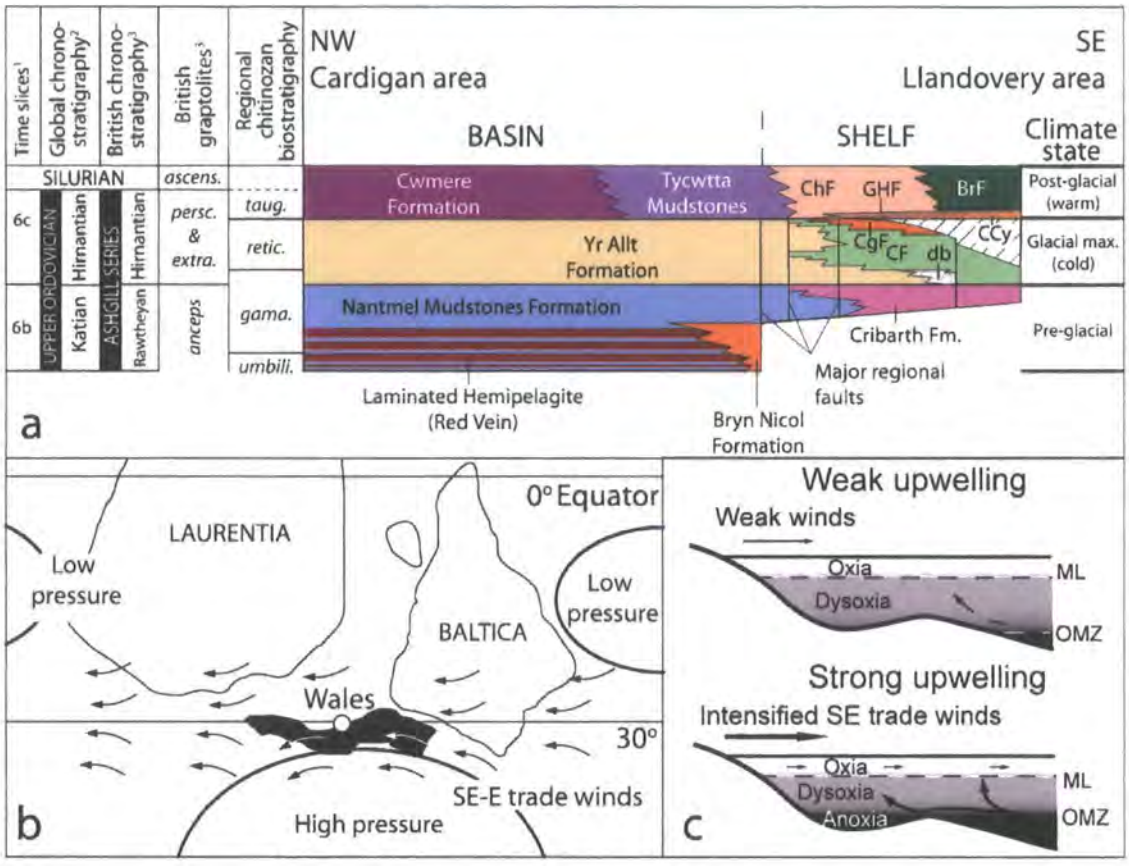

Figure 4.3: (a) Palaeogeographic and palaeoclimate setting of Avalonia and the Welsh Basin during Upper Katian warm climate state with SE trade winds directed over the southern margin of Iapetus. (b) hydrography of the Welsh Basin during weak coastal wind stress (top) and during increased coastal wind stress while situated beneath SE trade wind belt (bottom). (c) Chronostratigraphy, biostrataigraphy and lithostratigraphy between Basin (Cardigan area) and shelf (Llandovery area) with prevailing climate states indicated on the right. BrF=Bronydd Formation, db=disturbed beds, CCy=Cwm Clyd Sandstone Formation, CF=Ciliau Formation, CgF=Cwmcringlyn Formation, ChF=Chwefri Formation, ML=mixed layer, OMZ=oxygen minmum zone. [1]Webby *et al.* (2004); [2]Bergström *et al.* (2006a); [3]Fortey *et al.* (2000)

Gotland and seems to be consistent for the Chitinozoa throughout geological time. However, substrate alone reveals little in the way of vertical structure of plankton assemblages and may be more indicative of preservation potential rather than actual community structure. For instance, organic-rich sediments may only be preserved when burial rate is high and/or oxygenation is low.

Depth stratification in Chitinozoa was suggested by Grahn (1982) who derived a palaeoecological interpretation of Caradoc and Ashgill Chitinozoa from Gotland, Sweden, by first reconstructing the environmental conditions of the deposits. In this study, Grahn (1982)

proposed certain taxa had a benthic mode of life (e.g. *Cyathochitina reticulifera* and *Belonechitina robusta*) and he considered the sediment type to have had an important effect on the distribution of these Chitinozoa. Conversely, he noted that those forms considered to be benthic exhibit a far greater geographic range than modern benthic organisms. For those forms that were considered planktonic or epiplanktonic (e.g. *Hercochitina micracantha*, *Cyathochitina campanulaeformis*), Grahn (1982) noted that the range of dispersal is again greater than modern planktic organisms.

From the distribution of taxa in different facies, Grahn (1982) attempted to classify the Chitinozoa assemblages recovered into depth assemblages

1) Shallow depth: Chitinozoans preferentially recovered from shallow marine environments. This assemblage includes *Desmochitina minor*, *Cyathochitina campanulaeformis*, *Cyathochitina kuckersiana* and *Tanuchitina bergstroemi.*

2) Intermediate depth: Chitinozoans with a preference to restricted environment with reducing conditions predominantly comprising *Conochitina elegans* and *Lagenochitina baltica.*

3) Deep water: Chitinozoans found dominantly in carbonate mud environments.

Unfortunately, this model is not universally applicable being based on carbonate environments. Al-ameri (1983) further developed an ecological model for Silurian palynomorphs of Gondwana in siliciclastic environments establishing five 'palynofacies' ranging from terrestrial to marine and characterized by different suites and abundances of taxa. He recognized that any given chitinozoan taxon rarely occurs in more than one palynofacies from which he interpreted most Chitinozoa were benthic and their distribution correlated with water depth. However, ancyrochitinids were regarded as possibly being epiplanktonic and *Desmochitina* spp., recorded from shelfal sandstones, siltstones and shales and laminated shelfal siltones and mudstones were interpreted as having occupied the water column below tide level. In a similar vein to the graptolites (Cooper *et al.*, 1991), chitinozoan morphology has also been related to depth. Conical forms lacking appendages (e.g *Conochitina* spp.) have been suggested to have inhabited environments closer to shore and those with processes and delicate appendages (e.g. *Ancyrochitina* spp.) preferred deeper waters further out to sea (Al-ameri, 1983). Chitinozoans with short sculptural elements were prevalent in the deepest waters where diversity was low whereas forms recorded in shallower palynofacies had reduced or no appendages or ornamentation.

Non of these models integrated any dynamic oceanographical model into their schemes. No geochemical data has previously been utilized to suggest changing basin-shelf oxygenation

or carbon cycling/storage and basin hydrography associated with changing climate had any influence on chitinozoan distribution. Most recently, however, Achab & Paris (2007) compared chitinozoan biodiversity throughout the Ordovician with long-term trends in ocean circulation and eustatic change but comparisons with chemical parameters (e.g. Sr, Nd, $\delta^{18}O$ and $\delta^{13}C$) were largely uninformative or inconclusive, perhaps due to the broad comparison of taxa and low time resolution. In order to fully comprehend and understand the interrelationships between physio-chemical changes and chitinozoan distribution, specific, well-constrained examples and case studies are necessary.

4.5 Material and methods

Presence-absence data collected for the construction of a chitinozoan biozonation scheme between a basin setting (Cardigan area) and shelf break–shelf setting (Llandovery area) forms the dataset used herein for analysis (Figure 4.3).

For formations of *fossensis* to *taugourdeaui* chitinozoan Biozone age, a presence-absence matrix of chitinozoan taxa was constructed at the generic and specific level (Tables 4.1, 4.2). For the specific level matrix, specimens only identifiable at the generic level were excluded unless the specimens were the only representatives of their genus. This reduces loss of information because of poorly-preserved taxa. Analysing the dataset at the specific level provides a test for consistency of results from the generic analysis. Each of the formations investigated was categorized into one of three climate states according to when it was deposited: pre-Hirnantian glacial maximum, glacial maximum and post-glacial. These correspond to *fossensis*– upper *gamachiana* Biozones, upper *gamachiana–reticulatus* Biozones and *taugourdeaui* Biozones respectively (Figure 4.3 a). Formations were also categorized by their depositional environment into basin, shelf-break and shelf based on sedimentological interpretations of Davies *et al.* (1997, 2003) and Schofield *et al.* (2004). The data therefore represents two variables; water depth and time. The Nantmel Mudstones Formation, deposited before the glacial maximum, was further separated into burrow-mottled units and laminated hemipelagite units which were numbered consecutively from 0 to 3; the oldest (lowest) burrow-mottled unit referred to by OX^0, which is stratigraphically followed by LH^0, then OX^1, LH^1 and so forth.

The identification of biofacies and depth assemblages was made by identification of clusters of taxa and formations on plots of correspondence factor loadings in conjunction with results from unconstrained seriation. Unlike constrained seriation, unconstrained seriation allows the 'formation' variable to be repositioned during calculation as well as taxa. It therefore is not inhibited by the order the formations are placed in and so formations from different environments are free to be repositioned based on similarities in the taxonomic composition.

All analyses was conducted on the dataset at both the generic and specific level using the PAST software package (Hammer *et al.*, 2001).

4.6 Results

The presence absence matrix derived from the biozonation abundance data of Chitinozoa used for both correspondence analysis and unconstrained seriation are shown in Table 4.1 for genera and Table 4.2 for species.

4.6.1 Correspondence analysis

Plots of correspondence factor loadings for taxa present in samples at the generic and specific levels are presented in Figure 4.4. Key observations of the distribution of samples and chitinozoan taxa are: 1) Samples deposited during post-glacial transgression on the shelf (Bronydd, Cwmclyd Sandstone, Garth House formations) group with siphonochitinds, eisenackitinids, desmochitinids and belonechitinids. However, there is a distinct basin-shelf segregation of post-glacial samples and taxa. The Bronydd Formation retains an isolated position and appears isolated in the lower right corner of the specific-level plot and is associated with *Desmochitina juglandiformis* and *Lagenochitina* cf. *ponceti*. The basinal time equivalent Cwmere Formation is located in the extreme upper left of the same plot and is associated exclusively with *Ancyrochitina* cf. *primitiva*; 2) the Bryn Nicol Formation, representing a shelf-break environment, plots alongside samples from the basin environment; 3) hercochitinids, spinachitinids, ancyrochitinids and saharochitinds plot most closely to samples from pre-glacial maximum basin environments; 4) siphonochitinds, eisenackitinids, desmochitinids and belonechitinids plot most closely to samples from shelf environments; 5) the shelfal Cribarth and Ciliau Formations plot in the same region as samples from the basin environment;

Table 4.1: Presence–absence matrix for Chitinozoa identified to generic level for basin-shelf transect at the formations. BNF=Bryn Nicol Formation, BrF=Bronydd Formation, CCy=Cwm Clyd Sandstone, CeF=Cwmere Formation, CF=Ciliau Formation, CgF=Cwncringlyn Formation, GH=Garth House Formation, Garth House, YA=Yr Allt Formation.

	OX^0	LH^0	OX^1	LH^1	OX^2	LH^2	OX^3	LH^3	YA	CeF	BNF	Cri	CF	CgF	GHF	CCy	BrF
Cyathochitina	0	0	1	1	0	0	1	1	1	1	1	1	1	1	1	1	0
Saharochitina	0	0	0	0	0	1	0	0	1	0	1	0	0	0	0	0	0
Tanuchitina	1	0	0	0	0	0	0	0	0	0	1	0	0	1	0	1	1
Hercochitina	1	1	0	1	1	0	1	1	1	0	1	1	1	0	1	1	0
Ancyrochitina	0	0	0	1	0	1	0	0	1	1	1	0	0	0	0	1	1
Bursachitina	0	1	0	0	0	0	0	0	0	0	0	0	0	1	1	0	0
Spinachitina	1	1	0	1	0	1	1	1	1	0	1	1	1	0	1	1	0
Conochitina	0	1	0	0	1	0	0	1	1	0	0	1	0	0	1	0	0
Rhabdochitina	0	1	0	0	0	0	0	0	0	0	0	0	0	0	0	0	0
Belonechitina	0	1	0	0	0	0	0	0	1	1	0	1	1	1	1	1	0
Laufeldochitina	0	0	0	0	0	0	0	0	1	0	1	0	0	0	1	0	1
Eisenackitina	0	0	0	0	0	0	0	0	0	0	0	0	0	0	1	1	0
Desmochitina	0	0	0	0	0	0	0	0	1	1	0	0	1	0	1	1	1
Lagenochitina	0	0	0	0	0	0	0	0	0	0	0	0	0	0	1	0	1
Siphonochitina	0	0	0	0	0	0	0	0	0	0	0	0	0	0	1	1	0

Table 4.2: Presence–absence matrix for Chitinozoa identified to species level for basin-shelf transect at the formation level. See Table 3.1 for list of formation abbreviations.

	OX^0	LH^0	OX^1	LH^1	OX^2	LH^2	OX^3	LH^3	YA	CeF	BNF	Cri	CF	CgF	GHF	CCy	BrF
Cyathochitina campanulaeformis	0	0	1	1	0	0	1	1	1	1	1	1	1	1	1	1	0
Cyathochitina kuckersiana	0	0	0	0	0	0	0	0	1	0	1	0	0	0	1	0	0
Cyathochitina calix	0	0	0	0	0	0	0	0	1	0	1	0	0	0	1	1	0
Cyathochitina cf. *reticulifera*	0	0	0	0	0	0	0	0	0	0	0	0	0	0	1	0	0
Saharochitina sp.	0	0	0	0	0	1	0	0	1	0	1	0	0	0	0	0	0
Tanuchitina bergstroemi	1	0	0	0	0	0	0	0	0	0	0	0	0	0	0	0	0
Hercochitina sp. 1	0	0	0	0	0	0	0	0	0	0	0	1	0	0	0	0	0
Hercochitina cf. *normalis*	0	0	0	1	1	0	0	0	0	0	1	0	0	0	0	0	0
Hercochitina cf. *seriespinosa*	0	0	0	1	0	0	1	0	0	0	0	1	0	0	0	0	0
Hercochitina aff. *normalis*	0	0	0	1	0	0	0	1	0	0	1	0	0	0	0	0	0
Hercochitina micracantha	0	0	0	0	0	0	0	0	1	0	0	0	0	0	0	1	0
Hercochitina aff. *seriespinosa*	0	0	0	1	0	0	0	0	1	0	1	0	0	0	0	0	0
Hercochitina cf. *crickmayi*	0	1	0	0	1	0	0	0	0	0	1	1	0	0	0	0	0
Hercochitina cf. *gamachiana*	0	0	0	1	0	0	1	0	0	0	0	1	0	0	0	0	0
Hercochitina minuta	1	0	0	0	1	0	0	0	0	0	0	0	0	0	0	0	0
Hercochitina sp. A	0	0	0	0	0	0	0	1	1	0	0	0	0	0	0	0	0
Hercochitina cf. *grandispinosa*	1	0	0	0	0	0	0	0	0	0	0	0	0	0	0	0	0
Hercochitina turnbulli	0	1	0	0	0	0	0	0	0	0	0	0	0	0	0	0	0
Ancyrochitina cf. *primitiva*	0	0	0	0	0	0	0	0	0	1	0	0	0	0	0	0	0
Bursachitina umbilicata	0	1	0	0	0	0	0	0	0	0	0	0	0	0	0	0	0
Spinachitina taugourdeaui	0	0	0	0	0	0	0	0	0	0	0	0	0	0	1	0	0
Spinachitina penbryniensis	1	1	0	1	0	1	1	1	0	0	0	0	0	0	0	0	0
Spinachitina coronata	0	0	0	1	0	0	0	0	0	0	0	1	0	0	0	0	0
Spinachitina fossensis	1	0	0	1	0	0	0	0	0	0	1	0	0	0	0	0	0
Spinachitina cf. *bulmani*	1	1	0	0	0	0	0	0	0	0	0	0	0	0	0	0	0
Spinachitina sp. 2	0	0	0	1	0	0	0	0	0	0	0	0	0	0	0	0	0
Spinachitina sp. A	0	0	0	1	0	0	0	0	0	0	0	0	0	0	0	0	0
Spinachitina sp. 4	0	0	0	1	0	0	0	0	0	0	0	0	1	0	1	0	0
Conochitina rugata	0	1	0	0	0	0	0	0	0	0	0	0	0	0	0	0	0
Conochitina sp. 1	0	0	0	0	0	0	0	0	0	0	0	1	0	0	1	0	0
Conochitina cf. *homoclaviformis*	0	0	0	0	1	0	0	1	1	0	0	0	0	0	0	0	0
Rhabdochitina gracilis	0	1	0	0	0	0	0	0	0	0	0	0	0	0	0	0	0
Belonechitina capitata	0	0	0	0	0	0	0	0	0	0	0	1	0	0	1	0	0
Belonechitina ceredigioniensis	0	1	0	0	0	0	0	0	1	0	0	1	0	0	1	0	0
Belonechitina ?. americana	0	0	0	0	0	0	0	0	1	0	0	0	0	0	0	0	0
Belonechitina cf. *robusta*	0	0	0	0	0	0	0	0	1	0	0	0	0	0	0	0	0
Belonechitina reticulatus	0	0	0	0	0	0	0	0	1	0	0	0	0	0	0	1	0
Belonechitina sp. 12	0	0	0	0	0	0	0	0	1	0	0	0	0	0	1	0	0
Belonechitina wessenbergensis	0	0	1	0	0	0	0	0	1	0	0	0	1	0	1	0	0
Belonechitina sp. A	0	0	0	0	0	0	0	0	0	0	0	0	0	0	1	0	0
Laufeldochitina lardeuxi	0	0	0	0	0	0	0	0	1	0	0	0	0	0	1	0	0
Eisenackitina inconspicua	0	0	0	0	0	0	0	0	0	0	0	0	0	0	1	0	0
Eisenackitina cf. *rhenana*	0	0	0	0	0	0	0	0	0	0	0	0	0	0	0	1	0
Desmochitina cocca	0	0	0	0	0	0	0	0	1	0	0	0	0	0	1	1	0
Desmochitina minor	0	0	0	0	0	0	0	0	1	0	1	1	0	0	1	1	1
Desmochitina erinacea	0	0	0	0	0	0	0	0	0	0	1	0	0	0	1	0	0
Desmochitina juglandiformis	0	0	0	0	0	0	0	0	0	0	0	0	0	0	1	0	1
Lagenochitina cf. *ponceti*	0	0	0	0	0	0	0	0	0	0	0	0	0	0	0	0	1
Siphonochitina sp.	0	0	0	0	0	0	0	0	0	0	0	0	0	0	1	1	0

and 6) LH^0 from the basin environment is isolated from other samples from the pre-glacial maximum basin environment and is associated with a distinct fauna characterized by *Bursachitina umbilicata*.

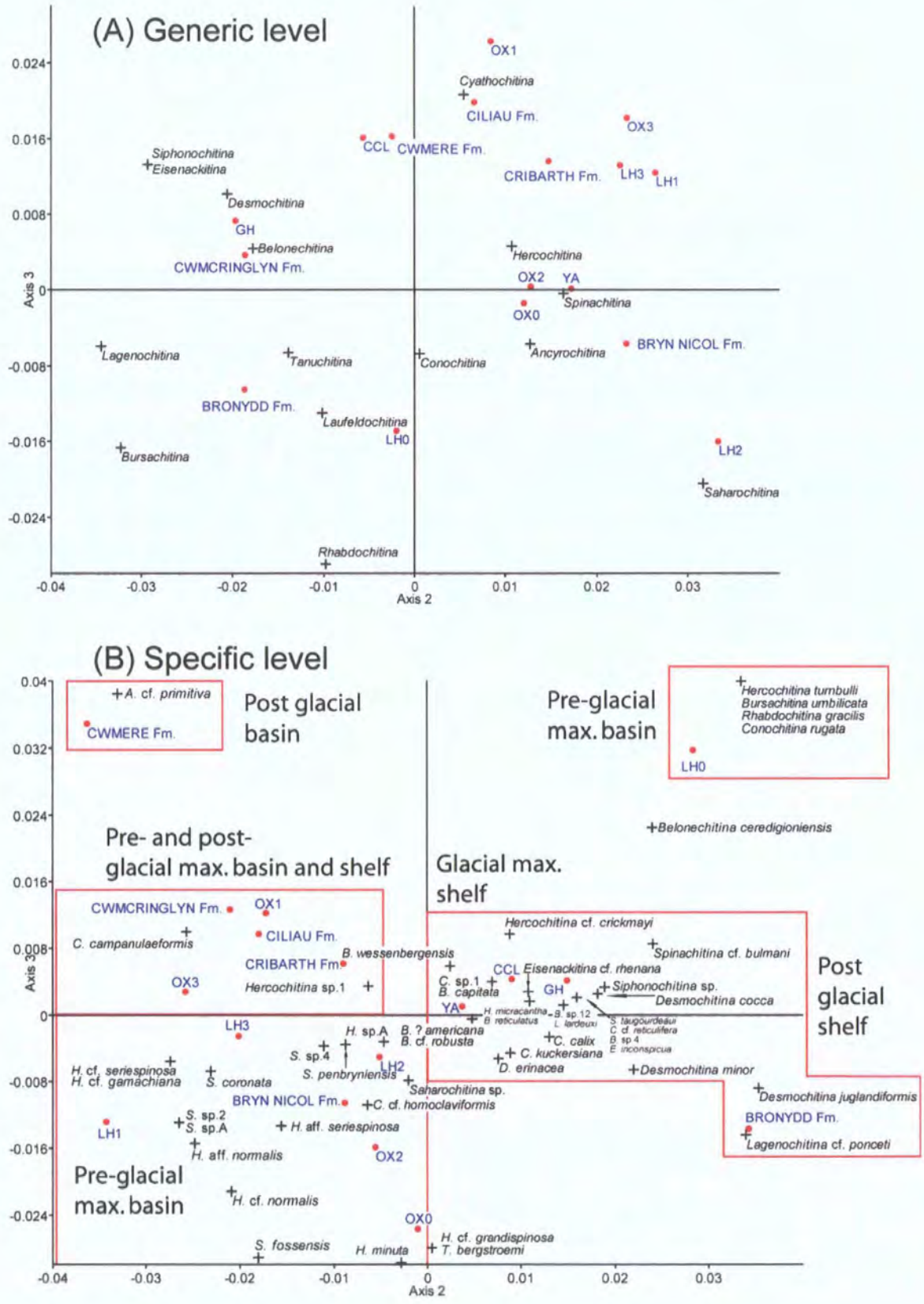

Figure 4.4: Plots of correspondence factor loadings for analysis of formations and taxa at the generic level (a) and the specific level (b). Axis 1 is not plotted because eigenvector 1 only represent total frequency in the presence-absence matrix. Discrete clusterings (in red boxes) represent formations from a distinct environment or climate state with shared taxa. Formations and taxa that plot around 0 in the negative half of axis 2 represent formations containing few taxa or taxa that occupy many environments and are long-ranging.

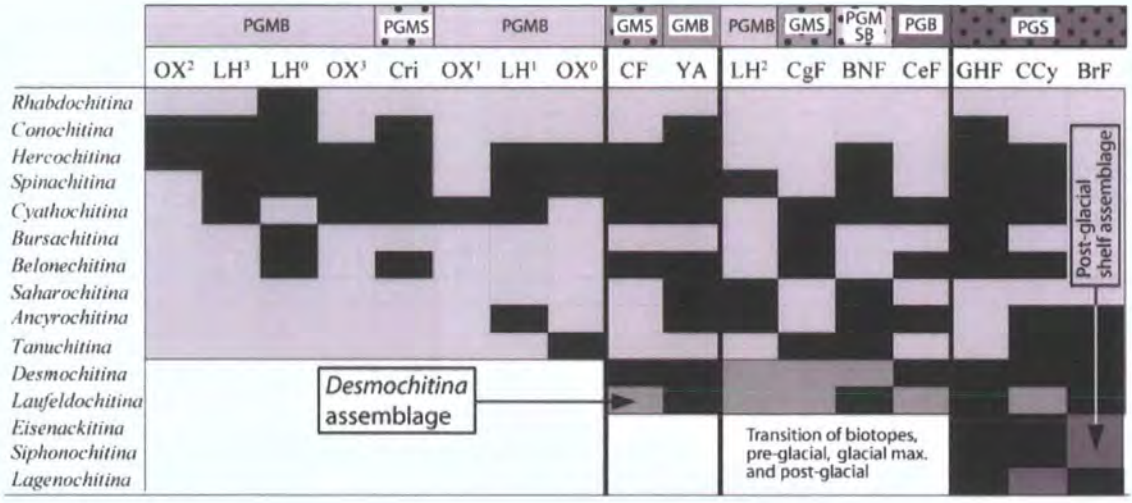

Figure 4.5: Unconstrained seriation matrix for chitinozoan genera present in formations from the basin, shelf-break and shelf. Light grey shading represents the open ocean biotopes (*Cyathochitina, Herchochitina-Spinachitina* and *Bursachitina* assemblages), medium grey shading represents the shelf biotope pre-glacial maximum *Desmochitina* assemblage and dark grey shading represents the shelf biotope post-glacial maximum assemblage. Seriation index = 0.62. Environment-time abbreviations: PGMB=Pre-glacial maximum basin, PGMS=Pre-glacial maximum shelf, PGMSB=Pre-glacial maximum shelf-break, GMB=Glacial maximum basin, GMS=Glacial maximum shelf, PGB=Post-glacial basin, PGS=Post-glacial shelf. See figure 4.3 for formation abbreviations.

4.6.2 Seriation

Unconstrained seriation at the generic level (Figure 4.5) groups all burrow-mottled units and laminated hemipelagite units (except LH^2) with the pre-glacial maximum Cribarth Formation from the shelf environment. Spinachitinids and hercochitinids are the most abundant chitinozoans throughout this assemblage. However, these units are not organized in stratigraphic order in the resulting analysis (Figure 4.5). Burrow-mottled units and laminated hemipelagite units do not show consistent segregation. A second distinguishable assemblage, marked by the appearance of desmochitinids and laufeldochitinids comprises samples from the glacial maximum and post-glacial shelf and basin as well as LH^2. This assemblage also contains the Bryn Nicol Formation from the pre-glacial shelf-break environment. Post-glacial deposits from the shelf environment form a third distinct assemblage that contains many of the taxa in the first two groups and additionally eisenackitinids, siphonochitinids and lagenochitinids. A group of formations from both shelf and basin environments representing all climate states and containing taxa from the *Hercochitina* and *Desmochitina* assemblages indicates mixing of biotopes during changing climate.

For unconstrained seriation analysis at the specific level, greater segregation of samples by taxa is evident and ordering of formations better fits stratigraphic order. Several distinct

differences are noticeable compared to the generic analysis. OX^0 and LH^0 form a discrete group comprising the same taxa as in the correspondence analysis and includes the zone fossils *Bursachitina umbilicata* and *Spinachitina fossensis*. The Bryn Nicol Formation groups with the pre-glacial maximum basin samples in its species composition rather than with the shelf samples as suggested by the generic level analysis. The Cwmere Formation, Cwmcringlyn Formation, Ciliau Formation and OX^1 form a group marked by the absence of numerous species of *Spinachitina* and *Hercochitina* with few additional taxa. The only taxon these formations have in common is the long-ranging *Cyathochitina campanulaeformis* and occurs in all environments and climate states. A final group comprising formations from the glacial maximum basin and the post-glacial shelf is characterized by the appearance of several species of *Desmochitina*, other than *Desmochitina minor*, *Belonechitina* defining a *Desmochitina* assemblage as recognized at the generic level analysis. Other taxa restricted to this assemblage are *Siphonochitina*, *Eisenackitina* and *Lagenochitina* cf. *ponceti* and *Laufeldochitina lardeuxi*. The latter two taxa are the only representatives of their genera identified to specific level. This assemblage contains the zone fossils *Belonechitina reticulatus* and *Spinachitina taugourdeaui*.

4.7 Interpretation: Biofacies organization and a depth model for chitinozoan distribution

The Graptoloidea are considered to be ecologically close to the chitinozoan animal (Achab & Paris, 2007; Cooper *et al.*, 2004) and similarities in the distribution of the two groups is therefore anticipated. In Laurentia during the late Katian (Cautleyan-Rawtheyan), and in Wales during the early Katian (Caradoc), the majority of graptolites lived in denitrification zone waters within and on the edges of oxygen minimum zones (OMZs) that developed around areas of intense upwelling (Berry *et al.*, 1985; Finney & Berry, 1997; Williams *et al.*, 2003a; Finney *et al.*, 2007) in an open ocean setting i.e. they are an open ocean biotope. The laminated hemipelagite units of the Nantmel Mudstones Formation contain an abundant low-diversity graptolite assemblage of *Orthograptus abbreviatus-truncatus* and may reflect a similar upwelling system to that of the Laurentian margin or the Caradoc in Wales. A preservation bias for the sudden appearance of graptolites present in the LH is excluded because graptolite thecal fragments and nemata are recovered from burrow-mottled mudstones alongside Chitinozoa. Based on similarity in facies distribution, Chitinozoa that occur *only* in Nantmel Mudstones Formation LH units likely occupied a similar zone in the water column to graptolites in upwelling waters on the edge of the OMZ. Conversely, the presence of abundant, diverse and well-preserved Chitinozoa in burrow-mottled sediments implies that some Chitinozoa inhabited water masses or depths outside the influence of upwelling and/or

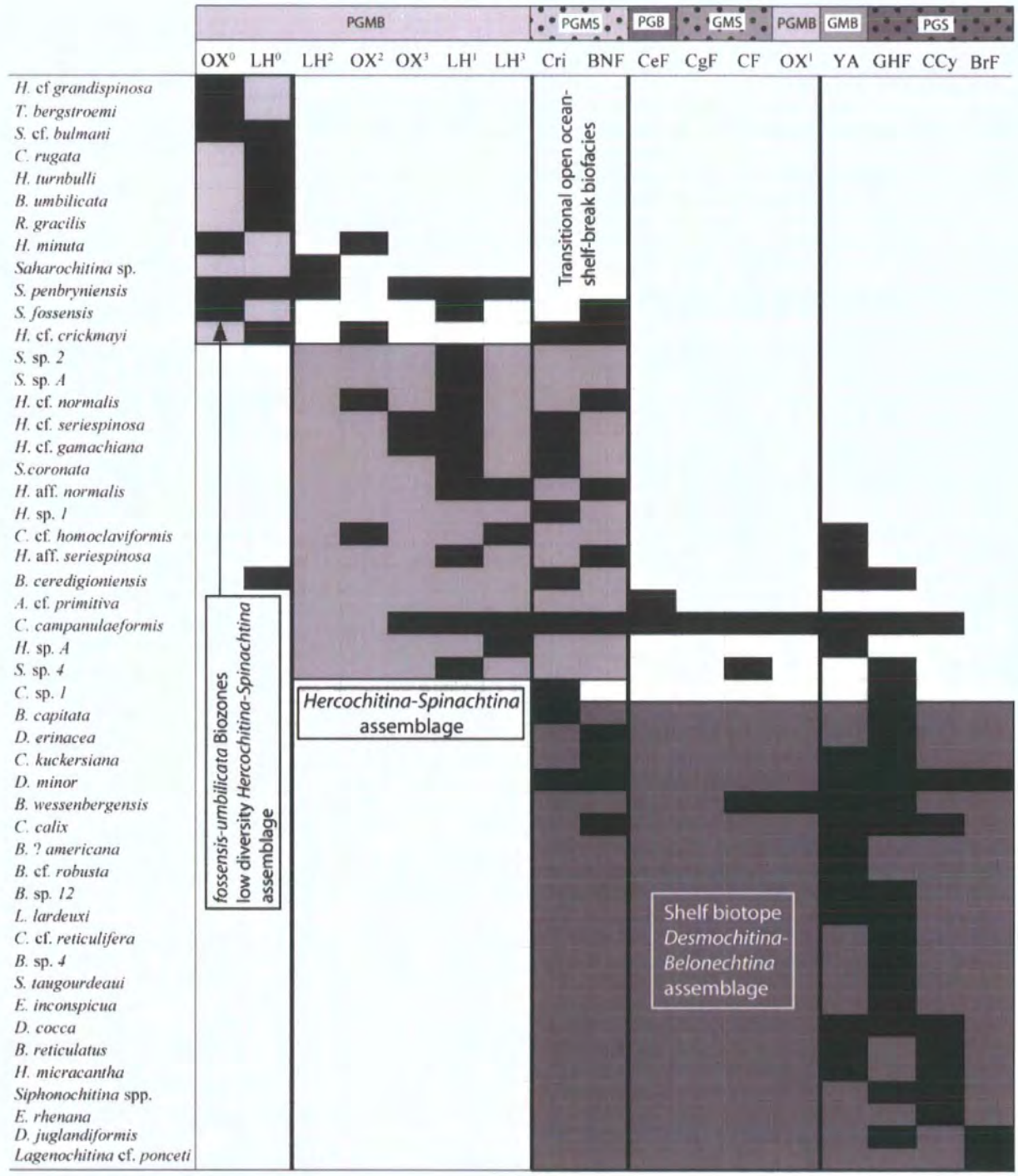

Figure 4.6: Unconstrained seriation matrix for chitinozoan species present in formations from the basin, shelf-break and shelf. Seriation index = 0.51. See figure 4.3 for formation abbreviations and Figure 4.5 for environment-time abbreviations.

expansion of the OMZ during LH deposition. Taxa that occur in the basin in both burrow-mottled and LH units as well as in shallower facies such as the shelf-break environment and the shelf environment e.g. *Hercochitina* cf. *crickmayi* are interpreted to comprise a biotope that occupied shallower waters than those that were affected or displaced by the expansion of the OMZ or those that are not present on the shelf. However, some Chitinozoa (e.g. *Hercochitina normalis, Hercochitina* aff. *seriespinosa*) and graptolites (*Orthograptus abbreviatus, Normalograptus normalis*) that only occur in the LH^1 unit in the basin are also recovered from the pre-glacial maximum shelfal Cribarth Formation. Because these taxa have only been recovered from the basin during a time of hemipelagite deposition (inferred to represent upwelling), I interpret that hydrospheric changes during these events were great enough to displace them from the basin into the shelf environment. This pattern is Finally, in the open ocean setting, there are taxa that are long-ranging, also occur in shelf-break and shelf settings and persist through all climate states. They can therefore tolerate perturbations in deeper water hydrography as well as changes in sealevel. Their inferred habitat is considered to be a shallow epipelagic one. Additionally, taxa that are restricted to the shelf environment or only occur in the basin during the Hirnantian glacial maximum, when sealevel was low, conform to the view of a shallow water shelf biotope.

The summation of these observations and interpretations is the recognition of four distinct biotopes during different climate states that segregate chitinozoan taxa in depth of depositional environment and in depth in the water column. These are an open ocean biotope with; 1) shallow-water; 2) middle-water; and 3) deep-water biotopes and 4) a shelf biotope. The open ocean biotope contains chitinozoan taxa that are exclusive to basin environments along with taxa that occur in basin and shelf environments. Within the open ocean biotope, three depth assemblage biotopes have been recognized; shallow water, middle water and deep water interpreted as epipelagic, mesopelagic and meso-bathypelagic respectively. The shallow depth biotope comprises taxa that occurs in both the basin and shelf environments and is characterized by *Cyathochitina campanulaeformis* (Figure 4.7 a). The middle depth assemblage constitutes the majority of the open ocean biotope that occurs in basin environment deposits. For the pre-glacial maximum this assemblage is dominated by hercochitinids from the *B. umbilicata* Biozone to the *Belonechitina reticulatus* n. sp. Biozone (Figure 4.7 a-b), and for post-glacial basin it is exclusively characterized by ancyrochitinids (Figure 4.7 d). The deep-water biotope contains an assemblage of taxa that only occurred in the basin environment during deposition of laminated hemipelagite and is interpreted as having entered the Welsh Basin from displacement by an expanding oxygen minimum zone during increased upwelling. The composition of this assemblage is not consistent; for LH^0 it is dominated by

Bursachitina umbilicata and for LH^{2-3} it is characterized by differing species of *Hercochitina* and *Spinachitina*.

The shelf biotope contains taxa that are exclusive to shelf environments but may be supplemented by taxa from the epipelagic open ocean biotope. It is discernable during all climate states and is dominated by *Desmochitina* and *Belonechitina* but is most distinct during the post-glacial climate with the appearance of *Laufeldochitina lardeuxi*, *Lagenochitina* cf. *ponceti* and several *Desmochitina* species not found in other samples (Figure 4.7 a-d).

It is possible from the discrete biotopes and diversity of depth assemblages established herein that even though some chitinozoan taxa do display similar palaeoecological patterns described by graptolites, graptolites cannot be used as a general comparison group or analogy for chitinozoan palaeoecology. Instead, the ecological structure of chitinozoans should be considered and established in their own context.

4.8 The depth model for chitinoza outside the Welsh Basin

Some of the most refined biostratigraphical schemes are heavily constrained by palaeoecological controls and most fully applicable to only a restricted palaeoclimate-geographic belt/region (e.g. Late Caradoc graptolite faunal gradients across the Iapetus Ocean Zalasiewicz *et al.* (1995)). Furthermore, modern restricted and semi-restricted basins (e.g. the Mediterranean Sea), can possess their own local circulation patterns and physiochemical gradients (Wignall, 1994). The Welsh Basin was a semi-restricted environment (Woodcock & Strachan, 2000) and therefore it is plausible that the distribution scheme of Chitinozoa proposed herein may be nothing more than a basin-specific signature. In order to test the appropriateness of the chitinozoan depth stratification model it is necessary to compare the model outwith the Welsh Basin. Because the Welsh Basin biozonation scheme compares well with the Avalonian regional biozonation scheme, other Avalonian localities are used for comparison. The test may be extended to other palaeocontinents for taxa not endemic to Avalonia and similar work identifying water mass indicators in Chitinozoa on a global scale is currently been carried out by Dr T. Vandenbroucke (Ghent University).

The type stratum for *B. umbilicata*, from the Cautley Mudstone Formation of northern England, is from a deep shelf setting. Furthermore, in the Condroz inlier in Belgium, the *umbilicata* Biozone is recorded from a deep outer-shelf to slope setting with graptolite-bearing horizons. Despite not having been recorded outside Avalonia, these other occurrences of *B. umbilicata* support the interpretation that this taxon is restricted to a deep water environment.

Of particular interest in the Cautley section is the occurrence of *S. fossensis* with *B. umbilicata*. Vandenbroucke *et al.* (2005) recorded a repeated appearance of *S. fossenis* within

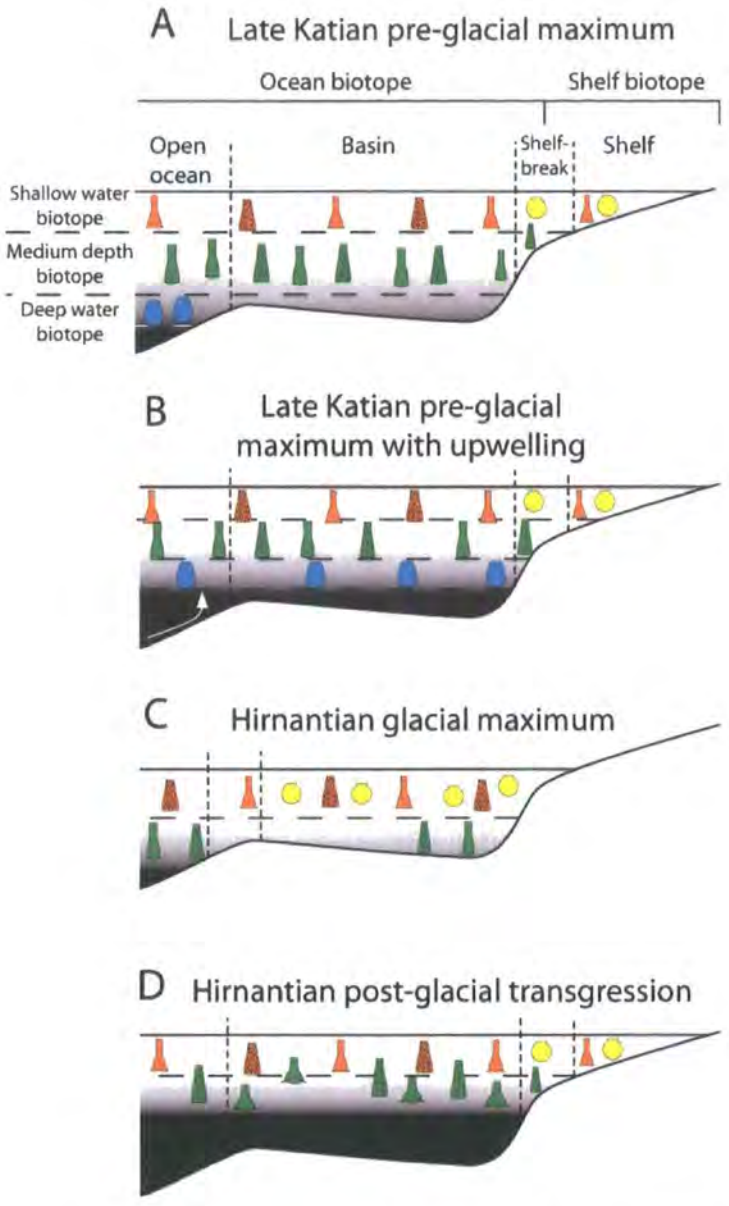

Figure 4.7: Proposed biotopes and depth stratification model for Chitinozoa during the late Ordovician in Avalonia based on data from the upper Katian and Hirnantian of the Welsh Basin. Four biotopes are recognized: a shelf biotope (yellow figures) characterized by *Desmochitina*, a shallow water open ocean biotope (orange figures) characterized by *Cyathochitina*, a medium depth open ocean biotope (green figures) characterized by *Hercochitina* and *Spinachitina* and a deep water biotope (blue figures) characterized by *Bursachitina*. A transitional zone around the shelf-break comprises mixtures of the biotopes. (a) In the pre-glacial maximum basin the deep water biofacies is absent during periods of oxia in the basin represented by burrow-mottling. (b) During upwelling the deep water biotope is displaced into the basin. (c) At the height of glaciation, fall in sea level expands the shelf biotope into what was previously the basin environment. (d) During the Hirnantian post-glacial transgression the medium depth to deep water biotope assemblage is replaced by one comprising *Ancyrochitina*.

the *B. umbilicata* Zone and attributed the reappearance of the gracile *S.fossensis* to changing palaeoecological conditions. In the Cardigan-Llangranog region, the same pattern is observed with *S. fossensis* occurring firstly in burrow-mottled facies of the Nantmel Mudstones Formation and secondly within laminated hemipelagite unit (LH^1) within the *B. umbilicata* Biozone. The demonstration of this repeating pattern in the Welsh Basin during changing hydrographical conditions suggests that *S. fossensis* was not greatly affected by changing palaeoecological conditions in a basin or deep shelf setting. Also, the occurrence of *S. fossensis* in both basin and shelf-break settings in the Cautley district and in the Welsh Basin reinforces the palaeoecological interpretation that these taxa occupied a middle depth mesopelagic habitat.

The Hirnantian *S. taugourdeaui* Biozone is recorded in Belgium from the Harelbeke well from dark muds and silts with bioturbated silt and sand horizons and slumped units (Vanmeirhaeghe, 2006). *Belonechitina reticulatus* is recovered alongside *S. taugourdeaui* from the same well. The depositional environment is not clear from the borehole description given by (Vanmeirhaeghe, 2006) but is similar to the description of the shelfal Ciliau Formation of the Welsh Basin given by Schofield *et al.* (2004) which was deposited during the Hirnantian glacial maximum and is of *B. reticulatus* n. sp. Biozone age. Though a tentative link in environment, this occurrence provides supplementary evidence that *S. taugourdeaui* only inhabited the shelf biotope.

4.9 Chitinozoan palaeoecological reorganization during the Hirnantian glaciation in the Welsh Basin

Major changes in chitinozoan diversity have previously been recognized at the first-order level during the late Katian and the Hirnantian (Paris *et al.*, 2004). Global chitinozoan diversity declined rapidly in the mid-Katian (beginning of the British Ashgill Series, Time Slice 6a of Webby *et al.* (2004)) and Chitinozoa were affected by the end-Ordovician mass extinction (during Time Slice 6a, Paris *et al.*, 2004), but details in the palaeoecological reorganization of chitinozoans during the onset of Upper Ordovician glaciation are not as well understood as for graptolites (e.g. Melchin & Mitchell, 1991) or shelly fossil groups. For instance, Owen & Robertson (1995) interpreted brachiopod and trilobite community structure breakdown from oceanic overturn to represent the onset of the Upper Ordovician glaciation at the Katian-(Rawtheyan) Hirnantian boundary. Chemostratigraphically, however, the onset of glaciation in the Upper Ordovician is interpreted to be marked by the beginning of the Hirnantian Isotopic Carbon Excursion (HICE, Brenchley *et al.*, 1994) and has been demonstrated to begin in the Upper Katian (Rawtheyan) in Laurentia (Underwood *et al.*, 1997; Melchin & Holmden, 2006; Bergström *et al.*, 2006a; Schmitz & Bergström, 2007). In Avalonia the base of the *Bursachitina umbilicata* Biozone is also placed in the upper Katian (mid-upper

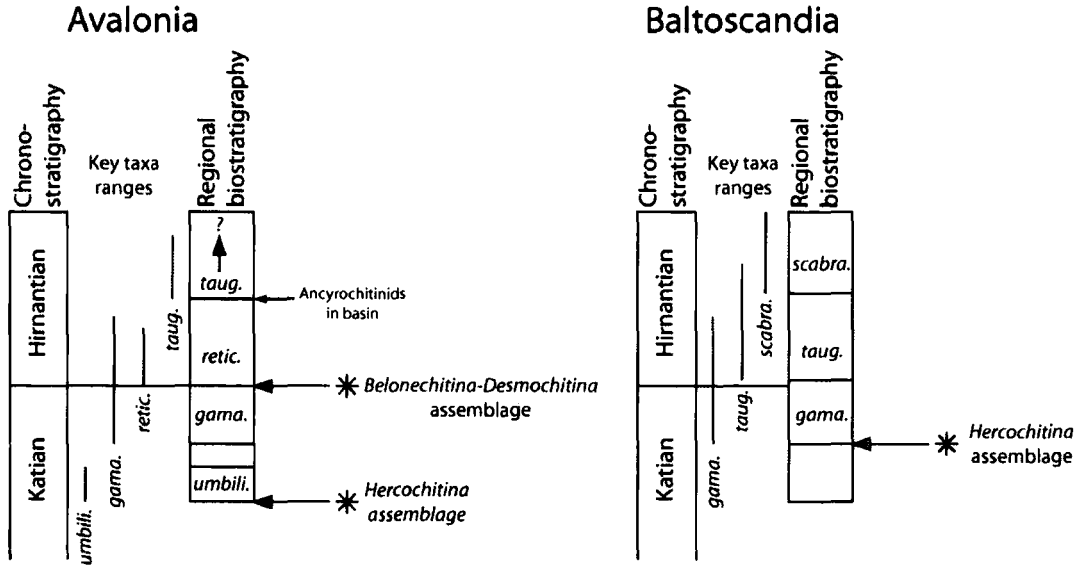

Figure 4.8: The timing of major chitinozoan assemblage reorganizations (marked by asterisks) between Avalonia and Baltoscandia differs. In Avalonia, major changes in biotope composition occur at the base of the *umbilicata* and *reticulatus* biozones whereas in Baltoscandia a major reorganization occurs at the base of the *gamachiana* biozone.

Rawtheyan) (Vandenbroucke, 2008) and in the Welsh Basin marks a change in the chitinozoan assemblage from a low-diversity spinachitinid–hercochitinid assemblage to a high diversity hercochitinid assemblage (Figure 4.6). Given the timing of this event in the Welsh Basin, such a reorganization in community structure could possibly also be attributed to the onset of global cooling. This would, however, mean that the initiation of coastal upwelling and deposition of the LH units was a product of cooling as well.

A further example of the effect of climate change on palaeoecological rearrangement in different biotopes is demonstrated through comparison of biotic events at the base of the *gamachiana* biozone in Baltoscandia and the Welsh Basin and the base of the *Belonechitina reticulatus* n. sp. Biozone in the Welsh Basin. In Baltoscandia, *H. gamachiana* is found in an epeiric sea setting and spans the uppermost Katian to Lower Hirnantian. The appearance of *H. gamachiana* in Baltoscandia is considered to mark, and be a major constituent of, a chitinozoan assemblage reorganization. In Wales, *H.* cf. *gamachiana* occurs in both a basin setting and on the shelf (i.e. it occupies a shallow-water epipelagic open ocean biotope Vandenbroucke *et al.*, submitted). In the Welsh Basin, however, major reorganizations of chitinozoan assemblages occur not at the base of the *H. gamachiana* Biozone but at the base of underlying *B. umbilicata* Biozone (see above) and the overlying *Belonechitina reticulatus* n. sp. Biozone. The latter occurs at the onset of the Hirnantian glacial maximum and involves a change from the open ocean hercochitinid biofacies assemblage to the shelf biofacies domi-

nated by belonechitinids and desmochitinids (Figure 4.8). Baltoscandia was predominantly a shallow epeiric carbonate sea whereas the Welsh Basin in Avalonia was a muddy distal shelf to basin environment. The difference in changes is interpreted as a result of regional environment and biotope composition at any one time. Changing climate affected composition of basin biotope assemblages prior to shelf biotope assemblages (Owen & Robertson, 1995).

4.10 Implications for chitinozoan biostratigraphy

In modern oceans, pelagic organisms are strongly controlled by water mass structure and water mass distribution which is directly controlled by climate (Norris, 2000). In the Palaeozoic we have no reason to believe pelagic organisms were any less susceptible to these constraints and numerous studies for different groups have demonstrated this to be the case (e.g. Armstrong & Owen (2002a) for conodonts; Cooper *et al.* (1991); Berry *et al.* (1989) amongst others for graptolites, Williams *et al.* (2003b) for ostracods; see also Webby *et al.* (2004) for a review of other individual groups. It can therefore be expected for even the most ubiquitous biozonation scheme to break down in some part of the world at some point in time because climatic zones are not universal (Christopher & Goodman, 1996). The consequences of these effects have long been recognized and understood for biostratigraphy and result in the construction of regional biostratigraphic schemes (Hedberg, 1965). For example, foraminifera and calcareous nannofossil biozonations constructed for the Tertiary are based on tropical oceanic assemblages and dinoflagellate zonations are based on shallow mid-latitude assemblages (Christopher & Goodman, 1996). It is through the combined use of these fossil groups, that can be independently correlated with a reliable chronostratigraphic data set (e.g. magnetostratigraphy) that a strong means of correlation over a wide range of palaeoenvironments and broad spatial extent can be achieved. But for chitinozoan biostratigraphy these effects, to a certain degree, have been ignored favoring the assumption that the geographical spread of a given species is synchronous and slight differences in the FAD of a taxon are not discernible at the scale of geological time (i.e. several hundred thousand to about one million years; Paris *et al.*, 1999b). Because distribution and origination of pelagic organisms is strongly climatically-controlled (Norris, 2000), this approach to biostratigraphy would also assume; 1) climatic perturbations that affect distribution of organisms do not occur over periods of time greater than several hundred thousand to about one million years, 2) chitinozoan distribution and origination was insensitive to climate change, and 3) climatic events at or shorter than the biozone level that may cause diachroneity are not discernible in the geological record. This is clearly not true as studies have exhibited the sensitivity of chitinozoans to climate change at short timescales. Dorning *et al.* (2006) recorded fourth and fifth order fluctuations in chitinozoan abudance in the intervals between the wet Telychian Snipklint Primo event

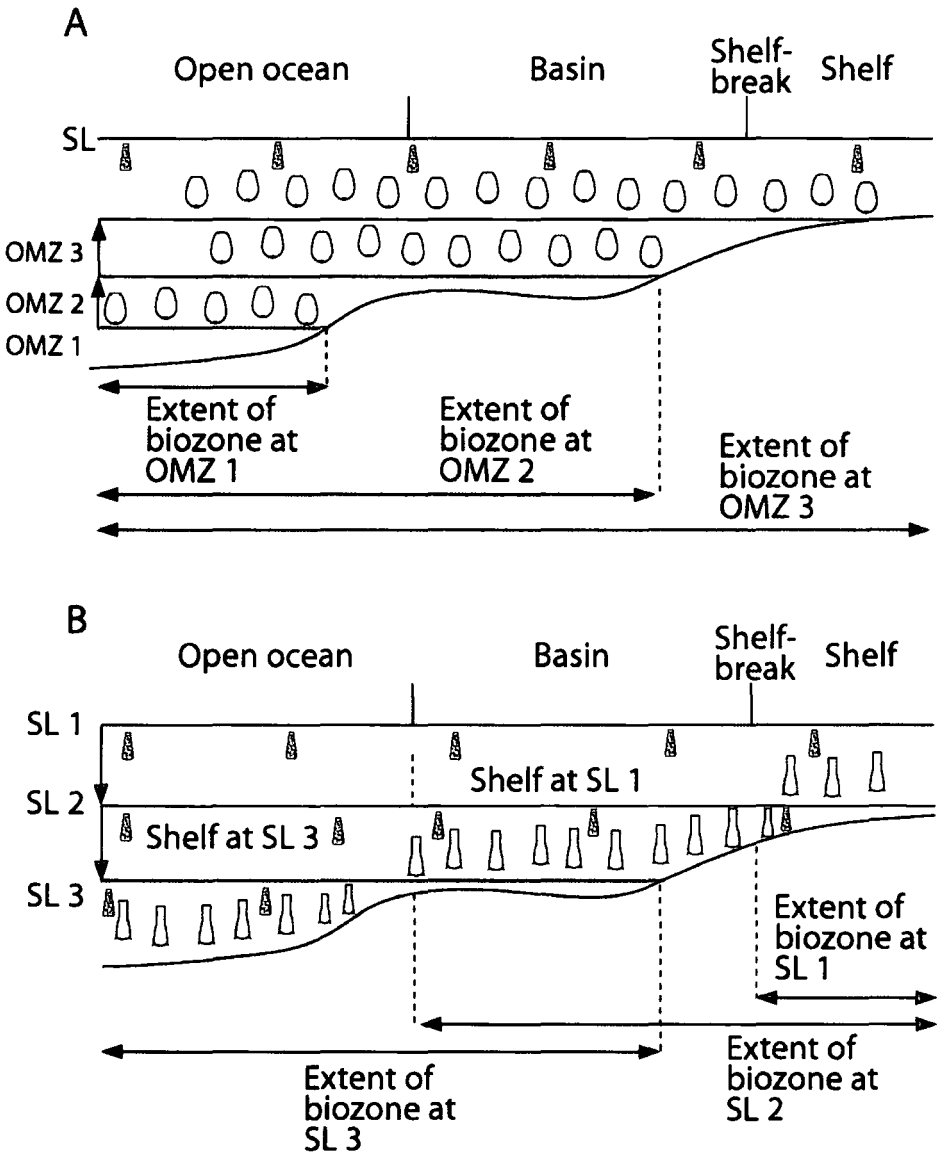

Figure 4.9: Index taxa that originate and are restricted to a particular biotope require climatic and/or environmental changes in their region for dispersal to occur and results in diachroneity of the biozone. (a) The index taxon *Bursachitina umbilicata* occupied, and was limited to, a deep open ocean biotope and would have required an expansion of a deep oxygen minimum zone (OMZ), for instance, to displace it into shallower ocean and shelf biotopes. OMZ 1-3=oxygen minimum zone at times 1-3. (b) *Spinachitina taugourdeaui*, on the other hand, may have been restricted to a shelf biotope and as such would require a fall in sea level (SL) to expand its environment into regions that were previously deep water environments. SL 1-3=sea level at times 1-3. Taxa that occupy an epipelagic open ocean biotope are insensitive to either effects e.g. *Hercochitina gamachiana* and continue to occur in both open ocean and shelf environments.

and the dry Sheinwoodian Vattenfallet Secundo episode. These high-resolution abundance fluctuations were recorded from marine shelf successions in Baltica, Laurentia and Avalonia. At even higher resolution, possibly, Laufeld (1974) calculated annual variations in chitinozoan abundance in Upper Visby marls (Sheinwoodian) calibrated to sub-annual growth increments in solitary rugose corals and noted that different taxa have their peaks of abundance at different times of the year. This was interpreted as being a means to calculate palaeoproductivity but, as Laufeld (1974) noted, a possible error with this method is that the figures obtained are considerably higher than any modern values for ocean productivity.

The detailed palaeoecological model for chitinozoans herein implies that if an index taxon originates in and occupies a discrete biotope and assemblage then there is potential for diachroneity of the biozone. Conversely, depending on the type of biotope occupied, open ocean or shelf, an index taxon may be less susceptible to diachroneity. The index taxon *Bursachitina umbilicata*, being restricted to deep water depths, may be one such example and could explain why this biozone is recorded in the basin but not in the shelf environment. Displacement of its environment during upwelling was not great enough to displace it into the shelf habitat. Consequently, a sealevel fall would not greatly affect the deep water assemblages because they would not lose their habitat, however, it would not aid their dispersal (Figure 4.7 a).

It follows from this that some index taxa that can be demonstrated to originate in and occupy a discrete biofacies (e.g. *Hercochitina* cf. *gamachiana* from the open ocean pelagic biotope), may be insensitive to some major climatic/hydrographic overhauls that may affect index taxa that originated in a different biotope (e.g. *Spinachitina taugourdeaui* from the shelf biotope). Indeed, index taxa that originate in a restricted biofacies e.g. shelf environment, could actually require a major environment change, such as sealevel fall, to aid their dispersal. The FAD of such an index taxon throughout a region, or even globally, would then be diachronous by virtue of its environmental requirements (Figure 4.7 b).

It therefore comes as no surprise that many of the chitinozoan biozone boundaries in Wales coincide with abrupt climatic changes and major reorganizations of chitinozoan assemblages. For instance, the base of the *umbilicata* Biozone occurs at the onset of upwelling and LH deposition, the *Belonechitina reticulatus* n. sp. Biozone appears at the beginning of the Hirnantian glacial maximum in the Yr Allt and Ciliau Formations and the base of the *S. taugourdeaui* Biozone is in the post-glacial transgressive Garth House Formation. *S. taugourdeaui* is not recorded in the basin but the basin assemblage changes from one dominated by *Hercochitina* and *Spinachitina* to one dominated by *Ancyrochitina*.

4.11 Conclusions

Where the palaeoecology of the fossil group is poorly understood, the risk of designating a zone fossil that may prove diachronous is greatly increased and potentially cause error in regional and/or global correlation. Only by careful analysis of facies distribution, temporal and geographic range and climatic tolerance of chitinozoan taxa can we begin to understand palaeoecological patterns and constrain the zonal schemes of the Chitinozoa better.

Correspondence analysis and unconstrained seriation of facies distribution of Upper Ordovician Avalonian Chitinozoa, through changing climate states with well-constrained basin hydrography, have allowed three open ocean depth-stratified biotopes and a shelf chitinozoan biotope to be recognized. Those taxa occupying only the shelf biotope experience segregation from the open ocean and their dispersal is influenced by sea level change. Dispersal of taxa originating in and occupying deep water biotopes (e.g. *Bursachitina umbilicata*), can be strongly affected by changes in basin hydrography such as the initiation of upwelling. Chitinozoan taxa that originate and occupy a shallow water epipelagic biotope are less affected or are insensitive to such changes (e.g. *Cyathochitina campanulaeformis, Hercochitina crickmayi* and *Belonechitina reticulatus* n. sp.) This distribution of biotope assemblages indicates, as previously suggested (Paris, 1981, for instance), that the Chitinozoa are almost exclusively planktonic and is further reinforced by their rapid response to changes in basin hydrography.

The distribution of biotope assemblages recognized herein replicates some of the interpretations of previous studies of chitinozoan palaeoecology based on facies comparison (Grahn, 1982; Al-ameri, 1983). *Desmochitina* occupies a shallow water shelf biotope and *Cyathochitina campanulaeformis* a shallow water open ocean biotope.

The chitinozoan biotope model demonstrates that the appearance and replacement of taxa that define regional biozones, and even pan-palaeocontinental biozones, can be the product of regional and global climate changes and changes in ocean hydrography. On the geological timescale and in global area these effects have typically been considered instantaneous but at the resolution of inter-basin, and even palaeocontinent-specific biostratigraphical schemes, such processes could be the cause of diachroneity as biotope assemblages respond to climate change, which varies with global latitudinal temperature gradient. The problem is also exacerbated the greater the resolution of the biostratigraphical scheme is.

Restriction of taxa and assemblages to specific biotopes may well help explain pockets of endemism e.g. *Bursachitina umbilicata* and *Spinachitina fossensis*, that remain during the collision of Avalonia with Baltica and the breakdown of provinciality during the closure of Iapetus. Good index taxa for chitinozoan biozonation need to have evolved in and to have occupied an epipelagic open ocean biotope to fulfill the criterion of wide dispersal. This does not appear to have been the case with all Avalonian chitinozoan biozonation index taxa.

Chapter 5

The HICE in Wales: carbon storage in the shelf and basin and regional carbon cycling.

Abstract

Stable carbon isotope profiles from the Hirnantian of the Welsh Basin are presented. Four positive $\delta^{13}C_{org}$ excursions, considered to represent the Hirnantian Isotopic Carbon Excursion (HICE) are recognized and correlate well between basin and shelf environments and also with a proposed sequence stratigraphic model for the Hirnantian in the Welsh Basin. Two excursions of up to 3 ‰ occur in the lower Hirnantian *reticualtus* chitinozoan Biozone and two excursions of 1 ‰ are present in the late Hirnantian *taugourdeaui* Biozone. Higher carbon storage in the basin, coincident with positive $\delta^{13}C_{org}$ excursions during glacial periods, indicate a shift in the locus of carbon burial from the shelf to the basin during low sealevel. The topology of the regional Hirnantian isotope curve for the Welsh Basin compares with only a few curves from other parts of the world indicating strong regional carbon cycling. Comparison of the relative timing of the onset of HICE and peak HICE values from other palaeocontinents demonstrate little, if any, consistency with palaeolatitude or basin setting. It is demonstrated that this chemostratigraphic diachroneity of HICE can be attributed to the process of signal rectification of $\delta^{13}C$ records most likely due to numerous local carbon cycling processes.

5.1 Introduction

The Hirnantian Stage of the Upper Ordovician was a period of abrupt global change in the biosphere, climate and ocean geochemistry. These events are marked by: 1) an abrupt positive Hirnantian isotopic carbon excursion (HICE); 2) one of the three global Phanerozoic mass

extinctions (Bambach *et al.*, 2004) and 3) an extensive drop in sealevel from the development of an ice-sheet over the high southern-latitude portion of the palaeocontinent of Gondwana. Evidence from initial osmium measurements from the Dob's Linn Global Stratotype Section Point (GSSP) for the base of the Silurian also suggests that the Hirnantian was a period of decreased weathering and detrital input into the world's oceans (Finlay *et al.*, 2007) that may well have influenced the global carbon isotopic composition.

The HICE event is documented predominantly from low-palaeolatitude, tropical to sub-tropical sections, but there are currently complete mid-palaeolatitude records. The HICE event has attracted considerable interest because of its coincidence with the end-Ordovician mass extinction (Brenchley *et al.*, 1995, 2003; Marshall *et al.*, 1997; Webby *et al.*, 2004), but a consensus on the mechanism for the HICE has not been reached. Four major hypotheses have been proposed: (1) increasing productivity and organic carbon burial (Brenchley *et al.*, 1995, 2003); (2) increased carbonate weathering (Kump & Arthur, 1999; Melchin & Holmden, 2006); (3) changes in ocean circulation patterns in shallow and deep-water settings during changing climate state (Holgate *et al.*, 2001, 2002; Holgate *et al.*, 2003); and (4) that individual records represent predominantly regional processes (Panchuk *et al.*, 2005; Holgate *et al.*, 2003).

Unfortunately, the first of these hypotheses, increased productivity and organic carbon burial, lacks physical evidence. There is a scarcity of extensive organic carbon deposition in basin or shelf environments coincident with the HICE. In the Welsh Basin at least, black shale deposition in the late-Katian was restricted to the basin environment and is proposed to have been caused by increased coastal upwelling (Challands *et al.*, 2008). However, climatic conditions in the Hirnantian contrast with those of the late Katian. Low sealevel, higher meridional temperature gradient and a northerly climate belt configuration (Chapter 3, Armstrong *et al.*, in revision), mean that mid-palaeolatitude basins and shelves may not have experienced the same nutrient or sediment fluxes as in the late Katian and the distribution of carbon burial could have been substantially different.

Generally speaking for the Early Palaeozoic, sequestration of carbon in shelf environments was largely restricted to the deposition of carbonates (Walker *et al.*, 2002) whilst organic carbon was primarily buried in anoxic deep-water basin environments (Page *et al.*, 2007). During the Upper Ordovician, a time of high pCO_2 when oceans may have been acidified and carbonate deposition restricted (Page *et al.*, 2007), organic carbon burial, on the shelf in particular, may have been an important mechanism for CO_2 draw-down that contributed to the onset and persistence of the Hirnantian glacial maximum (HGM; Brenchley *et al.*, 1995, 2003; Kump & Arthur, 1999). Further to this, burial efficiency of carbon is greater on the shelf than in the deep-marine environment in modern and Cretaceous oceans (Bjerrum *et al.*, 2006), with shelf environments accounting for approximately 90% of organic carbon burial under

oxygenated bottom waters along continental margins (Hedges & Keil, 1995). During periods of shelf-area expansion such as during post-glacial sealevel rise, organic carbon burial on the shelf may have increased, but during periods of glaciation such as the HGM, inferred global oceanographic conditions (i.e. low shelf area and high oxia from vigorous ocean thermohaline circulation and upwelling) would not have favored the preservation of sedimented carbon (Brenchley *et al.*, 1995).

It therefore seems unlikely that for the late Ordovician increased organic carbon burial in shelf environments can be described as *the* global mechanism responsible for the HICE. As Page *et al.* (2007) point out, there are many ways in which to sequester carbon regionally, particularly in isolated basins, and contribute to CO_2 drawdown and glaciation. There also stands the problem of achieving high organic carbon burial in oxygenated shelf environments, especially if sedimentation rate is low. Whereas vigorous upwelling may extend oxygen minimum zones onto shelves thus providing favorable conditions for organic carbon preservation (Wignall, 1994), continental configurations (Cocks & Torsvik, 2002, 2004) and the most recent GCM models (Herrmann *et al.*, 2005) suggest that global conditions in the late-Katian and Hirnantian were not generally favorable for coastal upwelling (Page *et al.*, 2007; Panchuk *et al.*, 2005, though see Armstrong (2007) for an alternative view). Increased burial of organic carbon in the shelf environment still remains a necessary hypothesis to test for the HICE. This applies particularly in regions with relatively scarce documentation of Hirnantian lithostratigraphy in contrasting basin-shelf environments such as at mid-palaeolatitudes. The Welsh Basin provides such a setting.

The increased productivity-burial model predicts high total organic carbon (TOC) burial coincident with the HICE. Increased organic carbon burial on the shelf during HICE can be tested for by contrasting TOC wt% and $\delta^{13}C$ between basin and shelf environments. TOC wt% is known to correlate with more direct measures of photosynthetic primary productivity such as total chlorophyll-a or total steryl chlorine esters (Nara *et al.*, 2005) and organic mass accumulation rate (Tyson, 1995; Vilinski & Domack, 1998; Twichell *et al.*, 2002; Kuypers *et al.*, 2002, 2004; Meyers & Arnaboldi, 2005) and therefore could possibly be a useful indicator of productivity and organic carbon burial.

However, the additional complexity of regional carbon-cycle processes on $\delta^{13}C$ values potentially hinders such a test. In the first instance, regional correlation of $\delta^{13}C$ curves provides an acceptable test that carbon-cycle processes in the same basin are homogenous. Provided this condition can be satisfied, correlation with other Hirnantian $\delta^{13}C_{org}$ curves from throughout the world performs a further test for the verification of a regional or global signal in Hirnantian of the Welsh Basin. Two further methods that can be used to test for regional effects for any given carbon isotope curve are: (1) reproducibility in different

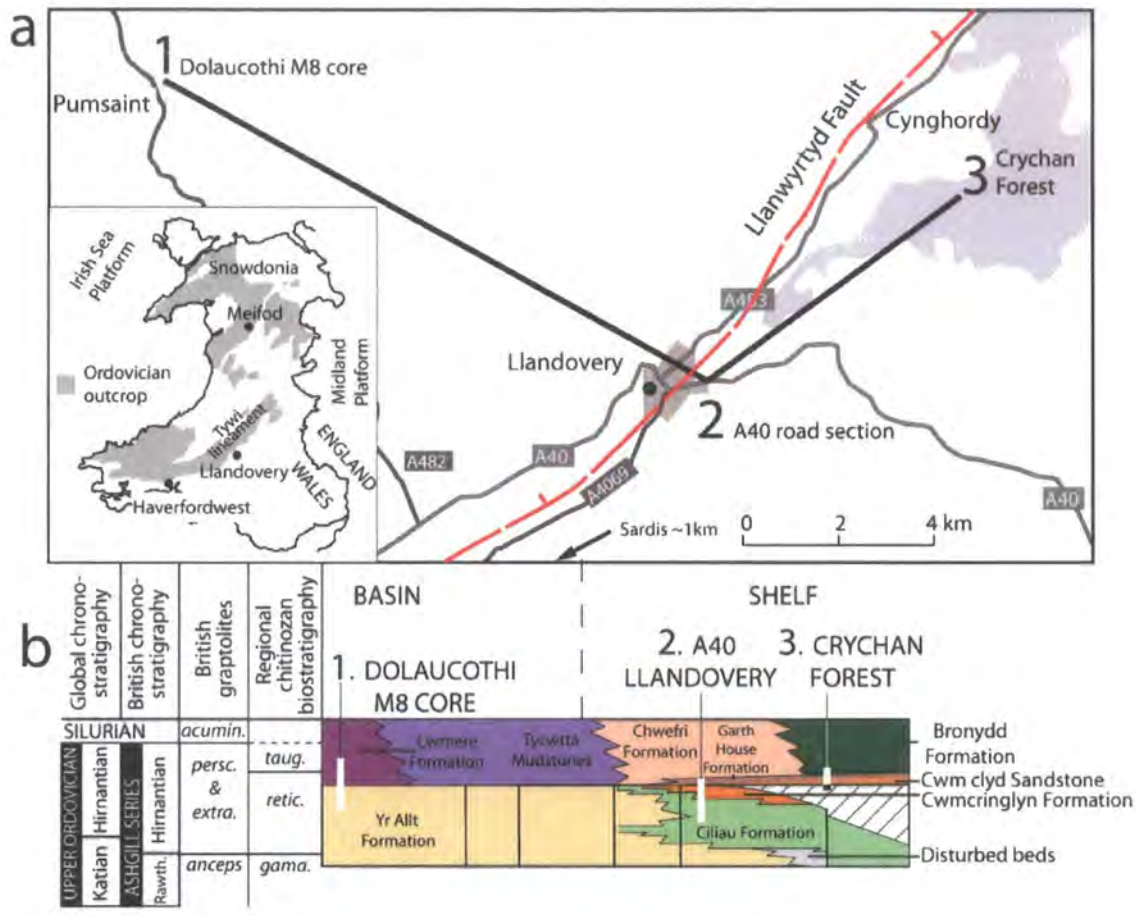

Figure 5.1: Field locations (a) and geological setting of the Hirnantian of the south central Welsh Basin around Llandovery (b) (redrawn from Schofield *et al.* (2004)).

environments of the same basin; and (2) comparison with predicted global patterns from numerical modeling. The first method has been carried out in many regions, in particular for Baltica (Brenchley *et al.*, 2003; Kaljo *et al.*, 2001, 2004, 2007) but the relative trends and differences of these curves from different environments have only been compared for correlative purposes. However, Melchin & Holmden (2006) compared shelf and basin profiles from the Upper Ordovician of Arctic Canada and noted isotopic heterogeneity between the two environments for the Hirnantian. Additionally, numerical studies by Panchuk *et al.* (2005) and Holgate *et al.* (2001, 2002) and Holgate *et al.* (2003) demonstrated regional differences in observed $\delta^{13}C$ curves from Laurentia compared to global predictions from numerical models. These examples suggest that influences from regional carbon-cycles are not uncommon for HICE curves. Numerical modeling for HICE in the Welsh Basin is explored in detail in Appendix E.

5.2 Geological setting

The Welsh Basin lay at mid-palaeolatitude on the northern margin of Avalonia during the Hirnantian with the Iapetus Ocean to the North. Hirnantian rocks in Wales crop out between Snowdonia in the North and Haverfordwest in the south. In the Llandovery region in south central Wales, Hirnantian shelf deposits crop out between Sardis (SN 747 289) in the south, northwards to Crychan Forest (SN 843 409) and are folded with axes striking NE-SW. Facies thin in the northern and southern extremes of the Llandovery region providing evidence of deposition control from the adjacent palaeo-shoreline to the east. To the west of the Llanwyrtyd Fault, basin facies prevail and Hirnantian rocks crop out in the center of the NE-SW-trending Twyi anticline. East of the Lanwyrtyd Fault, deposits are predominantly shelfal in character (Figure 5.1 b). Early Hirnantian deposits deposited in the shelf environment comprise weakly-burrowed mudstones and fine-grained calcareous sandstones of the Ciliau Formation with slumped and destratified disturbed beds common throughout. This facies grades into lenticular, wave-ripple cross-laminated sandstones with interbedded burrowed muds (the Cwmcringlyn Formation, west of Crychan Forest and east and south west of Llandovery) and are interpreted to represent deposition during the acme of the Hirnantian glaciation (Schofield *et al.*, 2004). These units are truncated by a pronounced disconformity and overlain by the Cwm Clyd Sandstone, a coarse-grained angular quartz sandstone with frequent mudstone rip-up clasts. The extent of erosion is variable locally, indicating active regional tectonism during marine regression, possibly a continuation of the Katian Shelveian deformation event of Lynas (1988) and Toghill (1992). During the early Hirnantian, the Midland Platform to the east was emergent and the basin received vast amounts of sedimentary debris from the eroding hinterland. Increased sediment supply from the exposed and destabilised basin platforms produced thick, slumped sandy deposits in the deeper parts of the basin (the Yr Allt Formation), with sediment bypassing the shallower shelves, whilst muddy-sand, tidally-influenced deposits accumulated in basin margin settings (Ciliau and Cwmcringlyn formations).

Postglacial conditions resumed in the late Hirnantian and deep marine sedimentation resumed over much of the Welsh Basin. In the Llandovery region, this is represented by smooth, dark mudstones of the Garth House Formation and muddy, bioturbated sands of the Ystrad Walter, Chwefri and Bronydd Formations in the shelf environment and turbiditic mudstones with laminated hemipelagite interbeds, the Cwmere Formation, in the basin setting. Initially sedimentation took place under oxic conditions, represented by the Mottled Mudstone Member of the Cwmere Formation, ubiquitous in the Welsh Basin, but soon anoxic conditions resumed and organic-rich laminated hemipelagite deposition occurred in slope apron settings (Schofield *et al.*, 2004).

5.2.1 Biostratigraphic framework

Biostratigraphical ties between basin and shelf sections are made using the chitinozoan biostratigraphical scheme for the Upper Ordovician of the Welsh Basin described in Chapter 1. The Ciliau and Cwmcringlyn Formations are both of *Belonechitina reticulatus* Biozone age placing them in the early-Hirnantian whereas the Garth House Formation is *Spinachitina taugourdeaui* Biozone age, the mid- to late-Hirnantian. The *persculptus* graptolite band is ubiquitous throughout the Welsh Basin and is located in the Llandovery area in shelf sediments at Ystrad Walter (SN 789 356) within the Ystrad Walter Formation. In basin sediments it occurs in within the Mottled Mudstone Member of the Cwmere Formation. The base of the Garth House Formation also provides a lithological datum which aids correlate between basin and shelf environments. In the basin section (Dolaucothi M8 core) the base of the Cwmere Formation (Mottled Mudstone Member) is equivalent to the base of the Cwm Clyd Sandstone (Figure 5.1 b).

5.2.2 Sequence stratigraphical framework

The Hirnantian glacio-eustatic regression has previously been documented in Wales by Brenchley *et al.* (2006) who recognized a triple regressive-transgressive system from channel infills containing karstified limestone mounds from the Meifod region in central Wales. Prior to this, Marshall *et al.* (1997) proposed that the onset of the positive $\delta^{13}C$ excursion at the base of the Hirnantian corresponds to sealevel fall and the HGM while the return to lower values is associated with mid-Hirnantian transgression. Most recently, mapping by the British Geological Survey in the Builth Wells region (British Geological Survey Builth Wells map, 1:50 000 scale, sheet number 196) and the type Llandovery area has proposed that Hirnantian shelf sediments record a similar triple regressive-transgressive pattern.

Disturbed units and sandy facies in the lower Ciliau Formation represent a sudden lowering in sealevel and destabilisation of shelf sediments following muddy-sand deposition of the Cribarth Formation in the late Katian (Figure 5.2). Subsequent undisturbed deposition of the Ciliau Formation was succeeded by rapid shallowing and deposition of the tidally-dominated Cwmcringlyn Formation sands during the HGM. Lowest sealevel, during the glacial maximum, are recorded by an unconformity at the base of the Cwm Clyd Sandstone Formation and laterally equivalent sandstones. Post-glacial transgression is recorded by the deposition of dark muds of the Garth House Formation on the shelf and laminated hemipelagite deposition of the Cwmere Formation in the basin. The upper Garth House Formation is interrupted by a large unit of disturbed beds in the shelf environment denoting a third period of regression. Recommencement of typical facies of the Garth House Formation and Cwmere Formation testify to the progression of the late Hirnantian post-glacial transgression.

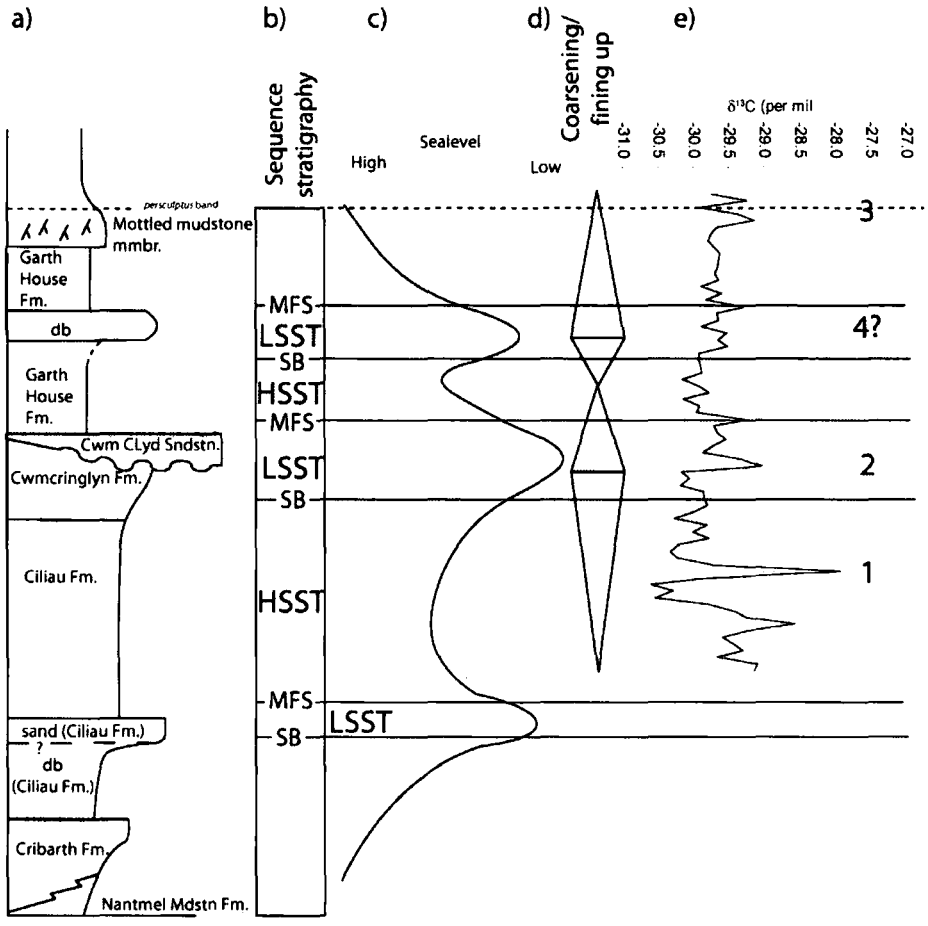

Figure 5.2: Composite lithostratigraphy, sealevel and sequence stratigraphy for the Hirnantian of the Llandovery region. Three lowstand periods are recognised: 1) in the lower Ciliau Formation (lower *reticulatus* Biozone; 2) at the base of the Cwm Clyd Sandstone Formation (uppermost *reticulatus* Biozone); and 3) in the mid-Garth House Formation (*taugourdeaui* Biozone. db=disturbed beds, *gama.=gamachiana*, *per.=persculptus*, *umb.=umbilicata*, HSST=Highstand systems tract, LSST=Lowstand systems tract, MFS=Maximum flooding surface, SB=Sequence boundary.

5.3 Materials and methods

5.3.1 Whole-rock $\delta^{13}C_{org}$ analysis

Three sections were sampled extensively for whole-rock stable carbon isotopes ($\delta^{13}C_{org}$) and total organic carbon (TOC wt%; Figure 5.1 a): Section 1, the Dolaucothi M8 core represents a section through Hirnantian basin facies, Section 2, A40 road section, Llandovery and Section 3, Crychan Forest both represent sections through Hirnantian shelf sediments.

Section 1, the Dolaucothi M8 core was one of sixteen boreholes sunk by the Department of Mining, Geological & Minerals Engineering for Anglo Canadian Exploration during ex-

ploration for mineral deposits, particularly gold, in the Pumsaint area in 1980. The British Geological Survey recently acquired all the boreholes totalling some 198 boxes of which only 9 have been logged with location information recorded. Fifteen whole-rock sub-samples were collected and analysed for $\delta^{13}C_{org}$ between 112 m and 20 m. All stated depths for $\delta^{13}C_{org}$ and TOC wt% values are corrected for a mean bedding dip of 42.25^o (see Figure 5.3 for a detailed sedimentary log of the Dolaucothi M8 core).

Section 2, the A40 Road section consists of a 280m thick outcrop between a small quarry 300m south of Dan Yr Allt farm (SN 780 348) and a 50m section along the A40(T) 1 km east of Llandovery (SN 787 343) (Figure 5.1 a, Figure 5.4). It exposes rocks of the upper Ciliau Formation, Cwmcringlyn Formation and the Garth House Formation with a prominent sandstone horizon between 247m and 252m taken to be equivalent to the transgressive Cwm Clyd Sandstone, which, at this position in the basin shelf lies conformably above the underlying Ciliau and Cwmcringlyn formations. The conformable nature of the section indicates that there has been no truncation through erosion during the acme of the glaciation though thin (< 1 m thick) disturbed units above and below the Cwm Clyd Sandstone Formation may indicate loss of strata. The non-erosive nature of the Cwm Clyd sandstone at this locality makes it a suitable locality for carbon isotope sampling through the Hirnantian glacial maximum. The base of the Ciliau Formation is not exposed nor is the top of the Garth House Formation but they are mapped to the north and west of the outcrop. No age diagnostic macrofossils have been recovered from the Ciliau or Cwmcringlyn Formations from the A40 road section. Sixty-two samples at 2 m intervals were collected and analysed for $\delta^{13}C_{org}$ and TOC wtwt% from the A40 road section at Llandovery. Sampling gaps from obscured outcrop occur between 28 m and 68 m, 73 m and 199 m and 205 m and 226 m.

Section 3, the Crychan Forest section was first exposed in the 1960's during the development of an extensive forest track system during the development of the Forestry Commission plantation system. Woodcock & Smallwood (1987) and Cocks *et al.* (1984) took advantage of this clear and extensive new exposure and studied the sections extensively. The sampled section crops out 350 m north of Scrach at (SN 849 396) and extends from the base of the Cwm Clyd Sandstone, 10 cm above the base of the disconformity, through the Garth House Formation and 10m into the overlying Bronydd Formation (Figure 5.6 and Figure 5.7 for graphic log). Forty-two samples were collected at 2 m intervals and analysed for $\delta^{13}C_{org}$ and TOC wt%

Rocks in the Llandovery area have experienced metamorphism up to low anchizone grade, indicating burial of around 4–5.5 km, whereas those in the Pumsaint region, from which the Dolaucothi M8 core originates, achieve high anchizone grade indicating burial of around 6-8 km. Using a regional geothermal gradient of *c.* 50^{o}C/km for the Welsh Basin (Bevins &

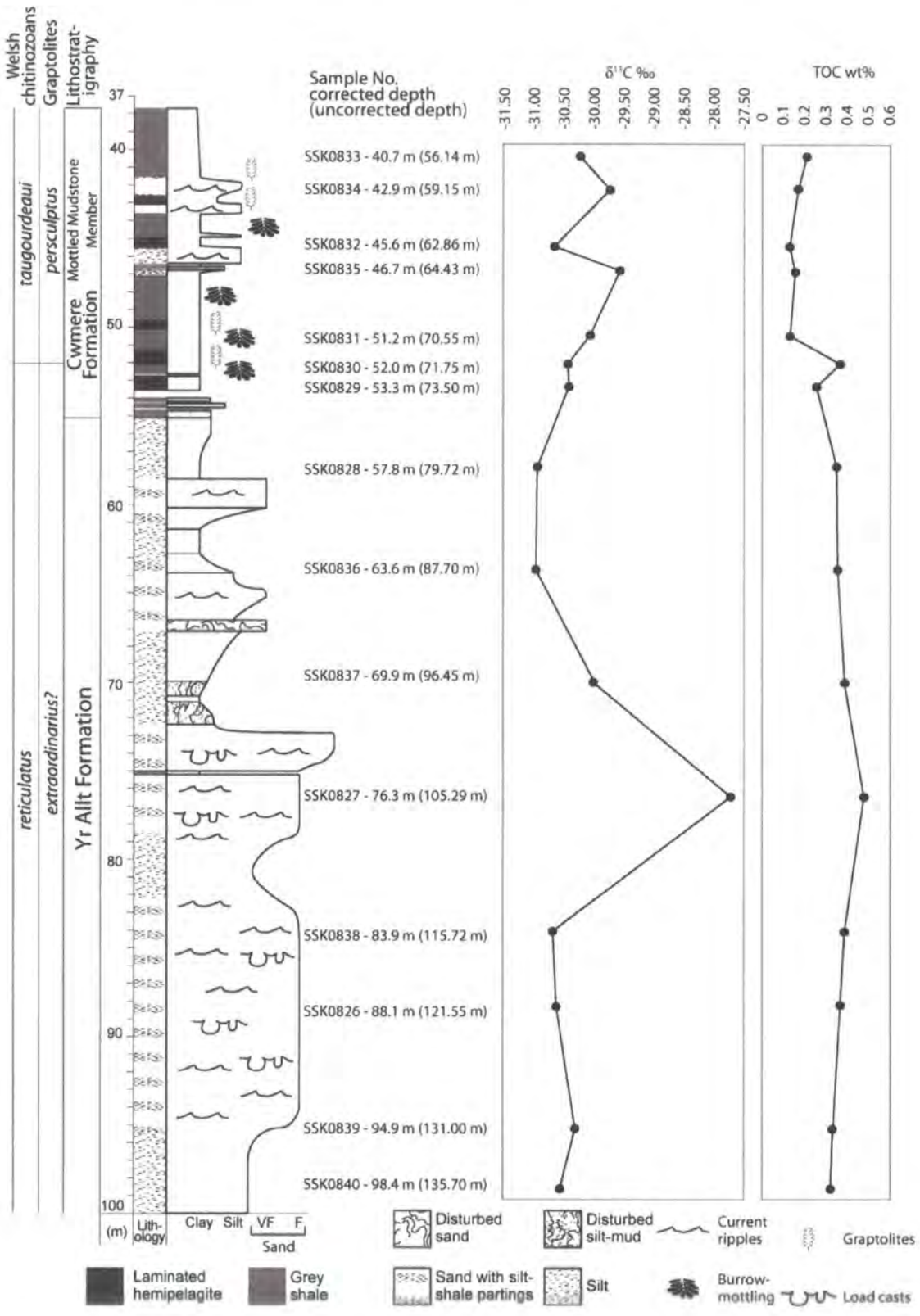

Figure 5.3: Graphic log and $\delta^{13}C$ profile and total organic carbon (TOCwt%) for Dolaucothi M8 core.

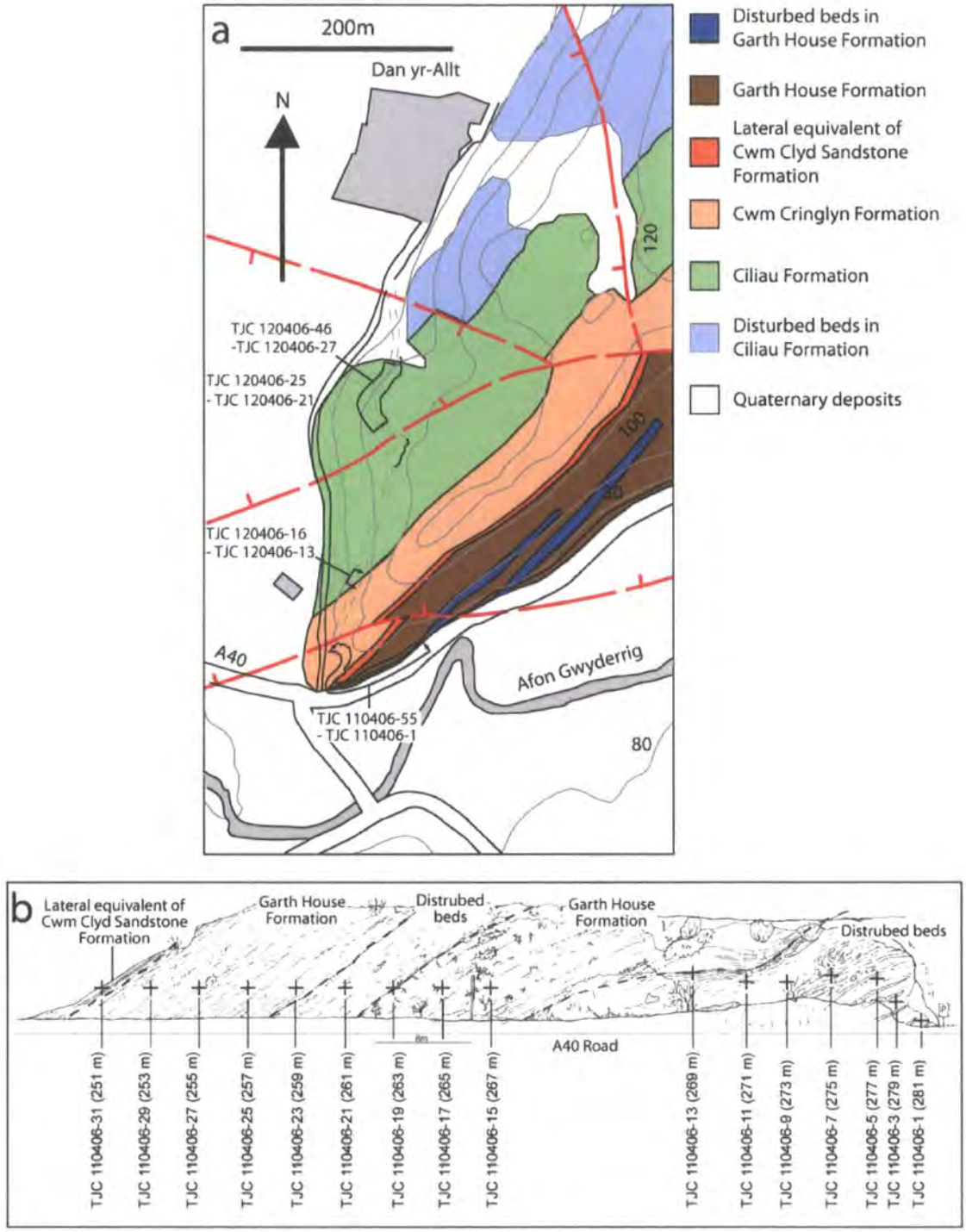

Figure 5.4: Geological map (a) indicating sample locations for the Hirnantian A40 Road section, Llandovery. (b) Field sketch of the A40 Road section which exposes the lateral equivalent of the Cwm Clyd Sandstone Formation to disturbed beds in the upper Garth House Formation. The sequence is overturned so the youngest units (Garth House Formation disturbed beds) are to the right (east). Geology from British Geological Survey Sheet 212, Llandovery (*unpublished*).

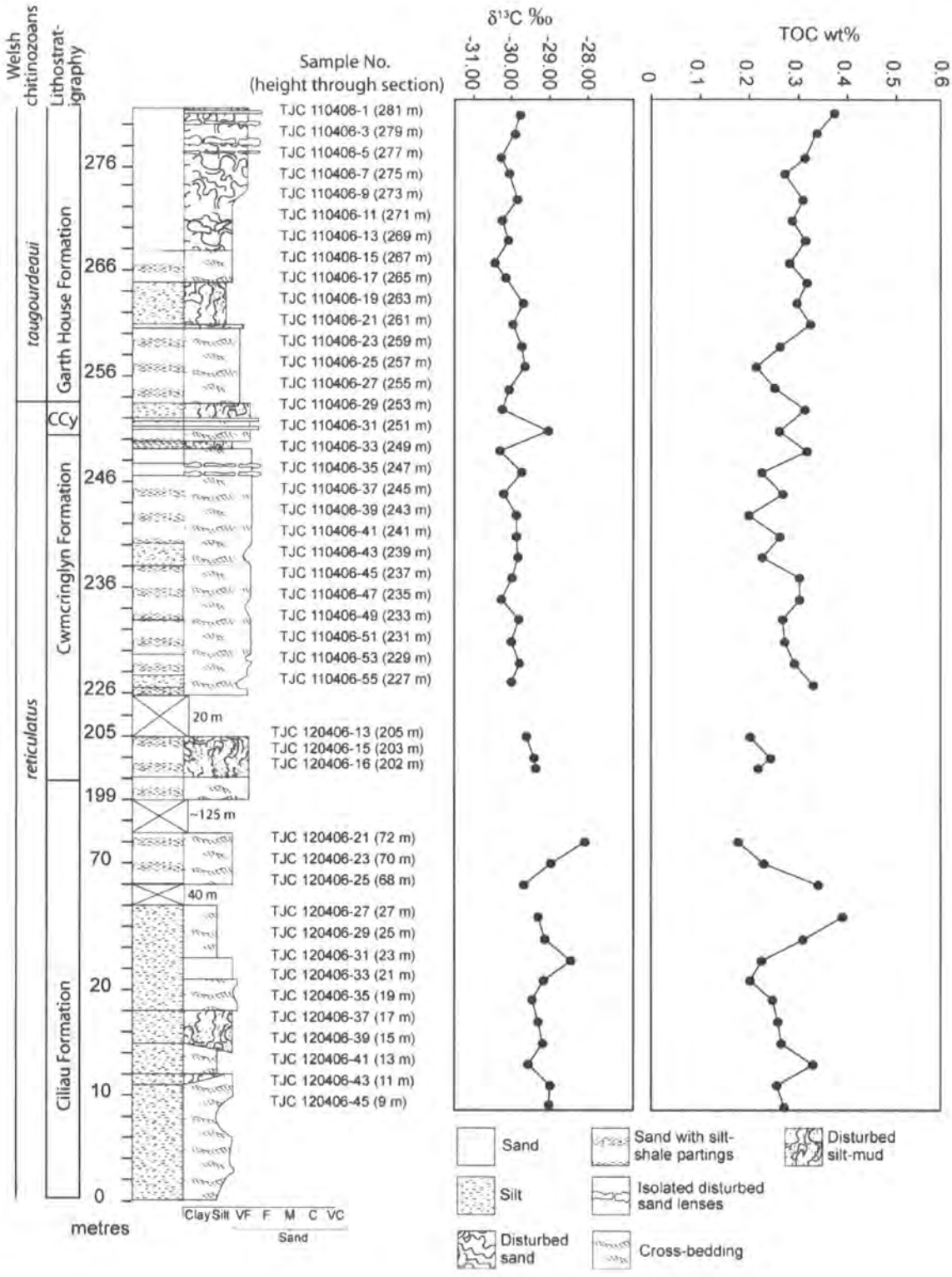

Figure 5.5: Graphic log and $\delta^{13}C$ profile and total organic carbon (TOCwt%) for A40 road section, Llandovery.

Merriman, 1988; Bottrell *et al.*, 1990; Roberts *et al.*, 1991), rocks in the Llandovery area experienced temperatures of up to 200–275°C during metamorphism and those in the Pumsaint area up to *c.* 300–400°C, both areas exceeding the post-mature oil-gas generation window (>165°C for oil, >220°C for gas, Killops & Killops, 1993; Cornford, 2001). $\delta^{13}C_{org}$ values have been shown to yield an unaltered environmental signal in greenschist facies rocks at Dob's Linn (Underwood *et al.*, 1997) and are therefore considered primary oceanic values in this study. Because the sections studied herein all come from regions that experienced post-oil and gas generation stage temperatures, TOC loss from maturation can be considered to be equivalent for each section. Because there was no extensive terrestrial vegetation in pre-Devonian times (Peters-Kottig *et al.*, 2006) Type III and Type IV kerogen (kerogen principally derived from vascular plant matter; Killops & Killops, 1993) can be considered to have had an insignificant contribution to the TOC values measured. All kerogen comprising sample TOCs is therefore assumed to be Type I and Type II kerogen i.e. marine in origin. All samples were taken from fresh exposure avoiding visible faults, fracture zones and mineralized veins. The Pumsaint area is noted for its high degree of epigenic metal mineralization, however, to avoid possible contamination, samples from the core were only taken from units devoid of any form of veining or mineralization.

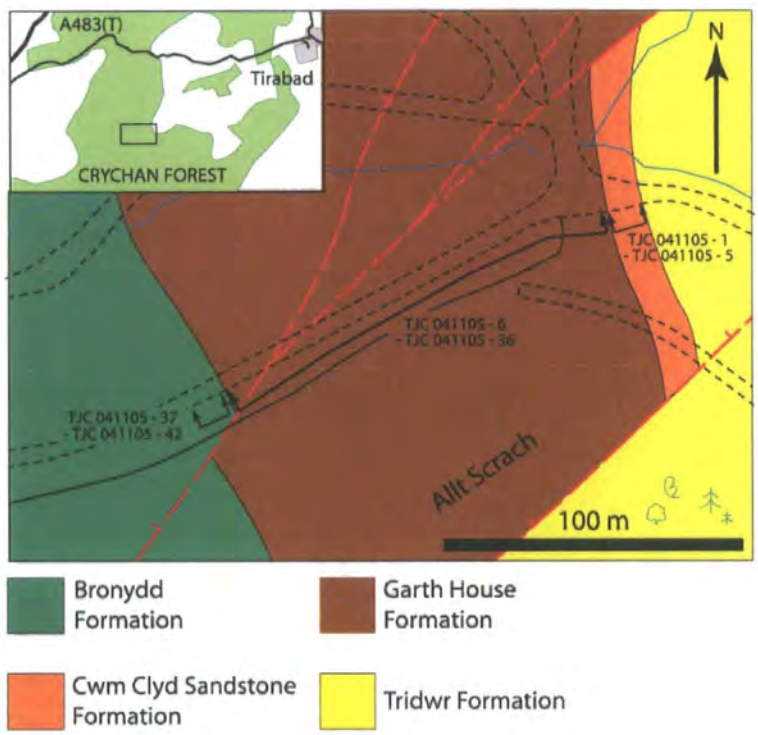

Figure 5.6: Geological map indicating sample locations for the Hirnantian Crychan Forest section. The sequence is younging to the southwest. Geology from British Geological Survey Sheet 212, Llandovery (*unpublished*).

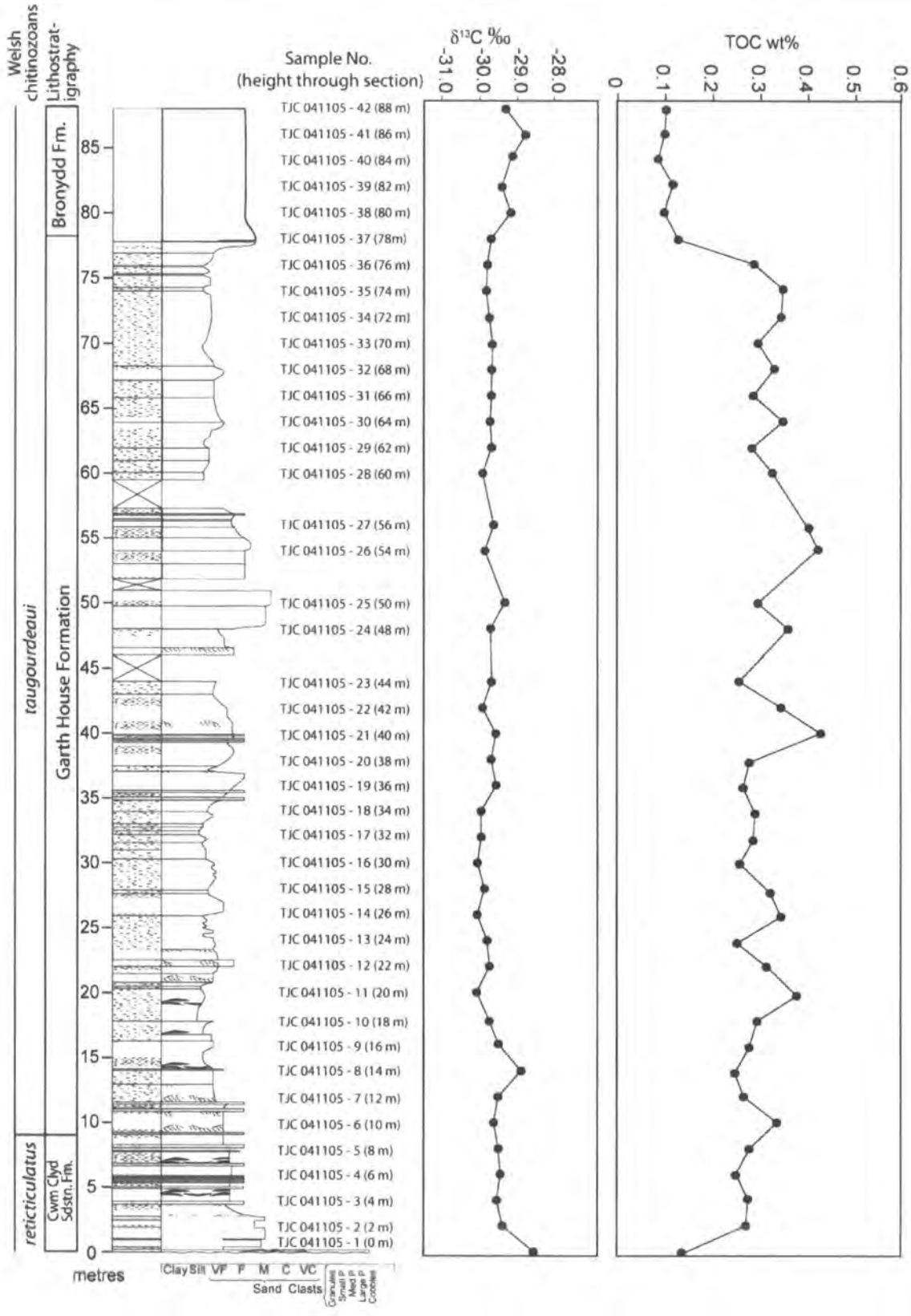

Figure 5.7: Graphic log and $\delta^{13}C$ profile and total organic carbon (TOCwt%) for the Crychan Forest section. See Figure 5.5 for graphic log key.

All $\delta^{13}C_{org}$ and TOC wt% measurements were made on a Thermo Finnigan MAT 253 Stable Isotope Mass Spectrometer at Durham University, Department of Earth Sciences. $Urea_2$, CH-7 and CH-6 isotopic standards were used for machine calibration and standard deviation was less than 0.15 ‰ for all standards. Duplicates were within ± 1%. Powdered samples were decarbonated in 10 % HCl for 24 hours and then thoroughly rinsed and dried prior to analysis. Carbon isotope ratios are expressed in the standard delta (δ) notation in per mil (‰) against the internationally accepted standard notation, Vienna Peedee Belemnite (VPDB).

5.4 Results

In the following descriptions and discussion, 'background values' refer to the mean sediment $\delta^{13}C_{org}$ value after subtraction of positive excursions.

5.4.1 Whole-rock $\delta^{13}C_{org}$ analysis.

Basin section - Dolaucothi M8 core The Dolaucothi M8 core profile is characterized by background values of -30.5 ‰ (Figure 5.8). Three noticeable positive excursions are present; a large excursion of 2.96 ‰ (-30.68 ‰ to -27.72 ‰) at 79.13 m (Yr Allt Formation), a small excursion of 1.4 ‰ (-30.96 ‰ to -29.56 ‰) at 48.68 m in the Mottled Mudstone Member and an excursion of 1.08 ‰ (-30.65 ‰ to -29.73 ‰) at 44.36 m (Cwmere Formation). Values for the third peak do not return to background values but remain at -30.22 ‰ (Figure 5.3).

TOC wt% values range between 0.12 to 0.47 wt% (mean = 0.29 wt%) through the Dolaucothi M8 core. Two distinct phases are recognizable that correspond with Formational boundaries and are separated by an abrupt decrease in TOC wt%: 1) the Yr Allt Formation with a high mean TOC wt% value of 0.36 wt% and 2) the Mottled Mudstone Member - Cwmere Formation characterized by low TOC wt% of mean value 0.16 wt%. The maximum value (0.47 wt%) coincides with the most positive $\delta^{13}C_{org}$ value at 79.13 m (Figure 5.3).

Shelf sections - A40 road section, Llandovery The A40 road section shows an overall decreasing trend in $\delta^{13}C_{org}$ with a mean value at the base of the section of -29.28 ‰ between 8 m to 28 m, and a mean value of -29.92 ‰ between 226-287m at the top (Figure 5.8). Values range between -30.45 ‰ to -28.17 ‰ throughout the entire section. The profile displays two significant positive excursions; a large excursion of 1.63 ‰ (maximum value = -28.58 ‰) at 69 m to 73 m and a smaller excursion of 1.27 ‰ (maximum value = -29.04 ‰) at 251 m. The first peak occurs within the Ciliau Formation and the second within an obvious sandstone body interpreted as representing the Cwm Clyd Sandstone between the Cwmcringlyn and Garth House Formations (Figure 5.5).

TOC wt% values range between 0.18 wt% to 0.39 wt% (mean = 0.28 wt%) and fluctuate between these values up to the base of the Garth House Formation at 253.5 m. From this point to the top of the section (253.5 m to 282 m) values exhibit an increasing trend from 0.31 wt% to 0.37 wt%. High TOC wt% values coincide with low $\delta^{13}C_{org}$ values e.g. at 27 m TOC wt% = 0.39 wt%, $\delta^{13}C_{org}$ = -29.42 ‰ (Figure 5.5).

Crychan Forest section $\delta^{13}C_{org}$ values range between -30.5 ‰ and -28.54 ‰ (mean = -29.58 ‰) with a low background value of -29.75 ‰. The section exhibits two noticeable excursions: 1) the largest excursion, a double-peaked excursion, of 1.21 ‰ from background values (peak value = -28.54 ‰) is recorded in the Cwm Clyd Sandstone Formation 10 cm from the base of the section at the unconformity with the second subsidiary peak occurring at 14 m from the base of the measured section in the Garth House Formation, 2) a smaller excursion of 1.04 ‰ (peak value = -28.76 ‰) at the top of the section (78 m to 88 m) in the bioturbated sandy Bronydd Formation 5.7).

TOC wt% values at the base of the section in the Cwm Clyd Sandstone at 0 m are low (0.13 wt%) and rise abruptly to 0.26 wt% by 2 m. Values then rise gradually to a maximum value of 0.41 wt% at 40 m after which they remain high and fluctuate between 0.24 wt% and 0.40 wt% (mean = 0.30 wt%) throughout the Cwm Clyd Sandstone and Garth House Formation. At the base of the Bronydd Formation at 78 m from the base of the section, values drop abruptly to 0.08 wt% and thereafter remain low with a mean value of 0.10 wt% (Figure 5.7).

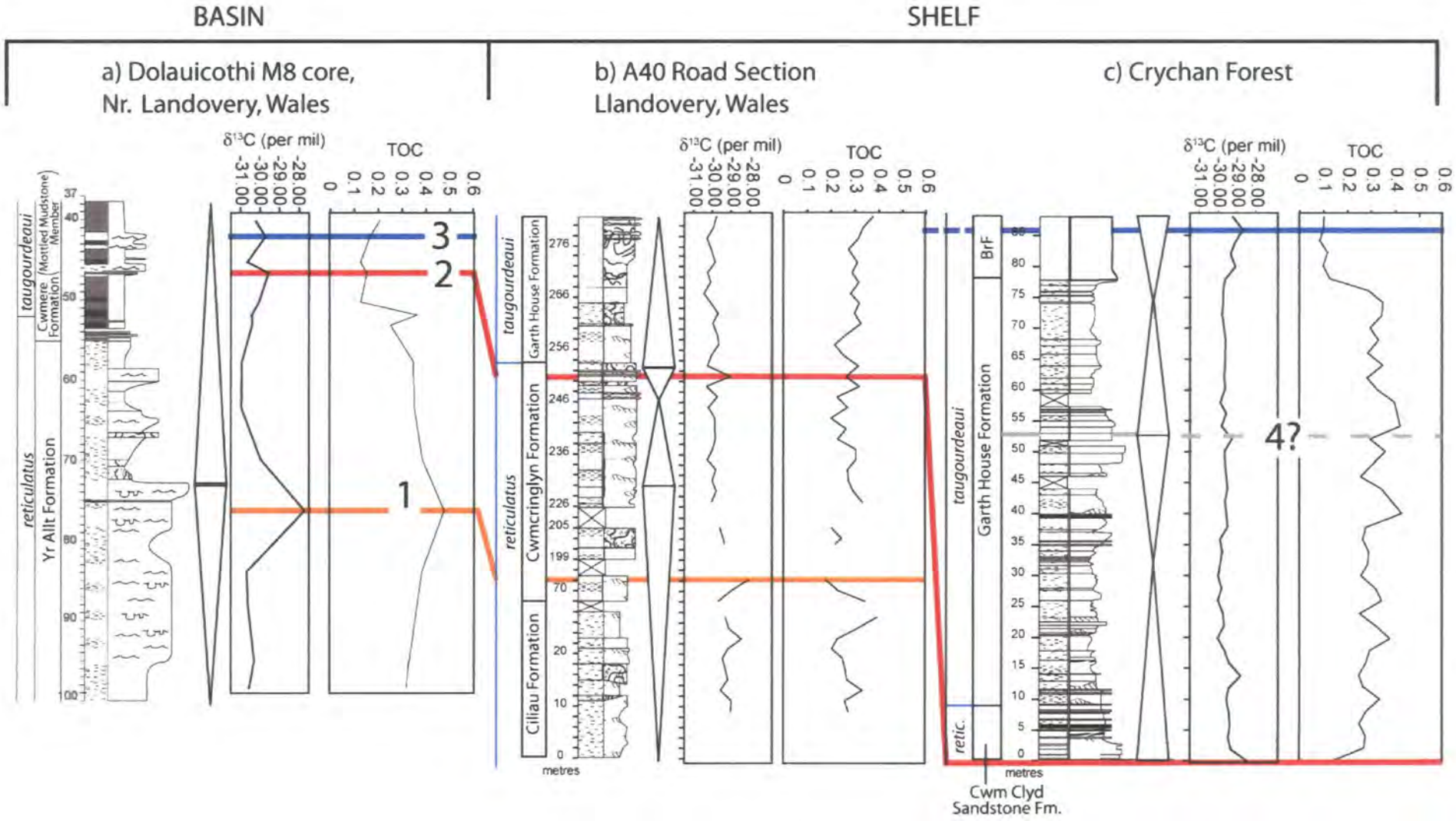

Figure 5.8: Regional $\delta^{13}C_{org}$ chemostratigraphic correlation chart between the basinal Dolaucothi M8 core (a) and the shelfal A40 road section (b) and Crychan Forest (c) sections from the Llandovery area. Positive isotopic excursions identified and correlated between sections that are referred to in the text are labeled 1-4. See Figure 5.5 and 5.3 for graphic log key

5.5 Regional correlation.

Construction of composite $\delta^{13}C_{org}$ curve A composite curve for the Hirnantian of the Welsh Basin was constructed from all three sections following regional correlation, by aligning correlative positive excursions and series of data and where more than one corresponding value occurred, taking the mean value. A three-point moving average was then applied to the curve as a filter to eliminate minor excursions representing noise.

The four separate positive $\delta^{13}C_{org}$ excursions identified between sections can be correlated primarily using regional chitinozoan biostratigraphy further supplemented by lithostratigraphic correlation (Figure 5.8). The first excursion of up to 2.96 ‰ occurs in the *reticulatus* Biozone and spans the early-Hirnantian Ciliau and Cwmcringlyn Formations in the A40 road section and occurs 28 m below the base of the Cwmere Formation in the Dolaucothi M8 borehole in the Yr Allt Formation. The second excursion of up to 1.27 ‰ occurs at the base of the post-glacial transgression in the uppermost *reticulatus* Biozone. It is present in the Cwm Clyd Sandstone of the the A40 road section and Crychan Forest section. The third positive excursion of up to 1.40 ‰ occurs towards the base of the *taugourdeaui* Biozone in the Cwmere Formation in the Dolaucothi M8 core and the Garth House Formation in

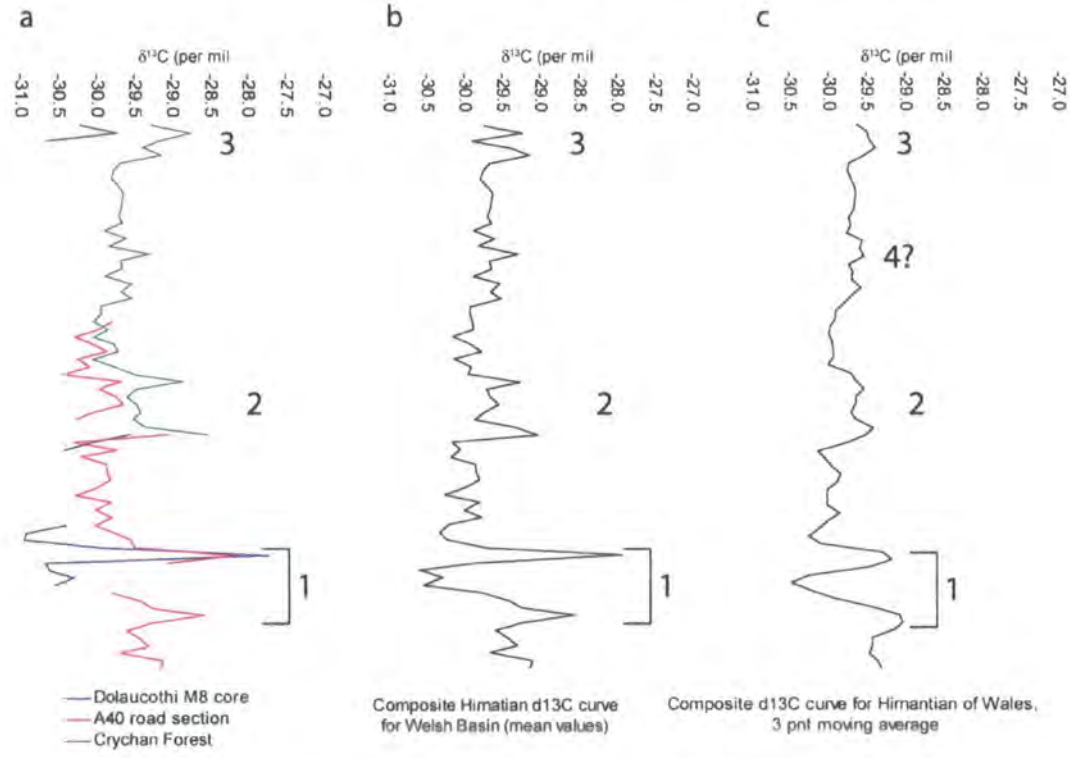

Figure 5.9: Composite $\delta^{13}C_{org}$ curve for Hirnantian of Welsh Basin.

the Crychan Forest section. The fourth excursion of 1.08 ‰ is of *taugourdeaui* Biozone age (*persculptus* graptolite Biozone) and is recorded in the Cwmere Formation in the Dolaucothi M8 core and the corresponding Bronydd Formation of the Crychan Forest section.

The lowest correlated excursion in the sections occurs in the Yr Allt Formation in the Dolaucothi M8 core and the Cwmcringlyn Formation of the A40 road section. In the A40 road section the peak is 1.63 ‰ compared to the equivalent Dolaucothi M8 core excursion of 2.96 ‰. These two peaks are correlated here on biostratigraphical and lithostratigraphical grounds and relative peak size compared to other parts of the sections

The positive excursion of 0.96 ‰ at the base of the Cwm Clyd Sandstone Member in the Crychan Forest section is correlated lithologically and biostratigraphically with the excursion in the Cwm Clyd Sandstone in the A40 road section (1.27 ‰).

The third positive excursion in the Cwmere Formation of the Dolaucothi M8 core and the Garth House Formation of the Crychan Forest Section is also correlated on biostratigraphical grounds. This excursion occurs towards the base of the *taugourdeaui* Biozone.

The fourth positive excursion, recognized in the Cwmere Formation of the Dolaucothi M8 core, is correlated with the positive excursion observed in Bronydd Formation of the Crychan Forest section. The magnitude of the excursion and the absolute $\delta^{13}C_{org}$ values are similar for both sections, 1.5 ‰ (-31.0 to 28.5 ‰) for the Dolaucothi M8 Cwmere Formation and 1.25 ‰ (-29.75 to -28.5 ‰) for the Crychan Forest section Bronydd Formation. Also, these two sections both yield age equivalent graptolite *N. persculptus* (Dolaucothi M8 core) and chitinozoan *S. taugourdeaui* (Crychan Foest section) further suggesting age equivalency in both sections.

The superposition of the individual curves from the regional correlation allows some important observations to be made. Values for the Dolaucothi M8 core basin section are noticeably higher for all excursions. Also, background $\delta^{13}C_{org}$ values are progressively more positive in more proximal shelf settings, however, corresponding excursions are greater in magnitude in the basin setting relative to the shelf (Figure 5.9a).

A three-point moving average curve has been used to eliminate spurious excursions that cannot be distinguished from background noise. When applied to the composite curve (Figure 5.9 b), the three-point moving average curve (Figure 5.9 c) exhibits some distinct differences. The amplitude of all excursions is reduced, by up 1.2 ‰, but still four excursions are evident.

5.6 Global correlation of the composite $\delta^{13}C_{org}$ curve for the Hirnantian of the Welsh Basin

Extensive work has been carried out on documenting and correlating the distinct Hirnantian isotopic carbon excursion (HICE) for the major palaeocontinents (Laurentia: Orth *et al.*,

1988; Long, 1993; Wang *et al.*, 1993; Underwood *et al.*, 1997; Saltzman & Young, 2005; Melchin & Holmden, 2006; Schmitz & Bergström, 2007), (Baltoscandia: Kaljo *et al.*, 2001; Brenchley *et al.*, 2003; Kaljo *et al.*, 2004, 2007; Schmitz & Bergström, 2007), China: Wang *et al.* (1997), Gondwana: Armstrong *et al.* (2005)) but there is a distinct lack of data from Avalonia. Only two $\delta^{13}C$ records have been published from the Ashgill of Avalonia; from the Genicot Formation, Belgium (Vanmeirhaeghe *et al.*, 2005) and, most recently, from Meifod in central Wales (Brenchley *et al.*, 2006). In the Belgian section the Hirnantian is missing (truncated) and rocks of the late-Katian *B. umbilicata* chitinozoan biozone are directly overlain by Silurian rocks of the *Conochitina eustachensis* chitinozoan biozone (Vanmeirhaeghe, 2006). The Meifod record only records five data points for the Hirnantian.

In this study, correlation of excursions between global sections from different palaeocontinents is based on chitinozoan and graptolite biostratigraphy. The biostratigraphic correlation scheme of Webby *et al.* (2004) is used except where more recent data have come to light e.g. the Avalonian chitinozoan biozonation scheme (Vandenbroucke & Vanmeirhaeghe, 2007) and the regional chitinozoan biostratigraphic scheme for the Welsh Basin (Chapter 2).

5.6.1 Baltoscandia

Much of the interval of rising $\delta^{13}C$ and the peak values occurs in the *persculptus* graptolite biozone (*taugourdeaui-scabra* Baltoscandian chitinozoan biozones) in the Baltoscandian sections indicating the early-Hirnantian interval in the Baltic sections is highly condensed (Melchin & Holmden, 2006). The potential for a similar problem in the Welsh Basin, where the basin section (Dolaucothi M8 core) may be condensed, and the shelf section (Crychan Forest) lacks the early-Hirnantian, has been eliminated through using an additional shelf section that is neither condensed nor has extensive erosion of the early-Hirnantian (the Llandovery A40 road section). Following the interpretation and correlation of Baltoscandia with other worldwide sections in Melchin & Holmden (2006), the two larger excursions in the *persculptus* Biozone in the Welsh Basin (excursions 2 and 4) could possibly be correlatives of the major peaks recorded by Kaljo *et al.* (2001) Brenchley *et al.* (2003), Kaljo *et al.* (2004) and Kaljo *et al.* (2007), in the *persculptus* Biozone (Figure 5.10).

Also, from Baltoscandia, Schmitz & Bergström (2007) recently produced a high-resolution $\delta^{13}C$ curve through the Boda Limestone Formation and recognized a pronounced positive isotopic excursion in this formation. However, contrary to the Schmitz & Bergström (2007) correlation, the beginning of the excursion is dated as late Katian from the presence of the brachiopod *Holorhyncus giganteus* (Brenchley *et al.*, 1997). Also, the Boda Limestone Formation studies by Schmitz & Bergström (2007) contains two unconformities towards the top of their section. It is uncertain, therefore, where the base of the Hirnantian is in this

section and whether late Hirnantian $\delta^{13}C$ peaks are missing, truncated by the unconformities. Because of these uncertainties, no attempt at correlation of the Welsh Basin curve with the curve of Schmitz & Bergström (2007) is made here.

5.6.2 Laurentia

At Dob's Linn, the GSSP for the Ordovician-Silurian boundary, the maximum $\delta^{13}C_{org}$ values occur in the *persculptus* graptolite Biozone (Underwood *et al.*, 1997; Melchin & Holmden, 2006). A minor peak is present in the *extraordinarius* graptolite Biozone at Dob's Linn may correlate with the lowest peak in the Welsh Basin section but is 2 ‰ smaller at Dob's Linn. The largest excursion at Dob's Linn is correlated with the youngest excursion (excursion 3) in the Welsh Basin sections. However, the maximum excursion in the *persculptus* Biozone at Dob's Linn is much greater than in the Welsh Basin (4 ‰ compared to 1.5 ‰ respectively) though the absolute values are similar (-28.2 ‰ at Dob's Linn, -28.54 ‰ Welsh Basin).

For sections from Anticosti Island, Long (1993) documented an increasing trend in $\delta^{13}C$ values through the *taugourdeaui* Biozone with maximum values in the very uppermost of part of the biozone whereas in the Welsh Basin, the maximum excursion values occur in the *reticulatus* Biozone (lower *taugourdeaui* Biozone of the Laurentian chitinozoan scheme). As such, the Anticosti Island sections are not easily related to the Welsh Basin section and the only confident similarities that can be drawn are that there are a series of positive $\delta^{13}C$ excursions within the *taugourdeaui* chitinozoan Biozone (including the *persculptus* graptolite Biozone).

Biostratigraphic control on the Hirnantian section from Nevada of Saltzman & Young (2005) is not strong enough to correlate individual peaks within the *extraordinarius* or *persculptus* Biozones.

From Arctic Canada, Melchin & Holmden (2006) stated that the rocks used to compile their $\delta^{13}C_{carb}$ curves have been subjected to diagenetic alteration and variable detrital carbonate flux. For these reasons, correlation of the Welsh Basin curve has not been attempted for Arctic Canada $\delta^{13}C_{carb}$ curves. All $\delta^{13}C_{org}$ sections for Arctic Canada, however, share a similar pattern of excursions to the Welsh Basin section. The largest positive excursion occurs in the *extraordinarius* graptolite biozone (*reticulatus*- lower-*taugourdeaui* Welsh Basin chitinozoan biozones) for the Arctic Canada sections except for Truro Island where the largest excursion occurs in the late-Katian *pacificus* graptolite biozone. This first large excursion is then followed by a decrease in values and a subsequent second positive excursion in the *persculptus* zone.

With respect to curve topology, the Arctic Canada $\delta^{13}C_{org}$ curves match very well with the Welsh Basin profile but all excursions are greater in magnitude, up to 7 ‰ for the Eleanor

Lake section compared to 3 ‰ for the Welsh Basin, and are more positive (up to 24 ‰ for Eleanor Lake section, 27.7 ‰ for the Welsh Basin).

No biozonation scheme is given for the HICE curves of Wang *et al.* (1993) or Orth *et al.* (1988) and so correlations of individual peaks between these sections and the Welsh Basin have not been made.

One other Laurentian $\delta^{13}C_{carb}$ curve from Copenhagen Canyon, Nevada, published by Schmitz & Bergström (2007) shows a similar pattern to the Arctic Canada $\delta^{13}C_{org}$ curves. The largest excursion occurs in the *extraordinarius* Biozone followed by a second excursion in the *persculptus* zone. However, the base of the *persculptus* Biozone occurs above a marked unconformity in the Copenhagen Canyon section and indicates loss of strata within the *extraordinarius* zone making any correlation of peaks below this horizon with the Welsh Basin Hirnantian curves uncertain.

5.6.3 China

In China, the *bohemicus* graptolite Biozone is equivalent to the *extraordinarius* graptolite biozone (Storch & Loydell, 1996). The Global Boundary Stratotype Section and Point (GSSP) for the Hirnantian is defined from the Wangjiawan North section in China (Chen *et al.*, 2006). The position of two excursions in the *extraordinarius* graptolite biozone from a $\delta^{13}C_{org}$ curve from the nearby Wangjiawan South section compares well with the positive $\delta^{13}C_{org}$ peaks in the age-equivalent *reticulatus-taugourdeaui* Biozones of the Welsh Basin curve. However, no excursion is recognized in the *persculptus* graptolite biozone from the GSSP section. The magnitude of the equivalent excursions also differs between the GSSP section and the Welsh Basin, the lower excursion in the Wangjiawan section being smaller than the upper excursion. The opposite pattern is observed in the Welsh Basin.

Only two sections from China (Huanghuachang and Tongguo; Wang *et al.*, 1997) exhibit the same topology of isotope excursions seen in the Welsh Basin. Other sections either have two large excursions in the *bohemicus* graptolite Biozone to *Hirnantia-Kinella* shelly fossil Biozone and none in the *persculptus* graptolite zone (e.g. Beigong) or they have an earlier excursion in the *mirus* graptolite Biozone and none in the *persculptus* Biozone (e.g. Fenxiang and Wangjiawan sections). The Datianba section only records one positive excursion at the base of the *Hirnantia-Kinella* Biozone which may be equivalent to the lowest peak in the Welsh Basin section. The peaks in the *persculptus* graptolite Biozone from the Welsh Basin are small relative to $\delta^{13}C_{org}$ from China (Wang *et al.*, 1997).

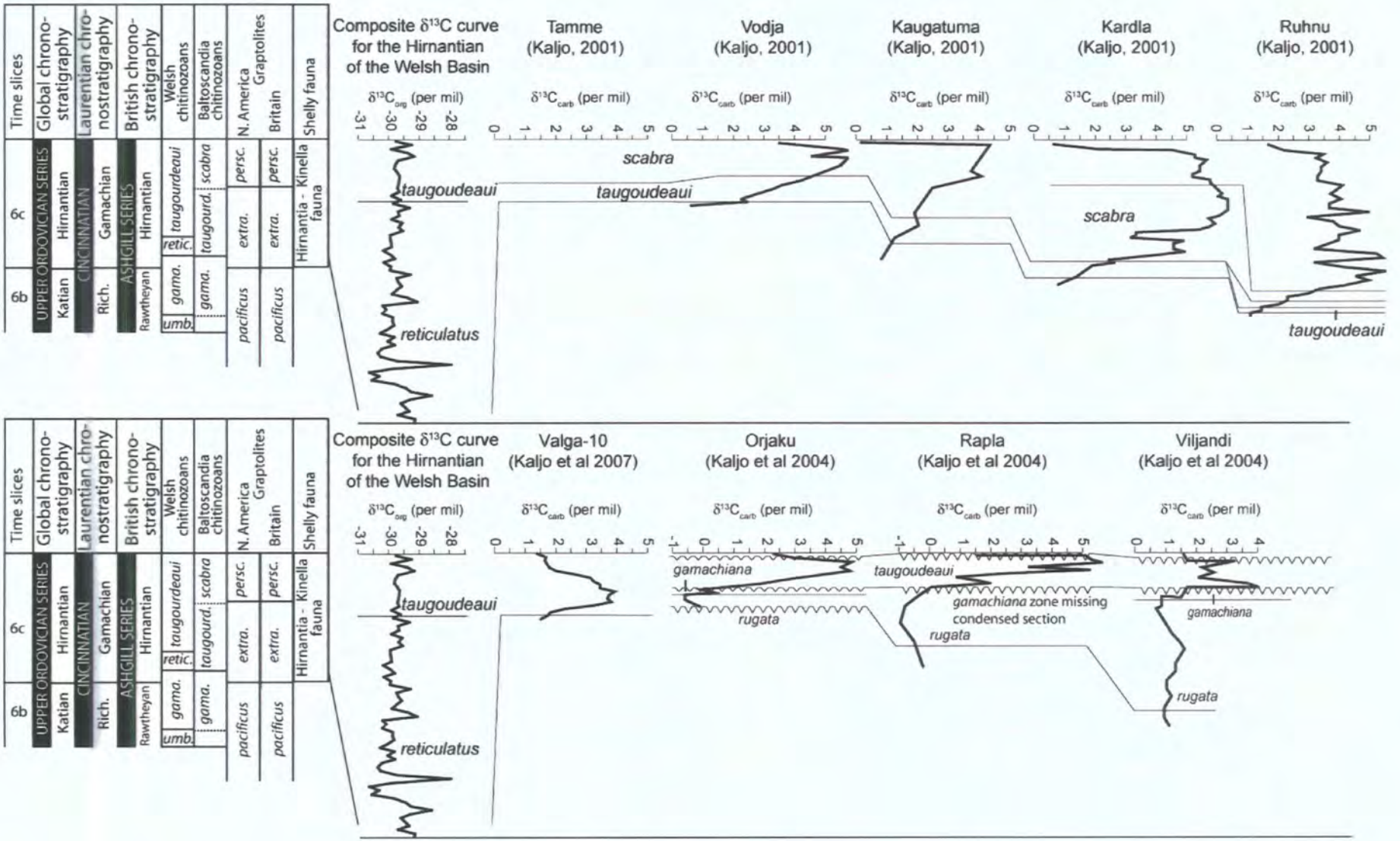

Figure 5.10: Composite $\delta^{13}C_{org}$ curve for the Welsh Basin (left) and correlation chart for Baltoscandia $\delta^{13}C$.

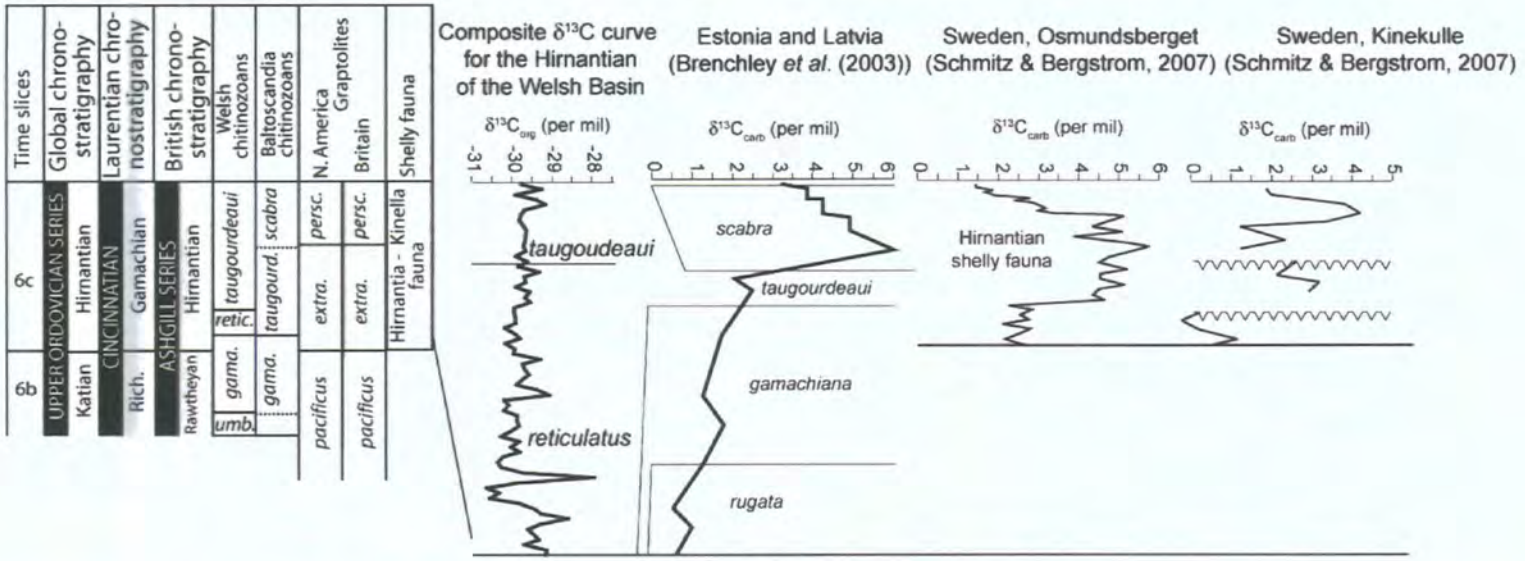

Figure 6.4 *cont.*: Baltoscandia correlation chart

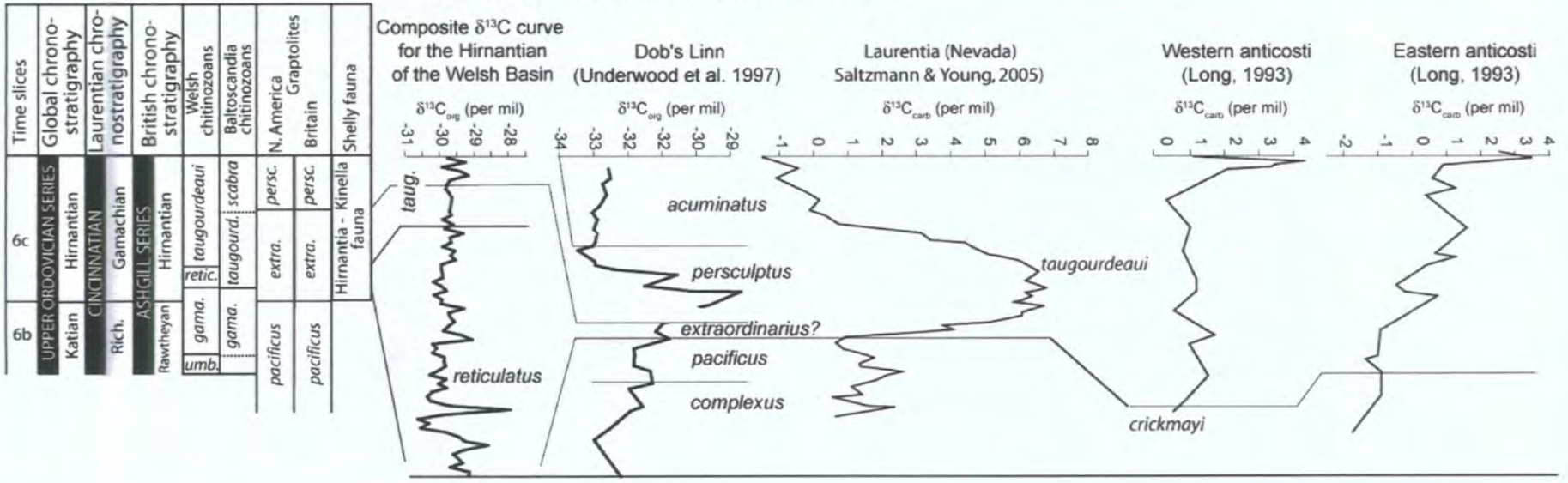

Figure 5.11: Composite $\delta^{13}C_{org}$ curve for the Welsh Basin (left) and correlation chart for Laurentia $\delta^{13}C$.

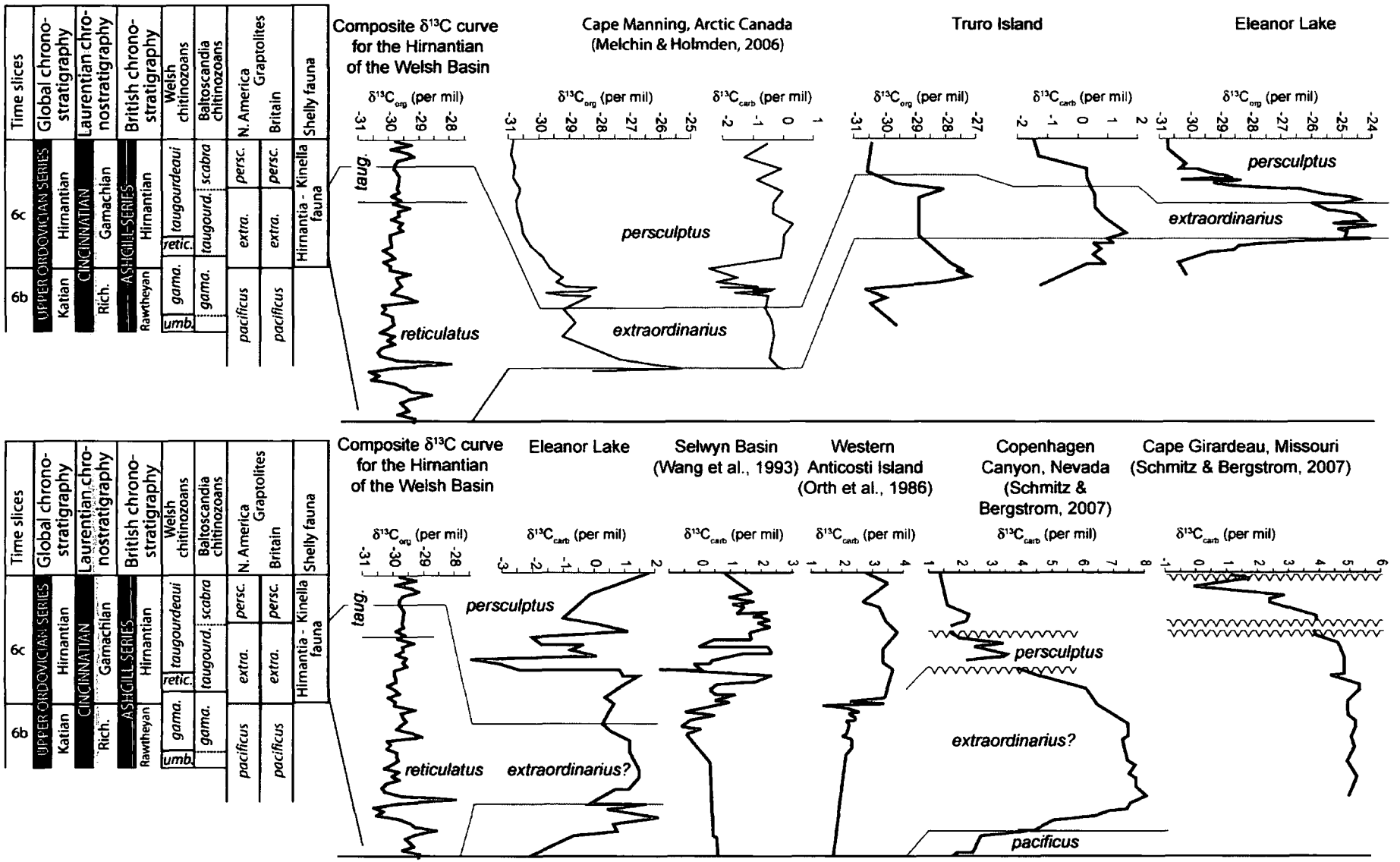

Figure 5.12: Composite $\delta^{13}C_{org}$ curve for the Welsh Basin (left) and correlation chart for Laurentia $\delta^{13}C$ *cont.*

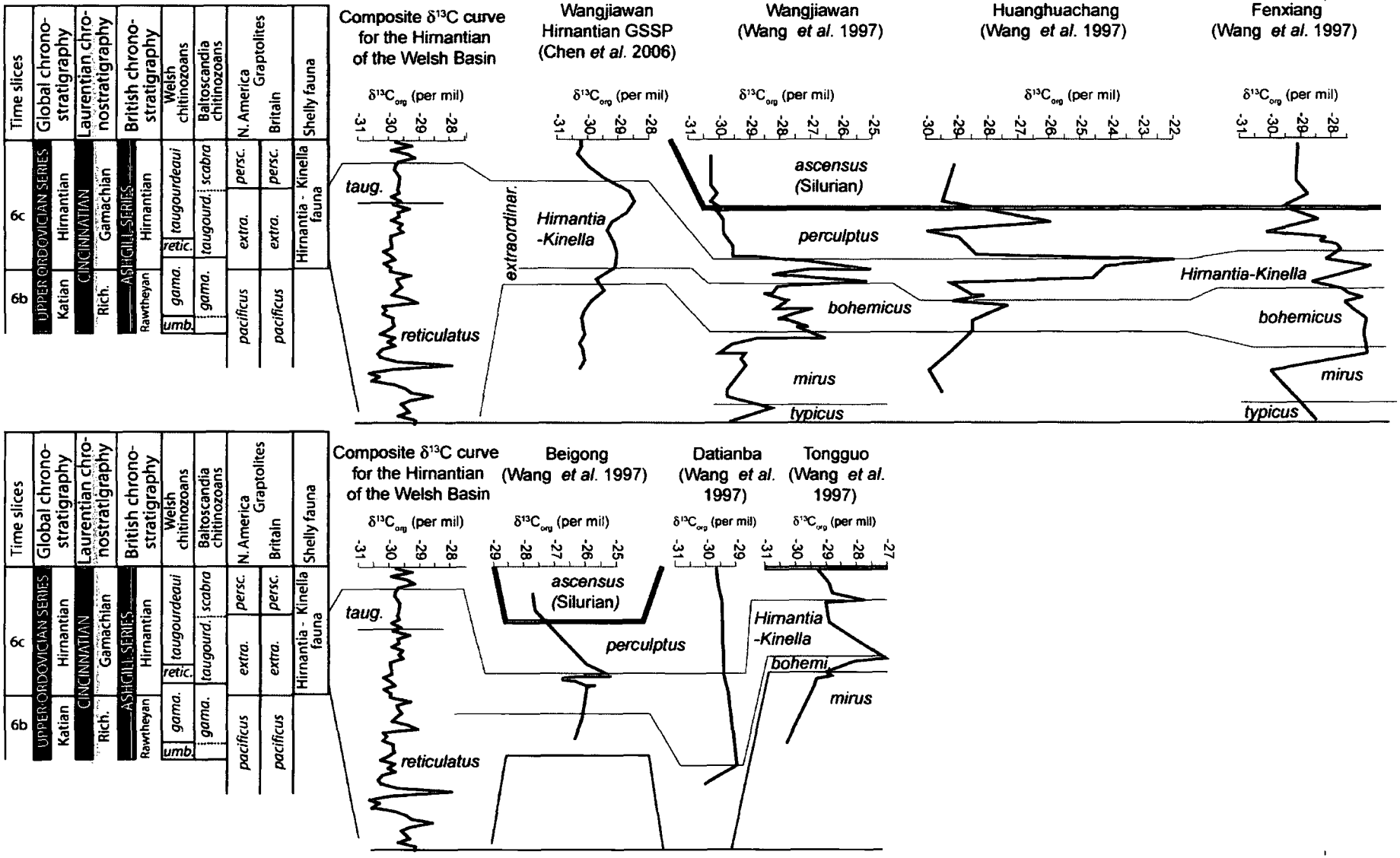

Figure 5.13: Composite $\delta^{13}C_{org}$ curve for the Welsh Basin (left) and correlation chart for China $\delta^{13}C$.

5.7 Sequence stratigraphical interpretation

Marshall & Middleton (1990) established that peak Hirnantian $\delta^{13}C$ values were coincident with sealevel fall and $\delta^{13}C$ values began to decline during sealevel rise. Establishing the timing of the Welsh Basin positive $\delta^{13}C_{org}$ excursions with respect to sealevel cycles and TOC peaks has important implications for testing the hypothesis of carbon burial contributing to the HICE. If TOC maxima coincide with $\delta^{13}C_{org}$ peaks on the shelf during low sealevel, it would be implied that carbon burial occurred in shelf environments and that such environments could be significant carbon sinks contributing to the HICE and/or Hirnantian glacial maximum.

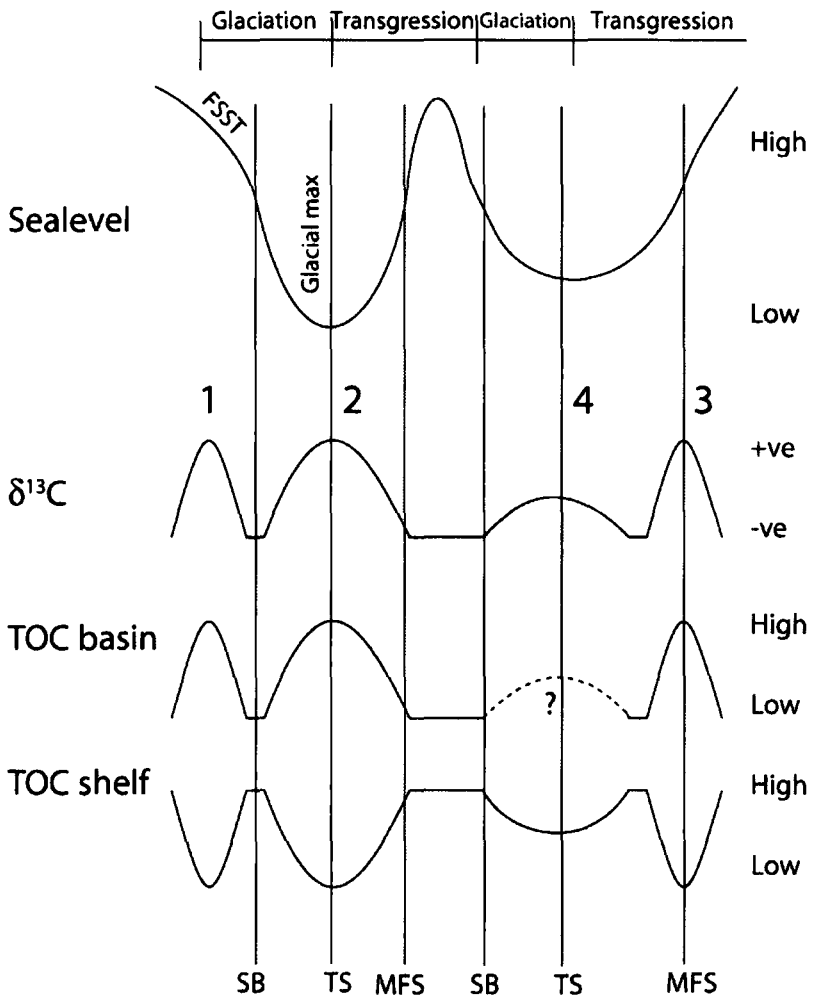

Figure 5.14: Sequence stratigraphy of Welsh Basin Hirnantian $\delta^{13}C_{org}$ excursions and TOC profiles for basin and shelf sections. $\delta^{13}C_{org}$ excursion 1 occurs during the falling stand systems tract (FSST), $\delta^{13}C_{org}$ excursion 2 begins on the sequence boundary (SB) and peaks at the transgressive surface (TS). $\delta^{13}C_{org}$ excursion 3 begins at the sequence boundary of the second sealevel cycle. The peak of $\delta^{13}C_{org}$ excursion 4 occurs at the maximum flooding surface of the second sealevel cycle.

A sequence stratigraphical interpretation of the Hirnantian sedimentary succession from the Llandovery region has been derived from analysis of detailed sedimentary logs for each measured section (Figure 5.8) and broadly confirms the patterns proposed for the Llandovery area (Figure 5.2). The Ciliau to Cwmcringlyn formations represent a coarsening-up sequence and the base of the Cwmcringlyn Formation has previously been interpreted as representing deposition during the acme of the Hirnantian glaciation (Schofield *et al.*, 2004) during sealevel lowstand. In the Dolaucothi M8 core, this interval is represented by the sand-rich Yr Allt Formation, which includes disturbed beds, and indicates sediment bypass into the basin. In the most marginal section sampled (Crychan Forest), the acme of marine regression is marked by an unconformity. The coarse-grained Cwm Clyd Sandstone Formation overlying the unconformity marks the beginning of the rising stand systems tract (RSST) and continues to fine up into the succeeding Garth House Formation until 22 m above the base of the Garth House Formation. After this point, sandy units become more abundant and the sequence becomes one of coarsening up indicating the falling stand systems tract (FSST) and low stand systems tract (LSST) up to the top third of the Formation. In the A40 section, the equivalent position of the FSST and LSST is represented by sandy disturbed units at the top of the section. Following the FSST and LSST, the Garth House Formation once again fines-upwards in the Crychan Forest section marking the RSST. In the Dolaucothi M8 core the equivalent RRST and the position of the ensuing maximum flooding surface (MFS) is likely represented by fining-up from the base of the Mottled Mudstone Member and the onset of persistent laminated hemipelagite deposition in the Cwmere Formation. In the Crychan Forest section, the section coarsens again at the base of the Bronydd Formation.

The peak of $\delta^{13}C_{org}$ excursion 1 occurs during the FSST of the HSST. Regional mapping in the Llandovery area by the British Geological Survey (unpublished data) suggests that lithostratigraphical position of this excursion is above a unit of coarse-grained sediment in the Ciliau Formation, deposited during a period of lower sealevel (Figure 5.2). Further to this, the position of the first $\delta^{13}C_{org}$ peak coincides with the boundary between the Ciliau and Cwmcringlyn Formations, indicative of the transition from high sealevel, mud-dominated deposition to sand-dominated deposition during glacial lowstand (Figure 5.8).

The beginning of excursion 2 occurs at the sequence boundary with the maximum value during the RSST and its peak occurs at the point of maximum regression, likely reflecting the HGM.

Excursion 3 occurs in the FSST-RSST during a second period of low sealevel, possibly a second glacial episode or a period of tectonism. In excursion 4, the maximum value occurs at the transgressive surface of the next sealevel cycle (Figure 6.1).

Evidence for syn-sedimentary faulting in the Ciliau and Cwmcringlyn formations could invalidate a glacioeustatic interpretation for sealevel and isotope control in the Welsh Basin. Discrete sandy units and disturbed beds in the lower Ciliau Formation along with progressive overstep at the base of the Cwm Clyd Sandstone testifies to the active nature of the localised Crychan Fault Belt prior to deposition of the Cwm Clyd Sandstone or the underlying Ciliau and Cwmcringlyn Formations (Schofield *et al.*, 2004). Tectonic effects are discounted for $\delta^{13}C_{org}$ excursions 2, 3 and 4 because they occur after cessation of fault activity. Excursion 1 though occurs during relative deep water sedimentation (mud-dominated Ciliau Formation) suggestive of subdued regional uplift and tectonic quiescence. However, the period of disturbed-bed deposition in the lower Ciliau Formation, not sampled in this study, could represent a period of tectonic activity.

5.8 Differential shelf and basin carbon burial

An increase in background $\delta^{13}C_{org}$ values from basin to shelf, seen in the Welsh Basin, is opposite to the pattern recognized in the Hirnantian in Arctic Canada where $\delta^{13}C_{org}$ excursions on the shelf were larger than basin sections (Melchin & Holmden, 2006). Melchin & Holmden (2006) attributed their pattern to the differences in terrestrial carbon-weathering flux having a greater influence in proximal basin settings on regional isotopic balances. In the Welsh Basin, variability in carbonate-weathering flux between basin and shelf sections is discounted for three reasons: 1) the sediments are entirely siliciclastic and were deposited beyond the mudline and therefore do not suffer the same detrital carbonate contamination as the Arctic Canada sections; 2) the 'background' conditions for each curve persists before and after excursions and appears to be a long-term state upon which excursions are superimposed, not an instantaneous event like in Arctic Canada; 3) modeled results (see Appendix E) suggest that a 17% increase in carbonate weathering is not sufficient to cause an excursion of the magnitude observed.

How else might such an isotopic gradient between basin and shelf environments occur? Upwelling of light carbon from the deep ocean is one possibility. Upwelling and reworking of light (^{12}C-rich) carbon in pre-Hirnantian (late Katian) Welsh Basin sediments produced a 1 ‰ negative excursion in deposited organic-rich sediments associated with elevated TOC levels (Chapter 2). A lack of black shales and phosphate nodules/horizons in both the basin and shelf during background $\delta^{13}C_{org}$, coupled with an absence of geochemical productivity proxy data (Ba/Al) weakens support for this interpretation. Another alternative is for higher shelf productivity, relative to basin productivity, during high sealevel interglacial periods (i.e. background $\delta^{13}C_{org}$ conditions). Coupled with favorable preservation conditions on the shelf for organic carbon during high sealevel (i.e. high sedimentation rate and organic carbon

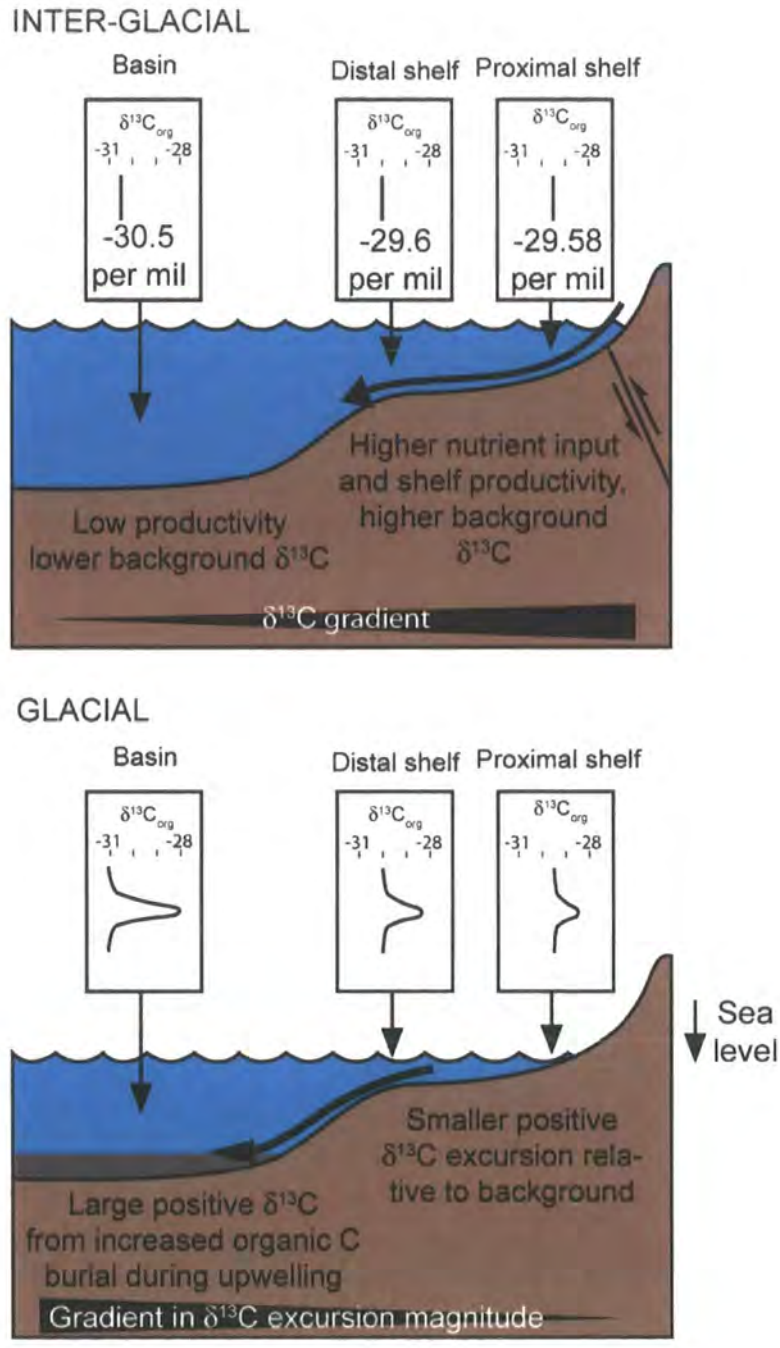

Figure 5.15: Interpretation of isotopic gradients and shifting organic carbon burial during interglacial-glacial periods in the Hirnantian of the Welsh Basin. Background productivity and organic carbon burial is lower in the basin during, interglacial periods in the Hirnantian, compared to the shelf, which receives high nutrient input. During glacial periods, sealevel falls and the locus of organic carbon burial shifts to the basin due to slumping and transport of organic carbon-rich shelf sediments into the basin. Shelf productivity decreases because of loss of shelf area during sealevel fall. $\delta^{13}C_{org}$ excursions are smaller in the shelf sections because the relative burial of ^{12}C is lower on the shelf relative to the basin or because of shelf-basin water mass segregation.

flux), shelf waters may have been depleted in ^{12}C relative to deeper basin waters because of higher carbon sequestration. This pattern is also reflected in the higher TOC values in shelf sediments during low $\delta^{13}C_{org}$ background values, compared to TOC values during excursions (Figure 5.15).

However, the burial of organic matter in sediments currently occurs largely within a relatively small surface area of seafloor in sediments of the continental shelf and slope (Archer, 2004; Hedges & Keil, 1995). Hallam & Wignall (1997) and Munnecke *et al.* (2003) recognize that Hirnantian shelf sediments from other parts of the world typically have low amounts of organic carbon prompting the suggestion that CO_2 drawdown and HICE may have been initiated by some other means than productivity and OC burial. The TOC values recorded in this study for both basin and shelf are very low (up to 0.45 wt%) and can be explained by loss of carbon during metamorphism and thermal maturation. Whole-rock kerogen (weight%) of organic-rich sediments can decrease by up to 50% when heated to post-oil generation temperatures (>165°C). Therefore, at the metamorphic temperatures experienced by the Welsh Basin rocks (≤400°C) the maximum TOC wt% values of basin and shelf sediments were probably originally no greater than 1 wt%.

The sections recorded herein demonstrate positive $\delta^{13}C_{org}$ excursions on the shelf accompanied by decreases in TOC wt% whereas positive $\delta^{13}C_{org}$ excursions in the basin correspond to increases in TOC wt%. This suggests that shelf OC deposition was low in the Welsh Basin during the HICE but that OC burial actually *increased* in the deeper basin environment during HICE relative to interglacial times. On longer time scales, during glacial periods, OC stored on shelves is transported into basins by turbidity currents (Van Weering *et al.*, 1997) reducing the role of shelves as OC sinks. However, during glaciation, the surface ventilated layer in the ocean would have increased the depth of the oxygen minimum zone favouring OC burial only in deeper anoxic parts of oceans and basin (Berry & Wilde, 1978).

Increased destability of shelf sediments, massive slumping and shelf bypass of sediment (e.g. thick sand units in the basinal Yr Allt Formation) are all lithological expressions of increased sediment transport from shelf to basin in the Welsh Basin during glacial times. This mechanism would have provided a 'conveyor' for shelf-derived OC into deeper waters where burial and preservation conditions were favourable during low sealevel (Figure 5.15). However, if this mechanism is responsible for the positive $\delta^{13}C_{org}$ excursions in the Welsh Basin, it requires that OC burial was greater from this process alone compared to shelf productivity during interglacial periods. Numerical modeling of carbon isotope mass balance demonstrates that a positive $\delta^{13}C_{org}$ excursion of the magnitude seen in the Welsh Basin can be achieved by increasing carbon burial by 50% (Kump *et al.*, 1999, see also Appendix E). This is, however, independent of the cause of the increased OC burial, be it increased

productivity or preservation although it cannot be ruled out that shelf and basin productivity may have contributed to carbon burial as well.

The greater magnitude of the basin $\delta^{13}C_{org}$ excursions relative to the shelf suggests some degree of isotopic segregation between the two environments and the presence of a 'continental boundary effect'. It would further suggest that $\delta^{13}C_{org}$ excursion values are higher in the basin relative to the shelf because greater sequestration of ^{12}C occurred in the basin. But, as noted for the interglacial periods, the background $\delta^{13}C_{org}$ values were initially lower in the basin than in the shelf. If shelf-basin segregation broke down during glaciation and lowering of sealevel, the shelf $\delta^{13}C_{org}$ excursion would be smaller than for the basin because shelf water dissolved inorganic carbon $\delta^{13}C$ was closer to the new steady state conditions of increased OC burial.

5.9 Global contribution to HICE

The relative timing of the positive $\delta^{13}C_{org}$ excursions and TOC excursions to sealevel fall in the Welsh Basin shows that OC burial in the deep basin was predominant at the start of sealevel fall and during glaciation and not before. Because of this timing, it therefore would have been an unlikely mechanism to contribute to CO_2 drawdown forcing the HGM. Additionally, there are no other shallow-deep clastic basin Hirnantian records to compare this mechanism with. The siliciclastic record from Dob's Linn, which formed as part of a deep-water, tropical, continental margin system (Armstrong, 2007; Underwood *et al.*, 1997), demonstrates a decrease in TOC values during HICE (A. Finlay, unpublished data) suggesting this mechanism was not active on the western margin of the Iapetus Ocean during HICE. Further to this, from a carbonate setting in Arctic Canada, TOC values are again low during HICE when $\delta^{13}C_{org}$ values are high in both proximal and distal ramp settings (Melchin & Holmden, 2006). The dataset for the Welsh Basin is relatively spartan but the unique pattern of the Welsh Basin TOC-$\delta^{13}C_{org}$ signal in the deep basin could suggest that this pattern may be a regional phenomenon implying that a global contribution of such carbon burial to the HICE could be, at the most, minimal.

5.9.1 Regional carbon cycling and mechanisms for HICE

Despite good regional correlation, the local variability in the size of isotopic excursions and background values between basin and shelf environments in the Welsh Basin is suggestive of the influence of a strong regional carbon cycle. Comparison with other HICE profiles throughout the world demonstrate that only a few other HICE curves from different palaeo-continents (Huanghuachang and Tongguo, China, Wang *et al.*, (1997); and Arctic Canada, Melchin & Holmden, (2006)) match the topology of HICE excursions in the Welsh Basin

(i.e. a large positive $\delta^{13}C_{org}$ excursion followed by a smaller positive $\delta^{13}C_{org}$, both in the *extraordinarius* graptolite biozone).

Although it is undeniable that positive $\delta^{13}C$ excursions do occur during the Hirnantian throughout the world (Marshall *et al.*, 1997) and that it is possible to correlate these peaks at the resolution of biozones, complex and variable $\delta^{13}C$ profile topologies, exhibited in all sections throughout the world, suggest that regional carbon cycle processes may have a stronger influence locally than a global signal. After all, a local record of increased carbon burial in deep basins during HICE does not constitute global confirmation of the productivity-burial hypothesis for HICE (Brenchley *et al.*, 1994). Consequently, the carbonate weathering hypothesis appears more credible. The global effect of increased carbonate weathering required to produce a $\delta^{13}C$ excursion consistent with HICE (using a target value of +7 ‰) has been modeled to only require a 16% increase in carbonate weathering rather than a 50-75% increase in OC burial (Kump & Arthur, 1999). A 16% increase in carbonate weathering is entirely reasonable given the reduction and exposure of carbonate-bearing shelves during the HGM (Kump & Arthur, 1999), whereas the loss of high-productivity shelf environment would probably have had drastic consequences for increasing burial of OC globally. However, like OC burial, the influence of regional carbonate weathering has been demonstrated to significantly affect HICE records regionally (Melchin & Holmden, 2006). For example, epicontinental sea basins contain smaller volumes of water and a less dissolved inorganic carbon (DIC) than open oceans. As a result, a small local perturbation in DIC from, for instance, increased carbonate weathering or OC productivity and burial, would produce a proportionately larger change in the $\delta^{13}C$ of the epicontinental sea DIC compared to an open ocean (Melchin & Holmden, 2006). This effect would be exacerbated if the sea was semi-restricted and communication from the open ocean was reduced, as is the case for the Welsh Basin in the the Upper Ordovician (Woodcock & Strachan, 2000).

In a global context, the shorter residence time of DIC in isolated basins and epicontinental seas serves to hasten the response time of these environments to local changes in carbon cycling, incited by global climate change, compared to the open global ocean (Panchuk *et al.*, 2005). The isotopic record of a global climate change episode in a restricted environment may therefore be expressed earlier than in an environment that is in open communication with the open sea DIC reservoir. This mechanism could explain why the positive $\delta^{13}C$ occurs in the late-Katian in some parts of the world e.g. China (Wangjiawan, Fenxiang and Tongguo sections, Wang *et al.*, 1997, ; Figure 5.13), Nevada (Copenhagen Canyon section, Schmitz & Bergström, 2007, Figure 5.12) and Arctic Canada (Truro Island and Eleanor Lake Melchin & Holmden, 2006, ; Figure 5.12).

Table 5.1: The relative timing of the onset of positive $\delta^{13}C$ excursion and peak excursion values at different localities throughout the world for the late-Katian to Hirnantian. British graptolite biozones are used to for timing of onset and peak HICE values. Climate zone abbreviations: ST=Sub-tropical (20-40° N & S), Trop.=Tropical (0-20° N & S). [1]Kaljo *et al.* (2004); [2]Kaljo *et al.* (2007); [3]Brenchley *et al.* (2003); [4]Saltzman & Young (2005); [5]Schmitz & Bergström (2007).

Location	Palaeocontinent	Climate Zone	Onset of +ve $\delta^{13}C$ excursion	Time of Peak HICE	Depositional setting
Welsh Basin	Avalonia	ST	*extraordinarius*	*extraordinarius*	Trans Iapetus, restricted clastic
Baltoscandia[1]	Baltoscandia	ST	*extraordinarius*	*persculptus*	Trans Iapetus, epeiric carbonate
Valga-10 core[2]	Baltoscandia	ST	*pacificus*	*extraordinarius*	Trans Iapetus, epeiric carbonate
Estonia & Latvia[3]	Baltoscandia	ST	*extraordinarius*	*persculptus*	Trans Iapetus, epeiric carbonate
Dob's Linn	Laurentia	Trop.	*pacificus*	*persculptus*	Trans Iapetus, deep clastic
Nevada [4]	Laurentia	Trop.	*extraordinarius*	*extraordinarius*	Open ocean, epeiric carbonate
Nevada[5]	Laurentia	Trop.	*pacificus*	*extraordinarius*	Open ocean, epeiric carbonate
Anticosti	Laurentia	Trop	*extraordinarius*	*persculptus*?	Trans Iapetus, clastic-carbonate shelf
Arctic Canada	Laurentia	ST	*pacificus*	*extraordinarius*	Open ocean, carbonate ramp
China	China	Trop.	*pacificus*	*extraordinarius*	Semi-restricted basin, clastic-carbonate basin

In addition to this, peak HICE values are not synchronous throughout the world. In Arctic Canada, Nevada and China, peak HICE $\delta^{13}C$ values occur in the *extraordinarius* graptolite biozone whereas at Dob's Linn, Anticosti Island and in Baltoscandia, peak HICE values are not achieved until the *persculptus* graptolite biozone (Melchin & Holmden, 2006). This delay, in the Baltoscandian and Estonian records, was attributed to limited carbonate platform exposure and weathering coupled with high subsidence rates and high siliciclastic input during the diminishing Taconic orogeny during the early Hirnantian (Kaljo *et al.*, 2004; Melchin & Holmden, 2006). A further example was demonstrated by Fanton & Holmden (2007) who showed that positive excursions in the late Ordovician of the mid-American continent were coincident with regional high sealevel rather than global low sealevel as Marshall *et al.* (1997) proposed for the HICE.

Unfortunately, there does not appear to be any consistency in the time of onset of the

positive $\delta^{13}C$ excursion and the timing of peak HICE values in relation to basin setting and current flow, as Melchin & Holmden (2006) proposed, or palaeolatitude (Table 5.1). It is inauspicious that $\delta^{13}C$ records alone cannot reveal information about changes in global or regional current configuration. Undoubtedly, however, regional changes in current configuration would have affected local ^{12}C cycling producing specific $\delta^{13}C$ profiles as Holgate *et al.* (2002) was able to model. This is confirmed, however, by Panchuk *et al.* (2005) and Holmden *et al.* (1998) for the Mohawkian epicontinental seas of Laurentia and also at other times throughout the Phanerozoic (Immenhauser *et al.*, 2003).

Attributing differences in timing purely to 'regional effects' gives us little help in understanding the relative timing of the HICE. A more informative explanation can be given from the process of signal rectification, that is, the truncation on one side or other of the full range of response due to the local climate system or from limitations of the proxy recorders (e.g. $\delta^{13}C$ Ruddiman, 2003). In the former, for example, in Cenozoic $\delta^{18}O$ records, oceans at high latitudes have a limited response to forcing towards colder sea surface temperatures once they reach the freezing point of water because further cooling cannot be recorded in the solid phase (Ruddiman, 2003). For $\delta^{18}O$, this process is better constrained if accepting that $\delta^{18}O$ can reliably recording sea surface temperature. But, because $\delta^{13}C$ profiles may be a record of numerous processes (carbonate weathering, carbon sequestration, photosynthetic fractionation), it is not possible to assign a mechanism to the rectification limit of a $\delta^{13}C$ profile at any given locality. However, the rectification principle would predict that localities where HICE begins early i.e. in the *pacificus* Biozone have a low rectification limit (Figure 6.3, a, top figure) whereas those where it starts late, in the *extraordinarius* Biozone, have a high rectification limit (Figure 6.3, a, lower figure). The opposite case - rectification of the upper limit of the record, is also possible (Ruddiman, 2003) and would cause a shift of the termination of HICE to earlier phases (Figure 6.3, b, lower figure).

5.10 Conclusions

Results from three Hirnantian sections from the Welsh Basin suggest four positive $\delta^{13}C_{org}$ excursions of 3 ‰ in the *extraordinarius* Biozone and one excursion of up 1.6 ‰ in the *persculptus* graptolite Biozone.

The *extraordinarius* excursion begins at the onset of sealevel fall and terminates just before the sequence boundary. The second excursion, just above the base of the *persculptus* Biozone, occurs during a period of oxygenation and sealevel fall whilst the third definite excursion occurs during marine transgression.

Positive excursions from a deep water basin setting, are accompanied by an increase in organic carbon burial whereas all the excursions from the shelf sections are associated with

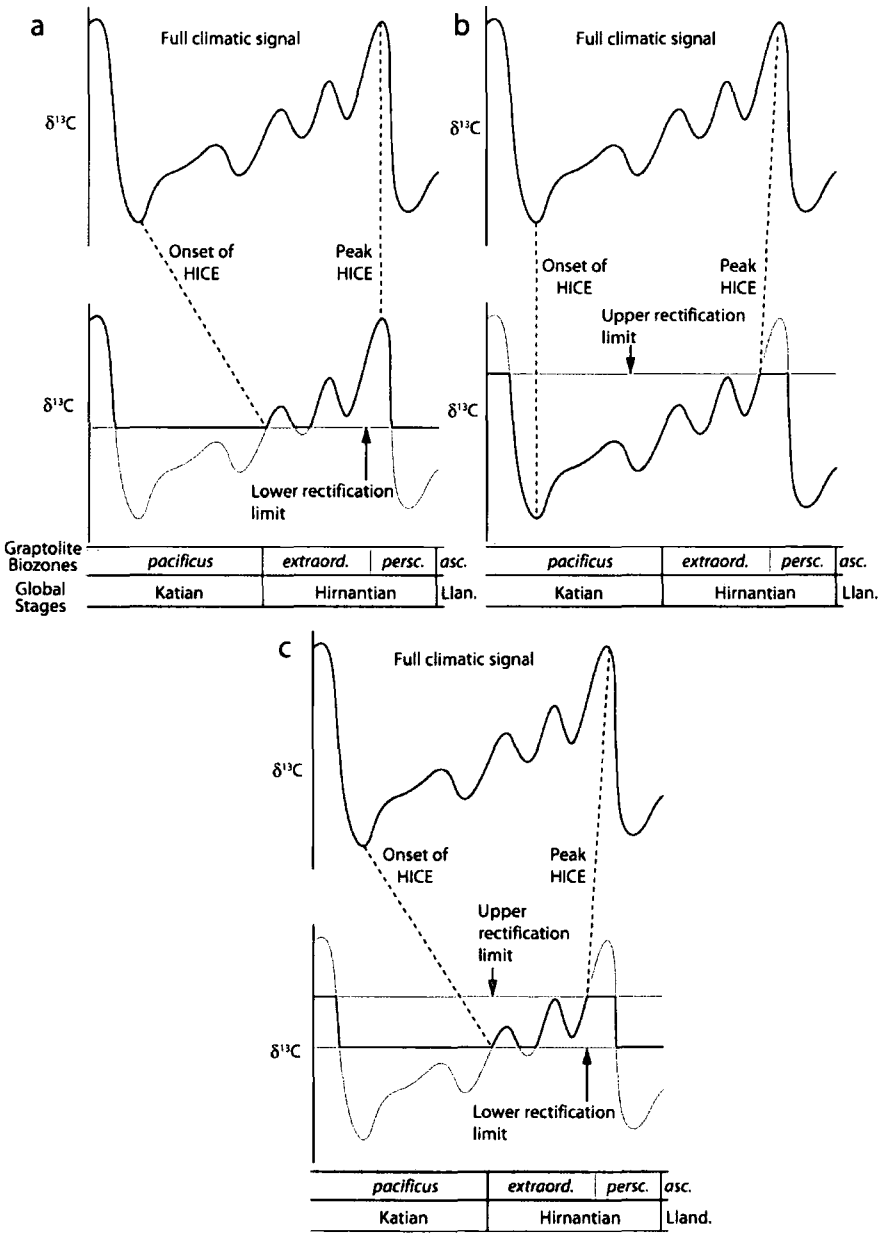

Figure 5.16: Differences in relative timing of the onset of HICE and peak HICE values can be caused by rectification of the isotopic signal. In a full climatic signal with no rectification (top figure in a-c), the onset of HICE occurs in the late Katian *pacificus* graptolite Biozone and peak HICE values occur in the *persculptus* graptolite Biozone. When the $\delta^{13}C$ signal is truncated at low values, the onset of HICE occurs in the *extraordinarius* graptolite Biozone e.g. the in Welsh Basin; a, lower figure). If the rectification limit is at high $\delta^{1(3}C$ values, the peak values of HICE occur in the *extraordinarius* Biozone (e.g. for Arctic Canada; b, lower figure). If rectification of upper and lower $\delta^{13}C$ occurs then the onset of the HICE and peak HICE values will occur in the *extraordinarius* Biozone (e.g. the Welsh Basin and Nevada; (Saltzman & Young, 2005, ; c, lower figure).

decreased organic carbon burial. For excursions that occur during lowering or low sealevel (excursions 1, 2 and 4) this is interpreted as being a shift in the locus of basin organic carbon burial from the highly productive shelf to the basin. Carbon burial and transport into the basin is aided by a 'sedimentary conveyor' from destabilised shelf sediment reworked and delivered directly into the basin during sealevel fall.

Whereas the Welsh Basin records increased burial of organic carbon during HICE as proposed by Brenchley *et al.* (1994), the inability to replicate this observation in other deep basin settings (e.g. Dob's Linn), demonstrates this to be a regional occurrence and does not confirm the productivity-burial hypothesis for the HICE. Further evidence for the regional nature of the Welsh Basin HICE record is observed in a shelf to basin gradient in background $\delta^{13}C_{org}$ values during interglacial periods. A lack of black shales and phosphates in both the basin and shelf, and an absence of supporting geochemical data, makes higher shelf area productivity a plausible explanation of this.

Inconsistent timing of the onset and maximum of the HICE throughout the world implies strong regional carbon cycling effects in regional semi-restricted basins (e.g. the Iapetus Ocean and epeiric seas such as the Baltoscandian regions), that do not appear to be constrained by basin setting or latitudinal setting. These local processes affect the rectification limit of the $\delta^{13}C$ record where a low lower rectification limit produces an early record of the onset of the HICE in the *pacificus* Biozone (e.g. Nevada, Arctic Canada, China) and a high lower response rectification limit produces a late record of the onset of the HICE (e.g. the Welsh Basin, Baltoscandia and Nevada) in the *extraordinarius* Biozone. Similarly, the rectification limit of the upper $\delta^{13}C$ response determines the timing of peak HICE. A high upper limit results in a late peak HICE in the *persculptus* Biozone (e.g. Baltoscandia, Anticosti Island) whereas a low upper response limit gives an early peak HICE in the *extraordinarius* Biozone (e.g. the Welsh Basin, Arctic Canada, Nevada). The Welsh Basin HICE record correlates well, in terms of topology and excursion magnitude, with only a limited number of HICE curves from sections elsewhere throughout the globe

It is proposed that the majority of HICE records have been subject to strong regional carbon input/cycling influences and that no individual HICE record, including that of the GSSP, can be regarded as a benchmark for chemostratigraphic correlation purposes. The likelihood of successful correlation of any carbon isotope curve can only be established where the regional carbon cycle processes are well constrained. In order for these conditions to be satisfied, the environmental position of the sample section needs to be accurately established (i.e. its position in the basin to shelf setting, and a comparative section in the same basin should be sampled to provide a means of determining shelf to basin isotopic effects). Chemostratigraphic correlation by comparing peaks of excursions within the same biozone

without regard for the effects of local processes and rectification of the signal, amounts to no more than elaborate, and expensive, wiggle matching.

Chapter 6

Conclusions

6.1 Introduction

This study has aimed to reconstruct the mechanisms of organic carbon (OC) burial and biotic change during the late Katian and Hirnantian (Upper Ordovician) in the context of changing regional and global climate and global climate belt configurations. Five current problems in our understanding of late Ordovician climate change, and for using the Welsh Basin to document climate change at this time are:

1. Global climate change processes in the Late Ordovician have a sparse record from mid-latitudes.

2. It is uncertain if the Boda Event is a warm event (Boucot *et al.*, 2003; Fortey & Cocks, 2005) or a cool event (Cherns & Wheeley, 2007).

3. Numerous mechanisms are proposed for HICE. Some lack physical evidence (sequestration of large amounts of carbon during HICE, Brenchley *et al.*, 1994) and others which have not been tested against each other using empirical data (e.g. Kump *et al.*, 1999). HICE is also regarded by some as a product of regional processes (Panchuk *et al.*, 2005).

4. There is currently no strong biostratigraphic correlation between basin and shelf in the upper Katian and Hirnantian of the Welsh Basin. This is essential if the Welsh Basin is to be used to test hypotheses for mechanisms of the Boda Event and the HGM.

5. Chitinozoan biostratigraphy is rapidly advancing without significant regard for the influences of their palaeoecology on biozonation schemes.

Five areas of investigation have been specifically addressed towards resolving these problems: (1) the mechanisms that drove organic carbon burial from the perspective of global climate belt reorganization in the Rawtheyan (late Katian); (2) trends of OC burial before,

during and after the Hirnantian glacial maximum; (3) the coupling of shelf and basin carbon burial and carbon-isotope mass balance during the Hirnantian glacial maximum and the Hirnantian Isotopic Carbon Excursion (HICE); (4) the development of a chitinozoan biostratigraphic scheme for the late Katian and Hirnantian in the Welsh Basin; and (5) the responses of chitinozoans to changing basin hydrography during changing climate.

The main conclusions from this study in the Welsh Basin are:

1. Changing aridity and wind stress record predicted changes in climate belt position at mid-palaeolatitudes during the Rawtheyan (late Katian) on the palaeocontinent of Avalonia.

2. Changing climate belt configuration induced coastal upwelling, increased productivity and carbon burial in the late Katian (Rawtheyan). This is interpreted as representing an expression of the Boda Event in Avalonia.

3. The Boda Event is associated with rearrangement of chitinozoan biotopes in the Rawtheyan (late Katian) in the Welsh Basin.

4. In the Welsh Basin, during the Hirnantian glacial maximum, the locus of organic carbon burial shifted from the shelf to the basin and is associated with three positive $\delta^{13}C_{org}$ excursions in both the basin and the shelf that represent local expressions of the HICE.

5. The onset of the HICE in the Welsh Basin occurs in the *extraordinarius* graptolite Biozone (regional *reticulatus* chitinozoan Biozone) and ends in the *persculptus* graptolite Biozone (*taugourdeaui* chitinozoan Biozone).

6. The HICE is potentially diachronous throughout the world.

7. Diachroneity of HICE could possibly be the product of rectification of $\delta^{13}C$ signals from regional carbon cycling processes.

8. Chitinozoa occupied distinct depth-stratified biotopes within open sea and shelf environments. Those chitinozoan taxa that originated in, and occupied, isolated biotopes were susceptible to regional effects of global climate change and may have relied on such changes for their dispersal. This may produce diachroneity of chitinozoan biozones if an index taxon originated in and occupied such a biotope.

6.2 Biostratigraphic framework

The study has focussed on the chronostratigraphic interval between the Pusgillian (mid- to late Katian) to the base of the Silurian (approximately 450.5 Ma to 443 Ma). Chapter 2 provided a chitinozoan biostratigraphic framework for the Welsh Basin region at this time and identified six chitinozoan biostratigraphic zones: the mid-Katian *Tanuchitina bergstroemi* Biozone, the mid-late-Katian *Spinachitina fossensis* Biozone, the late-Katian *Bursachitina umbilicata* and *Hercochitina gamachiana* biozones, the newly defined regional early Hirnantian *Belonechitina reticulatus* n. sp. Biozone and the mid-late Hirnantian *Spinachitina taugourdeaui* Biozone. The Cautleyan-Rawtheyan (late Katian) *rugata* Biozone of the Avalonian chitinozoan biostratigraphic scheme (Vandenbroucke, 2008) was not recognized in the Welsh Basin. The base of the Nantmel Mudstones Formation lies within the *T. bergstroemi* Biozone demonstrating that the Caradoc-Ashgill boundary (early Katian-late Katian) lies stratigraphically lower down in the Dinas Island Formation (cf. Vandenbroucke *et al.*, 2008) and that the transition from anoxic to oxic conditions within the Welsh Basin, marking decreased organic carbon preservation potential, occurred in the late Katian (Ashgill) and not at the Caradoc-Ashgill boundary as previously interpreted (Fortey *et al.*, 2000; Armstrong, 2007).

The reappearance of basin anoxia, and increased OC preservation potential, is recorded at the base of the Rawtheyan (late Katian) *B. umbilicata* Biozone and extends into the late Rawtheyan-early Hirnantian (late Katian-early Hirnantian) *H. gamachiana* Biozone. The *Hercochitina gamachiana* Biozone is recognized for the first time in Avalonia. Its base lies within laminated hemipelagite unit 1 (LH^1) in the Cardigan region and in the upper most Cribarth Formation in the Llandovery area.

The Hirnantian glacial maximum is represented in the Welsh Basin by the disappearance of infaunal bioturbation during the *H. gamachiana* and *B. reticulatus* biozones, coincident with the deposition of silty-sand units which frequently exhibit massive slumping (the Yr Allt Formation). At the same time in the shelf environment of the Llandovery area, infaunal burrowing also vanished and sedimentation comprised the silty-mud Ciliau Formation and the sand-dominated Cwmcringlyn Formation.

Deposits from the glacial maximum are overlain by post-glacial transgressive muds of *S. taugourdeaui* Biozone age of the Cwmere Formation in the basin and the Garth House Formation on the shelf. In the Llandovery area a distinct transgressive conglomerate-sandstone body, the Cwm Clyd Sandstone Formation, and associated time equivalent sandstone bodies, were deposited unconformably upon an erosional surface which is interpreted to have formed during low eustatic sea level coupled with local tectonic uplift.

This biostratigraphic scheme was applied to correlate between basin and shelf sections between the Cardigan and Llandovery areas of south Wales and to identify strata corresponding to intervals of specific climate change events i.e. the Boda Event, the Hirnantian glacial maximum and the Hirnantian post-glacial transgression.

6.3 Geosphere dynamics during end-Ordovician climate change

6.3.0.1 Recognition of the Boda Event in the Welsh Basin

The global Boda Event occurred during the Cautleyan and Rawtheyan (late-Katian Fortey & Cocks, 2005) and was originally recognized by the movement of low-palaeoatitude benthic faunas to high-palaeolatitudes and by an increase in endemic faunas at low-palaeolatitudes. The base of the *bergstroemi* Biozone to the upper *gamachiana* chitinozoan Biozone corresponds to the Cautleyan-Rawtheyan (late-Katian) in the Welsh Basin, and faunal or sedimentological patterns that occurred there during this time are considered to be of Boda Event age. In the Welsh Basin, sediments of *bergstroemi-fossensis* Biozone age (Cautleyan to early-Rawtheyan) comprise monotonous oxic burrow-mottled mudstones. However, two sedimentological and biological events are recognized in the mid- to late Rawtheyan (late-Katian): (1) periodic anoxia and deposition of organic-carbon rich (OC-rich) black shales; and (2) the rearrangement of the chitinozoan fauna comprising the proliferation of a hercochitinid and spinachitinid chitinozoan assemblage in open ocean biotopes (Figure 6.1). The appearance of environmentally-restricted, short-lived taxa such as *Bursachitina umbilicata* also occurred at the onset of organic-rich laminated hemipelagite deposition. These two events are interpreted to represent a mid-palaeolatitude expression of the Boda Event and are explicable in the context of climate belt rearrangement at mid-palaeolatiudes (section 6.5).

6.3.1 Carbon burial and geochemical responses during the Boda Event

Chapter 3 demonstrates that carbon burial increased in the Welsh Basin during the Boda Event. The deposition of OC-rich laminated hemipelagites, with post-anchizone metamorphism grade TOC values of up to 0.51 %, occurred during increased coastal upwelling and productivity resulting in basin anoxia. Increased upwelling is indicated from negative $\delta^{13}C_{org}$ excursions of up to 1 */permil* during OC-rich deposition from the remobilization of light carbon from deep ocean waters. Increased productivity, coincident with OC-rich laminated hemipelagite deposition, is demonstrated by elevated TOC values and elevated values of the inorganic productivity proxy Ba/Th. The deposition of OC-rich sediments did not extend onto the shelf at this time. The climate-sensitive weathering proxy K/Al increased during the

period of OC-rich deposition, indicative of a relative increase in minerals weathered under an arid climate regime, whilst Ti/Al, which is indicative of increased terrestrial run-off, did not change. The persistence of a burrowing infauna in the lower parts of the OC-rich laminated hemipelagite units demonstrates that basin anoxia lagged the onset of OC-rich deposition. At the cessation of OC-rich deposition, however, trace fossils indicate that oxia returned rapidly. The inorganic redox proxy Ni/Co is considered to have been altered from element remobilization within the C-rich unit. Other mobile elements including the, rare earth elements, do not change throughout OC-rich units indicating the integrity of other trace element proxies used in this study (Ba/Th, K/Al, Ti/Al).

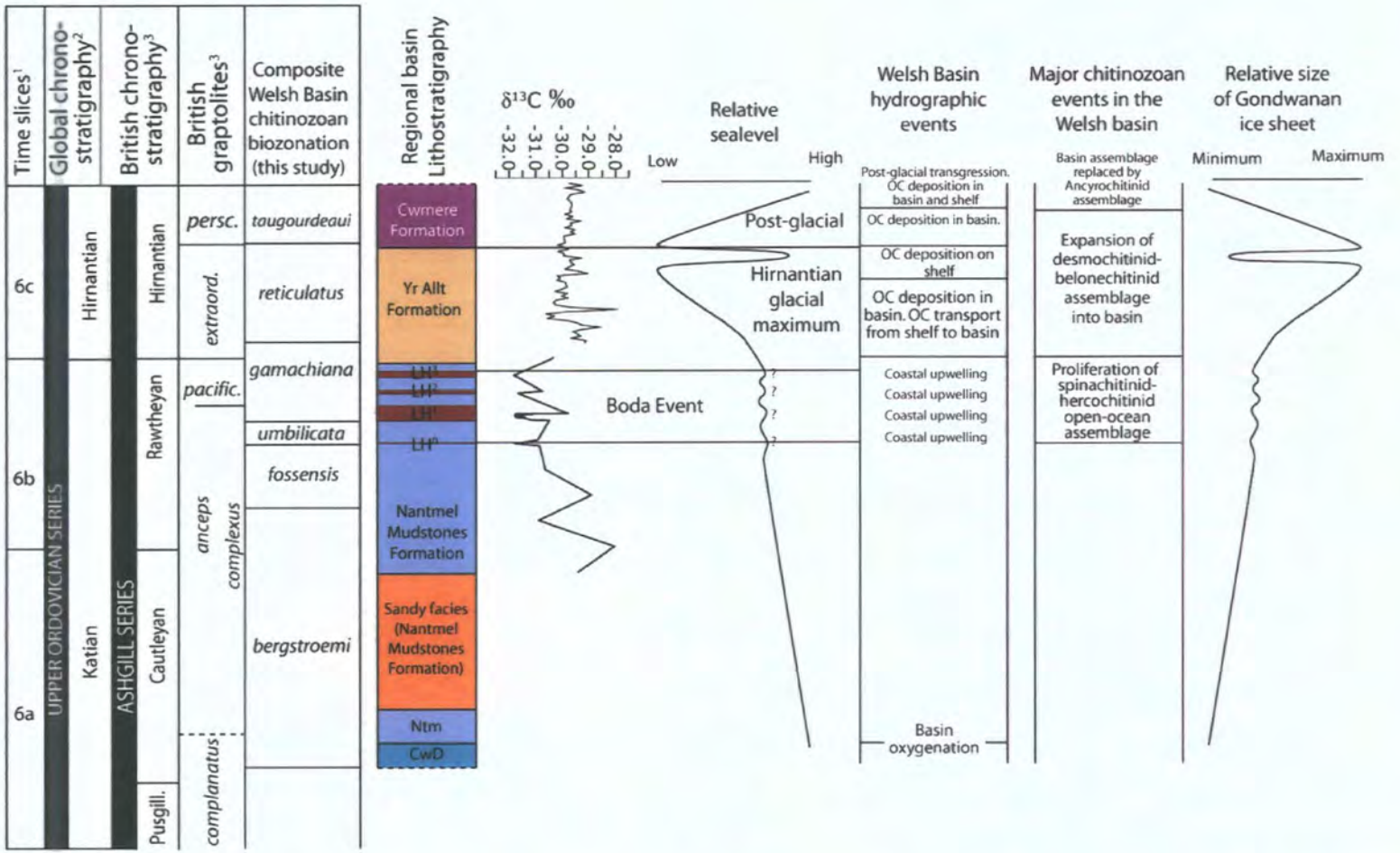

Figure 6.1: Diagram summarizing isotopic, sequence stratigraphic, hydrospheric, carbon burial and chitinozoan responses identified in this study to changing global climate state and interpolated size of the Gondwanan ice sheet. [1]Webby *et al.* (2004); [2]Bergström *et al.* (2006a); [3]Fortey *et al.* (2000). *pacific.*=*pacificus*; *extraord.*=*extraordinarius*; *persc.*=*persculptus*; Pusgill=Pusgillian; CwD=Cwm Degwel Mudstone Member; Ntm=Nantmel Mudstones Formation.

6.3.2 Hirnantian glacial maximum

6.3.2.1 HICE at mid-palaeolatitudes

Chapter 5 presents $\delta^{13}C_{org}$ results from three Hirnantian sections from the Welsh Basin. Two positive $\delta^{13}C_{org}$ excursions ($\delta^{13}C_{org}$ excursions 1 and 2) of up to 3 */permil* occur in the *extraordinarius* graptolite Biozone (*reticulatus* chitinozoan Biozone) and two excursions of up 1.6 */permil* in the *persculptus* graptolite Biozone (*taugourdeaui* chitinozoan Biozone).

The *extraordinarius* excursions began at the onset of sealevel fall and terminated just before the sequence boundary. The third small excursion of 0.5 */permil* occurred during a period of low sealevel ($\delta^{13}C_{org}$ excursion 3, Figure 6.1).

Inconsistent timing of the onset and peak $\delta^{13}C$ values of the HICE throughout the world implies that strong regional carbon cycling affected regional records. The timing of the onset and peak $\delta^{13}C$ values of the HICE does not appear to be constrained by basin setting or latitudinal setting. The Welsh Basin HICE record correlates well, in terms of topology and excursion magnitude, with only a limited number of HICE curves from sections elsewhere (those from China).

I propose that the majority of HICE records have been subject to strong regional carbon cycling influences and that no individual HICE record, even from the Hirnantian GSSP at Wangjiawang, China, can be regarded as a benchmark for chemostratigraphic correlation purposes. The likelihood of successful correlation of any carbon isotope curve is aided where the regional carbon cycle processes are well constrained. In order for these conditions to be satisfied, the environmental position of the sample section needs to be accurately established (i.e. its position in the basin to shelf setting), and a comparative section in the same basin should be sampled to provide a means of determining shelf to basin isotopic effects.

6.3.2.2 Carbon burial

Positive $\delta^{13}C_{org}$ excursions from a deep water basin setting during the Hirnantian in the Welsh Basin, are accompanied by an increase in organic carbon burial whereas all excursions from the shelf sections are associated with decreased organic carbon burial. For positive $\delta^{13}C_{org}$ excursions that occurred during lowering or low sealevel ($\delta^{13}C_{org}$ excursions 1, 2 and 4) this pattern is interpreted as representing a shift in the locus of organic carbon burial from the highly productive shelf to the basin. Carbon burial and transport into the basin was aided by a 'sedimentary conveyor' from destabilised shelf sediment reworked and delivered directly into the basin during sealevel fall and/or regional tectonic activity (Figure 6.1).

Whereas the Welsh Basin records possible increased burial of organic carbon during HICE, as proposed by Brenchley *et al.* (1994), the inability to replicate this observation in other

deep basin settings (e.g. Dob's Linn), demonstrates this to be a regional condition and does not confirm the productivity–OC-burial hypothesis for the HICE. Further evidence for the regional nature of the Welsh Basin HICE record is observed in a shelf to basin gradient in background $\delta^{13}C_{org}$ values during interglacial periods. A lack of black shales and phosphates in both the basin and shelf, and an absence of supporting geochemical data for upwelling, makes higher shelf area productivity a plausible explanation of this.

6.3.2.3 Post-glacial carbon burial

A third clear excursion of 1.6 */permil*, that can be correlated between basin and shelf sections in the Welsh Basin, is present just above the base of the *persculptus* graptolite Biozone (*taugourdeaui* chitinozoan Biozone) and occurred during post-glacial marine transgression. It again demonstrates increased carbon burial in the basin compared to the shelf.

6.4 Biosphere dynamics during end-Ordovician climate change

Having established the timing of the Boda Event and the HGM in the Welsh Basin from chitinozoan biostratigraphy in Chapter 2, Chapter 3 defined the hydrospheric responses in the Welsh Basin during the Boda Event in the Rawtheyan (late Katian). The fourth chapter has investigated in detail the distribution and reorganization of chitinozoan assemblages in the Welsh Basin during changing climate and hydrography to test the hypothesis of complex ecological structure amongst the Chitinozoa and their sensitivity to such changes.

Correspondence analysis and unconstrained seriation of facies distribution of Upper Ordovician Avalonian chitinozoa, during the Boda Event, Hirnantian glacial maximum and Hirnantian post-glacial transgression, have allowed three open-ocean depth-stratified biotopes and a shelf chitinozoan biotope to be recognized. These are: (1) an open-ocean shallow-water epipelagic biotope which includes *Cyathochitina campanulaeformis*; (2) an open-ocean middle-depth mesopelagic biotope comprising *Hercochitina* and *Spinachitina*; (3) an open-ocean deep-water meso-bathypelagic biotope characterized by *Bursachitina umbilicata*; and 4) a shelf biotope containing predominantly *Desmochitina*.

Those taxa occupying only the shelf biotope experienced segregation from the open-ocean and their dispersal was influenced by sea level change, for example, during the Hirnantian post-glacial transgression. Dispersal of taxa originating in, and occupying, deep water biotopes (e.g. *Bursachitina umbilicata*), can be strongly affected by changes in basin hydrography such as the initiation of upwelling and expansion of a deep oxygen minimum zone. Chitinozoan taxa that originated and occupied an open-ocean shallow water epipelagic

biotope were less affected or were insensitive to such changes (e.g. *Cyathochitina campanulaeformis, Hercochitina crickmayi* and *Belonechitina reticulatus* n. sp.). This distribution of biotope assemblages indicates, as previously suggested (Paris, 1981, for instance), that the chitinozoa were almost exclusively planktonic and is further reinforced by their rapid response to changes in basin hydrography.

The chitinozoan biotope model demonstrates that the appearance and replacement of taxa that define regional biozones, and even pan-palaeocontinental biozones, can be the product of regional and global climate changes and changes in ocean hydrography. On the geological timescale, and in global extent, these effects have previsouly been considered instantaneous (Achab & Paris, 2007), but at the resolution of inter-basin, and even palaeocontinent-specific biostratigraphical schemes, such processes could be the cause of diachroneity of biozones. Good index taxa for chitinozoan biozonation need to have evolved in and to have occupied an epipelagic open ocean biotope to fulfill the criterion of wide dispersal. This does not appear to have been the case with all Avalonian chitinozoan biozonation index taxa e.g. *Bursachitina umbilicata.*

6.5 Implications for climate belt rearrangement: confirmation of the Upper Ordovician shifting climate belt model?

During the Rawtheyan (late Katian), the Welsh Basin was located at approximately 30^{o} south of the equator (Cocks & Torsvik, 2004, 2002). The sedimentology and geochemistry of sediments deposited in the Welsh Basin at this time satisfies the predictions for climate belt movement at these palaeolatitudes. For a southerly shift in climate belts, mid-palaeolatitudes would have experienced a change in wind regime from one of low wind stress (beneath the Sub-tropical High Pressure Belt, STHP) to one of high wind stress beneath the southeasterly trade wind arid zone. Predictions for this scenario are: (1) increased coastal upwelling from increased wind stress inducing deposition of phosphates and OC-rich laminated hemipelagites; and (2) increased aridity from positioning below the sub-tropical arid zone.

The body of faunal, sedimentological and geochemical evidence from the mid-palaeolatitude Welsh Basin indicates that the onset of coastal upwelling along the northern margin of Avalonia (in the Welsh Basin) occurred in the late Katian (Rawtheyan) stage of the Boda Event. This is later than the onset of low-palaeolatitude responses to the Boda Event (e.g. negative $\delta^{18}O$ excursions e.g. Nevada, Saltzman & Young, 2005) which occur from the Çautleyan (lower late Katian) and contrasts with the climate belt configuration predicted by Armstrong *et al.* (in press) for this time. From an equatorial position of the Inter-Tropical Convergence

Zone (ITCZ) at this time, Armstrong *et al.* (in revision) imply mid-palaeolatitudes were positioned directly beneath the STHP, a zone of low wind stress in the Rawtheyan (late Katian). This model predicts mid-palaeolatitudes localities (e.g. Avalonia and the Welsh Basin), to have been positioned beneath southeast trade winds earlier, during the Cautleyan.

Chapter 5, however, demonstrated how the difference in timing of the onset of the HICE may be attributed to rectification of regional $\delta^{13}C$ signals by local carbon cycling processes. The demonstration herein that the expression of the Boda Event can occur at different latitudes at different times, suggests that climate belt position may, in part, be responsible for rectification of both faunal and geochemical expressions of the Boda Event too. Signal rectification is the truncation on one side or other of the full range of response of a system due to local climate system or from limitations of proxy recorders (Ruddiman, 2003; Weedon, 2003). In the Boda Event scenario a 'full range of response' would be represented by synchronous records of warming at all latitudes. Armstrong *et al.* (in revision) recognized this was not the case with temperature estimates (based on negative $\delta^{18}O$ excursions) from different localities at different latitudes relative to the ITCZ, and interpreted this as representing climate belts and water masses shifting through time in response to cooling and ice volume change. Inference from these observations suggests that ice volume and climate belts could cause rectification of global records of insolation and temperature, a hypothesis that could be tested during further work in Palaeozoic climate research.

6.6 Refining the dynamic climate belt model in the Upper Ordovician: new hypotheses

6.6.0.4 Contraction of atmospheric circulation cells

The Armstrong *et al.* (in revision) model assumes constant size of each atmospheric circulation cell during the progressive northward movement of the ITCZ. Armstrong *et al.* (in revision) recognized distinct $\delta^{18}O_{calcite}$ populations in the middle Katian (Caradoc), upper Katian (Cautleyan-Rawtheyan) and Hirnantian, that match changes in $\delta^{18}O_{calcite}$ values in marine waters beneath the present migrating ITCZ. They proposed that the ITCZ progressively moved northward in response to global cooling, from the beginning of the Late Ordovician glaciation in the mid-Katian (at GICE) to the Hirnantian (Figure 6.2). In particular, during the late Katian, an equatorial position of the ITCZ and convergent trade winds was conducive to transport of warm equatorial waters to high-latitudes, through entrainment in sub-tropical ocean gyres, resulting in a low meridional temperature gradient. This mechanism potentially

explains the Boda Event (Fortey & Cocks, 2005) as being the result of poleward redirection of warm water following climate belt rearrangement

However, global warming-cooling causes changes in the sizes of the climate zones and the Hadley, Ferrell and Polar atmospheric circulation cells (Lu *et al.*, 2007). Glacial episodes are characterized by an increase in the hemispherical latitudinal temperature gradient and subsequently result in contraction of the latitudinal extent of the Hadley and Ferrell cells (i.e. the Polar cell expands towards low-latitudes Rind, 1998; Lu *et al.*, 2007).

Figure 6.2: Armstrong *et al.* (in revision) Inter-Tropical Convergence Zone (ITCZ) model. From the inception of glaciation, $\delta^{18}O$ curves for the upper Katian and Hirnantian exhibit coincident positive excursions at discrete stages up to the glacial maximum in the Hirnantian. Each excursion event is interpreted as representing the isotopic response of ocean water, a combination of regional and global factors, to the position of the ITCZ during its northward migration. Bi-x= Boda isotopic event. Place name abbreviations: A. C.=Arctic Canada; Est.=Estonia; Nev.=Nevada; W. B.=Welsh Basin. Current abbreviations: EEC=Eastern Equatorial Current; NEC=Northern Equatorial Curent; PCPC=Panthalassic Counter-Polar Current; SEC=Southern Equatorial Current; SGC=South Gondwana Current.

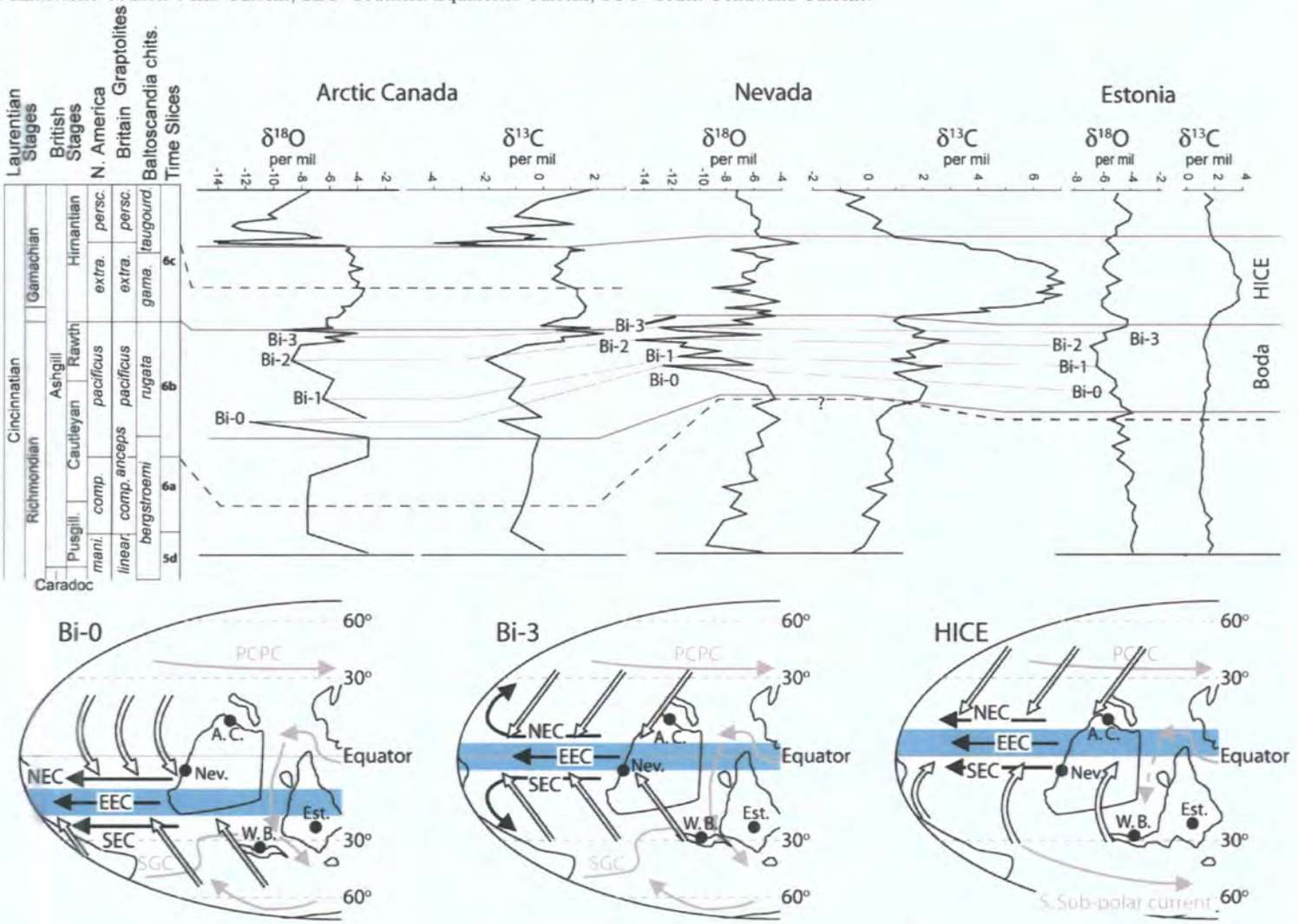

6.6.0.5 Orbital forcing and rectification

An additional implication in the Armstrong *et al.* (in revision) climate belt model is that orbital forcing on ice-sheet growth, in turn, paces the changing position of the ITCZ. Because the ITCZ and STHP move concomitantly (Nobre & Shukla, 1996), and the development of OC-rich laminated hemipelagites at mid-palaeolatitudes in the Welsh Basin have been demonstrated to be a product of shifting climate belts (Chapter 3), I interpret the repetitive nature of OC-rich laminated hemipelagite deposition in the Welsh Basin as also reflecting orbitally-moderated changes in the size of the Gondwanan ice.

Partial rectification of the upper limit of orbitally-moderated global insolation, potentially from ice volume, predicts greater extremes in insolation at the obliquity and precession periods when approaching eccentricity-modulated insolation minima (Figure 6.3). If the developing ice-sheet directly controls the position of the climate belts, as Armstrong *et al.* (in revision) and Chapter 3 propose, latitudinal shifts in climate belt position are predicted to become greater as the orbital system moves towards an eccentricity minimum and precession-obliquity insolation extremes become greater.

6.6.0.6 A refined model of climate belt dynamics during late Ordovician climate change

I propose a refined global model for late Ordovician climate belt dynamics that incorporates a rectified insolation model, coupled with contracting atmospheric circulation cells during continual global cooling (and increased ice-sheet growth), and progressive northward migration of the climate belts. The model accommodates both early (Cautleyan) expression of the Boda Event at low-palaeolatitudes and late (Rawtheyan) expression of the Boda Event at mid-palaeolatitudes (Figure 6.4). However, a caveat of the model, which remains to be tested, is that the ITCZ and STHP both migrate over approximately 30^o of latitude, greater than that currently recognized for the present day or in the Cenozoic.

Cautleyan. Pre-Boda conditions expressed at low- and mid-palaeolatitudes. The ITCZ lies south of the equator and the STHP lies over mid-latitudes (Figure 6.4 a). Cooling forces the climate belts north. Low-palaeolatitudes (e.g. Nevada), that lie beneath the ITCZ record a negative $\delta^{18}O$ excursion; Bi-1 of Armstrong *et al.* (in revision). The Welsh Basin still lay beneath the STHP (Figure 6.4 b). Obliquity/precession-paced ice ablation forced climate belts back southwards. The ITCZ lay south of the equator and the Nevada section recorded more positive $\delta^{18}O$ values as during pre-Boda times. The Welsh Basin still lay beneath the STHP and experienced no wind-driven coastal upwelling (Figure 6.4 c). Further orbitally-paced cooling drives the climate belts back northwards and low-latitude sections record the

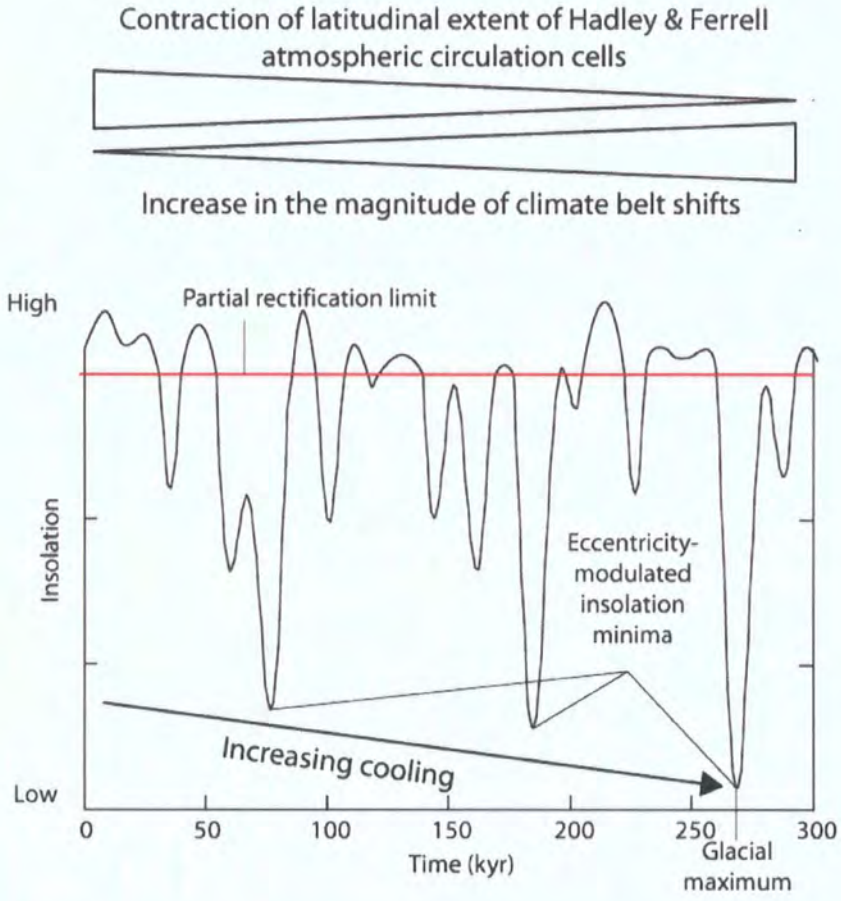

Figure 6.3: A partially-rectified insolation model composed of a composite sinusoid containing eccentricity (100 kyr), obliquity (40 kyr) and precession (21 kyr) periods. Glacial maximum is achieved when eccentricity was high, obliquity low and aphelion occurred during austral summer (Armstrong, 2007). In the model this occurs at approximately 270 kyr. During progressive insolation-driven global cooling the latitudinal extent in the southern hemisphere of the Hadley and Ferrell atmospheric circulation cells decreases as the Polar cell expands northwards synchronously with the developing Gondwanan ice-sheet. The orbitally-moderated north-south shift of the climate belts increases with greater extremes in insolation at the obliquity and precession periods when approaching the glacial maximum

same conditions as in 'b' (Figure 6.4 d). Early Rawtheyan. Further cooling and development of the Gondwanan ice-sheet aided by the 'snow gun' mechanism that operated during 'd' reduced the latitudinal extent of the atmospheric circulation cells (small, double-ended arrow on Figure 6.4 e, k). The ITCZ and STHP were subsequently positioned closer together. Climate belts moved south during an orbitally-forced ablation event (Figure 6.4 e). Climate belts continued to move south because of the larger insolation extreme caused by rectification of the insolation signal and now Avalonia lay under the southeasterly trade winds. Upwelling, productivity and deposition of OC-rich laminated hemipelagite occurred in the Welsh Basin. The ITCZ lay further south from the equator (Figure 6.4 f). Climate belts moved back north during a period of higher eccentricity and ice-advance (Figure 6.4 g). This process continued, back and forth, paced by obliquity and precession. The deposition of organic-rich laminated hemipelagites in the Welsh Basin records periods when the climate belts were in a far southerly position in the late Rawtheyan (Figure 6.4 h, j, l). Isotopic expression of the ITCZ ceased at low- and mid-palaeolatitudes once the Gondwanan ice-sheet had achieved a critical mass and no longer responded to precession-forced ice ablation i.e. at the Hirnantian glacial maximum (Figure 6.4 m). Under these conditions, the climate belts maintained a stable, cold northerly position.

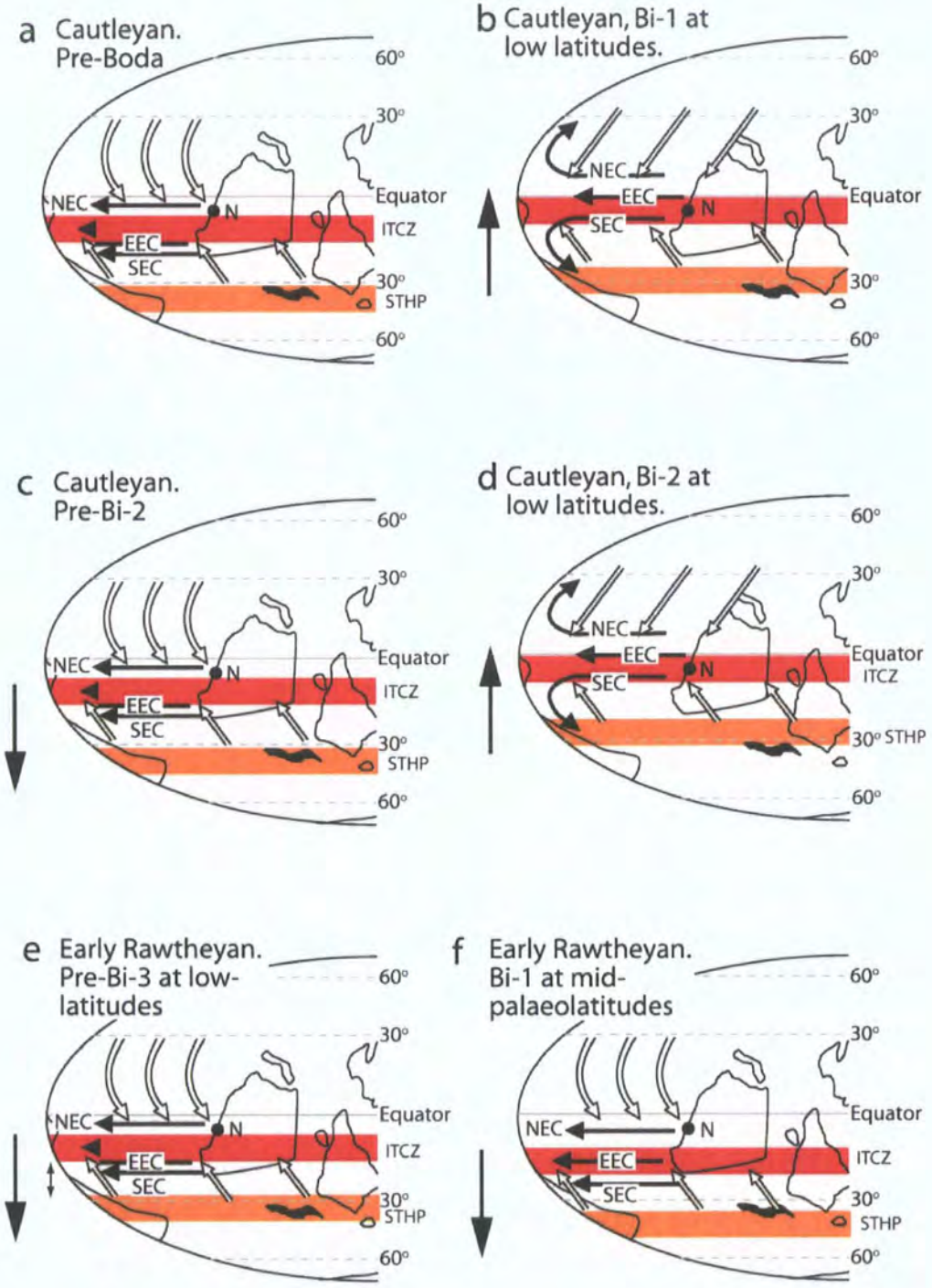

Figure 6.4: Changing climate belt configuration model accommodating contraction of low- and mid-latitude atmospheric circulation cells (Hadley and Ferrell Cells) paced by partially-rectified insolation signal. See text for description. ITCZ = Inter-Tropical Convergence Zone; STHP = Sub-Tropical high pressure belt; Bi-x = Boda isotopic event. Current abbreviations: EEC=Eastern Equatorial Current; NEC=Northern Equatorial Curent; SEC=Southern Equatorial Current.

g Mid-Rawtheyan, Bi-3 at low-latitudes, pre-Bi-2 at mid-latitudes.

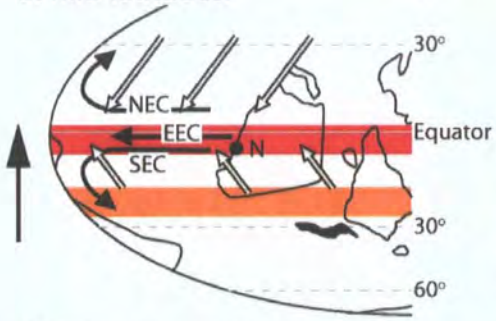

h Mid-Rawtheyan, pre-Bi-4 at low-latitudes, Bi-2 at mid-latitudes.

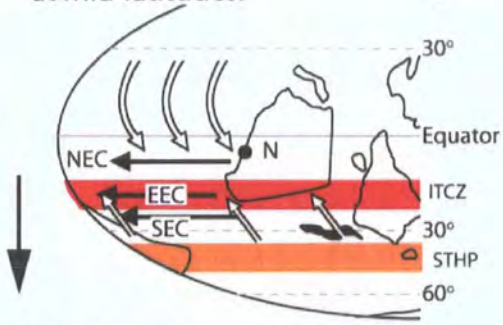

i Mid-Rawtheyan, Bi-4 at low-latitudes, pre-Bi-3 at mid-latitudes.

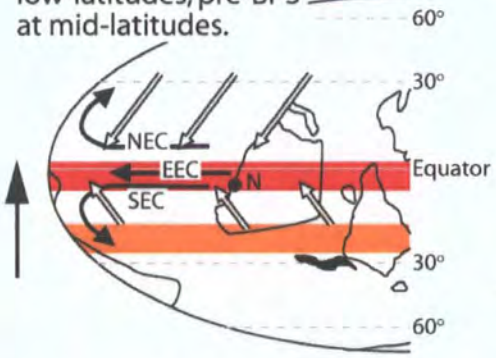

j Late Rawtheyan, Bi-3 at mid-latitudes.

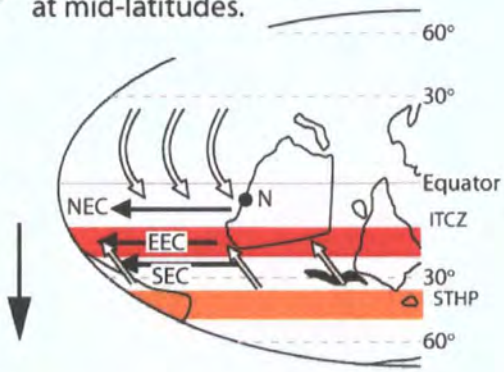

k Late Rawtheyan, pre-Bi-4 at mid-latitudes.

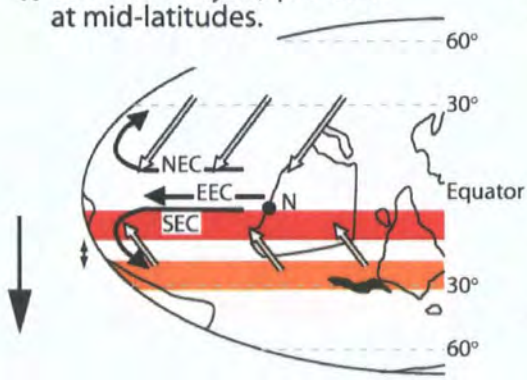

l Late Rawtheyan, Bi-4 at mid-latitudes.

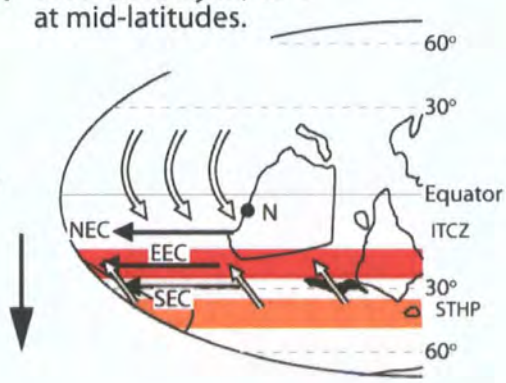

m Hirnantian. HICE and stabilisation of climate belt system in northerly mode from maximum ice-sheet volume

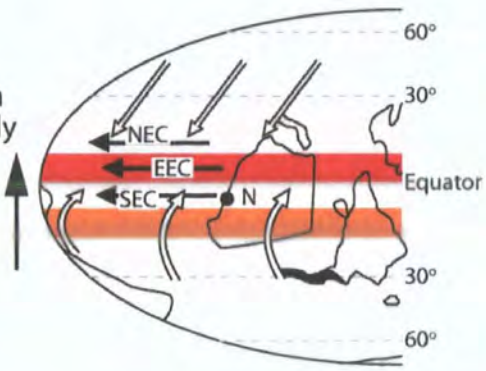

References

ABER-OUCHI A. & BLATTER H. (1993) On the initiation of ice sheets. *Glaciology*, **18**, 203–207.

ACHAB A. (1977a) Les chitinozoaires de la zone à *Climacograptus prominens elongatus* de la Formation de Vauréal (Ordovicien supérieur), île d'Anticosti, Québec. *Canadian Journal of Earth Sciences*, **14**, 2193–2212.

ACHAB A. (1977b) Les chitinozoaires de la zone à *Dicellograptus complanatus* Formation de Vauréal (Ordovicien supérieur), île d'Anticosti, Québec. *Canadian Journal of Earth Sciences*, **14**, 413–425.

ACHAB A. (1978) Les chitinozoaires de l'Ordovicien supérieur - Formations de Vauréal et d'Ellis Bay - de l' île d'Anticosti, Québec. *Palinologia*, **1**, 1–19.

ACHAB A. (1987) Chitinozoaires du Caradoc supérieur-Ashgill inférieur du Québec, Canada. *Canadian Journal of Earth Sciences*, **24**, 1212–1234.

ACHAB A. (1989) Ordovician chitinozoan zonation of Quebec and western Newfoundland. *Journal of Paleontology*, **63**, 15–24.

ACHAB A., ASSELIN E., LAVOIE D. & MUSSARD J.M. (1997) Chitinozoan assemblages from the third-order transgressive-regressive cycles of the Upper Gaspé Limestones (Lower Devonian) of eastern Canada. *Review of Palaeobotany and Palynology*, **97**, 155–175.

ACHAB A. & PARIS F. (2007) The Ordovician chitinozoan biodiversification and its leading factors. *Palaeogeography, Palaeoclimatology, Palaeoecology*, **245**, 5–19.

AL-AMERI T.K. (1983) Acid-resistant microfossils used in determination of Palaeozoic palaeoenvironments in Libya. *Palaeogeography, Palaeoclimatology, Palaeoecology*, **44**, 103–116.

ANKETELL J.M. (1963) *The geology of the Llangranog district, Southwest Cardiganshire*. Ph.D. Dissertation, Queen's University of Belfast.

ANKETELL J.M. (1987) On the geological succession and structure of South-Central Wales. In: *Sedimentation and Tectonics of the Welsh Basin. Geological Journal Vol. 22, Thematic issue, 1-5.* (Ed. W.R. Fitches & N.H. Woodcock), 155–165. Wiley.

ARCHER D. (2004) Biological fluxes in the ocean and atmospheric pCO_2. In: *The Oceans and Marine geochemistry* (Ed. H. Elderfield), vol. 6, chap. 6.10, 275–291. Elsevier Pergamon.

ARMSTRONG H.A. (2007) On the cause of the Ordovician glaciation. In: *Deep-Time Perspectives on Climate Change: Marrying the Signal from Computer Models and Biological Proxies* (Ed. M. Williams, A.M. Haywood, F.J. Gregory & D.N. Schmidt). Geological Society of London, The Micropalaeontological Society, London.

ARMSTRONG H.A., ABBOTT G.D. & TURNER B.R. (2006) High latitude $\delta^{13}C_{org}$ indicate pCO_2 levels of 3 x PAL for the late Ordovician. In: *IGCP 503 Glasgow conference abstracts.*

ARMSTRONG H.A., BALDINI J., CHALLANDS T.J., GRÖCKE D.R. & OWEN A.W. (in revision) Response of the Inter-Tropical Convergence Zone to Southern Hemisphere cooling during Ordovician glaciation. *Palaeogeography, Palaeoclimatology, Palaeoecology.*

ARMSTRONG H.A. & BRASIER M.D. (2005) *Microfossils.* Blackwell, 2nd edn. 296 p.

ARMSTRONG H.A. & COE A.L. (1997) Deep-sea sediments record the geophysiology of the late Ordovician glaciation. *Journal of the Geological Society, London*, **154**, 929–934.

ARMSTRONG H.A. & OWEN A.W. (2002a) Euconodont diversity changes in a cooling and closing Iapetus Ocean. In: *Palaeobiogeography and biodiversity change: The Ordovician and Mesozoic-Cenozoic radiations.* (Ed. A.W. Crame & A.W. Owen), vol. 194, 85–98. Geological Society (London) Special publication.

ARMSTRONG H.A. & OWEN A.W. (2002b) Euconodont palaeobiogeography and the closure of the Iapetus Ocean. *Geology*, **30**, 1091–1094.

ARMSTRONG H.A., TURNER B.R., MAKHLOUF I.M., WEEDON G.P., WILLIAMS M., AL SMADI A. & ABU SALAH A. (2005) Origin, sequence stratigraphy and depositional environment of an Upper Ordovician Hirnantian degalacial black shale, Jordan. *Palaeogeography, Palaeoclimatology, Palaeoecology*, **220**, 273–289.

ARNDT S., BRUMSACK H.J. & WIRTZ K.W. (2006) Cretaceous black shales as active bioreactors; a biogeochemical model for the deep biosphere encountered during ODP Leg 207 (Demerara Rise). *Geochimica et Cosmochimia Acta*, **70**, 408–425.

ARTHUR M. & SAGEMAN B. (1994) Marine black shales: Depositional mechanisms and environments of ancient deposits. *Annual Review of Earth and Planetary Sciences*, **22**, 499–551.

BAMBACH R.K., KNOLL A. & WANG S.C. (2004) Origination, extinction and mass depletions of marine diversity. *Paleobiology*, **30**, 522–542.

BARKER S., HIGGINS J.A. & ELDERFIELD H. (2003) The future of the carbon cycle: review, calcification response, ballast and feedback on atmospheric CO_2. *Philosophical Transactions of the Royal Society of London, A.*, **361**, 1977–1999.

BARNES C.R. (2004) Chapter 7. Ordovician Oceans and Climate. In: *The Great Ordovician Biodiversification Event.* (Ed. B.D. Webby, M.L. Droser, F. Paris & I. Percival), 72–76. New York: Columbia University Press.

BECKMANN B., FLÖGEL S., HOFMANN P., SCHULZ M. & WAGNER T. (2005) Orbital forcing of Cretaceous river discharge in tropical Africa and ocean response. *Nature*, **437**, 241–244.

BENGSTON P. (1988) Open nomenclature. *Palaeontology*, **32**, 223–227.

BERGER W.H., SMETACEK V.S. & WEFER G. (1989) *Productivity of the Oceans: Present and Past.*. Wiley Interscience, New York. pp. 471.

BERGSTRÖM S.M., FINNEY S.C., CHEN X., GOLDMAN D. & LESLIE S.A. (2006a) Three new Ordovician global stage names. *Lethaia*, **39**, 287–288.

BERGSTRÖM S.M. & GRAHN Y. (1985) Biostratigraphy and paleoecology of chitinozoans in the lower Middle Ordovician of the Southern Appalachians. *Appalachian Basin Industrial Associates*, **8**, 6–28.

BERGSTRÖM S.M., SALTZMAN M.M. & SCHMITZ B. (2006b) First record of the Hirnantian (Upper Ordovician) $\delta^{13}C$ excursion in the North American Midcontinent and its regional implications. *Geological Magazine*, **143**, 657–678.

BERNER R.A. (1992) Palaeo-CO_2 and climate. *Nature*, **358**, 114.

BERNER R.A. (1994) GEOCARB II: a revised model for atmospheric CO_2 over Phanerozoic time. *American Journal of Science*, **294**, 56–91.

BERNER R.A. (2006) Geocarbsulf: A combined model for Phanerozoic atmospheric O_2 and CO−2. *geochim*, **70**, 5653–5664.

BERNER R.A. & KOTHAVALA Z. (2001) GEOCARB III: a revised model for atmospheric CO_2 over Phanerozoic time. *American Journal of Science*, **301**, 182–204.

BERRY W.B.N. & WILDE P. (1978) Progressive ventilation of the oceans; an explanation for the distribution of the lower Paleozoic black shales. *American Journal of Science*, **278**, 257–275.

BERRY W.B.N., WILDE P. & QUINBY-HUNT M.S. (1985) The oceanic nonsulfidic oxygen minimum zone: a habitat for graptolites? *Bulletin of the Geological Society of Denmark*, **35**, 103–113.

BERRY W.B.N., WILDE P. & QUINBY-HUNT M.S. (1989) Palaeozoic (Cambrian through Devonian) anoxitropic biotopes. *Palaeogeography, Palaeoclimatology, Palaeoecology*, **74**, 3–13.

BERRY W.B.N., WILDE P. & QUINBY-HUNT M.S. (1991) Silurian oceanic and atmospheric circulation and chemistry. *The Murchison Symposium; proceedings of an international conference on the Silurian System. Special Papers in Palaeontology*, **44**, 123–143.

BEVINS R.E. & MERRIMAN R.J. (1988) Compositional controls on coexisting prehnite actinolite and prehnite pumpellyite facies assemblages in the Tal-Y-Fan metabasite intrusion, North Wales: - implications for Caledonian metamorphic field gradients. *Journal of Metamorphic Geology*, **6**, 17–39.

BEVINS R.E. & ROBINSON D. (1988) Low grade metamorphism in the Welsh Basin Lower Palaeozoic succession: An example of diastathermal metamorphism? *Journal of the Geological Society, London*, **145**, 363–366.

BIDIGARE R.R., FLEUGGE A., FREEMAN K.H., HANSON K.L., HAYES J.M., HOLLANDER D., JASPER J.P., KING L.L., LAWS E.A., MILDER J., MILLERO F.J., PANCOST R., POPP B.N., STEINBERG P.A. & WAKEHM S.G. (1997) Consistent fractionation of ^{13}C in nature and laboratory: growth-rate effects in some haptopyte algae. *Global Biogeochemical Cycles*, **11**, 279–292.

BILLUPS K. (2005) Snow maker for the ice ages. *Nature*, **433**, 809–810.

BIRCHFIELD G.E., WEERTMAN J. & LUNDE A.T. (1982) A model study of the role of high latitude topography in the climate response to orbital insolation anomalies. *Journal of Atmospheric Science*, **39**, 71–87.

BJERRUM C.J., BENDTSEN J. & LEGARTH J.J.F. (2006) Modeling organic carbon burial during sea level rise with reference to the Cretaceous. *Geochemistry, Geophysics, Geosystems - G (super 3)*, **7**. doi:10.1029/2005GC001032.

BLACKETT E., PAGE A., ZALASIEWICZ J., WILLIAMS M., RICKARDS B. & DAVIES J. (2008) Directional micro-evolution in the *Normalograptus persculptus* lineage from central Wales: a correlation tool for late Ordovician-early Silurian strata. *in press*.

BLUTH G.J.S. & KUMP L.R. (1991) Phanerozoic paleogeology. *American Journal of Science*, **291**, 284–308.

BOENING P., BRUMSACK H.J., BOETTCHER M.E., SCHNETGER B., KRIETE C. & BORCHERS S.L. (2004) Geochemistry of peruvian near-surface sediments. *Geochimica et Cosmochimia Acta*, **68**, 4429–4451.

BORCHERS S.L., SCHNETGER B., BÖNING P. & BRUNSACK H.J. (2005) Geochemical signatures of the Namibian diatom belt: Perennial upwelling and intermittent anoxia. *Geochemistry, Geophysics, Geosystems - G (super 3)*, **6**. doi:10.1029/2004GC000886.

BOTTRELL S.H., GREENWOOD P.B., YARDLEY B.W.D., SHEPHERD T.J. & SPIRO B. (1990) Metamorphic and post-metamorphic fluid-flow in the low-grade rocks of the Harlech Dome, North Wales. *Journal of Metamorphic Geology*, **8**, 131–143.

BOUCOT A.J., RONG J.Y., CHEN X. & SCOTESE C.R. (2003) Pre-Hirnantian Ashgill climatically warm event in the Mediterranean region. *Lethaia*, **36**, 119–132.

BRENCHLEY P.J. (2004) Chapter 9. End Ordovican Glaciation. In: *The Great Ordovician Biodiversification Event.* (Ed. B.D. Webby, M.L. Droser, F. Paris & I. Percival), 81–83. New York: Columbia University Press.

BRENCHLEY P.J., CARDEN G.A.F., HINTS L., KALJO D., MARSHALL J.D., MARTMA T., MEIDLA T. & NÕLVAK J. (2003) High-resolution stable isotope stratigraphy of Upper Ordovician sequences: constraints on the timing of bioevents and environmental changes associated with mass extinction and glaciation. *Geological Society of America Bulletin*, **116**, 89–104.

BRENCHLEY P.J., CARDEN G.A.F. & MARSHALL J.D. (1995) Environmental changes associated with the 'first-strike' of the Late Ordovician mass extinction. *Modern Geology*, **20**, 69–82.

BRENCHLEY P.J., MARSHALL J.D., CARDEN G.A.F., ROBERTSON D.B.R., LONG D.G., MEIDLA T., HINTS L. & ANDERSON T.F. (1994) Bathymetric and isotopic evidence for a short lived Late Ordovician glaciation in a greenhouse period. *Geology*, **22**, 295–298.

BRENCHLEY P.J., MARSHALL J.D., HARPER D.A.T., BUTLER C.J. & UNDERWOOD C.J. (2006) A late Ordovician (Hirnatian) karstic surface in a submarine channel, recording glacio-eustatic sea-level changes: Meifod, central Wales. *Geological Journal*, **41**, 1–22.

BRENCHLEY P.J., MARSHALL J.D., HINTS L. & NÕLVAK J. (1997) New isotopic data solving an old biostratigraphic problem: the age of the upper Ordovician brachiopod *Holorhyncus giganteus*. *Journal of the Geological Society, London*, **154**, 335–342.

BROECKER W.S. & PENG T.H. (1982) *Tracers in the Sea*. Lamont-Doherty Geological Observatory, Palisades, New York.

BRUMSACK H.J. (1989) Geochemistry of Recent TOC-rich sediment from the Gulf of California and the Black Sea. *Geologische Rundschau*, **78**, 851–882.

BRUMSACK H.J. (2006) The trace metal content of recent organic carbon-rich sediments: implications for Cretaceous black shale formation. *Palaeogeography, Palaeoclimatology, Palaeoecology*, **232**, 344–361.

CANFIELD D.E. (1989) Sulfate reduction and oxic respiration in marine sediments: implications for organic carbon preservation in euxinic environments. *Deep-sea Research*, **36**, 121–138.

CAVE R. (1965) The Nod Glas sediments of Caradoc age in North Wales. *Geological Journal*, **4**, 279–298.

CHALLANDS T.J., ARMSTRONG H.A., MALONEY D.P., DAVIES J.R., WILSON D. & OWEN A.W. (2008) Organic-carbon deposition and coastal upwelling mid-latitude during the Upper Ordovician (late Katian): a case study from the Welsh Basin, UK. *Palaeogeography, Palaeoclimatology, Palaeoecology*, , . *in press.*

CHALLINOR J. (1927) Further notes on the age of the rocks around the Teifi Estuary. *Geological Magazine*, **64**, 322–344.

CHANNELL J.E.T. & MCCABE C. (1992) Palaeomagnetic data from the Borrowdale Volcanic Group: volcanotectonics and Late Ordovician palaeolatitudes. *Journal of the Geological Society, London*, **149**, 881–888.

CHEN X., RONG J., FAN J., ZHAN R., MITCHELL C.E., HARPER D.A.T., MELCHIN M.J., PENG P., FINNEY S.C. & WANG X. (2006) The Global Boundary Stratotype Section and Point (GSSP) for the base of the Hirnantian Stage (the uppermost of the Ordovician System). *Episodes*, **29**, 183–196.

CHERNS L. & WHEELEY J.R. (2007) A pre-Hirnantian Late Ordovician interval of global cooling - the Boda Event re-assessed. *Palaeogeography, Palaeoclimatology, Palaeoecology*, **251**, 449–460.

CHRISTIANSEN J.L. & STOUGE S. (1999) Oceanic circulation as an element in palaeogeographical reconstructions: the Arenig (early Ordovician) as an example. *Terra Nova*, **11**, 73–78.

CHRISTOPHER R.A. & GOODMAN D.K. (1996) Chapter 15. Introduction to biostratigraphy and time scales. In: *Palynology: Principles and applications. Volume 2: Applications.* (Ed. J. Jansonius & D. McGregor), vol. 2, 463–492. AASP Foundation.

COCKS L.R.M. (2001) Ordovician and Silurian global geography. *Journal of the Geological Society, London*, **158**, 197–210.

COCKS L.R.M. & FORTEY R.A. (1982) Faunal evidence for oceanic separations in the Palaeozoic of Britain. *Journal of the Geological Society, London*, **139**, 465–478.

COCKS L.R.M., MCKERROW W.S. & VAN STAAL C.R. (1997) The margins of Avalonia. *Geological Magazine*, **134**, 627–636.

COCKS L.R.M. & TORSVIK T.H. (2002) Earth geography from 500 to 400 million years ago: A faunal and palaeomagnetic review. *Journal of the Geological Society, London*, **159**, 631–644.

COCKS L.R.M. & TORSVIK T.H. (2004) Chapter 5. Major Terranes in the Ordovician. In: *The Great Ordovician Biodiversification Event.* (Ed. B.D. Webby, M.L. Droser, F. Paris & I. Percival), 61–67. New York: Columbia University Press.

COCKS L.R.M. & TORSVIK T.H. (2005) Baltica from the late Precambrian to mid-Palaeozoic times: the gain and loss of a terrane's identity. *Earth Science Reviews*, **72**, 39–66.

COCKS L.R.M., WOODCOCK N.H., RICKARDS R.B., TEMPLE J.T. & LANE P.D. (1984) The Llandovery Series of the type area. *Bulletin of the British Museum (Natural History) Geology*, **38**, 131–182.

COLLINSON C. & SCHWALB H. (1955) North American Paleozoic Chitinozoa. Report of Investigations 186, Illinois State Geological Survey. 1-33.

COOPER R.A., FORTEY R.A. & LINDHOLM K. (1991) Latitudinal and depth zonation of early Ordovician graptolites. *Lethaia*, **24**, 199–218.

COOPER R.A., MALETZ J., TALOR L. & ZALASIEWICZ J.A. (2004) Graptolites: patterns of diversity across paleolatitudes. In: *The Great Ordovician Diversification Event* (Ed. B.D. Webby, F. Paris, M. Droser & I. Percival), 61–67. Columbia University Press, New York.

COPE J.W. (2007) What have they done to the Ordovician? *Geoscientist*, **17**, 19–21.

CORNFORD C. (2001) The use of organic geochemistry in hydrocarbon acreage evaluation. IGI Ltd. Bideford, Devon. University of London, Royal Holloway, unpublished MSc Petroleum Geoscience Lecture course notes.

CRAIG J. (1985) *Tectonic evolution of the area between Borth and Cardigan, Dyfed, West Wales*. Ph.D. Dissertation, University of Wales, Aberystwyth.

CROWLEY T.J. & BAUM S.K. (1995) Toward reconciling Late Ordovician (440 ma) glaciation with very high co_2 levels. *Journal of Geophysical Research*, **96**, 22597–22610.

CROWLEY T.J., YIP K.J. & BAUM S.K. (1994) Snowline instability in a general circulation model; Application to the Carboniferous glaciation. *Climate Dynamics*, **10**, 363–376.

DAVIES J.R., FLETCHER C.J.N., WATERS R.A., WILSON D., WOODHALL D.G. & ZALAZIEWICZ J.A. (1997) Geology of the country around llanilar and rhayader. memoir of the british geological survey, sheets 178 and 179 (england and wales).

DAVIES J.R., SHEPPARD T.H., WATERS R.A. & WILSON D. (2006) Geology of the Llangranog district - a brief explanation of the geological map. Sheet explanation of the British Geological Survey. 1 : 50000 Sheet 194 (England and Wales). British Geological Survey.

DAVIES J.R., WATERS R.A., WILBY P.R., WILLIAMS M. & WILSON D. (2003) Geology of the Cardigan and Dinas Island district - a brief explanation of the geological map. Sheet explanation of the British Geological Survey. 1 : 50000 Sheet 193 (including part of sheet 210) Cardigan and Dinas Island (England and Wales). 26 pp.

DE LA ROCHA C.L. (2004) The biological pump. In: *The Oceans and Marine Geochemistry* (Ed. H. Elderfield), vol. 6 of *Treatise on Geochemistry*, 83–112. Elsevier Pergamon.

DeConto R.M. & Pollard D. (2003) A coupled climate-ice sheet modelling approach to the Early Cenozoic history of the Antarctic ice sheet. *Palaeogeography, Palaeoclimatology, Palaeoecology*, **198**, 39–52.

Dorning K.J., Harvey C. & Washington-Evans J. (2006) Phytoplankton and chitinozoan evidence of small scale cyclicity in the Silurian. In: *Lyell Meeting 2006: Millenial-scale Events, 15 February 2006* (Ed. H.A. Armstrong & M. Tucker), 12. The Geological Society, Burlington House, London.

Droser M.L., Bottjer D.J., Sheehan P.M. & McGhee Jr G.R. (2000) Decoupling of taxonomic and ecologic severity of Phaerozoic marine mass extinctions. *Geology*, **28**, 675–678.

Dypvik H. (1984) Geochemical composition and depositional conditions of the Upper Jurassic and Lower Cretaceous Yorkshire clays, England. *Geological Magazine*, **121**, 489–504.

Eisenack A. (1931) Neue Mikrofossilien des baltischen Silurs. I. *Palaeontologische Zeitschrift*, **13**, 74–118.

Eisenack A. (1934) Neue Mikrofossilien des baltischen Silurs. III und Neue Mikfrofossilien des böhmischen Silurs. I. *Palaeontologische Zeitschrift*, **16**, 52–76.

Eisenack A. (1939) Chitinozoen und Hystrichosphaerideen im Ordovicium des Rheinischen Schiefergebirges. *Senckenbergiana lethaea*, **21**, 135–152.

Eisenack A. (1955) Neue Chitinozoen aus dem Silur des Baltikums und dem Devon der Eifel. *Senckenbergiana lethaea*, **36**, 311–319.

Eisenack A. (1959) Neotypen baltischer Silur-Chitinozoen und neue Arten. *Neues Jahrbuch für Geologie und Paläontologie. Abhandlungen*, **108**, 1–20.

Eisenack A. (1962) Neotypen baltischer Silur-Chitinozoen und neue Arten. *Neues Jahrbuch für Geologie und Paläontologie. Abhandlungen*, **114**, 291–316.

Eisenack A. (1964) Mikrofossilien aus dem Silur Gotlands. Chitinozoen. *Neues Jahrbuch für Geologie und Paläontologie. Abhandlungen*, **120**, 308–342.

Eisenack A. (1968) Microfossilien eines geschiebes der Borkholmer Stufe, baltisches Ordovizium, F–2. *Mittielungen aus dem Geologischen Staatinstitut in Hamburg*, **37**, 81–94.

Ekdale A.A. & Mason T. (1988) Characteristic trace-fossil associations in oxygen-poor sedimentary environments. *Geology*, **16**, 720–723.

EVANS D.C. (1906) The Ordovician Rocks of Western Carmarthenshire. *Quarterly Journal of the Geological Society, London*, **62**, 597–643.

FANTON K.C. & HOLMDEN C. (2007) Sea-level forcing and carbon isotope excursions in epeiric seas: implications for chemostratigraphy. *Canadian Journal of Earth Sciences*, **44**, 807–818.

FETTES D.J., LONG C.B., BEVINS R.E., MAX M.D., OLOVER G.J.H., PRIMMER T.J., THOMAS L.J. & YARDLEY B.W.D. (1985) Grade and time of metamorphism in the Caledonide Orogen of Britain and Ireland. In: *The nature and timing of orogenic activity in the Caledonian rocks of the British Isles.* (Ed. A.L. Harris). Blackwell for the Geological Society of London, U.K.

FINLAY A.J., SELBY D. & CHALLANDS T.J. (2007) Re-Os geochronology and end-Ordovician Os isotope seawater composition of the Ordovician/Silurian GSSP, Dob's Linn, Scotland. In: *Bicentennial Conference, The Geological Society of London: Earth Sciences in the service of society. Abstract book.*, 141.

FINNEY S.C. & BERRY W.B.N. (1997) New perspectives on graptolite distributions and their use as indicators of platform margin dynamics. *Geology*, **25**, 919–922.

FINNEY S.C., BERRY W.B.N. & COOPER J.D. (2007) The influence of denitrifying seawater on graptolite extinction and diversification during the Hirnantian (latest Ordovician) mass extinction event. *Lethaia*, **40**, 281–291.

FINNEY S.C., BERRY W.B.N., COOPER J.D., RIPPERDAN R.L., SWEET W.C., JACOBSEN S.R., SOUFIANE A., ACHAB A. & NOBLE P.J. (1999) Late Ordovician mass extinction; a new perspective from stratigraphic sections in central Nevada. *Geology*, **27**, 215–218.

FORTEY R.A. & COCKS L.R.M. (1986) Marginal fault belts and their structural implications, with examples from the Lower Palaeozoic. *Journal of the Geological Society, London*, **143**, 151–160.

FORTEY R.A. & COCKS L.R.M. (2005) Late Ordovician global warming - The Boda event. *Geology*, **33**, 405–408.

FORTEY R.A., HARPER D.A.T., INGHAM J.K., OWEN A.W., PARKES M.A., RUSHTON A.W.A. & WOODCOCK N.H. (2000) *A revised correlation of Ordovician rocks in the British Isles.*, vol. 24. Geological Society of London Special Report. 83 pp.

FORTEY R.A., HARPER D.A.T., INGHAM J.K., OWEN A.W. & RUSHTON A.W.A. (1995) A revision of Ordovician series and stages of the historical type area. *Geological Magazine*, **132**, 15–30.

FREEMAN K.H. (2001) *Reviews in Mineralogy and Geochemistry*, vol. 43, chap. 11. Isotopic biogeochemistry of marnie organic carbon., 579–605. Mineralogical Society of America and Geochemical Society, Washington, DC, United States.

FREEMAN K.H. & HAYES J.M. (1992) Fractionation of carbon isotopes by phytoplankton and estimates of ancient CO_2 levels. *Global Biogeochemical Cycles*, **6**, 185–198.

GIBBS M.T. & KUMP L.R. (1994) Global chemical weathering at the last glacial maximum and the present: sensitivity to changes in lithology and hydrology. *Paleoceanography*, **9**, 529–543.

GOERICKE R. (1994) Variations in marine $\delta^{13}C$ with latitude, temperature and dissolved CO_2 in the world ocean. *Global Biogeochemical Cycles*, **8**, 85–90.

GOERICKE R., MONTOYA J.P. & FRY B. (1994) Physiology of isotope fractionation in algae and cyanobacteria. In: *Stable isotopes in ecology* (Ed. K. Lajtha & B. Michener), 199–233. Blackwell Scientific, Boston.

GRAHN Y. (1981) Middle Ordovician Chitinozoa from Öland. *Sveriges Geologiska Undersökning C*, **5**, 1–41.

GRAHN Y. (1982) Caradocian and Ashgillian Chitinozoa from the subsurface of Gotland. *Sveriges Geologiska Undersökning C*, **788**, 1–66.

GRAHN Y. & MILLER M.A. (1986) Chitinozoa from the middle Ordovician Bromide Formation, Arbuckle Mountains, Oklahoma. *Neues Jahrbuch für Geologie und Paläontologie. Abhandlungen*, **172**, 381–403.

HALLAM A. (1992) *Phanerozoic sea-level changes.*, 266. Columbia University Press.

HALLAM A. & WIGNALL P.B. (1997) Latest ordovician extinctions: one disaster after another. In: *Mass extinctions and their aftermath* (Ed. A. Hallam & P.B. Wignall), 39–61. Oxford University Press.

HAMMER Ø., HARPER D.A.T. & RYAN P.D. (2001) Past: Paleontological statistics software package for education and data analysis. *Palaeontologia Electronica*, **4**, 9. http://palaeo-electronica.org/2001_1/*past*/*issue*$1_0$1.*htm*.

HANNIGAN R.E. & BASU A. (1998) Late diagenetic trace element remobilization in organic-rich black shales of the Taconic foreland basin of Quebec, Ontario and New York. In: *Shales and Mudstones vol. II* (Ed. W.Z. J. Schieber & P.S. Sethi), 209–233.

HATCH J.R., JACOBSEN S.B., WITZKE B.J., RISATTI J.B., ANDERS D.E., WATNEY W., NEWELL K.D. & VULETICH A.K. (1987) Possible Late Middle Ordovician organic carbon isotope excursion: evidence from Ordovician oils and hydrocarbon source rocks, mid-continent and east-central USA. *AAPG Bulletin*, **71**, 1342–1354.

HAUG G.H., GANOPOLSKI A., SIGMAN D.M., ROSELL-MELE A., SWANN G.E.A., TIEDEMANN R., JACCARD S.L., BOLLMANN J., MASLIN M.A., LENG M.J. & EGLINGTON G. (2005) North Pacific seasonality and the glaciation of North America 2.7. million years ago. *Nature*, **433**, 821–825.

HAY W.W. & BROCK J.C. (1992) Temporal variation in intensity of upwelling off southwest africa. In: *Upwelling Systems: evolution since the Early Miocene.* (Ed. P.W.L. Summerhayes C. P. & K.C. Emeis), 463–497. Geological Society Special Publication No. 64.

HAYS J.D. (1978) A review of the Late Quaternary history of Antarctic seas. In: *Antarctic Glacial History and World Paleoenvironments* (Ed. V.Z.B.E. M.). Rotterdam: A. A. Balkema.

HEDBERG H.D. (1965) Chronostratigraphy and biostratigraphy. *Geological Magazine*, **102**, 451–461.

HEDGES J.I. & KEIL R.G. (1995) Sedimentary organic matter preservation: an assessment and speculative synthesis. *Marine Chemistry*, **49**, 81–115.

HENDRIKS E.M.L. (1926) The Bala-Silurian succession in the Llangranog district (south Cardiganshire). *Geological Magazine*, **63**, 121–139.

HERRMANN A.D., HAUPT B.J., PATZKOWSKY M.E., SEIDOV D. & SLINGERLAND R.L. (2005) Response of Late Ordovician paleoceanography to changes in sea level, continental drift and atmospheric pCO_2: potential causes for long-term cooling and glaciation. *Palaeogeography, Palaeoclimatology, Palaeoecology*, **210**, 385–401.

HERRMANN A.D., PATZKOWSKY M.E. & POLLARD D. (2003) Obliquity forcing with 8-12 times preindustrial levels of atmospheric pCO_2 during the Late Ordovician glaciation. *Geology*, **31**, 485–488.

HERRMANN A.D., PATZKOWSKY M.E. & POLLARD D. (2004) The impact of paleogeography, pCO_2, poleward ocean heat transport and sea-level change on global cooling during the Late Ordovician. *Palaeogeography, Palaeoclimatology, Palaeoecology*, **206**, 59–74.

HEUSSER L.E. & VAN DE GEER G. (1994) Direct correlation of terrestrial and marine palaeoclimatic records from four glacial-interglacial cycles -DSDP Site 594, southwest Pacific. *Quaternary Science Reviews*, **13**, 275–282.

HOFMANN M., WOLF-GLADROW D.A., TAKASHASHI T., SUTHERLAND S.C., SIX K.D. & MAIER-REIMER E. (2000) Stable carbon isotope distribution of particulate organic matter in the ocean: a model study. *Marine Chemistry*, **72**, 131–150.

HOLGATE S.J., MARSHALL J.D. & WILLIAMS R.G. (2002) Carbon cycle changes and glaciation in the Late Ordovician. In: *AGU Ocean Sciences Meeting; programmes with abstracts*. American Geophysical Union.

HOLGATE S.J., MARSHALL J.D., WILLIAMS R.G. & BRENCHLEY P.J. (2001) An oceanographic mechanism for carbon cycle changes and glaciation in the Late Ordovician. In: *Earth system processes - Global Meeting; programmes with abstracts*. Session No. T4.

HOLGATE S.J., WILLIAMS R.G. & MARSHALL J.D. (2003) An explanation for the large positive carbon isotope excursion associated with the late ordovician glaciation? *EGS - AGU - EUG Joint Assembly, Abstracts from the meeting held in Nice, France, 6 - 11 April 2003, abstract #2784*, 2784.

HOLLANDER D.J. & MCKENZIE J.A. (1991) CO_2 control on carbon isotope fractionation during aqueous photosynthethesis: a palaeo-pCO_2 barometer. *Geology*, **19**, 929–932.

HOLMDEN C., CREASER R.A., MUEHLENBACHS K., LESLIE S.A. & BERGSTRÖM S. (1998) Isotopic evidence for geochemical decoupling between ancient epeiric seas and bordering oceans: implications for secular variations. *Geology*, **26**, 567–570.

IMBRIE J., BERGER A., BOYLE E.A., CLEMENS S.C., DUFFY A., HOWARD W.R., KUKLA G., KUTZBACH J., MARTINSON D.G., MCINTYRE A., MIX A.C., MOLFINO B., MORLEY J.J., PETERSON L.C., PISIAS N.G., PRELL W.L., RAYMO M.E., SHACKLETON N.J. & TOGGWEILER J.R. (1993) On the structure and origin of major glaciation cycles 2: the 100 000 year cycle. *Paleoceanography*, **8**, 699–735.

IMMENHAUSER A., PORTA D.G., KENTER J.A.M. & BAHAMONDE J.R. (2003) An alternative model for positive shifts in shallow-marine carbonate $\delta^{13}C$ and $\delta^{18}O$. *Sedimentology*, **50**, 953–959.

INGALL E.D., BUSTIN R.M. & VAN CAPPELLEN P. (1993) Influence of water column anoxia on the burial and preservation of carbon and phosphorus in marine shales. *Geochimica et Cosmochimia Acta*, **57**, 303–316.

JAHNKE R.A. (1990) Ocean flux studies: a status report. *Review of Geophysics*, **28**, 381–398.

JANSONIUS J. (1964) Morphology and classification of some Chitinozoa. *Bulletin of Canadian Petroleum Geology*, **12**, 901–918.

JENKINS W.A.M. (1969) Chitinozoa from the Ordovician Viola and Fernvale Limestones of the Arbuckle Mountains, Oklahoma. *Special Papers in Palaeontology*, **5**, 1–44.

JENKINS W.A.M. (1970) Chitinozoa from the Ordovician Sylvan Shale of the Arbuckle Mountains, Oklahoma. *Palaeontology*, **13**, 261–288.

JOHNSON R.J.E. & VAN DER VOO R. (1990) Pre-folding magnetiziation reconfirmed for the Late Ordovician-Early Silurian Dunn Point volcanics. *Tectonophysics*, **178**, 193–205.

JONES B. & MANNING D.A.C. (1994) Comparison of geochemical indices used for the interpretation of palaeoredox conditions in ancient mudstones. *Chemical Geology*, **111**, 111–129.

KALJO D., HINTS L., MARTMA T. & NÕLVAK J. (2001) Carbon isotope stratigraphy in the latest Ordovician of Estonia. *Chemical Geology*, **175**, 49–59.

KALJO D., HINTS L., MARTMA T., NÕLVAK J. & ORASPÕLD A. (2004) Late Ordovician carbon isotope trend in Estonia, its significance in stratigraphy and environmental analysis. *Palaeogeography, Palaeoclimatology, Palaeoecology*, **210**, 165–185.

KALJO D., MARTMA T. & SAADRE T. (2007) Post-Hunnebergian Ordovician carbon isotope trend in Baltoscandia, its environmental implications and some similarities with that of Nevada. *Palaeogeography, Palaeoclimatology, Palaeoecology*, **245**, 138–155.

KEEPING W. (1882) The geology of Cardigan town. *Geological Magazine*, **19**, 519–522.

KETO L.S. & JACOBSEN S.B. (1987) Nd and Sr isotopic variations of Early Palaeozoic oceans. *Earth and Planetary Science Letters*, **84**, 7–41.

KILLOPS S.D. & KILLOPS V.J. (1993) *An introduction to organic geochemistry*. Longman Scientific and Technical; Wiley, New York. 265 pp.

KUMP L.R. (1991) Interpreting carbon-isotope excursions: Strangelove oceans. *Geology*, **19**, 299–302.

KUMP L.R. & ARTHUR M.A. (1999) Interpreting carbon-isotope excursions: carbonates and organic matter. *Chemical Geology*, **161**, 181–198.

KUMP L.R., ARTHUR M.A., PATZKOWSKY M.E., GIBBS M.T., PINKUS D.S. & SHEEHAN P.M. (1999) A weathering hypothesis for glciation at high atmospheric pco_2 during the Late Ordovician. *Palaeogeography, Palaeoclimatology, Palaeoecology*, **152**, 173–187.

KUMP L.R. & GARRELS R.M. (1986) Modeling atmospheric O_2 in the global sedimentary redox cycle. *American Journal of Science*, **286**, 337–360.

KUYPERS M.M.M., LOURENS L.J., RIJPSTRA W., IRENE C., PANCOST R.D., NIJENHUIS I.A. & DAMSTE J.S. (2004) Orbital forcing of organic carbon burial in the proto-North Atlantic during oceanic anoxic event 2. *Earth and Planetary Science Letters*, **228**, 465–482.

KUYPERS M.M.M., PANCOST R.D., NIJENHUIS I.A. & SINNINGHE DAMSTÉ J.S. (2002) Enhanced productivity led to increased organic carbon burial in the euxinc North Atlantic basin during the late Cenomanian oceanic anoxic event. *Paleoceanography*, **17**.

LAPWORTH C. (1879) On the Tripartite Classification of the Lower Palaeozoic Rocks. *Geological Magazine*, **6**.

LATTER M.P. (1925) Note on the age of the rocks around the Teifi Estuary. *Geological Magazine*, **62**, 187–188.

LAUFELD S. (1967) Caradocian Chitinozoa from Dalarna, Sweden. *Geologiska Föreningens i Stockholm Förhandlingar*, **89**, 275–349.

LAUFELD S. (1974) Silurian chitinozoa from Gotland. *Fossils and Strata*, **5**, 1–130.

LEGGETT J.K. (1980) British Lower Palaeozoic black shales and their palaeo-oceanographic significance. *Journal of the Geological Society, London*, **137**, 139–156.

LEHMANN M.F., BERNASCONI S.M., BARBIERI A. & MCKENZIE J.A. (2002) Preservation of organic matter and alteration of its carbon and nitrogen isotope composition during simulated and in situ early sedimentary diagenesis. *Geochimica et Cosmochimia Acta*, **66**, 3573–3584.

LEV S.M., FILER J.K. & TOMASCAK P. (2008) Orogenesis vs. diagenesis: Can we use organic-rich shales to interpret the tectonic evolution of a depositional basin? *Earth Science Reviews*, **86**, 1–14.

LONG D.G.F. (1993) Oxygen and carbon isotopes and event stratigraphy near the Ordovician-Silurian boundary, Anticosti Island Quebec. *Palaeogeography, Palaeoclimatology, Palaeoecology*, **104**, 49–59.

LÖWEMARK L., SCHÖNFELD J., WERNER F. & SCÄFER P. (2004) Trace fossils as a paleoceanographic tool: evidence from late Quaternary sediments of the southwestern Iberian margin. *Marine Geology*, **204**, 27–41.

LU J., VECCHI G.A. & REICHLER T. (2007) Expansion of the Hadley cell under global warming. *Geophysical Research Letters*, **34**. doi:10.1029/2006GL028443.

LYNAS B.D.T. (1988) Evidence for dextral oblique-slip faulting in the Shelve Ordovician inlier, Welsh Borderland: implications for the south British Caledonides. *Geological Journal*, **23**, 39–57.

MACNIOCAILL C. (2000) A new Silurian palaeolatitude for eastern Avalonia and evidence for crustal rotations in the Avalonian margin of southwestern Ireland. *Geophysical Journal International*, **141**, 661–671.

MACQUEDA M., WILLMOTT A.J., MAMBER J.L. & DARBY M.S. (1998) An investigation of the small ice cap instability in the Southern Hemisphere with coupled atmosphere-sea-ice-ocean-terrestrial ice model. *Climate Dyanamics*, **14**, 329–352.

MANABE S. & BROCCOLI A.J. (1985) A comparison of climate model sensitivity with data from the last glacial maximum. *Journal of the Atmospheric Sciences*, **42**, 2643–2651.

MARSHALL J.D., BRENCHLEY P.J., MASON P., WOLFF A., ASTINI R.A., HINTS L. & MEIDLA T. (1997) Global isotopic events associated with mass extinction and glaciation in the Late Ordovician. *Palaeogeography, Palaeoclimatology, Palaeoecology*, **132**, 195–210.

MARSHALL J.D. & MIDDLETON P.D. (1990) Changes in marine isotopic composition and the Late Ordovician glaciation. *Journal of the Geological Society, London*, **147**, 1–4.

MASLIN M.A. & SWANN G.E.A. (2005) *Isotopes in Palaeoenvironmental Research*, chap. 6. Isotopes in marine sediments, 227–269. Springer.

MCCANN T. (1990a) Distribution of Ordovician-Silurian ichnofossil assemblages in Wales - implications for Phanerozoic ichnofaunas. *Lethaia*, **23**, 243–255.

MCCANN T. (1990b) *Palaeoenvironmental evolution of an Ordovician-Silurian deep-marine sedimentary succession in the Welsh Basin.*. Ph.D. Dissertation, University of Leicester.

MCKERROW W.S. & SCOTESE C.R. (1990) *Palaeozoic palaeogeography and biogeography. Memoir of the Geological Society of London, 12.*, 435. London, Blackwell (for the) Geological Society of London.

MEIDLA T., AINSAAR L., HINTS L., HINTS O., MARTMA T. & NÕLVAK J. (1999) The mid-Caradocian biotic and isotopic event in the Ordovician of the East Baltic. *Acta Universitatis Carolinae - Geologica*, **43**, 503–506.

MELCHIN M. & LEGAULT J. (1985) Evolutionary lineages in some Ordovician chitinozoa. *Palynology*, **9**, 199–210.

MELCHIN M.J. & HOLMDEN C. (2006) Carbon isotope chemostratigraphy in Arctic Canada: Sea-level forcing of carbonate platform weathering and implications for Hirnantian global correlation. *Palaeogeography, Palaeoclimatology, Palaeoecology*, **234**, 186–200.

MELCHIN M.J., HOLMDEN C. & WILLIAMS S.H. (2003) Correlation of graptolite zones, chitinozoan biozones, and carbon isotope curves through the Hirnantian. In: *Ordovician from the Andes - Proceedings of the 9th International Symposium on the Ordovician System* (Ed. B.M.S. Albanesi G. L. & S.H. Peralta), vol. 17, 101–104. INSUGEO, Serie Correlación Geológica.

MELCHIN M.J. & MITCHELL C.E. (1991) Late Ordovician extinction events in the Graptoloidea. In: *Advances in Ordovician Geology* (Ed. C.R. Barnes & S.H. Williams), vol. 90-9, 143–156. Geological Survey of Canada, Paper.

MELCHIN M.J. & WILLIAMS S.H. (2000) A restudy of the akidograptine graptolites from Dob's Linn and a proposed redefined zonation of the Silurian Stratotype. *Palaeontology Down Under 2000*, **61**, p. 63. Geological Society of Australia, abstracts.

MEYERS P.A. & ARNABOLDI M. (2005) Trans-Mediterranean comparison of geochemical productivity proxies in a mid-Pleistocene interrupted sapropel. *Palaeogeography, Palaeoclimatology, Palaeoecology*, **222**, 313–328.

MILLER M.A. (1982) The use of chitinozoans for recognition of sedimentary environments: concepts and examples. *Journal of Paleontology (Supplement to No. 2)*, **56**, 19. North American Paleontological Convention III, Abstracts of Papers.

MILODOWSKI A.E. & ZALASIEWICZ J.A. (1991) Redistribution of rare earth elements during diagenesis of turbidite/hemipelagite mudrock sequences of Llandovery age from central Wales. In: *Developments in sedimentary provenance studies* (Ed. A.C. Morton, S.P. Todd & P.D. Houghton), vol. 57 of *Geological Society Special Publication*, 101–124. Geological Society, London.

MU E., GE M., CHEN X., NI Y. & LIN Y. (1979) Lower Ordovician graptolites of southwest China. *Palaeontologica Sinica*, **156**, 1–192. in Chinese with English abstract.

MUNNECKE A., SAMTLEBEN C. & BICKERT T. (2003) The Ireviken Event in the lower Silurian of Gotland, Sweden, relation to similar Palaeozoic and Proterozoic events. *Palaeogeography, Palaeoclimatology, Palaeoecology*, **195**, 99–124.

MURCHISON R.I. (1839) *The Silurian System*, 768. London: John Murray.

NÕLVAK J. (1980) Chitinozoans in biostratigraphy of the northern East Baltic Ashgillian. A preliminary report. *Acta Palaeontologica Polonica*, **25**, 253–260.

NÕLVAK J. (1999) Ordovician chitinozoan biozonation of Baltoscandia. *Acta Universitatis Carolinae - Geologica*, **43**, 287–290.

NÕLVAK J. & GRAHN Y. (1993) Ordovician chitinozoan zones from Baltoscandia. *Review of Palaeobotany and Palynology*, **79**, 245–269.

NAISH T.R., WOOLFE K.J., BARRETT P.J., WILSON G.S., ATKINS C., BOHATY S.M., BUECKER C.J., CLAPS M., DAVEY F.J., DUNBAR G.B., DUNN A.G., FIELDING C.R., FLORINDO F., HANNAH M.J., HARWOOD D.M., HENRYS S.A., KRISSEK L.A., LAVELLE M., VAN DER MEER J., MCINTOSH W. C.; NIESSEN F., PASSCHIER S., POWELL R.D., ROBERTS A.P., SAGNOTTI L., SCHERER R.P., STRONG C.P., TALARICO F., VEROSUB K.L., VILLA G., WATKINS D.K., WEBB P.N. & WONIK T. (2001) Orbitally induced oscillations in the East Antarctic ice sheet at the Oligocene/Miocene boundary. *Nature*, **413**, 719–723.

NARA F., TANI Y., SOMA Y., SOMA M., NARAOKA H., WATANABE T., HORIUCHI K., KAWAI T., ODA T. & NAKAMURA T. (2005) Response of phytoplankton productivity to climate change recorded by sedimentary photosynthetic pigments in Lake Hovsgol (Mongolia) for the last 23,000 years. *Quaternary International*, **136**, 71–81.

NIELSEN A.T. (2004) Chapter 10. Ordovician sea level changes; a Baltoscandian perspective. In: *The Great Ordovician Biodiversification Event.* (Ed. B.D. Webby, M.L. Droser, F. Paris & I. Percival), 84–93. New York: Columbia University Press.

NOBRE P. & SHUKLA J. (1996) Variations of sea surface temperature, wind stress and rainfall over the tropical Atlantic and South America. *Journal of Climatology*, **9**, 2464–2479.

NORRIS R.D. (2000) Pelagic species diversity, biogeography and evolution. *Palaeobiology*, **26**, 236–258.

OGLESBY R.J. (1989) A GCM study of Antarctic glaciation. *Climate dynamics*, **3**, 719–729.

ORTH C.J., GILMORE J.S., QUINTANA L.R. & SHEEHAN P.M. (1988) Terminal Ordovician extinction: Geochemical analysis of the Ordovician/Silrian boundary, Anticosti Island, Quebec. *Geology*, **14**, 433–436.

OTTLEY C.J., PEARSON D.G. & IRVINE G.J. (2003) A routine method for the dissolution of geological samples for the analysis of REE and trace elements via ICP-MS. In: *Plasma Source Mass Spectrometry: Applications and Emerging Technologies.* (Ed. J.G. Holland & S.D. Tanner), 221–230. Cambridge: Royal Society of Chemistry.

OWEN A.W. & ROBERTSON D.B.R. (1995) Ecological changes during the end-Ordovician extinction. *Modern Geology*, **20**, 21–39.

PAGE A., ZALAZIWICZ J., WILLIAMS M. & POPOV L. (2007) Were transgressive black shales a negative feedback modulating glacioeustacy in the Early Palaeozoic icehouse? In: *Deep-Time Perspectives on Climate Change: Marrying the Signal from Computer Models and Biological Proxies.* (Ed. M. Williams, A.M. Haywood, F.J. Gregory & D.N. Schmidt), 123–156. The Micropalaeontological Society Special Publications. The Geological Society, London.

PANCHUK K., HOLMDEN C. & KUMP L. (2005) Sensitivity of the epeiric sea carbon isotope record to local-scale carbon cycle processes: Tales from the Mohawkian Sea. *Palaeogeography, Palaeoclimatology, Palaeoecology*, **228**, 320–337.

PANCOST R.D., FREEMAN K.H. & WAKEHAM S.G. (1999) Controls on the carbon-isotope compositions of compounds in Peru surface waters. *Organic Geochemistry*, **27**, 471–474.

PARIS F. (1981) Les chitinozaires dans le Paléozoïque du Sud-Ouest de l'Europe (Cadre géologique - Etude systématique - Biostratigraphie). *Mémoire de la Société géologique et minéralogique de Bretagne*, **26**, 1–496.

PARIS F. (1990) The Ordovician chitinozoan biozones of the Northern Gondwanan Domain. *Review of Palaeobotany and Palynology*, **73**, 549–570.

PARIS F. (1996) Chapter 17. chitinozoan biostratigraphy and palaeoecology. In: *Palynology: Principles and applications. Volume 2: Applications.* (Ed. J. Jansonius & D. McGregor), vol. 2, 531–552. AASP Foundation.

PARIS F., ACHAB A., ASSELIN E., XIAO-HONG C., GRAHN Y., NÖLVAK J., OBUT O., SAMUELSSON J., SENNIKOV N., VECOLI M., VERNIERS J., XIAO-FENG W. & WINCHESTER-SEETO T. (2004) Chapter 28. chitinozoans. In: *The Great Ordovician Biodiversification Event.* (Ed. B.D. Webby, M.L. Droser, F. Paris & I. Percival), 294–311. New York: Columbia University Press.

PARIS F., GRAHN Y., NESTOR V. & LAKOVA I. (1999a) A revised chitinozoan classification. *Journal of Paleontology*, **73**, 549–570.

PARIS F., VERNIERS J., ACHAB A., ALBANI R., ANCILLETTA A., ASSELIN E., CHEN X., FATKA O., GRAHN Y., MOLYNEUEX S., NOLVAK J., SAMUELSSON J., SENNIKOV N., SOUFIANE A., WANG X. & WINCHESTER-SEETO T. (1999b) Correlation of Ordovician regional chitinozoan biozonations. *Acta Universitatis Carolinae - Geologica*, **43**, 291–294.

PARRISH J.T. (1982) Upwelling and petroleum source beds, with reference to Palaeozoic. *AAPG Bulletin*, **66**, 750–774.

PEACOR D.R., VOVENEY R.M.J. & ZHAO G. (2000) Authigenic illite and organic matter; the principal hosts of vanadium in the Mecca Quarry Shale at Velpen, Indiana. *Clay and Clay Minerals*, **48**, 311–316.

PEETERS F.J.C., BRUMMER G.J.A. & GANSSEN G. (2002) The effect of upwelling on the distribution and stable isotope composition of *Globigerina bulloides* and *Globigerinoides ruber* (planktic Foraminifera) in modern surface waters of the NW Arabian Sea. In: *From process studies to reconstruction of the palaeoenvironment; advances in palaeoceanography, Global and Planetary Change* (Ed. G. Ganssen), vol. 34, 269–291. Elsevier, Amsterdam, Netherlands.

PERLMUTTER M.A. & MATTHEWS M.D. (1990) Global cyclostratigraphy - a model. In: *Quantitative Dynamic Stratigraphy.* (Ed. T.A. Cross), 233–260. Prentice Hall, New Jersey.

PETERS-KOTTIG W., STRAUSS H. & KERP H. (2006) The land plant delta ^{13}C record and plant evolution in the late Palaeozoic. *Palaeogeography, Palaeoclimatology, Palaeoecology*, **240**, 237–252.

POPE M.C. & STEFFEN J.B. (2003) Widespread, prolonged late Middle to Late Ordovician upwelling in North America: a proxy record of glaciation? *Geology*, **33**, 214–215.

POUSSART P.F., WEAVER A.J. & BARNES C.R. (1999) Late Ordovician glaciation and high atmospheric CO_2: addressing an apparent paradox via a coupled model approach. *Acta Universitatis Carolinae - Geologica*, **43**, 167–169.

PRAKASH BABU C., BRUMSACK H.J., SCHNETGER B. & BOETTCHER M.E. (2002) Barium as a productivity proxy in continental margin sediments; a study from eastern Arabian Sea. *Marine Geology*, **184**, 189–206.

PRENTICE M.L. & MATTHEWS R.K. (1991) Tertiary ice sheet dynamics: The snow gun hypothesis. *Journal of Geophysical Research*, **96**, 6811–6827.

PUGH W.J. (1923) The geology of the district around Corris and Aberllefenni (Merionethshire). *Quarterly Journal of the Geological Society, London*, **85**, 242–306.

RAILSBACK L.B., ACKERLY S.C., ANDERSON T.F. & CISNE J.L. (1990) Palaeontological and isotope evidence for warm saline deep waters in Ordovician oceans. *Nature*, **343**, 156–159.

RHOADS D.C. & MORSE J.W. (1971) Evolutionary and ecologic significance of oxygen deficient marine basin. *Lethaia*, **4**, 413–428.

RICKARDS R.B. (2002) The graptolitic age of the type Ashgill series (Ordovician) Cumbria. *Proceedings of the Yorkshire Geological Society*, **54**, 1–16.

RIND D. (1998) Latitudinal temperature gradients and climate change. *Journal of Geophysical Research*, **103**, 5943–5971.

ROBERTS B., MERRIMAN R.J., HIRONS S.R., FLETCHER C.J.N. & WILSON D. (1996) Synchronous very low-grade metamorphism, contractions and inversion in the central part of the Welsh lower Palaeozoic basin. *Journal of the Geological Society, London*, **153**, 277–285.

ROBERTS B., MERRIMAN R.J. & PRATT W. (1991) The influence of strain, lithology and stratigraphical depth on white mice (Illite) crystallinity in mudrocks from the vicinity of the Corris Slate Belt, Wales: - implications for the timing of metamorphism in the Welsh Basin. *Geological Magazine*, **128**, 633–645.

ROBINSON D. & BEVINS R.E. (1986) Incipient metamorphism in the Lower Palaeozoic marginal basin of Wales. *Journal of Metamorphic Petrology*, **4**, 101–113.

RONG J. (2006) Newsletter of the International Subcommission on Silurian Stratigraphy (ISSS). Silurian Times No. 14.

ROSS J.R.P. & ROSS C.A. (1992) Ordovician sea-level fluctuations. In: *Global Perspectives on Ordovician Geology* (Ed. B.D. Webby & J.R. Laurie), 327–336. Balkema.

ROYER D.L. (2006) CO_2-forced climate thresholds during the Phanerozoic. *Geochimica et Cosmochimica Acta*, **70**, 5665–5675.

RUDDIMAN W.F. (2000) *Earth's climate: past and future.* W. H. Freeman and Company, New York.

RUDDIMAN W.F. (2001) *Earth's climate, past and future*, 465 pp. W. H. Freeman and Co. , New York.

RUDDIMAN W.F. (2003) Orbital insolation, ice volume and greenhouse gases. *Quaternary Science Reviews*, **22**, 1597–1629.

RUSHTON A.W.A. (1994) Fossils from the area of Llanwrtyd Wells, Powys (1:10 000) sheet SN 84 NE. *British Geological Survey, Technical Report WH 94/269 R.*

SAGEMAN B.B., WIGNALL P.B. & KAUFFMAN E.G. (1991) Biofacies models for organic-rich facies: tool for paleoenvironmental analysis. In: *Cycles and Events in Stratigraphy.* (Ed. W.R. G. Einsele & A. Seilacher), 542–564. Springer - Verlag, Berlin.

SALTZMAN M.R. & YOUNG S.A. (2005) Long-lived glaciation in the Late Ordovician? Isotopic and sequence-stratigraphic evidence from western Laurentia. *Geology*, **33**, 109–112.

SAVRDA C.E. (1995) Ichnologic applications in paleoceanographic, paleoclimatic and sea-level studies. *Palaios*, **10**, 565–577.

SAVRDA C.E. & BOTTJER D.J. (1994) Ichnofossils and ichnofabrics in rythmically bedded pelagic/hemipelagic carbonates: Recognition and evaluation of benthic redox and scour cycles. In: *Orbital forcing and Cyclic Sequences*, 195–210. International Association of Sedimentologists, Special Publication.

SCHALLREUTER R. (1963) Neue Chitinozoen aus ordovizischen Geschieben und Bemerkungen zur Gattung. *Illichitina. Paläontologische Abhandlungen*, **1**, 391–405.

SCHMITZ B. & BERGSTRÖM S.M. (2007) Chemostratigraphy in the Swedish Upper Ordovician: Regional signifiance of the Hirnantian $\delta^{13}C$ excursion (HICE) in the Boda Limestone of the Siljan region. *GFF*, **129**, 133–140.

SCHNITKER D. (1980) North Atlantic oceanography as possible cause of Antarctic glaciation and eutrophication. *Nature*, **284**, 615–616.

SCHOFIELD D.I., DAVIES J.R., WATERS R.A., WILBY P.R., WILLIAMS M. & WILSON D. (2004) Geology of the Builth Wells district - a brief explanation of the geological map. Sheet Explanation of the British Geological Survey. 1:50 000 sheet 196 Builth Wells (England and Wales).

SHEEHAN P.M. (2001) The Late Ordovician mass extinction. *Annual review of Earth and Planetary Sciences*, **29**, 331–364.

SHIELDS G.A., CARDEN G.A.F., VEIZER J., MEIDLA T., RONG J.Y. & RONG Y.L. (2003) Sr, C and oxygen isotope geochemistry of Ordovician brachiopods: a major isotopic event around the Middle -Late Ordovician transition. *Geochimica et Cosmochimia Acta*, **67**, 2005–2025.

SHIMMIELD G.B. (1992) Can sediment geochemistry record changes in coastal upwelling palaeoproductivity? In: *Upwelling systems: Evolution since the Eary Miocene. Geological Society Special Publication 64.* (Ed. C.P. Summerhayes, W.L. Prell & K.C. Emeis), 29–46. The Geological Society, London.

SKEVINGTON D. (1974) Controls influencing the composition and distribution of Ordovician graptolite faunal provinces. *Special Papers in Palaeontology*, **13**.

SOBARZO M., BRAVO L., DONOSO D., GARCÉS-VARGAS J. & SCHNEIDER W. (2007) Coastal upwelling and seasonal cycles that influence the water column over the continental shelf off central Chile. *Progress in Oceanography.* in press.

SOUFIANE A. & ACHAB A. (2000) Chitinozoan zonation of the Late Ordovician and the Early Silurian of the Island of Anticosti, Québec, canada. *Review of Palaeobotany and Palynology*, **109**, 85–111.

STAPLIN F.L. (1961) Reef-controlled distribution of Devonian microplankton in Alberta. *Palaeontology*, **4**, 48–51.

STOLL H.M. (2006) The Arctic tells its story. *Nature*, **441**, 579–581.

STORCH P. & LOYDELL D.K. (1996) The Hirnantian graptolites *Normalograptus persculptus* and "*Glyptograptus*" *bohemicus*; stratigraphical consequences of their synonymy. *Palaeontology*, **39**, 869–881.

STOW D.A.V. & WETZL A. (1987) Hemiturbidite: a new type of deep-water sediment. In: *Proceedings of the Ocean Drilling Program, distal Bengal Fan; covering Leg 116 of the drilling vessel JOIDES Resolution, Colombo, Sri Lanka, to Colombo, Sri Lanka, sites 717-719, 2 July 1987-19 August 1987.*, vol. 116, 25–34. Texas A and M University, Ocean Drilling Program, United States.

STRAHAN A. & JONES O.T. (1914) *The Geology of the South Wales Coalfield. Part XI. The country around Haverfordwest.* Memoir of the Geological Survey of Great Britain, Sheet 228.

SUTCLIFFE O.E., DOWDESWELL J.A., WHITTINGTON R.J., THERON J.N. & CRAIG J. (2000) Calibrating the Late Ordovician glaciation and mass extinction by the eccentricity cycles of Earth's orbit. *Geology*, **28**, 967–970.

TARLING (1978) *Climatc change*, chap. 1, 3–24. Cambridge University Press.

TAUGOURDEAU P. (1965) Chitinozaires de l'Ordovicien des U.S.A; Comparison avec les faunes de l'Ancien Monde. *Journal of Paleontology*, **20**, 463–485.

TEMPLE J.T. (1988) Ordovician-Silurian boundaryin Wales. In: *A global analysis of teh Ordovician-Silurian boundary* (Ed. L.R.M. Cocks & R.B. Rickards), vol. 43 of *Geology Series*, 65–71. British Museum (Natural History).

TEMPLE J.T. & CAVE R. (1992) Preliminary report on the geochemistry and mineralogy of the Nod Glas and related sediments (Ordovician) of Wales. *Geological Magazine*, **129**, 589–594.

TOBIN K.J., BERGSTRÖM S.M. & DE LA GARZA P. (2005) A mid-Caradocian (453 Ma) drawdown in atmospheric pCO_2 without ice sheet development? *Palaeogeography, Palaeoclimatology, Palaeoecology*, **226**, 187–204.

TOGHILL P. (1992) The Shelveian event, a late Ordovician tectonic episode in southern Britain (Eastern Avalonia). *Proceedings of the Geologist's Association, London*, **103**, 31–35.

TORSVIK T.H. & REHNSTRÖM E.F. (2003) The Tornquist Sea and Baltica-Avalonia docking. *Tectonophysics*, **362**, 67–82.

TRIBOVILLARD N., RAMDANI & TRENTESAUX A. (2005) Controls on organic accumulation in upper jurassic shales of northwestern europe as inferred from trace-metal geochemistry. In: *The deposition of organic-carbon-rich sediments: models, mechnisms and consequences.* (Ed. N.B. Harris), 145–164. Society for Sedimentary Geology Special Publication No. 82.

TWICHELL S.C., MEYERS P.A. & DIESTER-HAASS L. (2002) Significance of high C/N ratios in organic carbon-rich Neogene sediments under the Benguela Current upwelling system. *Organic Geochemistry*, **33**, 715–722.

TYSON R.V. (1995) *Sedimentary organic Matter: Organic Facies and Palynofacies*. Chapman and Hall, London.

UNDERWOOD C.J., CROWLEY S.F., MARSHALL J.D. & BRENCHLEY P.J. (1997) High-resolution carbon isotope stratigraphy of the basal Silurian Stratotype (Dob's Linn, Scotland) and its global correlation. *Journal of the Geological Society, London*, **154**, 709–718.

URBAN J.B. & KLINE J.K. (1970) Chitinozoa of the Cedar City Formation, Midle Devonian of Missouri. *Revue de l'institut Français du Pétrolees et annales des Combustibles Liquides*, **44**, 69–76.

VAN WEERING T.C.E., HELDER W. & SCHALK P. (1997) The Netherlands Indian Ocean Expedition 1992-1993, first results and an introduction. *Deep-Sea Research II*, **4**, 1177–1193.

VANDENBROUCKE T.R.A. (2005) *Upper Ordovician Global Stratotype sections and points and the British Historical Type Area: A chitinozoan point of view*. Ph.D. Dissertation, Research Unit Palaeontology. Ghent, Ghent University.

VANDENBROUCKE T.R.A. (2008) An Upper Ordovician chitinozoan biozonation in British Avalonia (England and Wales). *Lethaia*, in press.

VANDENBROUCKE T.R.A. (in press) Upper ordovician chitinozoans from the historical type area in the uk. Monograph of the Palaeontographical Society.

VANDENBROUCKE T.R.A., HENNISSEN J., ZALASIEWICZ J.A. & VERNIERS J. (submitted) New chitinozoans from the historical type area of the Hirnantina and additional key sections in the Wye Valley, Wales, UK. *Geological Journal.*

VANDENBROUCKE T.R.A., RICKARDS B. & VERNIERS J. (2005) Upper Ordovician chitinozoan biostratigraphy from the type Ashgill area (Cautley district) and the Pus Gill (Dufton district, Cross Fell Inlier), Cumbria, Northern England. *Geological Magazine*, **142**, 783–807.

VANDENBROUCKE T.R.A. & VANMEIRHAEGHE J. (2007) An emerging chitinozoan biozonation for avalonia. *Acta Palaeontologica Sinica*, **46**, 497–501.

VANDENBROUCKE T.R.A., VERNIERS J. & CLARKSON E.N.K. (2003) A chitinozoan biostratigraphy of the Upper Ordovician and lower Siluria strata of the Girvan area, Midland Valley, Scotland. *Transactions of the Royal Society of Edinburgh: Earth Sciences*, **93**, 111–134.

VANDENBROUCKE T.R.A., VERNIERS J. & CLARKSON E.N.K. (2004) chitinozoan biostratigraphy of the Upper Ordovician Fågelsång GSSP, Scania, southern Sweden. *Review of Palaeobotany and Palynology*, **130**, 217–239.

VANDENBROUCKE T.R.A., WILLIAMS M., ZALASIEWICZ J.A., DAVIES J.R. & WATERS R.A. (2008) Integrated Upper Ordovician graptolite-chitinozoan biostratigraphy of the Cardigan and Whitland areas, southwest Wales. *Geological Magazine*, **145**, 199–214.

VANMEIRHAEGHE J. (2006) *The evolution of the Condroz-Brabant Basin from Middle Ordovician to Llandovery: lithostratigraphical and chitinozoan biostratigraphical approach.* Ph.D. Dissertation, Research Unit Palaeontology. Ghent, Ghent University.

VANMEIRHAEGHE J. (2007) A glacioeustatic sea-level drop at the Caradoc-Ashgill boundary? Global correlation based on chitinozoan biostratigraphy and facies analysis from Belgium. *Acta Palaeontologica Sinica*, **46**, 502–506.

VANMEIRHAEGHE J. & VERNIERS J. (2004) Chitinozoan bio-and lithostratigraphical study of the Ashgill Fosses and Génicot Formations (Condroz Inlier, Belgium). *Review of Palaeobotany and Palynology*, **130**, 241–267.

VANMEIRHAEGHE J., YANS J., PREAT A., GRASSINEAU N. & VERNIERS J. (2005) New evidence for the Hirnantian (Upper Ordovician) in Belgium? An integrated isotopical, biostratigraphic and sedimentological approach. In: *Pre-Cambrian to Palaeozoic Palaeopalynology and Palaeobotany* (Ed. P. Steemans & E. Javaux), vol. Memoir 2005/02 (CG2005-M02, 36–38. Carnets de Géologie - Notebooks on Geology.

VERNIERS J., PHARAOH T., ANDRÉ L., DEBACKER T.N., DE VOS W., EVERAERTS M., HERBOSCH A., SAMUELSSON J., SINTUBIN M. & VECOLI M. (2002) The Cambrian to mid Devonian basin development and deformation history of Eastern Avalonia, east of the Midlands Microcraton: new data and a review. In: *Geological Society, London, Special Publications, 201, Palaeozoic Amalgamation of Central Europe.* (Ed. P.T.C. Winchester J. A. & J. Verniers), 47–93. The Geological Society of London.

VILINSKI J.C. & DOMACK E. (1998) Temporal changes in sedimentary organic carbon from the Ross Sea Antarctica: inferred changes in ecosystems and climate. *Eos (Transactions, American Geophysical Union)*, **79**, 157.

VILLAS E., VENNIN E., ÁLVARO J.J., HAMMANN W., HERRERA Z.A. & PIOVANO E.L. (2002) The late Ordovician carbonate sedimentation as a major triggering factor of the Hirnantian glaciation. *Bulletin de la Société Géologique de France*, **173**, 569–578.

VIZAN H., CARNEY J.N., TURNER P., IXER R.A., TOMASSO M., MULLEN R.P. & CLARKE P. (2003) Late Neoproterozoic to Early Palaeozoic palaeogeography of Avalonia: some palaeomagnetic constraints from Nuneaton, central England. *Geological Magazine*, **140**, 685–705.

WALKER L.J., WILKINSON B.H. & IVANY L.C. (2002) Continental drift and Phanerozoic carbonate accumulation in shallow-shelf and deep-marin settings. *Journal of Geology*, **110**, 75–87.

WANG K. CHATTERTON B.D.E., ORTH C.J. & ATTREP M. (1993) Late Ordovician mass extinction in the Selwyn Basin: Geochemical, sedimentological and paleontological evidence. *Canadian Journal of Earth Sciences*, **30**, 1870–1880.

WANG K., CHATTERTON B.D.E. & WANG Y. (1997) An organic isotope record of Late Ordovician to Early Silurian marine sedimentary rocks, Yangtze Sea, South China: implications for CO_2 changes during the Hirnantian glaciation. *Palaeogeography, Palaeoclimatology, Palaeoecology*, **132**, 147–158.

WARNNIG B. & BRUMSACK H.J. (2000) Trace metal signatures of eastern mediterranean sapropels. *Palaeogeography, Palaeoclimatology, Palaeoecology*, **158**, 293–309.

WEBBY B.D. (2002) Patterns of Ordovician reef development. In: *Phanerozoic reef patterns* (Ed. W. Kiessling, E. Fluegel & J. Golonka), 129–179. SEPM Special Publication No. 72.

WEBBY B.D., DROSER M.L., PARIS F. & PERCIVAL I. (2004) *The Great Ordovician Biodiversification Event.*, 484. New York: Columbia University Press.

WEEDON G.P. (2003) *Time-series analysis and cyclostratigraphy: examining stratigraphic records of environmental signals.* Cambridge University Press. 259 pp.

WIGNALL P. (1991) Model for transgressive black shales? *Geology*, **19**, 167–170.

WIGNALL P.B. (1994) *Black shales.* Clarendon Press, Oxford.

WILDE P. (1991) Oceanography in the Ordovician. In: *Advances in Ordovician Geology* (Ed. C.R. Barnes & S.H. Williams), 283–298. Geological Survey of Canada, Paper 90-9.

WILLIAMS A. & WRIGHT A.D. (1981) The Ordovician-Silurian boundary in the Garth area of southwest Powys, Wales. *Geological Journal*, **16**, 1–39.

WILLIAMS G.E. (1991) Milankovitch-band cyclicity in bedded halite deposits contemporaneous with Late Ordovician–Early Silurian glaciation, Canning Basin, Western Australia. *Earth and Planetary Science Letters*, **103**, 143–155.

WILLIAMS M. (2001a) Ashgill graptolites from the 'Red Vein' at Traeth Penbryn, east of Tresaith, Wales. *British Geological Survey, Technical Report IR/01/114.*

WILLIAMS M. (2001b) BGS graptolite collections & biostratigraphy reports for the New Quay - Llangranog & Lampeter distrcits of Wales: a brief summary of in-house data (as of June, 2001). *British Geological Survey, Technical Report IR/01/117.*

WILLIAMS M., DAVIES J.R., WATERS R.A., RUSHTON A.W.A. & WILBY P.R. (2003a) Stratigraphical and palaeoecological importance of Caradoc (Upper Ordovician) graptolites from the Cardigan area, southwest Wales. *Geological Magazine*, **140**, 549–571.

WILLIAMS M., STONE P., SIVETER D.J. & TAYLOR P. (2003b) Upper Ordovician ostracods from the Cautley district, northern England: Baltic and Laurentian affinities. *Geological Magazine*, **138**, 589–607.

WOODCOCK N.H. (1990) Sequence stratigraphy of the Palaeozoic Welsh Basin. *Journal of the Geological Society, London*, **147**, 537–547.

WOODCOCK N.H. & SMALLWOOD S.D. (1987) Late Ordovician shallow marine environments due to glacio-eustatic regression: Scrach Formation, Mid-Wales. *Journal of the Geological Society, London*, **144**, 393–400.

WOODCOCK N.H. & STRACHAN R. (2000) *Geological history of Britain and Ireland*, 423. Blackwell.

YAPP C.J. & POTHS H. (1992) Ancient atmospheric CO_2 pressures inferred from natural goethites. *Nature*, **353**, 342–344.

YARINCIK K.M., MURRAY R.W. & PETERSON L.C. (2000) Climatically sensitive eolian and hemipelagic deposition in the Cariaco Basin, Venezuela, over the past 578,000 years. Results from Al/Ti and K/Al. *Paleoceanography*, **15**, 210–228.

ZACHOS J.C., QIUMM T.M. & SALAMY K.A. (1996) High-resolution (10^4 years) deep-sea foraminferal stable isotope records of the Eocene-Oligocene climate transition. *Paleooceanography*, **11**, 251–266.

ZALASIEWICZ J.A., RUSHTON A.W.A. & OWEN A.W. (1995) Late Caradoc graptolitic faunal gradients across the Iapetus Ocean. *Geological Magazine*, **132**, 611–617.

Appendix A

Chitinozoan sampling and treatment

Following discussions and fieldwork with the BGS Welsh mapping project team, several sections were identified and suggested as representing key outcrops spanning formation and chronostratigraphical boundaries. They were chosen on completeness, exposure and accessibility. More importantly, some sections (the Red Vein at Traeth Penrbyn) had previously yielded graptolites suggestive of the anceps graptolite Biozone and so could be used as a test for the age of those units. Twelve samples were collected from localities from Cardigan to Rhayader in the autumn of 2004 to test for chitinozoan yields. This was followed by more extensive sampling of chosen sections in the summer and spring of 2005 and 2006 to cover the entire Ashgill (mid to upper-Katian) of the Cardigan region and the Llandovery region. Extraction of organic residues followed the procedure outlined by Paris (1981) and is summarised below:

1. Samples should be broken down into approximately 0.5 cm^3 fragments before digestion using a rock crusher or, more simply, a hammer.

2. Weigh each sample, approximately 10-15g for a dark shale, up to 50 g for a limestone.

3. Transfer each sample to a Teflon beaker, if heating up to speed up digestion, or at least a 250ml polyethylene of fluorocarbon bottle with screw on lid. Label. Add 150ml HCl (20

4. Following dissolution of all carbonate (when no effervescence can be detected), wash thoroughly with distilled water.

5. Add 150ml HF (40%). If heating, heat at 80°C for 24 hours in a fume cupboard suitable for HF fumes.

6. Allow to cool, and wash thoroughly with distilled water in a neutralisation bucket.

7. If the samples are to be left at room temperature, stir thoroughly once daily until all silicates have dissolved.

8. Add 150ml HCl (20%) or enough to cover the residue, and leave at room temperature for 30 mins - 1 hour to remove any newly formed precipitates. Repeat this step two to three times washing thoroughly with distilled water in a neutralization bucket between each repetition.

9. Wash all samples with distilled water in a neutralisation bucket until neutral.

10. Transfer each sample in turn, or part of each sample, depending on abundance of residue to a 63 μm sieve and rinse until no more material passes through the mesh. Then transfer each sieved sample to a white-bottomed Petri dish, with enough water to cover the residue, for picking.

11. Sort under a binocular microscope and transfer either directly to an SEM stub or into well slides for retention using a capillary pipette. Use a fine brush to move material around in the Petri dish whilst picking if necessary.

Appendix B

Chitinozoan sample localities

All samples for each area are listed in stratigraphical order, stratigraphically lowest (oldest) first. All samples and specimens are stored at the British Geological Survey, Keyworth, Nottingham, UK.

B.1 Cardigan area

TJC D953: Cwm Degwel Mudstone Member, Cwm Degwel, St. Dogmaels, Near Cardigan. Sample from outcrop in small stream on north side of lane, 40 m north west from road bollard opposite small layby. British Ordnance Survey grid reference SN 15812 45155.

TJC D940: Nantmel Mudstones Formation, sandy facies (sa" on British Geological Survey Sheet 193, Cardigan and Dinas Island). Sample from mudstone between sandy turbiditic units in disused quarry on west side of B4548, Trwyn-yr-allt, 2 km north of Cardigan. N 052^o 05.985' W 004^o 09.982' British Ordnance Survey grid reference SN 17405 48045.

TJC D1006: Nantmel Mudstones Formation, burrow-mottled mudstone. Sample from south end of small cove, immediately south of Cliff Hotel, in cliff at the base of obvious slabs. British Ordnance Survey grid reference SN 16118 49970.

TJC D1007: Nantmel Mudstones Formation, burrow-mottled mudstone. Sample from light-grey silt with iron-oxide-lined burrows, Carreg Lydan, north Gwbert shore. British Ordnance Survey grid reference SN 16288 51336.

TJC D941: Nantmel Mudstones Formation, burrow-mottled mudstone. Sample from cleaved shale band in small cove and gully immediately east of Foel y Mwnt. N 052^o 08.268' W 004^o 08.006'.

TJC D942: Nantmel Mudstones Formation, burrow-mottled mudstone. Sample from dark, organic-rich fraction of silty-mudstone in small quarry on west side of Pen-y-Graig

farmyard. N 052^o 8' 10.4" W 004^o 36' 9.9".

TJC D943: Nantmel Mudstones Formation, burrow-mottled mudstone. Sample from dark, organic-poor fraction of silty-mudstone in small quarry on west side of Pen-y-Graig farmyard. N 052^o 8' 10.4" W 004^o 36' 9.9".

TJC D1003: Nantmel Mudstones Formation, burrow-mottled mudstone. Sample from burrow-mottled mudstone immediately below base of laminated hemipelagite unit 0 (LH^0), west side of Pen Traeth Bach, west of Aberporth. N 052^o 8' 5.4" W 004^o 32' 10.0", British Ordnance Survey grid reference SN 26525 51557.

TJC D1003: Nantmel Mudstones Formation, laminated hemipelagite unit (LH^0). Sample from 2 m above base of LH^0, west side of Pen Traeth Bach, west of Aberporth. N 052^o 8' 5.4" W 004^o 32' 10.0", British Ordnance Survey grid reference SN 26525 51557.

TJC D1013 TJC D1014: Nantmel Mudstones Formation, laminated hemipelagite unit 0 (LH^0). Sample from 2.4 m above base of LH^0, west side of Pen Traeth Bach, west of Aberporth. N 052^o 8' 5.4" W 004^o 32' 10.0", British Ordnance Survey grid reference SN 26525 51557.

TJC D1015: Nantmel Mudstones Formation, laminated hemipelagite unit 0 (LH^0). Sample from 3.8 m above base of LH^0, west side of Pen Traeth Bach, west of Aberporth. N 052^o 8' 5.4" W 004^o 32' 10.0", British Ordnance Survey grid reference SN 26525 51557.

TJC D1009: Nantmel Mudstones Formation, laminated hemipelagite unit 0 (LH^0). Sample from 1.2 m below top of LH^0, east side of Pen Traeth Bach, west of Aberporth. N 052^o 8' 6.2" W 004^o 32' 7.6".

TJC D1001: Nantmel Mudstones Formation, burrow-mottled mudstone. Sample from burrow-mottled mudstones below laminated hemipelagite unit 1 (LH^1), Traeth Penbryn. British Ordnance Survey grid reference SN 28631 52032.

TJC D1000: Nantmel Mudstones Formation, burrow-mottled mudstone. Sample from burrow-mottled mudstones immediately below base of laminated hemipelagite unit 1 (LH^1), east end of Tresaith Bay, Tresaith, 2 km east- northeast of Aberporth. British Ordnance Survey grid reference SN 280 516.

TJC D979: Nantmel Mudstones Formation, laminated hemipelagite unit 1 (LH^1). Sample from immediately above base of laminated hemipelagite unit 1 (LH^1), east end of Tresaith Bay, Tresaith, 2 km east northeast of Aberporth. British Ordnance Survey grid reference SN 280 516.

TJC D955 TJC D1002: Nantmel Mudstones Formation, laminated hemipelagite unit 1 (LH^1). Sample from 3 m above base of laminated hemipelagite unit 1 (LH^1), Traeth Penbryn. British Ordnance Survey grid reference SN 28508 51979.

TJC D967: Nantmel Mudstones Formation, laminated hemipelagite unit 1 (LH^1). Sample from 3.5 cm below top of (LH^1), Traeth Penbryn. British Ordnance Survey grid reference SN 28999 52254.

TJC D968: Nantmel Mudstones Formation, burrow-mottled mudstone. Sample from burrow-mottled mudstones 15 cm above top of laminated hemipelagite unit 1 (LH^1), Traeth Penbryn. British Ordnance Survey grid reference SN 28999 52254.

TJC D957: Nantmel Mudstones Formation, laminated hemipelagite unit 2 (LH^2). Sample from small outcrop along wooded path running from National Trust office at Penbryn cafe to Traeth Penbryn. British Ordnance Survey grid reference SN 2937 5229.

TJC D956: Nantmel Mudstones Formation, laminated hemipelagite unit 3 (LH^3). Sample from immediately above base of LH^3, bay northeast of Traeth Penbryn. British Ordnance Survey grid reference SN 29502 52784.

TJC D1010: Nantmel Mudstones Formation, laminated hemipelagite unit 3 (LH^3). Sample from 2 m below top of LH^3, bay northeast of Traeth Penbryn. British Ordnance Survey grid reference SN 29502 52784.

TJC D1005: Yr Allt Formation. Sample from silty mudstones at base of Yr Allt Formation exposed at northeast end of bay immediately northeast of Traeth Penbryn. British Ordnance Survey grid reference SN 29680 53004.

TJC D949: Yr Allt Formation: Sample from dark mudstones interbedded with thin sands exposed in Cilborth Bay, Llangranog. British Ordnance Survey grid reference SN 3115 5430.

TJC D946: TJC D949: Yr Allt Formation: Sample from dark silty mudstones exposed in Traeth yr Yscland, Llangranog. British Ordnance Survey grid reference SN 31247 54624.

TJC D947: Cwmere Formation, Mottled Mudstone Member *persculptus* bands. Sample from outcrop of *persculptus* bands at foot of path down to beach, Traeth-yr-Ynys, Llangranog. N 052° 10' 6.7" W 004° 27' 53.1".

TJC D948: Cwmere Formation. Sample from cliff outcrop 30 m southeast of *persculptus* band outcrop. N 052° 10' 6.0" W 004° 27' 50.9".

B.2 Llandovery area

Samples listed according to sections sampled in the Llandovery area. Samples in stratigraphical order, stratigraphically lowest (oldest) first, for each section.

B.2.1 Section A: Sugarloaf section

TJC D952: Nantmel Mudstones Formation. Sample from road cutting on corner of A483 west of Sugar Loaf car park, 7 m above base of Nantmel Mudstones Formation. British

Ordnance Survey grid reference SN 83516 42980.

TJC D950: Tridwr Formation. Sample from first appearance of sandy beds of Tridwr Formation in road cutting on corner of A483 west of Sugar Loaf car park, 31 m above base of Nantmel Mudstones Formation. British Ordnance Survey grid reference SN 83516 42980.

B.2.2 Section B: Bryn Nicol section

TJC D1033: Nantnel Mudstones Formation, Bryn Nicol Formation type section. Sampled from 30 cm above Pen Derlwyn facies – Nantmel Mudstones Formation contact.

TJC D960: Bryn Nicol Formation, Coed Ifan facies, Bryn Nicol Formation type section. Sample from finely-laminated silty muds immediately above disturbed bed at waterfall 15, immediately below contact with Bryn Nicol Formation and Nantmel Mudstones Formation.

TJC D959: Nantmel Mudstones Formation, Bryn Nicol Formation type section. Sample from bottom of second interdigitation of Nantmel Mudstones Formation with Bryn Nicol Formation, 100 m on log of section. British Ordnance Survey grid reference SN 82156 44390.

TJC D1032: Nantmel Mudstones Formation, Bryn Nicol type section. Sample from 50 m on log of section. British Ordnance Survey grid reference SN 82116 44391.

TJC D1031: Nantmel Mudstones Formation, Bryn Nicol type section. Sample from 20 m on log of section.

TJC D958: Nantmel Mudstones Formation, Bryn Nicol type section. Sample from 0 m on log of section. British Ordnance Survey grid reference SN 82066 44378.

B.2.3 Section C: Cribarth Formation, Glassallt Fawr

TJC D1021: Cribarth Formation. Sample from small quarry next to track to Coleg Elidyr, Glasallt Fawr Farm, 4 m from southeast end of outcrop. British Ordnance Survey grid reference SN 73016 30303.

TJC D1023: Cribarth Formation. Sample from small quarry next to track to Coleg Elidyr, Glasallt Fawr Farm, 5.5 m from southeast end of outcrop. British Ordnance Survey grid reference SN 73016 30303.

TJC D977: Cribarth Formation. Sample from small quarry next to track to Coleg Elidyr, Glasallt Fawr Farm, 12 m from southeast end of outcrop. British Ordnance Survey grid reference SN 73016 30303.

TJC D1024: Cribarth Formation. Sample from small quarry next to track to Coleg Elidyr, Glasallt Fawr Farm, 20 m from southeast end of outcrop. British Ordnance Survey grid reference SN 73016 30303.

TJC D1022: Cribarth Formation. Sample from small quarry next to track to Coleg Elidyr, Glasallt Fawr Farm, 32 m from southeast end of outcrop. British Ordnance Survey grid reference SN 73016 30303.

TJC D978: Cwm Clyd Sandstone. Sample from silty mud interbeds between thick, coarse sands, in disused, overgrown quarry in Glasallt Fawr wood, at top of track from Glasallt Fawr Farm drive. British Ordnance Survey grid reference SN 7295 3070.

B.2.4 Section D: Dan Yr Allt – A40 road section, Llandovery

TJC D971: Ciliau Formation. Sample from quarry by track from Dan yr Allt Farm to Y Grug, 0 m on log of section. See also Figure 3.3, Chapter 2.

TJC D972: TJC D972: Ciliau Formation. Sample from quarry by track from Dan yr Allt Farm to Y Grug, 7 m on log of section. See also Figure 3.3, Chapter 2.

TJC D973: Cwm Crimglyn Formation. Sample from outcrop on east side of public footpath, just after gate, by small quarry by entrance track to Dan yr Allt Farm, 71 m on log of section. See also Figure 3.3, Chapter 2.

TJC D943: Garth House Formation. Sample from A40 roadside outcrop by entrance track to Dan yr Allt Farm, 264 m on log of section. See also Figure 3.3, Chapter 2.

B.2.5 Section E: Llyn Brianne reservoir

TJC D975: Yr Allt Formation. Sample from outcrop of 'smooth mudstones' at bend in road above small inlet of reservoir at most easterly point of reservoir. British Ordnance Survey grid reference SN 81840 49373.

B.2.6 Section F: Garth House quarry, Garth House, Garth Bank

TJC D976: Garth House Formation. Sample from smooth muds between thin sands at left (west) end of main quarry face, small quarry immediately north of Garth House. British Ordnance Survey grid reference SN 94291 49926.

B.2.7 Section G: Crychan Forest

TJC D1016: Cwm Clyd Sandstone Formation. Sample from silty mud interbeds between thick, coarse sands in forest track cutting exposure, 6 m on log of section. British Ordnance Survey grid reference SN 84689 39635.

TJC D1027: Garth House Formation. Sample from smooth dark mudstones in forest track cutting exposure, 16 m on log of section. British Ordnance Survey grid reference SN 84689 39635.

TJC D1017: Garth House Formation. Sample from smooth dark mudstones in forest track cutting exposure, 20 m on log of section. British Ordnance Survey grid reference SN 84689 39635.

TJC D1028: Garth House Formation. Sample from smooth dark mudstones in forest track cutting exposure, 26 m on log of section. British Ordnance Survey grid reference SN 84689 39635.

TJC D1018: Garth House Formation. Sample from smooth dark mudstones in forest track cutting exposure, 36 m on log of section. British Ordnance Survey grid reference SN 84689 39635.

TJC D1019: Garth House Formation. Sample from smooth dark mudstones in forest track cutting exposure, 40 m on log of section. British Ordnance Survey grid reference SN 84689 39635.

TJC D1029: Garth House Formation. Sample from smooth dark mudstones in forest track cutting exposure, 48 m on log of section. British Ordnance Survey grid reference SN 84689 39635.

TJC D1030: Garth House Formation. Sample from smooth dark mudstones in forest track cutting exposure, 56 m on log of section. British Ordnance Survey grid reference SN 84689 39635.

TJC D1026: Garth House Formation. Sample from smooth dark mudstones in forest track cutting exposure, 76 m on log of section. British Ordnance Survey grid reference SN 84689 39635.

TJC D1020: Bronydd Formation. Sample from burrow-mottled sandy mudstones in forest track cutting exposure, 84 m on log of section. British Ordnance Survey grid reference SN 84689 39635.

TJC D1025: Bronydd Formation. Sample from burrow-mottled sandy mudstones in forest track cutting exposure, 86 m on log of section. British Ordnance Survey grid reference SN 84689 39635.

B.2.8 Dolaucothi M8 core

All depths given are for absolute borehole depths and are not stratigraphic depth. Numbers given in brackets are BGS specimen loan numbers.

TJC D980: (SSK 0826) Yr Allt Formation. 121.5 m.

TJC D981: (SSK 0827) Yr Allt Formation. 105.29 m.

TJC D982: (SSK 0828) Yr Allt Formation. 79.72 m.

TJC D983: (SSK 0829) Yr Allt Formation. 73.5 m.

TJC D984: (SSK 0830) Cwmere Formation, Mottled Mudstone Member. 70.5 m.

TJC D985: (SSK 0831) Cwmere Formation. 62.5 m.

Appendix C

Trace element data

Table C.1: Trace element data, LH[1], Traeth Penbryn. All depths from the base of LH[1]. Al, K, Ti are recorded as wt % oxide, Co, Ni and Ba are recorded as ppm.

Depth (cm)	Al	K	Ti	Co	Ni	Ba
1040	20.30	2.55	0.78	30.38	85.26	398.42
1020	21.48	3.30	0.97	20.15	57.48	523.08
1000	22.57	3.54	1.00	21.41	61.18	558.80
980	22.95	3.78	1.02	21.08	53.14	599.76
960	20.38	2.37	0.72	33.00	87.89	376.33
940	22.70	3.65	1.05	11.00	42.86	635.11
920	22.90	3.64	1.04	17.49	47.34	575.91
900	20.94	3.18	0.86	18.60	51.35	566.61
880	22.98	3.74	1.05	28.99	55.59	500.10
860	23.62	4.05	1.10	20.63	51.74	582.61
840	22.20	3.93	1.01	10.03	42.02	636.98
834.5	20.46	3.77	0.90	8.31	29.55	603.73
833.5	22.31	3.87	1.08	11.18	41.09	645.21
832	22.91	4.14	1.11	7.00	46.88	677.80
830.5	22.65	3.79	1.03	8.59	33.52	658.14
829.75	21.86	3.62	0.99	8.18	35.54	641.16
828.25	17.02	3.60	1.07	5.48	28.45	674.28
826.5	19.19	3.40	1.01	5.47	26.77	719.64
824	21.85	3.71	1.08	8.01	27.05	713.92
823	22.11	4.06	1.10	6.80	29.65	615.95
822	10.31	1.90	0.53	5.85	10.32	293.64
820.75	7.84	1.41	0.40	9.41	14.24	230.62
819.5	9.14	1.60	0.43	40.09	54.74	265.87
800	22.30	3.77	1.00	49.61	92.95	629.64
780	22.87	3.74	1.00	44.51	81.83	624.06

continued on next page

Table C.1: *continued*

Depth (cm)	Al	K	Ti	Co	Ni	Ba
760	23.67	3.84	1.06	25.08	68.19	597.80
740	22.83	3.75	1.00	25.56	65.33	626.40
720	23.10	3.76	1.06	27.61	74.06	624.73
700	24.14	3.98	1.03	23.87	64.82	666.42
680	24.13	3.98	1.02	24.02	65.15	667.03
660	24.57	4.08	1.05	27.66	73.52	695.30
640	24.03	3.88	1.00	26.37	69.57	650.20
620	25.41	4.21	1.09	23.45	56.92	690.73
600	24.51	4.01	1.04	25.36	70.33	668.63
580	24.70	4.12	1.06	26.79	65.52	695.13
560	25.09	4.10	1.05	21.28	56.08	674.47
540	23.73	3.92	1.06	26.13	65.38	658.18
520	23.97	3.96	1.06	22.87	62.66	674.32
500	24.25	3.90	1.05	23.69	67.88	648.63
480	24.74	4.05	1.08	27.24	66.99	674.07
460	24.89	4.09	1.05	23.53	63.67	687.62
440	25.28	4.10	1.07	22.01	60.39	677.77
420	25.30	3.94	1.05	20.51	59.14	665.27
400	26.06	4.24	1.07	21.12	65.18	709.96
380	25.31	3.95	1.03	16.86	54.90	676.80
360	24.55	3.96	1.08	17.04	56.47	675.72
340	23.31	3.70	0.95	19.84	54.56	625.34
320	24.36	3.86	1.04	21.68	60.80	660.32
300	24.00	4.00	1.03	20.92	49.83	675.16
280	25.50	4.21	1.11	19.22	53.81	694.27
260	24.38	4.07	1.03	18.90	50.77	694.41
240	23.65	3.83	1.00	17.61	52.36	648.93
220	27.61	4.53	1.15	21.29	58.55	757.73
200	23.94	4.00	0.98	24.96	56.25	700.33
180	22.83	3.97	1.01	32.36	64.47	704.44
160	23.51	4.04	1.01	32.18	63.07	717.06
140	22.41	3.76	1.00	29.52	64.09	681.81
120	22.15	3.83	0.97	26.24	56.33	679.47
100	22.03	3.77	0.99	34.86	62.89	670.49
80	22.23	3.82	0.99	24.67	56.95	682.50
60	22.52	3.85	1.01	39.03	60.55	677.27
40	22.32	3.83	0.99	41.11	62.00	675.94
20	22.38	3.80	0.97	53.31	55.01	671.13
-40	22.63	3.28	0.99	21.23	60.44	572.60
-60	23.57	3.57	1.05	20.54	56.13	629.54
-80	22.67	3.64	0.98	17.79	48.51	640.86
-100	22.58	3.56	1.00	18.84	48.24	620.59
-120	23.38	3.81	1.10	18.65	45.47	663.89

continued on next page

Table C.1: *continued*

Depth (cm)	Al	K	Ti	Co	Ni	Ba
-140	23.02	3.25	1.05	24.11	65.62	584.37
-160	22.64	3.64	1.06	18.56	45.67	649.10
-180	23.21	3.68	1.09	21.44	56.50	659.44
-200	20.26	2.98	0.90	22.06	53.96	520.37

Appendix D

Carbon isotope mass balance model for the Hirnantian

This appendix study attempts to replicate the analytical approaches of Panchuk *et al.* (2005), Kump (1991); Kump *et al.* (1999) and Holgate *et al.* (2001, 2002); Holgate *et al.* (2003) towards investigating carbon isotope systems in the Palaeozoic. These authors attempted to replicate $\delta^{13}C$ curves for the late Ordovician using numerical modeling of carbon isotope mass balance during changes in isotopic fluxes between carbon reservoirs and sinks. Here I use a similar isotope mass balance model to that of Kump *et al.* (1999) and Kump *et al.* (1999) to derive predictions for the topology of the HICE in the Welsh Basin using different simulated mechanisms. Each mechanism simulated serves a hypothesis for the mechanism of a regional HICE.

This study has not been included in the main body of this thesis because the assumptions made in the model (Section D.2) cannot be fully justified at this stage to consider the model an accurate representation of the late Ordovician Welsh Basin or of the Palaeozoic world. For instance, a silled-basin component, used in the model of Panchuk *et al.* (2005) is necessary for the Welsh Basin which was semi-restricted and bound by bathymetric highs to the west and south (Woodcock & Strachan, 2000). Suggestions for further work required for refinement of the current model are given at the end of this appendix.

However, the model described in this appendix represents a work in progress that potentially contributed to further understanding of the HICE, particularly in light of the results of this thesis i.e. recognition of remobilization of light carbon in the Welsh Basin in the late Katian (Chapter 3) and the change in locus of the regional carbon burial during the Hirnantian glacial maximum (Chapter 5).

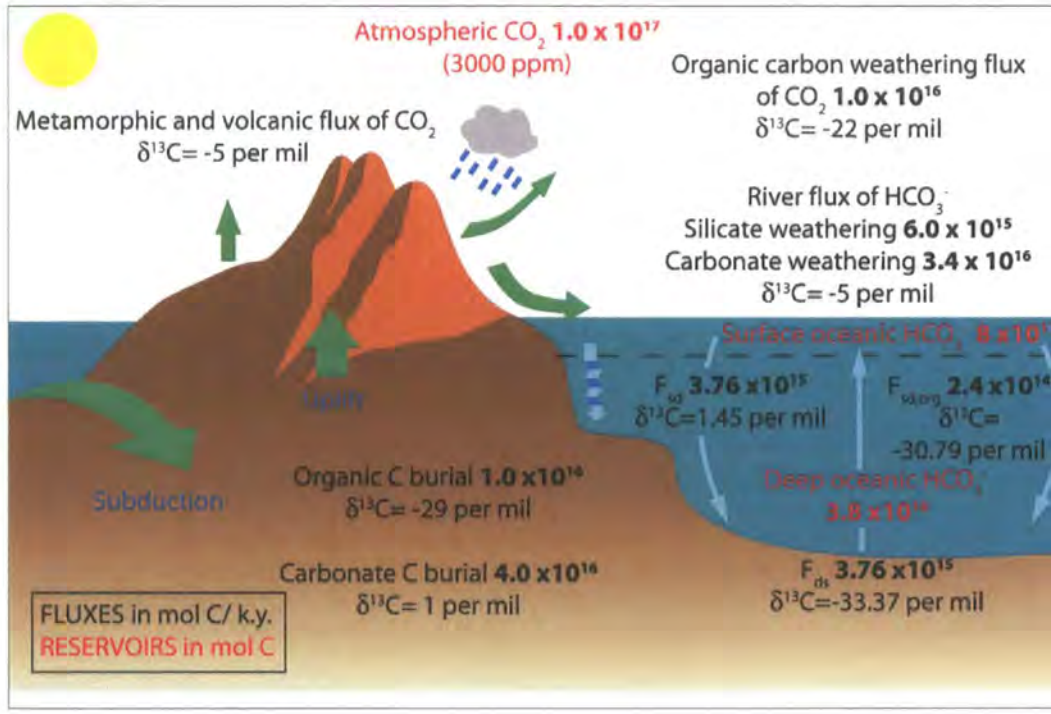

Figure D.1: The long-term carbon cycle showing fluxes and isotopic compositions. The values are presumed representative of the Phanerozoic average state. F_{sd} is surface-ocean to deep-ocean inorganic carbon flux, $F_{sd,org}$ is surface-ocean to deep-ocean organic carbon flux and F_{ds} is deep-ocean to surface-ocean inorganic flux.

D.1 Numerical modeling: isotopic response predictions

The model derived herein is a combination of the models from Kump & Arthur (1999) and Kump (1991). It simulates the isotopic response of carbon reservoirs in the surface-ocean and deep-ocean incorporating a two-box ocean-atmosphere mass balance model for inorganic carbon and a two-layer ocean model derived from Kump (1991). The model outputs responds to changes in fluxes to and from carbon sources and sinks (Figure D.1). Using this, it is possible to investigate plausible conditions responsible for the carbon isotope patterns observed in the Hirnantian of the Welsh Basin.

The amount of inorganic carbon in the ocean surface (M_s) is a function of organic weathering ($F_{w,org}$), inorganic weathering ($F_{w,carb}$), the inorganic carbon flux from the deep ocean to the surface ocean (F_{dps}), organic carbon burial ($F_{b,org}$), inorganic burial ($F_{b,carb}$), silicate weathering ($F_{w,sil}$), the inorganic carbon flux from the surface ocean to the deep ocean (F_{sd}) and the organic carbon flux from the surface ocean to the deep ocean ($F_{sd,org}$). This mass

balance is represented by,

$$\frac{dM_s}{dt} = (F_{w,org} + F_{volc} + F_{dps}) - (F_{b,org} + F_{w,sil} + F_{sd} + F_{sd,org}) \tag{D.1}$$

and for the deep ocean reservoir (M_d):

$$\frac{dM_d}{dt} = F_{sd} + F_{sd,org} - F_{dps} \tag{D.2}$$

For isotopic mass balance in the surface ocean,

$$\begin{aligned}\frac{dM_s\delta_{s,carb}}{dt} &= F'\delta'_w + F_{ds,carb}\delta_{d,carb} - (F_{b,carb}\delta_{s,carb} + F_{sd,carb}\delta_{s,carb}) \\ &\quad +((F_{b,org} + F_{sd,org})(\delta_{s,carb} + \Delta_B))\end{aligned} \tag{D.3}$$

and in the deep ocean,

$$\frac{dM_s\delta_{s,carb}}{dt} = F_{sd,org}\delta_{scarb} + F_{sd,org}(\delta_{s,carb} + \Delta_B) - F_{dps}\delta_{d,carb} \tag{D.4}$$

where F' is the combined weathering flux which includes the volcanic flux ($F_{volc} + F_{worg} + F_{wcarb}$) assuming that δ_{volc} and δ_w approximate the mantle isotopic value (Kump & Garrels, 1986). δ'_w is the isotopic composition of F'. This value is derived from estimates of relative volumes of rocks of different compositions that are being weathered (Bluth & Kump, 1991; Gibbs & Kump, 1994) and is assumed to initially be -5 ‰ for all scenarios. $\delta_{s,carb}$ is the isotopic composition of the surface ocean and $\delta_{d,carb}$ is the isotopic composition of the deep ocean.

The associated isotopic change in the surface ocean inorganic carbon reservoir as reflected in the isotopic composition of carbonate sediments deposited from it ($\delta_{s,carb}$) is represented by:

$$\frac{d\delta_{s,carb}}{dt} = \frac{F'(\delta'_w - \delta_{s,carb}) + F_{dps}(\delta_{d,carb} - \delta_{s,carb}) - (F_{b,org} + F_{sd,org})\Delta_B}{M_s} \tag{D.5}$$

and for the deep ocean reservoir:

$$\frac{d\delta_{d,carb}}{dt} = \frac{F_{sd,carb}(\delta_{s,carb} - \delta_{d,carb}) + F_{sd,org}(\delta_{s,carb} - \delta_{d,carb})\Delta_B}{M_d} \tag{D.6}$$

Δ_B is the isotopic difference between organic matter and carbonate deposited from the ocean (derived from Bidigare *et al.*, 1997, and pagani98) and relates CO_2 and phosphate concentration to the photosynthetic isotope effect (ϵ_p) with an assumed maximum enzymatic isotope effect of 25 ‰.

$$25 - \epsilon_p = \left(\frac{(159.5[PO_4]) + 38.9}{[CO_2(aq)]} \right) \tag{D.7}$$

At 25°C, a reasonable value for low-latitude temperature,

$$\epsilon_p = -(\Delta_B + 8) \tag{D.8}$$

and, following the procedure of Kump & Arthur (1999), substituting atmospheric pCO_2 for $[CO_{2(aq)}]$, assuming equilibration according to Henry's Law, the following expression for Δ_B is obtained:

$$\Delta_B = \left(\frac{(159.5[PO_4]) + 38.9}{0.034 pCO_2} \right) - 33 \tag{D.9}$$

PO_4 concentration is 0.25μmol/kg in all cases, a typical oligotrophic ocean value (Kump & Arthur, 1999).

For each scenario with a flux increase or decrease, unless otherwise stated, fluxes changed asymptotically. The function used for an asymptotic increase ($F_{b,org}$ taken as an example) is:

$$F_{b,org} = 1.5 \times 10^{16} - 0.5 \times 10^{16} e^{\frac{-t+101}{100}} \tag{D.10}$$

Following perturbation, the flux values return to the original value with an e-folding time or 10^5 years (Broecker & Peng, 1982). The function used for the 100 Kyr e-folding time ($F_{b,org}$ used as an example) is:

$$F_{b,org} = 1.0 \times 10^{16} + 0.5 \times 10^{16} e^{\frac{-t+601}{100}} \tag{D.11}$$

Three carbon cycle perturbation scenarios have been run, each scenario being a hypothesis for the mechanism for the HICE; 1) Increased regional weathering of inorganic carbon and increased organic carbon burial from regional uplift (50% increase in $F_{w,org}$, $F_{w,carb}$, $F_{w,sil}$, $F_{b,org}$ and $F_{sd,org}$), 2) decreased global silicate weathering from glaciation (instantaneous 100% decrease in $F_{w,sil}$, instantaneous 50% decrease in $F_{w,org}$ and $F_{w,carb}$ instantaneously set at 3.9×10^{16}) and 3) Increased regional upwelling (50% increase in F_{dps}, $F_{sd,org}$, $F_{b,org}$ and PO_4). All flux and reservoir values used in the model were taken from (Kump & Arthur, 1999) (Figure D.1, Table D.1). The programming script for the simulations was written using Matlab software and the script for each simulation is included at the end of this appendix.

Steady state values for $\delta_{s,carb}$ and $\delta_{d,carb}$ at a pCO_2 of 8 × PAL (3000 ppm), a lower estimate for late Ordovician pCO_2 (Yapp & Poths, 1992; Berner, 1992, 1994; Berner & Kothavala, 2001) can be found by setting the derivatives of D.1, D.2, D.3 and D.4 to zero and rearranging to give,

$$\delta_{s,carb} = \delta'_w - \Delta_b(F_{b,org}/F_{b,org} + F_{b,carb}) \quad \text{(D.12)}$$

$$\delta_{d,carb} = \delta_{s,carb} + \Delta_b(F_{sd,org}/F_{sd,org} + F_{sd}) \quad \text{(D.13)}$$

Under these atmospheric conditions, $\delta_{s,carb}$ = 1.45 ‰ and $\delta_{d,carb}$ = -1.13 ‰. Δ_B = -32.23 and $\delta_{s,org}$ is simply $\delta_{s,carb}+\Delta_B$ (= -30.79 ‰). Similarly, $\delta_{d,org}$ is $\delta_{d,carb}+\Delta_B$ = -33.37 ‰.

D.2 Assumptions

The length of the Hirnantian Stage has been hotly contended and ranges from between 1 Ma and 200 kyr (two eccentricity-modulated glacial-interglacial cycles) (Brenchley *et al.*, 1994; Saltzman & Young, 2005; Armstrong, 2007). I use two periods of 100 kyr for each perturbation with a 100 ky period between perturbations when fluxes and reservoirs set to pre-perturbation values once again.

The model used herein is an attempt at representing the carbon-cycle and carbon isotope mass balance in a simple yet informed manner. It is therefore by no means perfect and several assumptions that cause it to deviate from reality are necessary for the model to be manageable. Future work of integrating other models (e.g. Panchuk *et al.*, 2005; Holgate *et al.*, 2003) will refine the model predictions and address these assumptions.

Assumption (1), The ocean responds instantaneously to silicate weathering production of alkalinity by deposition of $CaCO_3$ (increased $F_{b,carb}$) and so $F_{w,sil}$ represents a carbon sink rather than a source in equation D.1. However, the Lower Palaeozoic lacked calcifying plankton and the contribution to carbonate compensation from coral reefs and other calcifying organisms was probably not comparable to the carbonate buffer provided by modern calcifying plankton (Barker *et al.*, 2003).

Assumption (2), Phosphate availability limits productivity (Broecker & Peng, 1982).

Assumption (3), Values for reservoirs and fluxes represent mean Phanerozoic global values. These are the most appropriate values that can be used for the Lower Palaeozoic carbon reservoirs where there is no evidence as to whether ocean basins were anoxic or oxic for instance.

Therefore all changes in variables during simulations indicate global changes and not regional changes.

Finally, for simplification in comparison in $\delta^{13}C_{org}$ response between simulations, each tectonic episode in simulation 1 (increased weathering from regional tectonic uplift) is set for the same amount of time as the glacial episode (100 ky).

Table D.1: Initial conditions for model calculations.

Fluxes ($\times 10^{12}$mol C/yr)	Reservoirs ($\times 10^{15}$mol C)	Isotopic values (‰)
$F_{w,org}$=1000	Ms=800	$\delta_{s,carb}$=1.45
$F_{w,carb}$=3400	Md=3000	$\delta_{d,carb}$=-1.13
$F_{w,sil}$=600		δ'_w=-5
F'_w=5000		$\delta_{s,org}$=-30.79
F_{volc}=600		$\delta_{d,org}$=-33.37
$F_{b,org}$=1000		Δ_B=-32.23
F_{sd}=2760		
$F_{sd,org}$=240		
F_{dps}=3000		

D.2.1 Numerical modeling results

All empirical initial $\delta^{13}C_{org}$ values are greater than the steady state for initial model atmospheric conditions (steady state = -30.79 ‰ for $\delta^{13}C_{s,org}$ and -33.37 ‰ $\delta^{13}C_{d,org}$). Initial $\delta^{13}C_{org}$ background values, as recorded from each Welsh Basin section are -30.5 ‰, -29.6 ‰ and -29.58 ‰ for Dolaucothi M8 core, A40 Road section and Crychan forest respectively.

Simulation 1: Increased regional weathering of inorganic carbon and increased organic carbon burial from regional uplift: 50% increase in $F_{w,org}$, $F_{w,carb}$, $F_{w,sil}$, $F_{b,org}$ and $F_{sd,org}$, Figure D.2 a, b. The isotopic response of the surface-ocean carbonate reservoir ($\delta^{13}C_{s,carb}$) to this perturbation is two separate abrupt positive excursions followed by a return to a slightly lower steady state conditions. The deep-ocean responds with two small negative excursions establishing a new lower steady state value after perturbations. Both the surface- and deep ocean organic reservoirs exhibit a response of two positive excursions of up to 0.6 ‰ (surface-ocean at 401 kyr), after the perturbation has ceased. The new steady state value for the surface-ocean organic reservoir is the same as pre-perturbation steady state whereas the deep-ocean reservoir new steady state is slightly higher by 0.03 ‰ (Table D.2).

Simulation 2: Decreased global silicate weathering from glaciation: instantaneous 100% decrease in $F_{w,sil}$, instantaneous 50% decrease in $F_{w,org}$ and $F_{w,carb}$ instan-

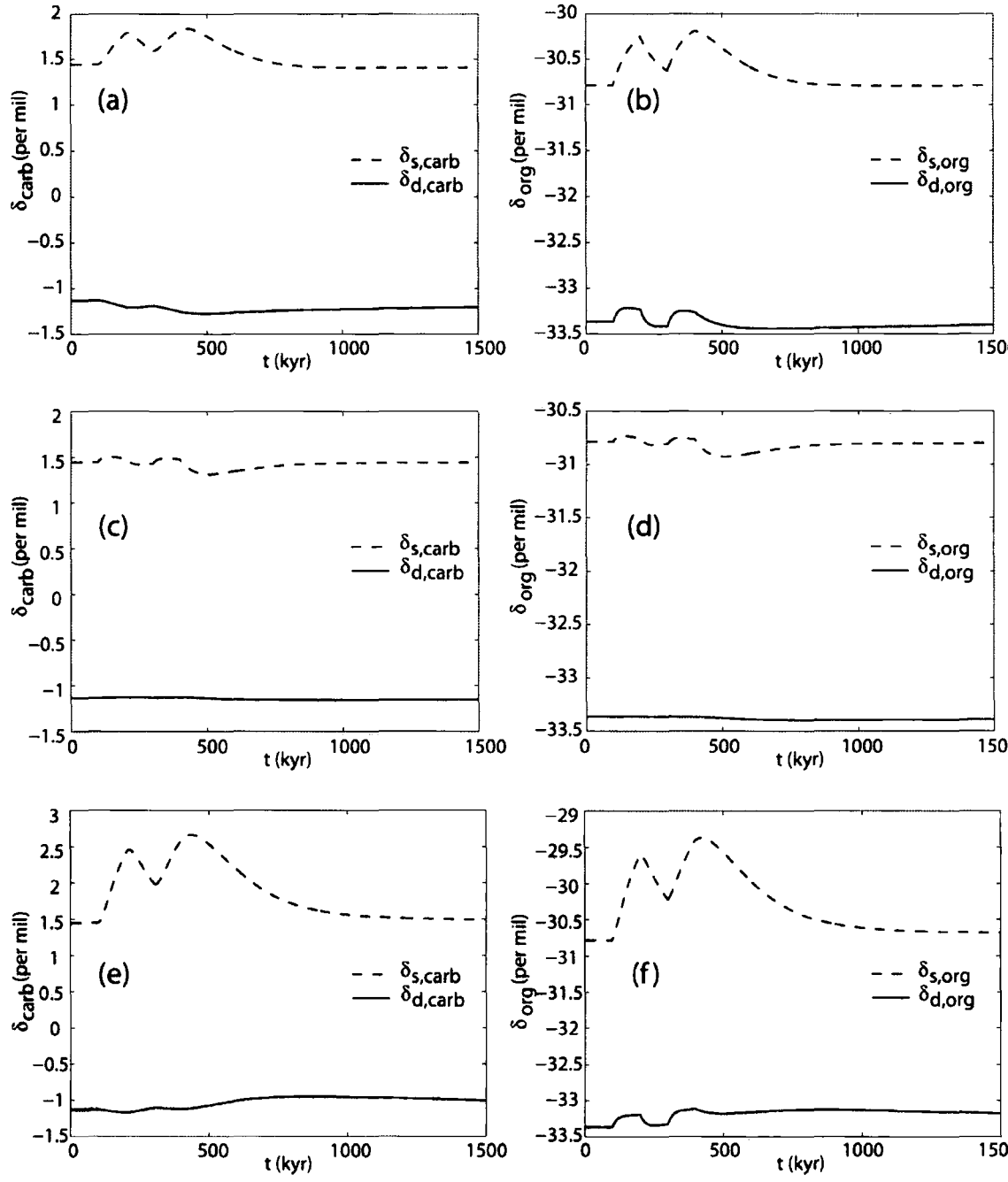

Figure D.2: The isotopic response of the marine inorganic and organic reservoirs to perturbations in the carbon cycle. Inorganic (a) and organic (b) reservoir response to a 50% increase in weathering simulating abrupt tectonic uplift. Inorganic (c) and organic (d) reservoir response to an instantaneous 100% decrease in silicate weathering ($F_{w,sil}$) and 50% decrease in organic carbon weathering ($F_{w.org}$) and a 17% increase in carbonate weathering $F_{w,carb}$). Inorganic (e) and organic (f) reservoir response to a 50% increase in organic carbon burial ($F_{b,org}$), deep-ocean to shallow-ocean inorganic carbon flux (F_{dps}) and surface-ocean to deep-ocean organic carbon flux ($F_{sd,org}$).

Table D.2: Isotopic changes during simulated carbon cycle perturbations. P1 = perturbation 1 (101-200 Kyr), P2 = perturbation 2 (301-400 Kyr). All values ‰.

		Initial	P1	P2	New steady state at 1500 kyr
Simulation 1	$\delta_{s,carb}$	1.45	0.339	0.389	1.41
	$\delta_{d,carb}$	-1.13	-0.08	-0.15	-1.2
	$\delta_{s,org}$	-30.79	0.54	0.61	-30.79
	$\delta_{d,org}$	-33.37	0.16	0.13	-33.4
Simulation 2	$\delta_{s,carb}$	1.45	0.0523	0.030	1.44
	$\delta_{d,carb}$	-1.13	0.002	0.0025	-1.15
	$\delta_{s,org}$	-30.79	0.058	0.040	-30.8
	$\delta_{d,org}$	-33.37	0.010	0.010	-33.39
Simulation 2	$\delta_{s,carb}$	1.45	1.0	1.24	1.49
	$\delta_{d,carb}$	-1.13	-0.045	0.1	-1.00
	$\delta_{s,org}$	-30.79	1.19	1.42	-30.68
	$\delta_{d,org}$	-33.37	0.18	0.26	-33.18

taneously set at 3.9×10^{16}, Figure D.2 c, d. A total cessation of silicate weathering associated with decreased organic weathering and increased carbonate weathering causes a negligible response in the deep-ocean reservoir $\delta^{13}C_{d,carb}$ and $\delta^{13}C_{d,org}$. In the surface-ocean reservoir, both $\delta^{13}C_{s,carb}$ and $\delta^{13}C_{s,org}$ exhibit a small positive increase during each perturbation followed by a negative excursion to values lower than steady state after cessation of the perturbations (1.31 ‰ $\delta^{13}C_{s,carb}$ at 507 kyr and -30.92 ‰ $\delta^{13}C_{s,org}$ at 508 kyr). New steady state values, following equilibration of the ocean reservoirs, are negligibly different from pre-perturbation values (Table D.2).

Simulation 3: Increased regional upwelling and nutrient supply to surface waters from increased thermohaline circulation during glaciation: 50% increase in F_{dps}, $F_{sd,org}$, $F_{b,org}$ and PO_4, Figure D.2 e, f. Both the surface-ocean inorganic and organic reservoirs respond with a depletion in ^{13}C-depleted organic matter represented by positive excursions which decline following removal of the perturbation. The new steady state value for these records is higher than the initial steady state indicating permanent depletion in ^{13}C in these reservoirs. However, the deep-ocean carbonate reservoir exhibits an initial negative excursion during perturbation but increases when the perturbation is removed to a maximum value at 912 Kyr. As a result of this, the new steady state for these reservoirs is also depleted in ^{13}C. The deep-ocean organic reservoir similarly exhibits two positive excursions during the perturbations and a third positive excursion of 0.25 ‰ at 838 Kyr during the return to steady state (Table D.2).

D.2.2 Discussion: $\delta^{13}C$ systematics interpretation

In simulation 1, each $\delta^{13}C_{carb}$ increase corresponds to a decline in pCO_2, associated with increased silicate weathering and the increased burial of organic carbon. In turn, this brings about an increase in Δ_B. The decrease in deep-ocean carbonate $\delta^{13}C_{d,carb}$ values may be attributed to the flux increase of C^{13}-depleted organic matter to the deep ocean associated with increased OC burial. The deep-ocean organic reservoir $\delta^{13}C_{d,org}$ on the other hand, increases because of increasing Δ_B being greater than the negative $\delta^{13}C_{d,carb}$ excursion.

During total cessation of silicate weathering (simulation 2), the deep-ocean reservoirs remain essentially unchanged because there is no increase or decrease in carbon fluxes to and from the deep-ocean. The slight perturbation observed may be accounted for by the increase in pCO_2 from decreased silicate weathering which results in a decrease in Δ_B. In the surface-ocean reservoirs, both $\delta^{13}C_{s,carb}$ and $\delta^{13}C_{s,org}$ exhibit positive excursions because of the reduction in ^{13}C-depleted organic matter entering the surface ocean from weathering and the increase in weathering of heavier carbonate material. Conversely, the negative excursion

following cessation of the perturbations indicates the return to higher influx of ^{13}C-depleted organic matter from weathering. Note that altering $F_{w,sil}$ does not add or subtract carbon from the ocean or atmosphere system via riverine sources, it converts atmospheric inorganic carbon to oceanic inorganic carbon (HCO_3^-) reducing pCO_2 (Kump & Arthur, 1999).

Simulation 3 suggests that thermohaline circulation can increase the shelf $\delta^{13}C_{s,org}$ by 1.4 ‰ (recorded background values) with a 50% increase in $F_{b,org}$, F_{dps}, $F_{sd,org}$ and PO_4, with a corresponding positive excursion of around 0.25 ‰ for deep-ocean $\delta^{13}C_{org}$. Like simulation 1, the basin $\delta^{13}C_{carb}$ exhibits a negative excursion from increased transport of light organic carbon from the surface waters to deep waters ($F_{sd,org}$ during increased productivity. However, the new $\delta^{13}C_{carb}$ steady state value is higher than the initial steady state because of lowered pCO_2 from increased $F_{b,org}$. The positive $\delta^{13}C_{org}$ excursions, compared to the negative $\delta^{13}C_{carb}$ excursions, in the deep-ocean can again be attributed to increasing Δ_B with decreasing pCO_2.

D.3 Suggestions for further work required to refine the current carbon isotope mass balance model

1. Quantitative estimation of regional carbon flux and reservoir values e.g. from modern analogues.

2. Incorporation of elements of the Panchuk *et al.* (2005) model. In particular, account for the fact that the Welsh Basin was a semi-restricted basin by considering the basin and the open ocean as being made of two separate carbon reservoirs with indirect coupling and exchange between them via the surface-ocean reservoir.

3. Account quantitatively for the synthesis of carbonate and organic matter in the deep-ocean.

4. Differentiation of burial fluxes, $F_{b,org}$ and $F_{b,carb}$, in surface- and deep-oceans.

5. Derivation of dissolved inorganic carbon exchange rates between the basin and surface-ocean reservoirs (see Panchuk *et al.*, 2005).

D.4 Matlab script

D.4.1 Simulation 1: Increased regional weathering of inorganic carbon and increased organic carbon burial from regional uplift: 50% increase in $\mathbf{F}_{w,org}$, $\mathbf{F}_{w,carb}$, $\mathbf{F}_{w,sil}$, $\mathbf{F}_{b,org}$ and $\mathbf{F}_{sd,org}$

```
F_volc=6e15; F_worg=1e16; F_wcarb=3.4e16; F_wsil=6e15; F_bcarb=4e16;
d_w=-5; dt=1; PO4=0.25; d_b=-29; t0=101; t1=201; t2=301; t3=401;
elife1=20; elife2=20; elife3=100;

F_ww=F_volc+F_worg+F_wcarb;

nt=1500;

time=zeros(1,nt); time(1)=0;

M0=zeros(1,nt); M0(1)=3.8e18;

d_carbDOL=zeros(1,nt); d_carbDOL(1)=1.73;

d_carbA40=zeros(1,nt); d_carbA40(1)=2.632696078;

d_carbSHELF=zeros(1,nt); d_carbSHELF(1)=2.652696078;

d_carbTEST=zeros(1,nt); d_carbTEST(1)=1.3690;

CO2=zeros(1,nt); CO2(1)=3000;

F_borg=zeros(1,nt); F_borg(1)=1e16;
```

```
d_b=zeros(1,nt); d_b(1)=-32.2277;

d_orgDOL=zeros(1,nt); d_orgDOL(1)=d_carbDOL(1)+d_b(1);

d_orgA40=zeros(1,nt); d_orgA40(1)=d_carbA40(1)+d_b(1);

d_orgSHELF=zeros(1,nt); d_orgSHELF(1)=d_carbSHELF(1)+d_b(1);

d_orgTEST=zeros(1,nt); d_orgTEST(1)=d_carbTEST(1)+d_b(1);

F_wcarb=zeros(1,nt); F_wcarb(1)=3.4e16;

F_worg=zeros(1,nt); F_worg(1)=1e16;

dd_carbDOL=zeros(1,nt);
dd_carbDOL(1)=((F_volc(1)+F_worg(1)+F_wcarb(1))*(d_w-d_carbDOL(1))
-F_borg(1)*d_b(1))/M0(1);

dd_carbA40=zeros(1,nt);
dd_carbA40(1)=((F_volc(1)+F_worg(1)+F_wcarb(1))*(d_w-d_carbA40(1))
-F_borg(1)*d_b(1))/M0(1);

dd_carbSHELF=zeros(1,nt);
dd_carbSHELF(1)=((F_volc(1)+F_worg(1)+F_wcarb(1))*(d_w-d_carbSHELF(1))
- F_borg(1)*d_b(1))/M0(1);

dd_carbTEST=zeros(1,nt);
dd_carbTEST(1)=((F_volc(1)+F_worg(1)+F_wcarb(1))*(d_w-d_carbTEST(1))
- F_borg(1)*d_b(1))/M0(1);
```

```
F_wsil=zeros(1,nt); F_wsil(1)=6e15;

PO4=zeros(1,nt); PO4=0.25;

for it=2:nt
   if it<101
      F_borg(it)=1e16;
      F_wsil(it)=6e15;
      F_worg(it)=1e16;
      F_wcarb(it)=3.4e16;
      %F_volc(it)=6e15;
      PO4(it)=0.25;
      MO(it) = MO(it-1) + dt*(F_worg(it)+F_volc-F_borg(it)-F_wsil(it));
      CO2(it) = (MO(it)/MO(1))^2 * CO2(1);
      d_b(it) = -32.2277;
      dd_carbTEST(it)= 0;
      d_carbTEST(it) = 1.3680;
      d_orgTEST(it) = d_carbTEST(it)+d_b(it);
   end
   if it>100 & it<202
      F_borg(it)=1.5e16-0.5e16*exp((-it+t0)/elife1);
      F_wsil(it)=9.0e15-3.0e15*exp((-it+t0)/elife1);
      F_worg(it)=1.5e16-0.5e16*exp((-it+t0)/elife1);
      F_wcarb(it)=5.1e16-1.7e16*exp((-it+t0)/elife1);
      %F_volc(it)=9.0e15-3.0e15*exp((-it+t0)/elife1);
      PO4(it)=0.375-0.125*exp((-it+t0)/elife1);
      MO(it) = MO(it-1) + dt*(F_worg(it)+F_volc-F_borg(it)-F_wsil(it));
      CO2(it) = (MO(it)/MO(1))^2 * CO2(1);
```

```
   d_b(it) = (((159.5 * PO4(it)) + 38.39)/(0.034*CO2(it)))-33;
   dd_carbTEST(it)=((F_volc+F_worg(it)+F_wcarb(it))*(d_w-d_carbTEST(it-1))
   -F_borg(it)*d_b(it))/MO(it);
   d_carbTEST(it) = d_carbTEST(it-1) + dt*dd_carbTEST(it);
   d_orgTEST(it) = d_carbTEST(it)+d_b(it);

end
if it>201 & it<302
   F_borg(it)=1e16+0.5e16*exp((-it+t1)/elife3);
   F_wsil(it)=6.0e15+3.0e15*exp((-it+t1)/elife3);
   F_worg(it)=1e16+0.5e16*exp((-it+t1)/elife3);
   F_wcarb(it)=3.4e16+1.7e16*exp((-it+t1)/elife3);
   PO4(it)=0.25+0.125*exp((-it+t1)/elife3);
   MO(it) = MO(it-1) + dt*(F_worg(it)+F_volc-F_borg(it)-F_wsil(it));
   CO2(it) = (MO(it)/MO(1))^2 * CO2(1);
   d_b(it) = (((159.5 * PO4(it)) + 38.39)/(0.034*CO2(it)))-33;
   dd_carbTEST(it)= ((F_volc+F_worg(it)+F_wcarb(it))*(d_w-d_carbTEST(it-1))
   -F_borg(it)*d_b(it))/MO(it);
   d_carbTEST(it) = d_carbTEST(it-1) + dt*dd_carbTEST(it);
   d_orgTEST(it) = d_carbTEST(it)+d_b(it);
end
 if it>301 & it<402
   F_borg(it)=(F_borg(301)*1.5)-((F_borg(301)*1.5)
   -F_borg(301))*exp((-it+t2)/elife1);
   F_wsil(it)=(F_wsil(301)*1.5)-((F_wsil(301)*1.5)
   -F_wsil(301))*exp((-it+t2)/elife1);
   F_worg(it)=(F_worg(301)*1.5)-((F_worg(301)*1.5)
   -F_worg(301))*exp((-it+t2)/elife1);
   F_wcarb(it)=(F_wcarb(301)*1.5)-((F_wcarb(301)*1.5)
```

```
      -F_wcarb(301))*exp((-it+t2)/elife1);
      PO4(it)=(PO4(301)*1.5)-((PO4(301)*1.5)-PO4(301))*exp((-it+t2)/elife1);
      MO(it) = MO(it-1) + dt*(F_worg(it)+F_volc-F_borg(it)-F_wsil(it));
      CO2(it) = (MO(it)/MO(1))^2 * CO2(1);
      d_b(it) = (((159.5 * PO4(it)) + 38.39)/(0.034*CO2(it)))-33;
      dd_carbTEST(it)= ((F_volc+F_worg(it)+F_wcarb(it))*(d_w-d_carbTEST(it-1))
      -F_borg(it)*d_b(it))/MO(it);
      d_carbTEST(it) = d_carbTEST(it-1) + dt*dd_carbTEST(it);
      d_orgTEST(it) = d_carbTEST(it)+d_b(it);
    end
    if it>401
      F_borg(it)=1e16+(F_borg(401)-1e16)*exp((-it+t3)/elife3);
      F_wsil(it)=6.0e15+(F_wsil(401)-6.0e15)*exp((-it+t3)/elife3);
      F_worg(it)=1e16+(F_worg(401)-1e16)*exp((-it+t3)/elife3);
      F_wcarb(it)=3.4e16+(F_wcarb(401)-3.4e16)*exp((-it+t3)/elife3);
      PO4(it)=0.25+(PO4(401)-0.25)*exp((-it+t3)/elife3);
      MO(it) = MO(it-1) + dt*(F_worg(it)+F_volc-F_borg(it)-F_wsil(it));
      CO2(it) = (MO(it)/MO(1))^2 * CO2(1);
      d_b(it) = (((159.5 * PO4(it)) + 38.39)/(0.034*CO2(it)))-33;
      dd_carbTEST(it)= ((F_volc+F_worg(it)+F_wcarb(it))*(d_w-d_carbTEST(it-1))
      -F_borg(it)*d_b(it))/MO(it);
      d_carbTEST(it) = d_carbTEST(it-1) + dt*dd_carbTEST(it);
      d_orgTEST(it) = d_carbTEST(it)+d_b(it);
    end
   time(it)=time(it-1)+dt;
end
```

D.4.2 Simulation 2: Decreased global silicate weathering from glaciation: instantaneous 100% decrease in $F_{w,sil}$, instantaneous 50% decrease in $F_{w,org}$ and $F_{w,carb}$ instantaneously set at 3.9×10^{16}

```
F_volc=6e15; F_worg=1e16; F_wcarb=3.4e16; F_wsil=6e15; F_bcarb=4e16;
d_w=-5; dt=1; PO4=0.25; d_b=-32.2277; t0=101; t1=201; t2=301;
t3=401; elife1=100; elife2=100;



nt=1500;

time=zeros(1,nt); time(1)=0;

MO=zeros(1,nt); MO(1)=3.8e18;

d_carbDOL=zeros(1,nt); d_carbDOL(1)=1.73;

d_carbA40=zeros(1,nt); d_carbA40(1)=2.632696078;

d_carbSHELF=zeros(1,nt); d_carbSHELF(1)=2.652696078;

d_carbTEST=zeros(1,nt); d_carbTEST(1)=1.4455;

CO2=zeros(1,nt); CO2(1)=3000;

F_borg=zeros(1,nt); F_borg(1)=1e16;

d_b=zeros(1,nt); d_b(1)=-32.2277;
```

```
d_orgDOL=zeros(1,nt); d_orgDOL(1)=d_carbDOL(1)+d_b(1);

d_orgA40=zeros(1,nt); d_orgA40(1)=d_carbA40(1)+d_b(1);

d_orgSHELF=zeros(1,nt); d_orgSHELF(1)=d_carbSHELF(1)+d_b(1);

d_orgTEST=zeros(1,nt); d_orgTEST(1)=d_carbTEST(1)+d_b(1);

F_wcarb=zeros(1,nt); F_wcarb(1)=3.4e16;

F_worg=zeros(1,nt); F_worg(1)=1e16;

dd_carbDOL=zeros(1,nt);
dd_carbDOL(1)=((F_volc(1)+F_worg(1)+F_wcarb(1))*(d_w-d_carbDOL(1))
-F_borg(1)*d_b(1))/M0(1);

dd_carbA40=zeros(1,nt);
dd_carbA40(1)=((F_volc(1)+F_worg(1)+F_wcarb(1))*(d_w-d_carbA40(1))
-F_borg(1)*d_b(1))/M0(1);

dd_carbSHELF=zeros(1,nt);
dd_carbSHELF(1)=((F_volc(1)+F_worg(1)+F_wcarb(1))*(d_w-d_carbSHELF(1))
- F_borg(1)*d_b(1))/M0(1);

dd_carbTEST=zeros(1,nt);
dd_carbTEST(1)=((F_volc(1)+F_worg(1)+F_wcarb(1))*(d_w-d_carbTEST(1))
- F_borg(1)*d_b(1))/M0(1);

F_wsil=zeros(1,nt); F_wsil(1)=6e15;
```

```
PO4=zeros(1,nt); PO4=0.25;

for it=2:nt
   if it<101
      F_borg(it)=1e16;
      F_wsil(it)=6e15;
      F_worg(it)=1e16;
      F_wcarb(it)=3.4e16;
      PO4(it)=0.25;
      MO(it) = MO(it-1) + dt*(F_worg(it)+F_volc-F_borg(it)-F_wsil(it));
      CO2(it) = (MO(it)/MO(1))^2 * CO2(1);
      d_b(it) = -32.2277;
      dd_carbTEST(it)= 0;
      d_carbTEST(it) = 1.4455;
      d_orgTEST(it) = d_carbTEST(it)+d_b(it);
   end
   if it>100 & it<202
      F_borg(it)=1e16;
      F_wsil(it)=0;
      F_worg(it)=0.5E16;
      F_wcarb(it)=3.9E16;
      PO4(it)=0.25;
      MO(it) = MO(it-1) + dt*(F_worg(it)+F_volc-F_borg(it)-F_wsil(it));
      CO2(it) = (MO(it)/MO(1))^2 * CO2(1);
      d_b(it) = (((159.5 * PO4(it)) + 38.39)/(0.034*CO2(it)))-33;
      dd_carbTEST(it)= ((F_volc+F_worg(it)+F_wcarb(it))*(d_w-d_carbTEST(it-1))
      -F_borg(it)*d_b(it))/MO(it);
      d_carbTEST(it) = d_carbTEST(it-1) + dt*dd_carbTEST(it);
```

```
    d_orgTEST(it) = d_carbTEST(it)+d_b(it);

end
if it>201 & it<302
    F_borg(it)=1e16;
    F_wsil(it)=6e15;
    F_worg(it)=1e16;
    F_wcarb(it)=3.4e16;
    PO4(it)=0.25;
    MO(it) = MO(it-1) + dt*(F_worg(it)+F_volc-F_borg(it)-F_wsil(it));
    CO2(it) = (MO(it)/MO(1))^2 * CO2(1);
    d_b(it) = (((159.5 * PO4(it)) + 38.39)/(0.034*CO2(it)))-33;
    dd_carbTEST(it)= ((F_volc+F_worg(it)+F_wcarb(it))*(d_w-d_carbTEST(it-1))
    -F_borg(it)*d_b(it))/MO(it);
    d_carbTEST(it) = d_carbTEST(it-1) + dt*dd_carbTEST(it);
    d_orgTEST(it) = d_carbTEST(it)+d_b(it);
end
 if it>301 & it<402
    F_borg(it)=1e16;
    F_wsil(it)=0;
    F_worg(it)=0.5E16;
    F_wcarb(it)=3.9E16;
    PO4(it)=0.25;
    MO(it) = MO(it-1) + dt*(F_worg(it)+F_volc-F_borg(it)-F_wsil(it));
    CO2(it) = (MO(it)/MO(1))^2 * CO2(1);
    d_b(it) = (((159.5 * PO4(it)) + 38.39)/(0.034*CO2(it)))-33;
    dd_carbTEST(it)= ((F_volc+F_worg(it)+F_wcarb(it))*(d_w-d_carbTEST(it-1))
    -F_borg(it)*d_b(it))/MO(it);
    d_carbTEST(it) = d_carbTEST(it-1) + dt*dd_carbTEST(it);
```

```
      d_orgTEST(it) = d_carbTEST(it)+d_b(it);
    end
    if it>401
      F_borg(it)=1e16;
      F_wsil(it)=6e15;
      F_worg(it)=1e16;
      F_wcarb(it)=3.4e16;
      PO4(it)=0.25;
      MO(it) = MO(it-1) + dt*(F_worg(it)+F_volc-F_borg(it)-F_wsil(it));
      CO2(it) = (MO(it)/MO(1))^2 * CO2(1);
      d_b(it) = (((159.5 * PO4(it)) + 38.39)/(0.034*CO2(it)))-33;
      dd_carbTEST(it)= ((F_volc+F_worg(it)+F_wcarb(it))*(d_w-d_carbTEST(it-1))
      -F_borg(it)*d_b(it))/MO(it);
      d_carbTEST(it) = d_carbTEST(it-1) + dt*dd_carbTEST(it);
      d_orgTEST(it) = d_carbTEST(it)+d_b(it);
   end
   time(it)=time(it-1)+dt;
end
```

D.4.3 Simulation 3: Increased regional upwelling and nutrient supply to surface waters from increased thermohaline circulation during glaciation: 50% increase in F_{dps}, $F_{sd,org}$, $F_{b,org}$ and PO_4

```
F_volc=6e14; F_worg=10e15; F_wcarb=3.4e15; F_wsil=6e14;
F_bcarb=4e15; d_w=-5; dt=1; PO4=0.25; d_b=-32.2377; t0=101; t1=201;
t2=301; t3=401; elife1=20; elife2=20; elife3=100;

nt=1500;

time=zeros(1,nt); time(1)=0;
```

```
Ma=zeros(1,nt); Ma(1)=1e17;

Ms=zeros(1,nt); Ms(1)=8e17;

Md=zeros(1,nt); Md(1)=3e18;

d_scarb=zeros(1,nt); d_scarb(1)=1.4465;

d_dcarb=zeros(1,nt); d_dcarb(1)=-1.1325;

CO2=zeros(1,nt); CO2(1)=3000;

F_worg=zeros(1,nt); F_worg(1)=1e15;

F_volc=zeros(1,nt); F_volc(1)=6e15;

F_wcarb=zeros(1,nt); F_wcarb(1)=3.4e15;

F_dps=zeros(1,nt); F_dps(1)=3e15;

F_borg=zeros(1,nt); F_borg(1)=1e15;

F_bcarb=zeros(1,nt); F_bcarb(1)=4e15;

F_wsil=zeros(1,nt); F_wsil(1)=6e14;

F_sd=zeros(1,nt); F_sd(1)=2.76e15;
```

```
F_sdorg=zeros(1,nt); F_sdorg(1)=2.4e14;

d_sorg=zeros(1,nt); d_sorg(1)=d_scarb(1)+d_b(1);

d_dorg=zeros(1,nt); d_dorg(1)=d_dcarb(1)+d_b(1);

d_b=zeros(1,nt); d_b(1)=-32.2377;

dd_scarb=zeros(1,nt); dd_scarb(1)=0;

dd_dcarb=zeros(1,nt);
dd_dcarb(1)=(F_sd(1)*(d_scarb(1)-d_dcarb(1))
+(F_sdorg(1)*(d_scarb(1)+d_b(1)-d_dcarb(1))))/Md(1);

PO4=zeros(1,nt); PO4(1)=0.25;

for it=2:nt
   if it<101

      F_worg(it)=1e15;
      F_wcarb(it)=3.4e15;
      F_dps(it)=3e15;
      F_borg(it)=1e15;
      F_bcarb(it)=4e15;
      F_wsil(it)=6e14;
      F_sd(it)=2.76e15;
      F_sdorg(it)=2.4e14;
      F_volc(it)=6e14;
      PO4(it)=0.25;
```

```
    Ms(it) = Ms(it-1) + (dt*(F_worg(it)+F_wcarb(it)+F_dps(it))
    -(F_borg(it)+F_bcarb(it)-F_wsil(it)+F_sd(it)+F_sdorg(it)));
    Md(it) = Md(it-1) + (dt*(F_sd(it)+F_sdorg(it)-F_dps(it)));
    CO2(it) = 3000;
    d_b(it) = -32.2327;
    dd_scarb(it)=0;
    d_scarb(it)=1.4465;
    d_sorg(it) = d_scarb(it)+d_b(it);
    dd_dcarb(it)=0;
    d_dcarb(it)=-1.1325;
    d_dorg(it) = d_dcarb(it)+d_b(it);
end
if it>100 & it<202
     F_borg(it)=1.5e15-0.5e15*exp((-it+t0)/elife1);
    F_dps(it)=4.5e15-1.5e15*exp((-it+t0)/elife1);
    F_sdorg(it)=3.6e14-1.2e14*exp((-it+t0)/elife1);
    F_wsil(it)=6e14;
    F_worg(it)=1e15;
    F_wcarb(it)=3.4e15;
    F_bcarb(it)=4e15;
    F_sd(it)=2.76e15;
    F_volc(it)=6e14;
    PO4(it)=0.375-0.125*exp((-it+t0)/elife1);
    Ms(it) = Ms(it-1) + dt*(F_worg(it)+F_wcarb(it)
    +F_dps(it))-(F_borg(it)+F_bcarb(it)-F_wsil(it)+F_sd(it)
    +F_sdorg(it));
    Md(it) = Md(it-1) + dt*(F_sd(it)+F_sdorg(it)-F_dps(it));
    CO2(it) = ((Md(it)+Ms(it))/(Md(1)+Ms(1)))^2 * CO2(1);
    d_b(it) = (((159.5 * PO4(it)) + 38.39)/(0.034*CO2(it)))-33;
```

```
    dd_scarb(it)=((F_volc(it)+F_worg(it)+F_wcarb(it))
    *(d_w-d_scarb(it-1))+(F_dps(it)*(d_dcarb(it-1)-d_scarb(it-1)))
    -(F_borg(it)+F_sdorg(it))*d_b(it))/Ms(it);
    d_scarb(it)=d_scarb(it-1)+(dt*dd_scarb(it));
    d_sorg(it) = d_scarb(it)+d_b(it);
    dd_dcarb(it)=(F_sd(it)*(d_scarb(it-1)-d_dcarb(it-1))
    +(F_sdorg(it)*(d_scarb(it-1)+d_b(it)-d_dcarb(it-1))))/Md(it);
    d_dcarb(it)=d_dcarb(it-1)+(dt*dd_dcarb(it));
    d_dorg(it) = d_dcarb(it)+d_b(it);
end
if it>201 & it<302
    F_borg(it)=1e15+0.5e15*exp((-it+t1)/elife2);
    F_dps(it)=3e15+1.5e15*exp((-it+t1)/elife2);
    F_sdorg(it)=2.4e14+1.2e14*exp((-it+t1)/elife2);
    F_wsil(it)=6e14;
    F_worg(it)=1e15;
    F_wcarb(it)=3.4e15;
    F_bcarb(it)=4e15;
    F_sd(it)=2.76e15;
    F_volc(it)=6e14;
    PO4(it)=0.25+0.125*exp((-it+t1)/elife2);
    Ms(it) = Ms(it-1) + dt*(F_worg(it)+F_wcarb(it)+F_dps(it))-(F_borg(it)
    +F_bcarb(it)-F_wsil(it)+F_sd(it)+F_sdorg(it));
    Md(it) = Md(it-1) + dt*(F_sd(it)+F_sdorg(it)-F_dps(it));
    CO2(it) = ((Md(it)+Ms(it))/(Md(1)+Ms(1)))^2 * CO2(1);
    d_b(it) = (((159.5 * PO4(it)) + 38.39)/(0.034*CO2(it)))-33;
    dd_scarb(it)=((F_volc(it)+F_worg(it)+F_wcarb(it))*
    (d_w-d_scarb(it-1))+(F_dps(it)*(d_dcarb(it-1)-d_scarb(it-1)))-
    (F_borg(it)+F_sdorg(it))*d_b(it))/Ms(it);
```

```
    d_scarb(it)=d_scarb(it-1)+(dt*dd_scarb(it));
    d_sorg(it) = d_scarb(it)+d_b(it);
    dd_dcarb(it)=(F_sd(it)*(d_scarb(it-1)-d_dcarb(it-1))
    +(F_sdorg(it)*(d_scarb(it-1)+d_b(it)-d_dcarb(it-1))))/Md(it);
    d_dcarb(it)=d_dcarb(it-1)+(dt*dd_dcarb(it));
    d_dorg(it) = d_dcarb(it)+d_b(it);
end
    if it>301 & it<402
    F_borg(it)=(F_borg(301)*1.5)-((F_borg(301)*1.5)
    -F_borg(301))*exp((-it+t2)/elife1);
    F_dps(it)=4.5e15-1.5e15*exp((-it+t2)/elife1);
    F_sdorg(it)=(F_sdorg(301)*1.5)-((F_sdorg(301)*1.5)
    -F_sdorg(301))*exp((-it+t2)/elife1);
    F_wsil(it)=6e14;
    F_worg(it)=1e15;
    F_wcarb(it)=3.4e15;
    F_bcarb(it)=4e15;
    F_sd(it)=2.76e15;
    F_volc(it)=6e14;
    PO4(it)=(PO4(301)*1.5)-((PO4(301)*1.5)-PO4(301))*exp((-it+t2)/elife1);
    Ms(it) = Ms(it-1) + dt*(F_worg(it)+F_wcarb(it)+F_dps(it))-
    (F_borg(it)+F_bcarb(it)-F_wsil(it)+F_sd(it)+F_sdorg(it));
    Md(it) = Md(it-1) + dt*(F_sd(it)+F_sdorg(it)-F_dps(it));
    CO2(it) = ((Md(it)+Ms(it))/(Md(1)+Ms(1)))^2 * CO2(1);
    d_b(it) = (((159.5 * PO4(it)) + 38.39)/(0.034*CO2(it)))-33;
    dd_scarb(it)=((F_volc(it)+F_worg(it)+F_wcarb(it))*(d_w-d_scarb(it-1))+
    (F_dps(it)*(d_dcarb(it-1)-d_scarb(it-1)))-(F_borg(it)+F_sdorg(it))*d_b(it))
    /Ms(it);
    d_scarb(it)=d_scarb(it-1)+(dt*dd_scarb(it));
```

```
d_sorg(it) = d_scarb(it)+d_b(it);
dd_dcarb(it)=(F_sd(it)*(d_scarb(it-1)-d_dcarb(it-1))+
(F_sdorg(it)*(d_scarb(it-1)+d_b(it)-d_dcarb(it-1))))/Md(it);
d_dcarb(it)=d_dcarb(it-1)+(dt*dd_dcarb(it));
d_dorg(it) = d_dcarb(it)+d_b(it);
end
if it>401
F_borg(it)=1e15+(F_borg(401)-1e15)*exp((-it+t3)/elife3);
F_dps(it)=3e15+1.5e15*exp((-it+t3)/elife3);
F_sdorg(it)=2.4e14+(F_sdorg(401)-2.4e14)*exp((-it+t3)/elife3);
F_wsil(it)=6e14;
F_worg(it)=1e15;
F_wcarb(it)=3.4e15;
F_bcarb(it)=4e15;
F_sd(it)=2.76e15;
F_volc(it)=6e14;
PO4(it)=0.25+(PO4(401)-0.25)*exp((-it+t3)/elife3);
Ms(it) = Ms(it-1) + dt*(F_worg(it)+F_wcarb(it)+F_dps(it))
-(F_borg(it)+F_bcarb(it)-F_wsil(it)+F_sd(it)+F_sdorg(it));
Md(it) = Md(it-1) + dt*(F_sd(it)+F_sdorg(it)-F_dps(it));
CO2(it) = ((Md(it)+Ms(it))/(Md(1)+Ms(1)))^2 * CO2(1);
d_b(it) = (((159.5 * PO4(it)) + 38.39)/(0.034*CO2(it)))-33;
dd_scarb(it)=((F_volc(it)+F_worg(it)+F_wcarb(it))*
(d_w-d_scarb(it-1))+(F_dps(it)*(d_dcarb(it-1)
-d_scarb(it-1)))-(F_borg(it)+F_sdorg(it))*d_b(it))/Ms(it);
d_scarb(it)=d_scarb(it-1)+(dt*dd_scarb(it));
d_sorg(it) = d_scarb(it)+d_b(it);
dd_dcarb(it)=(F_sd(it)*(d_scarb(it-1)-d_dcarb(it-1))
+(F_sdorg(it)*(d_scarb(it-1)+d_b(it)-d_dcarb(it-1))))/Md(it);
```

```
      d_dcarb(it)=d_dcarb(it-1)+(dt*dd_dcarb(it));
      d_dorg(it) = d_dcarb(it)+d_b(it);
      end
   time(it)=time(it-1)+dt;
end
```

Appendix E

E.1 δ^{13}C and TOC% data for Dolaucothi M8 core, Pumsaint

Table E.1: δ^{13}C and TOC% data for Dolaucothi M8 core

Sample number	Core depth (m)	Stratigraphic depth (m)	$\delta^{13}C_{org}$ (‰)	TOC%
SSK0833	56.14	40.7	-30.22	0.21
SSK0834	59.15	42.9	-29.73	0.17
SSK0832	62.86	45.6	-30.65	0.15
SSK0835	64.43	46.7	-29.46	0.15
SSK0831	70.55	51.2	-30.06	0.13
SSK0830	71.75	52.0	-30.43	0.37
SSK0829	73.50	53.3	-30.41	0.25
SSK0828	79.72	57.8	-30.93	0.34
SSK0836	87.70	63.6	-30.96	0.36
SSK0837	96.45	69.9	-29.96	0.39
SSK0827	105.29	76.3	-27.72	0.48
SSK0838	115.72	83.9	-30.68	0.38
SSK0826	121.55	88.1	-30.62	0.36
SSK0839	131.00	94.9	-30.30	0.33
SSK0840	135.70	98.4	-30.55	0.32

E.2 δ^{13}C and TOC% data for Crychan Forest section, Llandovery

Table E.2: δ^{13}C and TOC% data for Crychan Forest section, Llandovery

Sample number	Stratigraphic height from base of section (m)	$\delta^{13}C_{org}$ (‰)	TOC%
TJC 041105-1	0	-28.54	0.13
TJC 041105-2	2	-29.36	0.26
TJC 041105-3	4	-29.51	0.26
TJC 041105-4	6	-29.42	0.24
TJC 041105-5	8	-29.47	0.26
TJC 041105-6	10	-29.59	0.32
TJC 041105-7	12	-29.48	0.25
TJC 041105-8	14	-28.86	0.24
TJC 041105-9	16	-29.47	0.26
TJC 041105-10	18	-29.75	0.28
TJC 041105-11	20	-30.05	0.36
TJC 041105-12	22	-29.71	0.31
TJC 041105-13	24	-29.77	0.24
TJC 041105-14	26	-30.04	0.33
TJC 041105-15	28	-29.84	0.31
TJC 041105-16	30	-30.03	0.25
TJC 041105-17	32	-29.94	0.27
TJC 041105-18	34	-29.93	0.28
TJC 041105-19	36	-29.54	0.25
TJC 041105-20	38	-29.66	0.26
TJC 041105-21	40	-29.54	0.41
TJC 041105-22	42	-29.89	0.33
TJC 041105-23	44	-29.66	0.24
TJC 041105-24	48	-29.68	0.34
TJC 041105-25	50	-29.30	0.28
TJC 041105-26	54	-29.83	0.40
TJC 041105-27	56	-29.61	0.38
TJC 041105-28	60	-29.89	0.31
TJC 041105-29	62	-29.65	0.27
TJC 041105-30	64	-29.70	0.33
TJC 041105-31	66	-29.66	0.27
TJC 041105-32	68	-29.65	0.31
TJC 041105-33	70	-29.64	0.28
TJC 041105-34	72	-29.72	0.33
TJC 041105-35	74	-29.80	0.33
TJC 041105-36	76	-29.77	0.27
TJC 041105-37	78	-29.67	0.12
TJC 041105-38	80	-29.15	0.09

continued on next page

Table E.2: *continued*

Sample number	Stratigraphic height from base of section (m)	$\delta^{13}C_{org}$ (‰)	TOC%
TJC 041105-39	82	-29.38	0.11
TJC 041105-40	84	-29.17	0.08
TJC 041105-41	86	-28.76	0.10
TJC 041105-42	88	-29.28	0.10

E.3 δ^{13}C and TOC% data for A40 road section, Llandovery

Table E.3: δ^{13}C and TOC% data for A40 road section, Llandovery

Sample number	Stratigraphic height from base of section (m)	$\delta^{13}C_{org}$ (‰)	TOC%
TJC 120406-45	9	-29.16	0.37
TJC 120406-43	11	-29.12	0.33
TJC 120406-41	13	-29.68	0.31
TJC 120406-39	15	-29.31	0.27
TJC 120406-37	17	-29.43	0.31
TJC 120406-35	19	-29.59	0.29
TJC 120406-33	21	-29.28	0.31
TJC 120406-31	23	-29.58	0.28
TJC 120406-29	25	-29.26	0.31
TJC 120406-27	27	-29.42	0.30
TJC 120406-25	68	-29.80	0.32
TJC 120406-23	70	-29.07	0.26
TJC 120406-21	72	-28.17	0.21
TJC 120406-16	202	-29.51	0.25
TJC 120406-15	203	-29.54	0.31
TJC 120406-13	205	-29.75	0.26
TJC 110406-55	227	-30.02	0.31
TJC 110406-53	229	-29.79	0.23
TJC 110406-51	231	-30.01	0.27
TJC 110406-49	233	-29.81	0.20
TJC 110406-47	235	-30.27	0.26
TJC 110406-45	237	-30.00	0.23
TJC 110406-43	239	-29.82	0.30
TJC 110406-41	241	-29.86	0.30
TJC 110406-39	243	-29.87	0.27
TJC 110406-37	245	-30.20	0.27
TJC 110406-35	247	-29.73	0.29
TJC 110406-33	249	-30.31	0.33
TJC 110406-31	251	-29.04	0.20
TJC 110406-29	253	-30.25	0.24
TJC 110406-27	255	-30.04	0.22
TJC 110406-25	257	-29.65	0.18
TJC 110406-23	259	-29.74	0.23
TJC 110406-21	261	-29.96	0.34
TJC 110406-19	263	-29.68	0.39
TJC 110406-17	265	-30.06	0.31
TJC 110406-15	267	-30.45	0.23
TJC 110406-13	269	-30.09	0.20
TJC 110406-11	271	-30.25	0.25
TJC 110406-9	273	-29.86	0.26

continued on next page

Table E.3: *continued*

Sample number	Stratigraphic height from base of section (m)	$\delta^{13}C_{org}$ (‰)	TOC%
TJC 110406-7	275	-30.07	0.26
TJC 110406-5	277	-30.28	0.33
TJC 110406-3	279	-29.96	0.25
TJC 110406-1	281	-29.79	0.27